OIL SHALE PYROLYSIS: BENCHSCALE EXPERIMENTAL STUDIES AND MODELING

by

Pankaj Tiwari

A dissertation submitted to the faculty of
The University of Utah
in partial fulfillment of the requirements for the degree of

Doctor of Philosophy

Department of Chemical Engineering

The University of Utah

August 2012

The University of Utah Graduate School

STATEMENT OF DISSERTATION APPROVAL

The dissertation of **Pankaj Tiwari**

has been approved by the following supervisory committee members:

Milind D. Deo	, Chair	**5/30/2012**
Eric G. Eddings	, Member	**5/30/2012**
Edward M. Trujillo	, Member	**5/30/2012**
Hong Y. Sohn	, Member	**5/30/2012**
Edward M. Eyring	, Member	**5/30/2012**

and by **JoAnn Lighty** , Chair of the Department of **Chemical Engineering**

and by Charles A. Wight, Dean of The Graduate School.

ABSTRACT

Oil shale is a complex material that is composed of organic matter, mineral matrix and trace amount of bound and/or unbound water. The endothermic decomposition of the organic matter generates liquid and gaseous products. The yield and the desired quality of the product (shale oil) are controlled by the operational conditions. Pyrolysis of a small batch of finely ground oil shale provides chemically controlled intrinsic kinetic rate of organic decomposition. Pyrolysis of large size block/core samples is governed by temperature distributions and the time required for product expulsion. Heat and mass transfer considerations influence the distribution of products and alter the yield and quality.

The experimental studies on oil shale pyrolysis performed in this work were designed to understand the relevant coupled phenomena at multiple scales. Oil shale in the Mahogany zone of the Green River formation was used in all experiments. Experiments were conducted at four scales, powdered samples (100 mesh) and core samples of ¾", 1" and 2.5" diameters. Batch, semibatch and continuous flow pyrolysis experiments were designed to study the effect of temperature (300°C to 500°C), heating rate (1°C/min to 10°C/min), pressure (ambient and 500 psi) and size of the sample on product formation. Comprehensive analyses were performed on reactants and products - liquid, gas and spent shale.

The activation energies of organic decomposition derived from advanced isoconversional method were in the range of 93 to 245 kJ/mol with an uncertainty of about 10%. Lighter hydrocarbons evolved slightly earlier and their amounts were higher in comparison to heavier hydrocarbons. Higher heating rates generated more alkenes compared

to respective alkanes and as the carbon number increased, this ratio decreased. Oil yield decreased and the amount of coke formed increased as the sample size and/or pressure increased. Higher temperature, higher heating rate and low pressure favored more oil yield. The quality of oil improved with an increase in the temperature, pressure and size of the sample.

A model in COMSOL multiphysics platform was developed. A general kinetic model was integrated with important physical and chemical phenomena that occur during pyrolysis. The secondary reactions of coking and cracking in the product phase were addressed. The multiscale experimental data generated and the models developed, provide an understanding of the simultaneous effects of chemical kinetics, heat and mass transfers on oil quality and yield. The comprehensive data collected in this study will help advance the move to large scale oil production from the pyrolysis of shale.

To My Family

TABLE OF CONTENTS

LIST OF TABLES

LIST OF FIGURES

ABBREVIATIONS

ASTM	American Society for Testing and Materials
BPR	Back Pressure Regulator
BT	Batch Pyrolysis
CB	Combustion (Air Environment)
CF	Continuous Flow Pyrolysis
CHNS	Carbon Hydrogen Nitrogen Sulfur -Elemental Analysis
CO	Core Oil Shale
CP	Core Powdered
CT	Computed Tomography
FID	Flame Ionization Detector
FTIR	Fourier Transform-Infrared spectroscopy
GC	Gas Chromatography
GC-MS	Gas Chromatography- Mass Spectrometry
GR	Green River Oil Shale from Skyline 16 location
ISO	Isothermal
HP	High Pressure Pyrolysis
HR	Heating Rate
HY	Hydrous Pyrolysis
HO	Heavy Oil
HPTGA	High Pressure Thermal gravimetric Analysis

LO	Light Oil
MW	Molecular Weight
NISO	Non-Isothermal
OS	Oil shale
PO	Powdered oil shale
PY	Pyrolysis (Nitrogen Environment)
RMS	Root Mean Square
SCN	Single Carbon Number
SG	Shale Gas
SO	Shale Oil
SS	Spent Shale
SB	Semi-batch Pyrolysis
TCD	Thermal Conductivity Detector
TGA	Thermal Gravimetric Analysis
TC	Temperature Control
TCC	Temperature Control from Center of the Sample
TCO	Total Organic Carbon
TGA-DSC	Thermal Gravimetric Analysis-Differential Scanning Calorimetry
TGA-MS	Thermal Gravimetric Analysis- Mass Spectrometry
TIC	Total Ion Chromatogram
WS	Water Soaked Sample
WAT	Wax Appearance Temperature
XRD	X-Ray Diffraction Analysis

NOMENCLATURE

A	Preexponential (Frequency) Factor [min^{-1}]
a'_1	Constant [1.1275]
a'_2	Constant [1.149e-4]
α	Conversion
β	Heating Rate
b'_1	Constant [3.6667e-7]
b'_1	Constant [-0.01843]
C_i	Mass/Concentration of Component i
cO	Concentration of oil [mol/m^3]
Cp	Heat capacity [J/(kg×K)]
D_{AB}	Diffusion Coefficient of A in B (10^{-50} m^2/s)
D_p	Average Pore Diameter [50×10^{-6} meter]
E	Activation Energy [kJ/mol]
E_α	Activation Energy at Conversion α
ε	Porosity of Oil Shale
$f(\alpha)$	Reaction Model
$f(T)$	Temperature Dependency of the Reaction Rate
Grade_OS	Grade of Oil Shale = 30 [gallon/ton]
I	Integral symbol

k	Rate Constant
K	Thermal Conductivity [W/(m×K)]
K_p	Permeability [mili darcy]
Org	Organic content of the material [initially, 0.18 wt% unit less]
M	Molar Mass
N	Number of Heating Rates
p	Pressure
Q	Heat Source (Heat Absorbed by Reactions)
Qm	Mass Source
R	Gas Constant [8.314 kJ/(mol× K)]
Rho_org	Density of Organic Material [1050 [kg/m^3]
Rho_rock	Density of Rock (other than organic) Material [2700 [kg/m^3]
r_i	Reaction Rate of Component i
r	Radial Coordinate
T	Temperature [°C or K]
$T0$	Initial Temperature
T_{max}	Temperature when Reaction Rate is Maximum
t	Time (second (s)/ minute (min)/ hour (hr))
u	Velocity Vector
μ	Viscosity
ρ	Density
ρos	Density of Oil Shale [kg/m^3]
W_0	Initial Weight of the Sample
W_t	Weight of the Sample at time, t

W_∞	Weight of the Sample at the End of the Experiment
xK	Conversion of Kerogen
ΔH	Heat of Reaction
∇p	Pressure Gradient
∇T	Temperature Gradient

ACKNOWLEDGMENTS

I would like to express my sincere thanks and gratitude to Professor Milind D. Deo for his invaluable guidance and support throughout the period of my doctoral work. Working with him provided an enriching experience to my academic endeavor at the University of Utah. His encouragement and support were instrumental in the completion of my dissertation. Sincere thanks are also extended to the members of my supervisory committee, Dr. Eric G. Eddings, Dr. Edward M. Trujillo, Dr. Edward M. Eyring and Dr. Hong Y. Sohn, for their invaluable help during the course of my work through discussions and their input to this dissertation.

The funding for this project was made available through U.S. Department of Energy, project number DE-FE0001243. The samples were provided by Utah Geological Survey. I also would like to acknowledge the efforts of my colleagues at the Petroleum Research Center and their contribution to this work.

I wish to thank my family members for their love and support throughout this endeavor. Special thanks are due to my parents who have always believed in me and have always provided their encouragement and support for every move in my life. Finally, special thanks are also due to my friends in Salt Lake City, Naveen, Surya, Prashanth, Jake, Madhu and Palash, and my lovely friend Pinki for providing me with a family away from home.

1. INTRODUCTION

With the rapid rise in energy requirements, a strong need to search for alternative fuels to furnish future energy demand is quintessential. Alternative fuels can be generated from various sources, such as bioenergy, wind, solar, nuclear, etc. Oil shale and oil sands can contribute significantly to energy requirements by producing unconventional oils through thermal treatment. Oil shale can be exploited as a viable source to produce oil and gas by pyrolysis and electricity by direct combustion. The technologies for oil shale development need to be improved for the process to be economically feasible. Oil shale is a complex heterogeneous material that contains significant quantities of organic matter, with kerogen being the principal component. Kerogen is a complex compound with a high molecular weight. During thermal retorting, kerogen decomposes and releases liquid (shale oil) and gaseous products. This decomposition process requires heat input. The source of heat input might emit greenhouse gases. Hence, pyrolysis of oil shale is questionable due to economic and environmental constraints.

The concept of obtaining useful hydrocarbons from oil shale is not new, and extraction has been in practice since the 14^{th} century. The first patent for a shale oil extraction process was granted during the 17^{th} century [1]. Historically, the cost of oil derived from oil shale has been significantly higher than conventional oil. The development of efficient technologies to derive oil from oil shale might reduce its cost [2]. The oil shale industry has gone through a revolution of sorts. After the oil crisis in the 1970s, a great deal of effort was spent on research and development and on pilot scale

technologies. Extensive research was conducted both in on-surface and in-situ production methods. Even though some large pilot underground retorting operations were performed, the on-surface (mining and processing) methods were closest to full scale (~10,000 barrels/day) commercial implementation. Oil prices collapsed in the early and mid-1980s, which led to the total discontinuation of oil shale research and development programs. Recently, crude oil prices have again risen to levels that may make shale-based oil production commercially viable. The interest of governments and industries in developing the technologies for oil shale as an alternative to conventional oil may contribute to reduce the cost of production significantly.

There has been active research on the production of oil from oil shale since 1913 [3]. Currently, most of the commercial methods in operation or under development are direct heating retorts. In-situ production technologies have seen a significant revival with recent advancements in understanding the inherent technical logistics of the process. This involves a slow thermal pyrolysis of the organic matter in shale which leads to a light oil product that would not require additional thermal upgrading. The variability in composition and geologic setting of worldwide oil shale deposits affects the applicability of various technologies. Water content, minerals, and organic maturity (amount and H/C ratio) vary with source rocks causing different product distribution when subjected to retorting conditions [4]. Despite the application of existing technologies, some key fundamental questions concerning kerogen decomposition, the quality and yield of the generated oil remain unanswered. Improved knowledge of detailed kerogen decomposition mechanisms, kinetic rates, and product compositions are required to efficiently design and optimize the processes. The process of scaling up the laboratory

data to field scale for large production by insitu and exsitu means is not yet well established.

1.1. Research Objectives

A detailed study of the pyrolysis process at different scales provides data that can generate the information needed for developing kinetic rate models for predicting kerogen decomposition and product composition. Heat and mass transfer resistances affect the rates and product compositions depending on the process configuration. An understanding of the pyrolysis process at different experimental scales aids in efficient formulation of the process at field scale. Development of a kinetic model for these phenomena and the development of a possible mechanistic pathway for the generation of products are required to optimize the effects of operational parameters.

The goal of this study is to provide a comprehensive understanding of the kinetics of the oil shale pyrolysis process. This understanding includes the development of a kinetic model to represent the compositional distribution of products obtained from a large pool of experimental conditions. The emphasis of this research is on a bench scale understanding of the tradeoff between simplicity (the macro mechanism of the product formation) and complexity (the detailed micro chemistry) involved in the decomposition process.

The principal goal of this research is to evaluate the kinetics and dependency of product composition on the scale and operating conditions. The research in this study is focused on the multiscale thermal pyrolysis of oil shale. Experimental studies conducted were under a wide range of operating conditions. A mathematical model simulating the

complex physical and chemical process was developed in a multiphysics simulation suite, COMSOL.

The following activities were carried out to achieve this goal:

- Thermal treatment of oil shale with thermal gravimetric analysis (TGA) and understand the kinetics.
- Use of the best available kinetic models for the complex material decomposition.
- Conduct TGA and bench scale experiments on cores of different sizes to understand the conversion of kerogen to oil
- Obtain product distribution under different conditions.
- Multiscale pyrolysis to address the multiphysics issues involved.
- Conduct experiments at high temperature (with different heating rates) and high pressure, emulating insitu conditions.
- Develop a comprehensive model which combines, heat and mass transport mechanisms along with reaction kinetics.

1.2. Background

Fast depleting conventional oil reserves may be substituted by the vast resources of petroleum generating source rock known as oil shale. There are significant resources of oil shale in the western United States, which if exploited in an environmentally responsible manner, would provide secure access to transportation fuels. Oil shale is a compact sedimentary rock that contains organic matter laminated with a complex mineral matrix. The organic matter undergoes chemical decomposition on thermal heating or retorting to produce volatile matter. The generated volatile products are both lighter gases

as well as condensable higher boiling point substances known as shale oil. Shale oil is an oil-like liquid that can be used to produce transportation fuels. Oil shale may contain small amounts of bound and/or unbound water. During the decomposition of organic material in oil shale several coupled processes occur simultaneously and regulate the distribution of the products. The yield and desired quality of the shale oil is controlled by the operational parameters to which the raw oil shale is exposed.

The distribution of the products from oil shale retorting depend on the composition of the source material [4-6], the temperature-time history [7, 8], pressure [9-11], residence time (secondary reaction) [12, 13] and presence of other reactants such as water [14-17], methane [18], oxygen [19] carbon dioxide [20] , and a host of other factors. Because of the chemical composition of the oil produced, moderate to significant upgrading (nitrogen removal and/or hydrogen addition) may be required to convert the oil into a refinery feedstock [21-23].

Worldwide recoverable reserves of oil shale have been estimated at about 2.8 to 3.3 trillion barrels of shale oil [24]. The largest known and most studied oil shale deposits are in the Green River Formation, which is spread among the states of Colorado, Utah, and Wyoming [2, 25, 26]. The Green River Formation reserves could yield 1.5 to 1.8 trillion barrels of shale oil. The oil produced from Green River Formation promise a significant domestic oil source [25, 27]. The Mahogany zone in the Green River Formation region is an organically rich deposit (10-15 weight % organic) of type-1 kerogen [28]. The decomposition of kerogen produces more than 15 gallons of oil per ton of oil shale source rock, according to the Fischer Assay method [2, 28, 29].

The knowledge necessary for the commercial implementation of a process to produce oil from oil shale is growing due to extensive research efforts. The thermal treatment of oil shale can be carried out in surface reactors (exsitu mode) in controlled settings or in-situ under prevailing geologic conditions. Mining the source material to the surface and then retorting are the major steps in exsitu (surface) processing, while in-situ processes are performed underground where the source material is originally deposited. Each mode has certain advantages and drawbacks. Controlling the process parameters is more difficult in insitu processes than in exsitu processes. But, on the other hand, it has been reported that the oil produced in an insitu process is better quality and may be used as a direct feedstock for a petroleum refinery. The yield and quality of the products generated vary significantly with differing heating conditions. The time-temperature history to which the organic matter in the shale (kerogen) is subjected to is important in all of these configurations. The configuration in which the reacting materials are placed is also important in establishing the product amounts and compositions. In most reactor (exsitu) or in-situ configurations, the products evolved undergo secondary reactions. The operational parameters determine the yield and the oil quality, which in turn directly impact the economic and environmental aspects of the process. Producing shale oil with desirable characteristics (low heteroatom content and molecular weight, and high hydrogen content) requires an understanding of the decomposition mechanisms and kinetic parameters associated with kerogen decomposition. Kinetic parameters include activation energy E, preexponential factor A, and the reaction model $f(\alpha)$, also known as kinetic triplet, which describe the progress of the reaction. Determining the kinetics of the decomposition and the rates of products formation will help guide process development.

Technologies have been proposed for feasible commercial development of the process. Currently, many major oil companies are applying different technologies to develop these processes. For example, Shell has developed their InSitu Conversion Process (ICP) technology (on a pilot scale) [30], ExxonMobil has developed the ElectroFrac process [31], and Chevron has developed the CRUSH process [32]. Other production activities include Redleaf's confined capsule retorting, AMSO's CCR_{TM} in-situ process, and the retorting of targeted organic matter by radio frequency heating.

1.3. Significance of the Research and Original Contribution

Extensive research has been carried out on the recovery of oil from oil shale by different means over the last eighty years. However, certain issues, in particular concerning decomposition mechanisms and associated kinetics, remain inconclusive, either due to contrary findings, or due to limitations with the data. Studying the compositional and material characteristics of each phase generated in the process, would help develop a better understanding of this complex reaction set. The framework for creating distribution of activation energy based kinetic models exists in the literature. The generalized methodology for scaling up data from the laboratory to industrial or field scales has not been reported in published literature.

The purpose of this research is to generate oil shale specific kinetics using the distribution of activation energy methodology, understand the compositional aspects and create generalized scale up procedures. The research needed for both surface and subsurface processing were reported in this work. A study was conducted to address the issues of oil production by pyrolyzing the oil shale in the laboratory. Detailed kinetics were examined. Apart from grain-scale samples used in TGA, the cores of different

diameters were studied to understand scale up effects. Experiments were conducted at pressures close to the in-situ processes. The detailed compositional analyses of the products were performed. A multiphysics model for the formation of the product component was established. The reaction network was constrained based on material and elemental balances.

This work provides a comprehensive laboratory data set to improve existing compositional simulators. This study would also resolve the existing ambiguity on the physics of this process and also would significantly improve the accuracy of existing compositional simulators by providing a comprehensive kinetic data set. The outcome of this research advances the understanding of reaction mechanisms, product evolution rates, and the kinetics of the pyrolysis products generated from complex material, kerogen in oil shale.

1.4. Thesis Outline

Chapter 2 contains a comprehensive literature review on oil shale pyrolysis, kinetic studies and compositional analysis, and then a review of modeling efforts. Chapter 3 outlines the experimental setup, analysis and the characterization protocols for the reactants and the products. This section also summarizes the experimental procedures. The characterization of the raw material is summarized in Chapter 4. Chapter 5 discusses the results of the detailed thermal gravimetric analysis (TGA) kinetic studies of organic decomposition. The compositional analysis of the evolved products and their kinetics using thermal gravimetric analysis-mass spectrometry (TGA-MS) are discussed in Chapter 6. The results of mutiscale pyrolysis of oil shale pyrolysis under a wide range of operational parameters and experimental configurations are summarized in Chapter 7.

The studies of hydrous treatment of oil shale pyrolysis and the heterogeneity in the raw samples are included in Chapter 8 and Chapter 9, respectively. The results of a generalized mathematical model simulating this complex multiphysics process are summarized in Chapter 10. Chapter 11 contains a comprehensive summary of study and recommendations for future work.

2. LITERATURE REVIEW

The extent of the literature on oil shale retorting is comprehensive and covers various approaches for the production of shale oil including compositional analysis of materials (raw shale, products formed and spent shale), development of mechanisms and kinetic parameters as well as the effects of retorting conditions on the product distribution. However, due to the very complex nature of the organic matter in oil shale, unraveling the kinetics has not been straightforward. An accurate kinetic model that is able to adequately represent the mechanism of kerogen conversion to generated products is necessary.

2.1. Oil Shale Pyrolysis Process

Oil shale is a wide variety of compact, laminated, complex and heterogeneous sedimentary rock material that contains organic matter, mineral matrix and small amount of bound and/or unbound water [33]. The main constituent of the organic part of the shale is kerogen which, in some publications is approximated as $C_{200}H_{300}SN_5O_{11}$ [34]. Pure kerogen is not considered to be a chemical compound of fixed composition and properties. It is a heterogeneous mixture of organic matter derived from materials such as spore exines, algae, resins, cuticles and woody fragments [33]. Rich oil shale contains about 10 weight percent kerogen. The kerogen portion of the organic matter is insoluble in ordinary solvents. Oil shale also contains a small percentage of bitumen which is a benzene-soluble organic material naturally present in the oil shale. This soluble material

(natural bitumen) normally amounts to only 8 to 10% by weight of the total organic matter present [35].

The common understanding is that kerogen, which is a cross linked high molecular weight solid, breaks down and undergoes chemical decomposition into products when subjected to thermal heating or retorting. Producing oil from oil shale requires heating out of contact with air in a process called pyrolysis. Pyrolysis, which is carried out in an inert atmosphere, is likely to exhibit different characteristics than combustion, which is carried out in the presence of air. Oil shale pyrolysis is analogous to what happens on a geological time scale to produce conventional oil. The production of oil from oil shale is considered unconventional because the material is being artificially and thermally treated at a much faster rate. Upon supplying the energy (heat) to the source rock, the decomposition rate of the organic portion in the shale is accelerated and produces volatile materials. This volatile material ranges from light organic and inorganic gases to very heavy liquid including bitumen. The condensation of the evolved products yields shale oil. Because of hydrogen deficiency, a significant portion of kerogen is converted to char/coke, a carbonaceous residue. Carbonaceous residue is a benzene insoluble portion of the kerogen that remains in the spent shale [36].

The potential products evolve when kerogen reaches a definitive temperature. This reaction continues to completion with appropriate temperature and/or time. The necessary temperatures for oil shale retorting mentioned in the literature are 300°C-550°C for laboratory conditions [33, 37]. The temperature can be lower if the duration of the experiment is long, or on the contrary to reduce the time required, the temperature can be increased. The compositional form of kerogen in shale is such a complicated

heterogeneous mixture of organic compounds that the sequence of several reactions that take place to produce numerous chemical compounds are mostly unknown [27]. Some investigations have led to the conclusion that the kerogen exhibits properties of pyro-bitumen and, upon heating, decomposes by a consecutive reaction into bitumen. The bitumen does not vaporize but remains in the shale [33] and may behave as a solvent for the remaining organic matter [35]. Upon subsequent heating, this bitumen decomposes or cracks to oil, gas, and a carbonaceous residue [38, 39]. Few studies were also reported on the extraction of the soluble bitumen [3] and insoluble kerogen [40] from oil shale and their pyrolysis processes. Frank and Goodier [40] reported that the primary products from the extracted kerogen in the temperature range of 300°C to 350°C were formed without producing any oil. At higher temperatures, the decomposition was much faster and said to resemble that of a cracking process.

Hubbard and Robinson [33] studied Colorado (Parachute and Rifle) oil shale samples with different amounts of organic material, at different temperatures (350^{o}-525^{o}C) and atmospheric pressure in the absence of oxygen. The samples were extracted (removal of naturally present bitumen) and only insoluble organic material in the oil shale was studied. They found that the soluble organic material (bitumen) in the raw oil shale has no appreciable effect upon the rate of thermal decomposition of kerogen. Extracted kerogens from oil shale of different sources follow comparatively the same reaction rate at corresponding temperatures. Allred [35] reinterpreted the Hubbard and Robinson data and concluded stating that the bitumen has a catalytic or solvent action on kerogen decomposition.

2.2. Mechanism of Oil Shale Pyrolysis and Product Formation

The definitive knowledge of the chemical structure of kerogen is not known. It is assumed that kerogen is largely a material of high molecular weight consisting mainly of a loosely interconnected structure of partly unsaturated chains and rings. The rupture of cross-linkage of these interconnected structures occurs first and then true thermal decomposition follows [41]. The complexity of the decomposition during the oil shale pyrolysis was hypothesized based on experimental observations and measurements, such as bitumen formation as an intermediate and subsequent reactions [33]. Analysis of the compositions of the products is important for understanding the competitive reaction mechanisms. There are several reactions that occur during oil shale pyrolysis. Table 2-1 summarizes a list of the reaction networks that may represent the overall decomposition process of oil shale [42]. Rajeshwar et al. [43] listed various mechanisms proposed for oil shale retorting in the literature. The most common pyrolysis decomposition mechanism can be explained in two steps: primary pyrolysis, followed by secondary pyrolysis as shown in Figure 2-1 [27]. All these reactions progress with competitive reaction mechanisms and with different rates that depend on the conditions of pyrolysis process.

The gas products include very light hydrocarbons and inorganic gases, CO_2 and H_2, while the oil is a mixture of condensable hydrocarbons (heavy and light oils) in vapor-liquid equilibrium. The fraction of oil in vapor and liquid phases depends on the boiling point distribution of the mixture components and pyrolysis temperature and pressure [27]. The water may also be generated from other sources such as free water and bound water from organic and mineral decomposition. The rates of competitive reactions depend primarily on the time-temperature history and on other process parameters that

Table 2- 1: Reaction network (organic, water and mineral reactions) during the pyrolysis of oil shale.

Organic phase reaction	Reactant	Products
Primary Pyrolysis	Kerogen	$Oil_{(l)}$ + $Gas_{(v)}$ + $H_{2(v)}$ + $CH_{4(v)}$ + $CO_{2(v)}$ + $H_2O_{(v)}$ + $Char_{(s)}$
Secondary Pyrolysis	Char	$H_{2(v)}$ + $CH_{4(v)}$ + $ROC_{(s)}$ + $ROH_{(s)}$
Carbon Gasification	$ROC_{(s)}$ + $CO_{2(v)}$	$CO_{(v)}$
Oil degradation	$Oil_{(l)}$	$H_{2(v)}$ + $CH_{4(v)}$ $ROC_{(s)}$ + $Coke_{(s)}$
Oil Distillation/Condensation	Oil (l)	Oil(v)
Water-gas Shift	$CO_{(v)}$ + $H_2O_{(v)}$	$CO_{2(v)}$ + $H_{2(v)}$
Bound water loss	$H_2O_{(s)}$	$H_2O_{(v)}$
Mineral reactions		
Dolomite decomposition	$MgCa(CO_3)_{2(s)}$	$CaCO_{3(s)}$ + $MgO_{(s)}$ + $CO_{2(v)}$
Calcite decomposition	$CaCO_{3(s)}$ + $SiO_{2(s)}$	$Ca_2SiO_{4(s)}$ + $CaO_{(s)}$ + $CO_{2(v)}$

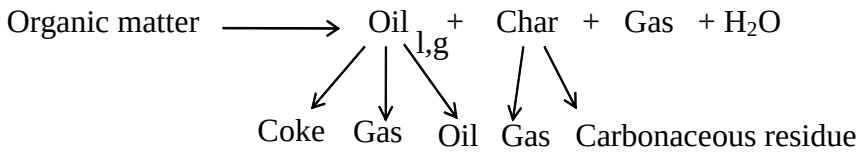

Figure 2- 1: The simplest mechanism of oil shale pyrolysis.

are responsible for the secondary reactions. Secondary pyrolysis refers to the decomposition of the primary products due to coking (liquid phase oil to coke), cracking (vapor phase oil to light gases), and further decomposition of the char and carbon residue to gas. Oil coking takes place when the generated oil has a long residence time. The presence of the significant aromatic components in the oil makes it hydrogen deficient and susceptible to coking [13]. Burnham and Happe [13] hypothesized that the carbon residue may also form from a material that loses minor fragments but retains its basic three dimensional structure during pyrolysis. Burnham and Singleton [9] reported that

enough hydrogen is available from coke formation to saturate the products formed by cracking of the large normal and cyclic hydrocarbons. Fausett and Mikinis [44] have proposed a mechanism in which kerogen pyrolysis can be considered simply as a conversion of most of the aliphatic carbon to oil, while most of the aromatic carbon is converted directly to a carbon residue. Although these workers acknowledged that other reactions such as conversion of aromatic carbon to oil and coking of oil to carbon residue may also occur.

There are a few more complex reaction mechanisms reported in the literature. These address the effect of the mineral matrix and its inorganic products formed on organic matter decomposition mechanisms [45-47], diffusion controlled kinetics [48] and free radical mechanisms [49, 50]. Galan and Smith [48] determined the influence of transport effects (heat and mass) on the observed rate of thermal decomposition of kerogen of Colorado shale (Anvil point mine) in a TGA type apparatus. They concluded that if the particle size was greater than about 0.4×10^{-3} m and if there are more than two to three layers of particles, the transport of heat and mass through intra-particle, particle to bulk fluid, and interparticle, influenced the rate of decomposition. Charlesworth [49] proposed a more complex temperature dependent diffusion mechanisms which follows the following steps; 1-Diffusion controlled reactions, 2- Phase boundary controlled processes, 3- Nucleation controlled processes, 4- Reaction with nucleation and linear growth of nuclei, and 5- Processes governed by nucleation and bulk growth of nuclei which may occur during pyrolysis.

2.3. Complexity Involved in the Process

The parental source rock is complex and impermeable. During thermal treatment products are formed. Voids and fissures are generated as the converted kerogen moves out of its original site due to thermal expansion and volatility**.** This provides an interconnecting network and an internal porosity and permeability in the shale [18]. The coke formed may fuse the porous network. Galan and Smith [48] reported the influence of heat and mass transports. There is a possibility of intraparticle diffusion limiting the generation rate, and the rate controlling step may change as the decomposition progresses. These rate-control transport phenomena also favor the residence time conditions for secondary reactions. Depending on the processing condition, the oil produced may be degraded into less desirable products: coke and gas [51]. The heterogeneity of reactant molecules may produce different amounts of desired products generated from different segments, which influence the reactivity distributed around the complex mechanism.

During the pyrolysis of large particles/blocks of oil shale, several coupled physical and chemical phenomena occur simultaneously, such as heat transfer, chemical reaction kinetics, multiphase flow, phase changes, and mineral alteration and interaction. These processes are highly coupled and interrelated. The changes in the physical properties (density, heat capacity, permeability, porosity, etc.) due to the local thermodynamic conditions may also alter the product distribution. Isolating each phenomenon accurately is impractical. For example, the chemical reaction kinetics of oil shale pyrolysis are quite complex. Several hundred products are formed during decomposition. The distribution of these products (vapor or liquid) and their formation

rates depend on the local conditions. Attempts to address some of these issues during experimental and modeling investigation of Colorado and other oil shales' retorting were reported in the literature [37, 42, 52].

2.4. Kinetic Analysis of Organic Decomposition

Reliable kinetic data are essential for the accurate mathematical modeling of various on-surface and in-situ oil shale processes. The rate of the individual reaction in a complex reaction network is different at different temperature profiles (heating rates) because of time and temperature history the material is exposed to. The appropriate mechanism for representing the decomposition kinetics is uncertain. The simplest representation is a global reaction mechanism. However, oil shales have different origins and geological environments resulting in different compositions. They may behave differently when subjected to pyrolysis conditions, and consequently the proposed mechanisms and derived kinetics vary.

Analysis of the oil shale pyrolysis has appeared in the literature; Colorado oil shale (Green River Formation) [48, 53, 54], Spanish oil shale (Puetrollano) [6], Chinese oil shales [55-57], Pakistani oil shale [58], Jordanian oil shale [20], Moroccan oil shale [59], etc. Elemental analysis and pyrolysis kinetics of oil shales from all over the world were summarized by Nuttal et al. [4] who observed that there were considerable variations in the kinetic parameters of the different shales. A number of researchers have derived relatively simple but effective kinetic expressions for oil evolution during the pyrolysis of Green River and other oil shales based on first-order reaction [60, 61], consecutive first-order reactions [33], parallel first-order reactions [62], and logistic or autocatalytic mechanisms [35]. Campbell et al. [61] postulated a first-order

decomposition mechanism for the pyrolysis of Colorado oil shale and reported an activation energy of 214.4 kJ/mol and a frequency factor of 2.8E13 s^{-1}. Leavitt et al. [62] proposed two parallel first-order lumped reactions and, obtained activation energies of 191.02 kJ/mol for temperature above 350°C and 87 kJ/mol for temperature below 350°C. A controversial two-step mechanism has also been proposed by Braun and Rothman [36].

The kinetic analysis round table [63-67] convened to study the kinetics of reactions involving complex solid materials concluded that it was inappropriate to use a single heating rate and a prescribed kinetic model to derive kinetic parameters. The basic flaw in methods which followed this procedure was that they resulted in activation energies that were heating rate dependent. By using a variety of computational methods, the panel observed that isoconversion and multi heating methods were particularly useful in describing kinetics of complex material reactions [63]. Burnham and Braun [68] reviewed various kinetic analysis approaches for obtaining kinetic parameters for reactions involving complex materials. They argued for the use of well chosen models that are able to fit the data and extrapolate beyond the time-temperature range of the data. For complex materials such as kerogen, generalized distributed reactivity models were found to be suitable. When studying the oil shale pyrolysis data, Burnham and Braun [68] used modified Friedman and the modified Coats and Redfern methods while also employing the discrete activation energy model. Burnhan and Dihn [69] also compared the isoconversional methods to models obtained using nonlinear parameter estimation. They concluded that reactivity distribution of parallel reactions involving complex materials can be modeled effectively using either the isoconversional methods or

parameter fitting approaches; however, they observed that the isoconversional methods are fundamentally inappropriate for use in modeling competing reactions.

It is argued [70] that the variation in activation energy for the decomposition of a complex material is caused by the fact that the overall rate measured by thermal analysis is a combination of the rates of several parallel reactions, each of which has its own energy barrier, and hence an activation energy. The effective activation energy derived from these global rate measurements becomes a function of the individual activation energies.

Burnham [14, 71] has argued convincingly by using multiple sets of data that this two step decomposition mechanism is not appropriate for oil shale pyrolysis. More complex kinetic analysis procedures have also been used in deriving kinetics of decomposition of oil shales [5, 72-74]. It has also been reported that kinetics parameters obtained using one apparatus do not agree well with those derived using a different system. Burnham [71] notes that these differences are primarily due to the use of poor kinetic analysis methods.

Most of these studies recommended the use of distributed reactivity or similar methods, where the reaction rate is inherently independent of heating rates. Variations in the application of these concepts exist in the literature [69, 75-77], particularly in the manner in which the equations are solved. One the first applications of the isoconversion method, based on the differential form of the rate equation [78] is the Friedman method. Modifications and applications to different complex materials have been reported [68, 75, 79]. A general application of this concept is the postulation of a model-free isoconversional method [80], where a functional form of the reaction model is not

presupposed. Extensions of this basic theory in the form of advanced isoconversional method have been applied to a number of complex solid materials [79, 81, 82]. A comprehensive suite of kinetic analysis models based on the concepts discussed by Burnham and Braun [68] is available for use (*Kinetic05*).

2.4.1. Isothermal and Nonisothermal Kinetic Studies

A kinetic model should be coherent under isothermal and nonisothermal conditions. The overall mechanism of decomposition is independent of the temperature and reaction progress. Kinetics should not depend on the methods used for its derivation. Hence, nonisothermal kinetics is obliged to give the same results as isothermal kinetics. However, comparison of isothermal and nonisothermal data can be tainted by some uncontrolled experimental factor according to the Parametric Sensitivity of Thermal Analysis (PSTA) principle [66]. Thakur and Nuttal [59] reported that at lower temperatures, rates of isothermal decomposition are equivalent to those obtained under nonisothermal conditions with high heating rates (>50^{O}C/min). In high temperature isothermal experiments, the thermal induction period is sufficient to decompose a significant amount. Braun and Rothman [36] recognized this fact and reanalyzed the results of Hubbard and Robinson [33] by making corrections to account for the thermal induction period. Other researchers [34, 48] also determined the intrinsic kinetics of Colorado oil pyrolysis by incorporating the induction period. Campbell et al. [27] performed combined kinetic analysis of isothermal and nonisothermal TGA measurements on oil shale data.

2.5. Compositional Analysis of Pyrolysis Products

There has been some published work on the compositional information of the products of oil shale pyrolysis. Campbell et al. [27] deduced mechanisms of the formation of different products, oil and gas, but did not focus on the detailed chemistry of the formation of different components. Most of the studies focused on the compositional analysis of the bulk products collected during or after the completion of the experiment at different conditions [5, 7, 14, 27]. Analysis of products as they are formed using online techniques provides additional information about mechanisms of product formation.

Compositional measurements of products have been performed using both online gas chromatography (GC) and online gas chromatography combined with mass spectrometry (GC-MS). Burnham and Ward [50] analyzed noncondensable gases evolved during pyrolysis using the online flame ionization detector (FID) (C_2 and C_3 hydrocarbons) and thermal conductivity detector (H_2, N_2 and CO). They proposed a free radical mechanism to study the alkene/alkane evolution. Chalesworth [8, 49] studied the pyrolysis of two Australian oil shales and monitored the products using an online GC-FID. Alkene to alkane ratios and kinetic parameters for selected organic compounds were reported. Espitalie et al. [83] studied the kinetics of hydrocarbon evolution produced from the pyrolysis of type II and III kerogens using online GC-FID, and grouped them into C_1, C_2-C_5, C_6-C_{15}, C_{15}+ classes. They concluded that the T_{max} (temperature at which the rate of product evolution is highest) values for each class of compounds increased as the molecular weight of the class decreased. Programmed pyrolysis-gas chromatography of artificially matured Green River kerogen was also reported [84].

The use of mass spectrometry (MS) to identify compounds from the pyrolysis of oil shale is not new. Both offline and online analyses have been used. It was shown that a complex molecule like porphyrin survives retorting temperatures, but attached alkyl and other compounds break off and evolve separately [85]. Shale oil derived from a novel perchloroethylene extraction scheme was analyzed by a number of analytical methods, including tandem mass spectrometry [86]. The principal components found in the extracted oil from Indiana oil shale (Devonian member) were hydrogen rich paraffins and cycloparaffins, having a carbon number range extending to approximately C_{35}+. The benzene concentration in the extracted oil was reported to be 3.94 volume percent. Lee [87] summarized detailed compositional analyses of produced oils from seven different oil shale sources and identified approximately 173 compounds using mass spectrometry. Several different types of compounds ranging from a carbon number of five (pentane) to 37 (heptatricontane) were identified. The compound types included alkanes, alkenes, alkynes, cyclic saturated compounds and aromatics. Oils produced from different sources and under different conditions differed in alkane to alkene ratios and other key parameters. Greenwood and George [88] performed the GC-MS analysis on solvent extracted hydrocarbon fraction of Tasmanite oil shale to study the mass spectral characterization of several C_{19} and C_{20} tricylcic terpanes in the oil.

Online MS analyses have also been reported. Hydrocarbons and inorganic compounds up to 200 atomic mass units were observed by Steck et al. [89] using online mass spectrometric analyses of the pyrolysis of Colorado oil shale. The temperature range studied was divided into three zones, 25-350°C, 350-450°C and 450-1250°C and at higher temperatures, compounds with a greater degree of unsaturation were observed.

Chakravarty et al. [90] pyrolyzed micro-scale samples of four different oil shales and their kerogens. The compositions of the pyrolysis products did not vary significantly when oil shale or kerogens were used as feed. The variation in the total ion chromatograms (TIC) of the products was possibly due to the variations in the raw material composition.

A significant body of work on oil shale pyrolysis with associated compositional and kinetic analysis was compiled at the Lawrence Livermore National Laboratory (LLNL). Campbell et al. [91, 92] studied the kinetics of the evolution of various gas species, CO_2, CO, H_2, and hydrocarbons (CH_4, C_2 and C_3) on the pyrolysis of Colorado oil shale using a mass spectrometer (Finnegan model-3200 quadrupole) at heating rates ranging from 0.5 to 4°C/min. They considered the pyrolysis temperature from 25 to 900°C and reported that the change in the distribution and amount of the evolved components depended on the heating rate. First order reaction was assumed and kinetic expressions for some of the compounds were reported. Huss and Burnham [93] conducted similar studies to measure the rates of evolution of the light gases (CO_2, CO and H_2, CH_4 and C_2 and C_3 hydrocarbons) during the pyrolysis of seven Colorado oil shale samples. They analyzed the gases in the pyrolysis temperature range 200-500°C. T_{max} of these components were used to derive the kinetic parameters. In a later study with oil shales from saline zones in the Green River formation, Burnham et al. [94] reported decomposition kinetics of several minerals in addition to kinetics of pyrolysis by using online GC-MS.

Oh et al. [95] studied real-time evolution of over 30 species by means of a triple quadrupole mass spectrometry (TQMS) to monitor the evolution of water and naphtha up

to C_9 from five different shales. They reported that the exact T_{max} varies with shale and, to a lesser extent, with the molecular weight of the species. The higher molecular weight hydrocarbons have lower T_{max} than the low molecular weight species. A single first order reaction model with the Gaussian-distributed activation energy was applied to ethane and total hydrocarbon evolution rates. Activation energy distributions for single hydrocarbons were narrower than for mixtures.

Reynold at el. [96] studied the kinetics of oil generation of several oil shales and petroleum source rocks of marine and lacustrian origin. They used programmed-temperature pyrolysis at various heating rates, from room temperature to 900°C and analyzed the products using TQMS. T_{max} depended on the sample and the species evolving. Nonhydrocarbon gas formation, particularly H_2S, CO_2, CO, and H_2O was highly dependent on the mineral matrix and mineral matrix-kerogen interactions of the shale.

Burnham et al. [97] determined the rates of product evolution during pyrolysis of several petroleum source rocks and isolated kerogens by nonisothermal techniques including Rock Eval pyrolysis and pyrolysis-MS/MS. Burnham et al. [98] used Py-TQMS (Pyromat; a pyrolysis furnace connected to a triple quadrupole mass spectrometer) to understand the maturity of the rock material and evolution rate profiles of light hydrocarbons. The generation rates of methane, ethane and hydrogen gases were compared along with Rock Eval -T_{max} of overall products for different sources oil shales. Burnham [99] also studied Bakken oil shale decomposition in detail with different instruments (including Py-TQMS) and reported the organic and inorganic gases

generation rates by mass spectrometry. He was able to derive an activation energy of decomposition of about 217 kJ/mol.

Braun at el. [100] conducted TQMS analysis of the pyrolysis products of seven oil shales, and petroleum source rocks at heating rates of 1°C/min and 10°C/min to monitor volatile compounds evolution. Kinetic parameters were determined for evolution of hydrocarbons and of various heteroatomic species using the Gaussian distribution method. Activation energies for benezene formation (211.96 kJ/mol) and other light gases were reported.

Mass spectroscopic studies have also been conducted to look at the formation of specific heteroatomic species. Ammonia (NH_3) evolution during pyrolysis of three Green River formation shales and one Eastern (Devonian) shale was studied using TQMS [101]. Oh et al. [102] reported the decomposition of buddingtonite mineral in the Green River oil shale and monitored the evolution of H_2, NH_3, H_2O, N_2 and CO_2. Wong et al. [103] used the TQMS setup for the kinetics studies of 10 sulfur species produced from the pyrolysis of raw shales and acid treated shales. Wong and Cowford [104] used a triple quadrupole MS/MS to study high explosives and sulfur-containing pyrolysis gases from oil shale.

In addition to the work at LLNL, Meuzelaar et al. [105] studied Py-MS (Pyrolysis followed by online mass spectrometry) of oil shale kerogens and separated alginites of different geological and depositional origins. Oils from Torbanite shale were rich in straight chain hydrocarbons; carboxylic acids dominated the product from Tasmanite, while the Colorado shale oil contained significant amounts of branched chain aliphatic and sulfur compounds. Combined TGA-MS analysis was reported by Khan [106] on

selected gaseous products (CO_2 and H_2O) produced during the study of weathering and preoxidation of eastern (Colorado) and western (Kentucky) oil shales. Marshall et al. [47] also used a TGA-MS unit to study the generation kinetics of key components (CO_2, H_2O and CH_4) during Australian oil shale decomposition. They explained the inflection in the TGA weight loss by different sequential mechanisms such as, moisture loss, organic and mineral decompositions.

2.6. Effect of Operational Parameters on Oil Shale Pyrolysis

The pyrolysis conditions such as temperature, heating rate, sweep gas compositions and flow rate, size of the particle and the pressure regulate the product distribution as well as the composition. The study of the combined effect of many factors on oil yield is important in the recovery of shale oil [41]. The yield of the pyrolysis product may also be affected by the raw material composition. However, Stout et al. [107] reported that it is not the organic content in oil shale but the secondary reactions in the oil phase which affects the oil yield. A similar conclusion was reported by Mikien and Maclel [108] for the presence of aromatic carbons in the residual of retorted shale from several geological formations by analyzing the ^{13} NMR data. The pyrolysis parameters affect the oil quality simultaneously and it was reported that the effects are not additive [9, 41]. The reported results on the effect of pyrolysis conditions in the literature are contradictory.

Hill et al. [18] summarized that the cracking of kerogen at minimum decomposition temperature produces primary products with a relatively low molecular weight. These product molecules are sufficiently stable and do not undergo polymerization. At higher temperature, secondary cracking and polymerization reactions

occur producing the usual higher pour point and low gravity material. Secondary reactions, cracking and coking, control the distribution of the collected products. Secondary reactions depend not only on the pressure but also on the temperature/heating rate and flow rate of the sweep gas. High temperature pyrolysis offers a low residence time for the oil produced (causing less coking), but exposes the oil to high temperatures (causing more cracking) [52]. But, the opposite is true for low temperature pyrolysis. The dependence of oil yield on the heating rate has been attributed to a competition between evaporation, and the coking and cracking of the oil [13]. The effect of oil cracking on yield is less important when compared to oil coking [9]. Condensation and polymerization are other possibilities for changes in the quality of oil produced [9]. The studies of the organic residue in the spent shales showed that the samples yielding decomposition products contained less organic residue than the samples that had been heated longer at the same temperature [33].

The particle size is important in the pyrolysis of oil shale. The effects of heating rate, temperature and holding time on the pyrolysis of different particle sizes have been reported in the literature. The increase in the size of the particle increases the transport resistance. The effects of size under different operating temperature on oil and gas production rates were interpreted by taking into consideration different physical process occurring during the pyrolysis [109-111]. Charlesworth [49] studied the pyrolysis rate of different particle sizes and concluded that the rate of heat transfer is more important than any physical transport phenomenon as the particle size increases. Torrente and Galan [6] found that transport affected the observed rate when the heating rates are higher (more

than 10°C/min). However, they did not observe significant effects of heat and mass transport on the kinetic parameters.

The high flow rate of sweep gas, or reduced pressure increases the oil yield by aiding oil evaporation and thereby reducing the liquid phase coking reactions [5, 10, 11]. Higher pressure and lower heating rates during pyrolysis cause a decrease in the oil yield [9]. Carbonate decomposition is also possible at high temperatures. This might fuse the spent shale resulting in a less permeable or porous network in the shale [18].

The loss in oil yield is due to reactions in the liberated oil [107, 112]. The oil degradation process occurs mainly in the liquid phase not in the vapor phase [27, 98, 112]. The decrease of oil yield under high pressure may also be caused by the slow diffusion of oil from the mineral matrix [41]. Burnham and Singleton [9] reported that the chemical mechanism affecting oil yield and composition are somewhat different at higher pressures. The alkene/alkane ratio in the oil decreases with both decreased heating rate and increased pressures [9].

Chalesworth [8, 49] studied the infrared absorbance results during the progress of pyrolysis process and concluded that the destruction of a significant number of the functional groups containing heteroatoms occurs very early in the pyrolysis. The predominant species in the vapors at short contact times or low temperatures are aromatics, isoprenoids, and saturated cyclic and branched compounds. In the middle and later stages of the reaction, the major components in the vapor are 1-alkenes and n-alkanes. The l-alkene to n-alkane ratios depend on the pyrolysis temperature, the type of oil shale, and to a lesser extent on the degree of conversion. The individual 1-alkene to n-alkane ratios were reported to be high at short times and at low conversions. This was

interpreted in terms of the thermal destruction of specific functional groups, particularly esters and amides. He also suggested that the reaction leading to the alkanes occurs mostly within the kerogen rather than in the gaseous phase.

Burnham and Happe [13] analyzed NMR data of five Green River shale oils to predict the aromaticity and yield of liquid product. They reported that slow heating rates cause hetroaromatic compounds in the oil to be converted to coke, and excessive temperature cause aliphatic moieties to crack to gas. The distribution of aromatic carbon depends on pyrolysis conditions. Marshall et al. [47] also reported a correlation of aromaticity with the yield of volatiles. However, they concluded that during cooling the rearrangement of the products can occur and yield products with varying degree of quality.

Noble et al. [113] demonstrated that increasing pressure significantly retards all aspects of the organic matter decomposition. Pressure affects not only the fractional distribution of liquid and vapor of the primary oil but also the degree of oil degradation during secondary reactions. At elevated pressures the rate of thermal cracking increases and significant decrease in specific gravity occurs. Bae [41] reported that the rate is retarded at elevated pressures and polymerization reactions accelerate. Higher pressure reduces the oil yield significantly and produces a large volume of light hydrocarbon gas. The oil produced under high pressure contains higher aromaticity and lower pour point and sulfur and nitrogen do not change significantly [41]. He also reported that the variation in different aspects of oil shale pyrolysis is not significant at pressures higher than 500 psig. Burnham and Singleton [9] reported oil yield, compositions, and rate of evolution from Green River oil shale (Anvil Point mine) for heating rates from 1^{o}-

100^{o}C/hr and pressures of 1.5 and 27 atm. They concluded that higher pressures and lower heating rates during pyrolysis cause a decrease in oil yield. The oil produced under high pressure was reported to be mixture of lower boiling point substances.

Voge and Good [114] reported that the rate constant increases at elevated pressures while the activation energy of overall first order kinetics of Colorado oil shale was relatively constant over various pressures. A similar conclusion was reported by other researchers on the effect of elevated pressure [113, 115] and reduced pressure, vacuum [10], on the activation energy of organic matter decomposition process.

2.7. Modeling of Oil Shale Pyrolysis

The decomposition process requires heat input. Several interrelated physical and chemical phenomena occur simultaneously, such as heat transfer, chemical reaction kinetics, multiphase flow, phase changes, and mineral alteration and interaction. Oil shale pyrolysis involves all three phases- liquid, gas and solid. In addition, there is an aqueous phase also involved. Currently, there is no thermal simulator available that includes all the coupled physical processes necessary to effectively model in-situ oil shale conversion [116]. Numerous mathematical models of oil shale thermal treatments have been developed over the last few decades. These models address the oil shale pyrolysis using a rather simpler model to very complicated coupled model. Reservoir Thermal Simulator (STARS) from Computer Modeling Group (CMG) [117] and CKT (model developed at the Petroleum Engineering Research Center, University of Utah) [118], adequately simulate the oil shale thermal treatment to a certain level of complexity.

Granoff and Nuttall [119] studied pyrolysis kinetics for single particles (12.7 mm diameter cylinders and spheres) of 22 gal/ton oil shale and developed two mathematical

models; shrinking core and homogeneous. They reported that the shrinking core model describes the observed pyrolysis process very well at high temperatures while the nonisothermal homogeneous model applies well to low temperature pyrolysis. The homogeneous model was found to be preferable as it matched the high and the low temperature conversion curves.

The models PYROL [120] and PMOD [121] were developed by Lawrence Livermore National Laboratory (LLNL) which include many possible reaction pathways, and constrain the product distribution based on the material and elemental balance. The governing equations for PYROL consist of the time derivatives of 150 variables. These ordinary differential equations are expressed in terms of 100 chemical reaction rates and 32 vaporization/condensation relations. A modified Redlich-Kwong-Soave equation of state is used in calculating the vapor/liquid equilibria and *PVT* behavior [120]. PMOD [121] is a computer program to model chemical reactions, which are constructed interactively by supplying the empirical formula of the reactants and products and desired reactions. PMOD calculates stoichiometric coefficients which conserve elemental balance. For pressure driven expulsions this model uses the Redlich-Kwong-Soave (RKS) equation of state calculations for an assumed single hydrocarbon phase. A global model for the generation of oil and gas from petroleum source rocks was also presented by Braun and Burnham [122]. This model consists of 13 chemical species and 10 reactions and incorporates alternative mechanistic pathways for type I and type II kerogens.

A model developed by Parker at al. [42] includes kerogen pyrolysis, oil coking, residual carbon gasification, carbonate mineral decomposition, water gas shift reaction,

and phase equilibria reactions (Table 2-1). Fractured rock was modeled consisting of fracture porosity in which advective and dispersive gas and heat transfer occur and the rock matrix in which diffusive mass transport and thermal conduction occur. They focused on the development and testing of more efficient formulations to simulate heat and mass transfer processes in rubbelized oil shale during in-situ retorting. They noted that the heat and mass transfer rates between permeable fracture porosity and low permeability rock matrix are limited by thermal and mass transport properties of the oil shale. Exxon's electro-frac process model was studied by Symington et al. [116]. They examined the impact of varying process parameters such as heating geometry, size, spacing, total heat input and heating duration using screening tools and basin modeling. A complex Shell Genex model for oil generation and diffusion limited expulsion for 23 lumped species was also reported [123]. In this model, the rate-limiting step of primary migration is considered to be the slow diffusion of the petroleum through the kerogen itself.

2.8. Hydrous Pyrolysis

Hydrous pyrolysis involves heating organic-rich rocks in the presence of liquid water [15, 16]. Liquid oil is generated and expelled from the rock and accumulates on the water surface within the reactor. When water is associated with the shale, the pyrolysis process has the potential of producing water [124]. A steady stream of water loss before and after 400°C is because of water formed during thermal loss of organic as water and through some mineral dehydration [47, 124]. The application of water vapor, a source of hydrogen and oxygen, in surface retorting of oil shale has been shown to improve the quality of the oil product [14, 16].

3. EXPERIMENTAL METHODS AND ANALYTICAL TECHNIQUES

This section details the experimental apparatus and various analytical standard techniques used in this research. The general view of the experimental section is described in the first part (section 3.1). A high pressure experimental system was installed to perform multiscale (sanples of different size) pyrolysis. Specific modifications in the experimental setup are mentioned in the chapters where the results obtained are discussed. The second part of this section, Section 3.2, includes the details of analytical instruments that were used for the raw material and product characterizations. Some of these analytical techniques and experimental setups used standard procedures and methods and some of them were developed during this research.

3.1 Experimental Section

3.1.1. Material

The oil shale samples used in this study were collected from different locations. The samples were from the Mahogany zone of the Green River formation and were provided by the Utah Geological Survey (UGS). The samples were designated as sample #1 (powdered oil shale (PO)) and sample #2 (core oil shale (CO)). This nomenclature was adopted throughout this dissertation study to represent these samples. The oil shale samples were crushed and dried for 4 hrs at 100°C to remove the inherent moisture, if any. There was no significant weight loss observed during drying and hence the samples were used as received. The samples were screened to 100 mesh size (1.49×10^{-4} m) for

the raw material characterization. Another set of samples was used from the fresh core drilling of skyline 16 locations and these samples were titled as GR (Green River) samples.

3.1.2. Experimental Procedure

Pyrolysis of the fine powdered and small amounts of oil shale provides chemically controlled intrinsic kinetic rate of organic decomposition. Pyrolysis of large size block/core illustrates the distribution of temperature and product generation profiles across the sample. Heat and mass transfer factors influence the distribution of products. Secondary reactions, coking and cracking, in liquid and vapor phases are important and alter the yield and quality of the desired product.

The following tasks were designed to study the effects of the operational parameters on the decomposition mechanisms, and on the generation rates of different products.

Task 1: Thermal gravimetric analysis (TGA) of the powdered oil shale

- Kinetic modeling and validating the intrinsic rate.

Task-2: Thermal gravimetric analysis mass spectrometry (TGA-MS) study of the powdered oil shale samples

- Continuous monitoring of the targeted components in the generated products.
- Study of the compositional analysis and kinetics.

Task-3: Multiscale pyrolysis in batch, semibatch and continuous modes

- Conduct experiments to study the thermal behavior and product distribution.
- Estimate the effect of the transport resistances on yield and quality of the products.

- Perform pyrolysis under elevated pressure.
- Study the secondary reactions (coking and cracking).

Task-5: Analytical analyses of bulk products

- Perform compositional analyses to study the quality and yield of the products, material balances.
- Obtain single carbon number distribution, alkane/nonalkene ratios and residue in oils produced.
- Ratio of the products (oil to coke, and noncondensable to condensable gases).
- Physical property estimations of the products such as density, viscosity, pour point, etc.

In order to accomplish these tasks an experimental matrix was designed and several process configurations were examined. Experiments were performed at four scales; grain size (powdered of finer than 100 mesh) and core samples of ¾", 1" and 2.5" diameters. The apparatuses used for the samples are summarized in Table 3-1. Batch, semibatch and continuous flow pyrolysis experiments were designed to capture the effect of temperature (300°C to 500°C), heating rates (1°C/min to 10°C/min), pressure (ambient and 500 psi) and sample sizes on product formation. The products obtained were condensed vapors (liquids), noncondensable gases, and solid residue (spent shale). The overview of the different reactors, experiment assembly and experimental conditions are listed in Table 3-2. In addition to the tasks mentioned above, hydrous treatment of oil shale pyrolysis and the heterogeneity within the samples were also studied. The results from these experiments are discussed in separate chapters.

Table 3- 1: List of the oil shale samples and scales (size) used to study the pyrolysis process with different apparatus.

Oil shale sample	Scale	Apparatus			
Sample #1	Powder	TGA	TGA-MS	HPTGA	Reactor
Sample #2	Powder	TGA		HPTGA	Reactor
	3/4"				Reactor
	1"				Reactor
	2.5"				Reactor
GR	Powder	TGA			
	1"				Reactor

Table 3- 2: List of the experimental apparatus, configurations and conditions used to study the pyrolysis process.

Reactors	1" Swagelok	1.25" Swagelok	1.25" Flange	3" Flange
Samples	Powder	3/4" Core	1" Core	2.5" Core
Experiments	Batch	Semibatch	Continuous	
Liquid collection	Condenser	Receiver	Periodic samples	Direct
Temperature control	Reactor surface	Core surface	Center of Core	
Temp program	Isothermal	Nonisothermal		
Pressure	Ambient	500 psi		

3.1.2.1. Thermal Gravimetric Analysis (TGA)

Thermal gravimetric analysis (TGA) is a well-known technique to monitor the progress of chemical processes as weight changes. A TGA device (Q500) from TA Instruments was used. This TGA is rated for 1000°C and total of 100ml/min of sweep/reacting and balance gases. The center part of the TGA is a furnace which is electrically heated and allows for a good control of the temperature (under isothermal and nonisothermal temperature programs). A maximum heating rate, 100°C/min, and minimum 0.1°C/min can be employed. The TGA was heated via electric heating elements in the furnace vessel. An accurate control on mass flow rate and ramping heating rate

provide the reproducibility in the data. A thermocouple with four ports measured and controlled the temperature just above the sample basket. TGA experiments were conducted with approximately 20 milligrams of samples in a platinum basket. The basket was suspended from a thin wire attached to a microbalance. Curie point calibration of metals to determine and to adjust the offset in the temperature was carried out using ASTM E 1582 [125]. The calibration of the empty basket and standard sample of calcium oxalate was performed periodically to account for the buoyancy and other instrumental factors affecting the real data generation. The TGA furnace was purged with an inert gas for approximately 15 mins prior to any experiment. For all the experiments, the flow rate of balance gas (N_2) was kept constant at 40 ml/min while the purge gas (N_2) flow rate was 60 ml/min. The sizes of the particles used along with other conditions employed were specifically designed to reduce the heat and mass transport effects.

3.1.2.2. Thermal Gravimetric Analysis Mass Spectrometry (TGA-MS)

A thermal gravimetric analysis mass spectrometry (TGA-MS) instrument was used for inline compositional analysis of the products formed during pyrolysis. TGA-MS affords the opportunity to obtain compositional information while the decomposition is being measured quantitatively. A TGA instrument (TA Instruments Q500) coupled with a mass spectrometer (Thermostat model GSD 301 T3 from Pfeiffer Vacuum) was used. This machine uses the TGA principle and procedure as mentioned in section 3.1.2.1 for TGA apparatus (TGA Q500). The TGA furnace chamber outlet was connected to the MS instrument through a hot capillary column heated to 150°C. Total flow rate of nitrogen was 100 ml/min (90 ml/min as purge and 10 ml/min as balance gas). A maximum of 63 compounds can be analyzed in a single run with this instrument. Compounds of about

300 atomic mass units were targeted in the mass spectrometric analyses. The components of the vapor product were identified by single ion monitoring response of mass spectrometry based on molecular weight.

3.1.2.3. High Pressure Thermal Gravimetric Analysis (HPTGA)

The high pressure TGA pyrolysis experiments were performed using a Cahn TherMax 500 high-pressure thermo gravimetric analyzer from Thermo Fischer. This instrument is rated up to 1100°C under ambient pressure and 1000°C at 1000 psi and up to a 100 gram sample. A quartz crucible (18 mm diameter and 20 mm height) was used to load the sample. The crucible was suspended from a ceramic coil attached to a microbalance. The furnace and balance were purged with N_2 prior to each experiment. Mass data were recorded approximately every second. The buoyancy effect was corrected by using the empty basket data.

3.1.2.4. Multiscale Pyrolysis: Reactor Pyrolysis

The experimental matrix was designed to address the effect of active parameters such as temperatures, heating rates, pressures, and scale on pyrolysis products. A schematic of the experimental setup is shown in Figure 3-1. This set up was designed and built for high pressure experiments. This system is fully automated and capable of performing the experiments at different scales (size of the sample). The images of the system are depicted in Figure 3-2. The left panel shows the condenser and autosampler assembly while right panel depicts the reactor position. A simpler form of this setup was also used to perform the experiments, especially for batch, semibatch and ambient pressure conditions.

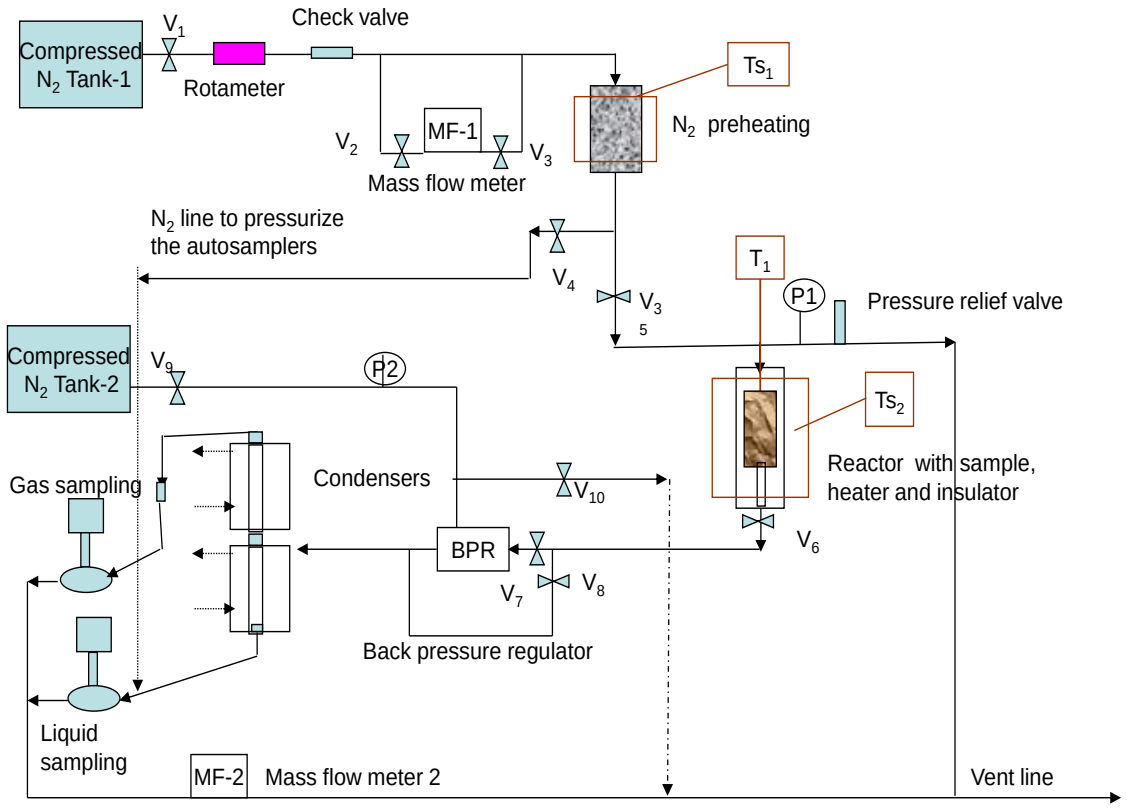

Figure 3- 1: Schematic of the experimental setup to study the effect of operational parameters on yield and quality of the product distribution.

Figure 3- 2: Images of the experimental setup to study the effect of operational parameters on yield and quality of the product distribution at different size of sample.

Four different types of reactors were used (Table 3-1). All the reactors are made of 316 stainless steel rated to 4000 psi at 600°C. The Swagelok reactors, 1" diameter (6" long) and 1.25" diameter (12" long) were equipped with high pressure Swagelok fittings on each end. The flange reactors, 1.25" diameter (8" long) and 3" diameter (10" long) were sealed using graphite flange at both ends. The reactors of 1" diameter and 1.25" diameter were heated with heating tapes while for the 3" diameter reactor, a ceramic heater band was used. The reactor assembly was insulated with self-adhesive high temperature silicon tape and glass wool along the reactor assembly and the fittings. The flange reactors had addition holes to measure the temperature within the core sample. The thermocouples were inserted in the core (approximately 0.6" deep) via drilling a hole of the size of the thermocouple (1/8" diameter). Figure 3-3 shows the positions of the temperature measurement probes (at 5 locations) with 2.5" core samples in 3" reactor. This flange reactor was designed to measure the temperature at three locations (TC-1, TC-4 and TC-5) within the core sample. The Swagelok reactors provide the means to measure the temperature at two locations (TC-1 and TC-5). The temperature of the process was controlled using a bench–top temperature controller with SPECVIEW as the interface via K-type thermocouples. The measuring temperatures and flow readings of mass flow meters were recorded using Labview interface.

A Swagelok back pressure regulator (BPR) was used on the outlet line to maintain the process pressure. The metal tube which connects the reactor outlet to back pressure regulator was heated at 200°C. The temperature of condensers was maintained using a Brookfield TC501 programmable temperature bath with controller. The position of the 12 port autosampler was regulated using a VCOM interface.

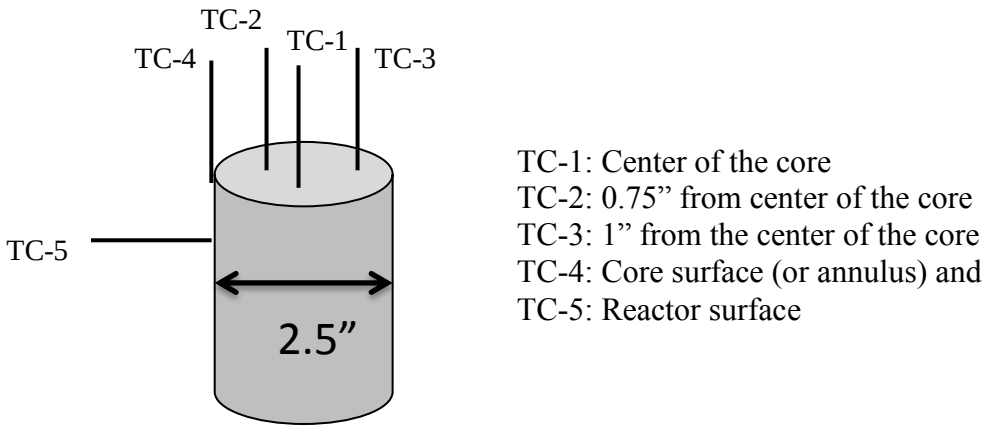

Figure 3- 3: Schematic of temperature distribution measurements during the pyrolysis of large size (2.5”) sample.

Nitrogen was used to purge the reactor, sweep the products (100 ml/min) in open system pyrolysis and to pressurize the system for high pressure experiments. The resulting spent shale and oil were weighed. The isothermal pyrolysis runs were conducted by using a rate of 100°C/min to achieve the desired stable temperature. The amount of noncondensable gases (gas loss) was estimated by material balance, difference of weight loss and oil yield. A sampling protocol for gas and liquid samples was set up to collect the fractions of the fluid product at different times and temperatures during the continuous flow (open reactor) pyrolysis. The gaseous products were collected in a tedlar bag of 1 liter capacity. Gas chromatography analyses were conducted on collected oil and gas samples without further treatment.

Batch experiments (closed system) were conducted under initial ambient and pressure, 500 psi. The sample was fed in the reactor and purged with nitrogen to displace the air in the reactor. To perform the batch pyrolysis, the reactor assembly was sealed at both the ends and the pressure measurements were recorded as the reaction progressed.

After the pyrolysis, the reactor assembly was cooled down to room temperature and samples were collected through a needle valve.

The semibatch (autogenous) pyrolysis involves no sweep gas. The products were allowed to escape from the top of the reactor as they formed due to autogenous pressure and were collected in the chilled condenser maintained at -6°C using acetone and ice in a bath.

The continuous flow experiments, also known as open system pyrolysis, were designed to collect the products as they are formed using a sweep gas, nitrogen. The nitrogen gas was heated to the process heating rate and temperature before passing through the center of the reactor. The products were swept out from the reactor with the nitrogen and then passed through the condenser. Periodic sampling of the products was carried out. The aim of these experiments was the collection of the liquid and gaseous samples at different time intervals and subsequent analyses of the samples to obtain the distribution of the products.

Specific modifications were also made in the experimental setup as per the need of the experiments. For example, the control of the heat supply, to maintain the process temperature, was controlled using TC-1 (center of the core) or TC-5 (surface of the reactor) thermocouple, and a setup to minimize the dead volume was built. In some of the ambient pressure experiments, a receiver was used to collect the heavy fraction of liquid, which otherwise would plug the condenser assembly. The modifications are discussed in the study appropriately.

The experimental conditions and results are summarized in Appendix C for all the experiments discussed in Chapter 4. There was a temperature gradient across the large

size shale upon applying the heat from external sources. Therefore the different sections of the shale were at different temperatures. The temperature and pressure profiles (batch pyrolysis) are shown in Appendix D.

3.2. Analytical Techniques

This section describes the procedures and principles which were applied to analyze the raw and product materials. Raw material characterization was conducted using elemental analysis (CHNSO), thermal gravimetric analysis (TGA) and X-ray diffraction (XRD) analysis. Thermal gravimetric coupled with Mass spectrometry (TGA-MS) was used to perform the compositional analysis of the products formed during the pyrolysis process. The bulk fluid products, gas and liquid, of the pyrolysis process were analyzed using gas chromatography (GC) and gas chromatography mass spectrometry (GCMS). A TGA-DSC (Differential scanning calorimetric) instrument is used to estimate unreacted organic and coke formation in spent shales. Fourier transformation infrared spectroscopy (FTIR), densitometer and rheometer were used to estimate the physical properties of the oils produced.

3.2.1. Material Characterization

The total organic matter contains in the oil shale samples of different origin; geological depth and horizon were suspected. Thus, it becomes important to understand the raw material and the variability which exists in different samples. Elemental analysis (CHNSO), TGA (weight loss due to organics and decomposable minerals) and XRD (minerals) analyses were conducted to characterize the oil shale samples used in this research work.

3.2.1.1. Elemental Analysis

The elemental analyses of the samples were performed using LECO CHNS-932 for CHNS (carbon, hydrogen, nitrogen, sulfur and oxygen) and VTF-900 for oxygen analysis in the samples. LECO analyzer (LECO Corp., St. Joseph, Michigan) used IR and thermal conductivity detectors to determine the percentage of elements in the sample. A combustion method was employed to measure C, H, N, S content. A CHNS run uses approximately 2 mg of sample. A separate oxygen analysis also requires the same amount of the sample. Standard materials, sulfamethazine ($C_{12}H_{12}N_4O_2S$) acetanilide ($C_8H_9N_O$) along with blank air runs were used to calibrate the instrument periodically. All the samples were duplicated several times and the results were averaged to determine the percentage of the elements in the sample.

3.2.1.2. X- Ray Diffraction (XRD) Analysis

X-ray diffraction (XRD) analyses of the crushed oil shale samples and separated clay fractions were performed using a Bruker D8 Advance X-ray diffractometer. Phase quantification was performed using the Reitveld method and the TOPAS software. The following operating parameters were used when analyzing the powdered samples: Cu-K-α radiation at 40 kV and 40 mA, $0.02^o 2\theta$ step size, 0.4 and 0.6 seconds per step, for clay and bulk samples respectively. Clay samples were examined from 2 to 45^o 2θ, and the bulk from 4 to 65^o 2θ. The instrument was equipped with a detector (lynx eye) which collects data over 2.6 mm, rather than at a point. Rietveld method calculates intensities from a model of the crystalline structure and fit to the observed X-ray powder pattern by a least squares refinement. The samples were ground in a micronizing mill until they were fine enough to pass through a 325 mesh screen (particle size < 44 micrometers). The

clay fraction from each sample was separated from the bulk by using prticle sedimentation. The fraction used for the bulk analysis was rolled approximately 50 times to randomly orient the mineral grains before being scanned. The air dried and glycolated scan patterns were compared to determine if expandable clays were present. The amount of the identified clay minerals were determined by using the Rietveld refinement of the bulk scans.

3.2.2. Compositional Analysis

A Thermal Gravimetric Analysis Mass Spectrometry (TGA-MS) instrument was used for inline compositional analysis of the products formed during pyrolysis (Section 3.1.2.2). Gas chromatography (GC) and gas chromatography combined with mass spectrometry (GC-MS) analyses were performed to characterize the bulk products, liquid and gas collected from reactor pyrolysis. Spent shale analyses were performed with thermal gravimetric analysis differential scanning calorimetry (TGA-DSC) and LECO elemental analyzer instruments.

3.2.2.1. Gas Chromatography (GC)

GC was used for qualitative as well as quantitative analysis in this study. Fluid products, liquid and gas, from the pyrolysis were analyzed using Gas chromatography. Agilent GC HP 5890 and GC HP 6890 were used in this study. GC 5890 used cool on column injection assembly while with GC HP 6890, split injection were carried out. As the hydrocarbons are the main products of interest, a conventional flame ionization detector (FID) was employed in most gas chromatographs. Few analyses of gaseous products were performed with thermal conductivity detector (TCD) followed by FID detector assembly to identify the composition of inorganic and very light hydrocarbons.

Oil samples were analyzed using the principle of High Temperature Gas Chromatography (HTGC) to obtain retention time information for the hydrocarbons and residual calculation [126]. The GC simulated distillation (GC-SIMDIS) analysis was also performed on the liquid samples. The procedure provides the weight percent of a given SCN as well as the weight percent of n-alkane and non n-alkane portions for each SCN. The GC-SIMDIS method is intended to simulate the true boiling point (TBP) method by providing single carbon number (SCN) distributions. GC-SIMDIS was used to obtain a single carbon number (SCN) distribution of the sample up to carbon number C_{44}.The samples were prepared according to the ASTM-5703 [127] standard using dichloromethane (DCM) solvent. DCM is selected as the solvent because it dissolves hydrocarbons (oil) well and also has a lower boiling point (40°C) that helps in separating the signal in chromatogram. Two SIMDIS samples were prepared for each sample analyzed. One sample was diluted with DCM. An internal standard (HP part no 5080-8723), a mixture of normal paraffins , C_{14} to C_{17}, was added to the other sample followed by dilution with DCM. The sample injections (0.2µl) were performed by the autosampler (HP-7683). Restek MXT-1(steel coated fused silica capillary) column (dimension, 30m x 0.28 mm x 0.1µm) with stationary phase of cross bonded dimethyl polysiloxane was used for the liquid sample analyses. The operating conditions of the gas chromatography for the GC-SIMDIS method are summarized in Table 3-3.

The FID detector responses were manually integrated. The integrated area under the curve for each carbon number peak was used to determine the SCN distribution. A retention time table, developed by analyzing a laboratory standard containing normal paraffin ranging from C_{12} to C_{60} was used to identify the n-alkane peaks for each SCN.

Table 3- 3: Operating conditions of gas chromatography for cool on column injection (GC 6890) and split injection (GC6890).

Oven	Initial Temperature	30°C
	Ramp Rate	10°C/min
	Final Temperature	410°C
	Isothermal	10 mins at 410°C
Inlet	Carrier Gas	Helium at 1ml/min, constant flow
	Temperature	Tracked over (3°C over oven temperature) for cool on column injection
		350°C for split injection with split ratio (20:1)
Detector	Temperature	450°C
	Flows	Air- 450 ml/min
		Hydrogen- 40 ml/min
		Nitrogen-45 ml/min

The procedure was described in detail in the standard test method ASTM D 5307 [127] and Neer and Deo [126].

Several standard samples were used to calibrate the chromatograms. The changes in the conditions of gas chromatography for both liquid and gas samples over the time period of this research were calibrated using the standards periodically, especially, each time before running the batch of the samples. A *MATLAB* program was developed to classify the chromatogram in SCN, normal alkane and non normal alkane, and residual calculation.

3.2.2.2. Gas Chromatography Mass Spectrometry (GC-MS)

A GC-MS equipment from Agilent was used in this study. The machine is an assembly of Agilent GC-6890 and a triple quadrupole MS (5397N). A 60 meter long capillary column, HP-5 (5% phenyl methyl siloxane) of J&W Scientific was used. The transfer line temperature was kept at 280°C. The program of GC operation was the same as described in the section 3.2.2.1. Several standard normal paraffin samples were used to

judge the predictability of the of library match from National Institute Standard and Technology (NIST) for the peaks detected by MS.

3.2.2.3 Thermal Gravimetric Analysis and Differential Scanning Calorimetry (TGA-DSC)

The spent shale obtained from the pyrolysis of oil shale may contain unreacted organic and the coke formed during the process. A combined TGA-DSC unit, SDT Q 600, from TA Instruments was used to characterize the spent shale and estimate the unreacted organic and coke. TGA Q-600 works on the same principle as TGA Q-500. The thermograms of DSC were used to judge the energy input, endothermic, organic and mineral decomposition, and exothermic, coke burning.

The experimental scheme of different stages was designed to separate the weight losses of the organic matter, mineral matter and of the coke formation. Initially, pyrolysis till 500°C (stage-1) was carried out for organic decomposition, followed by the second pyrolysis up to 900°C or 1000°C (stage-2) for mineral decompositions and then without opening the TGA chamber, the furnace was cooled down to 400°C and the remaining material was combusted from 400°C to 900°C or 600°C (stage-3) to estimate the amount of coke. A heating rate of 10°C/min was used for these analyses. It is hypothesized that in the first pyrolysis, only organic, in the second pyrolysis, only minerals and in the combustion process, only carbon residue material (coke) contributes to the weight loss. It was also hypothesized that coke was formed only during the pyrolysis in the reactor and not during further TGA pyrolysis of the spent shale. Unreacted organics in spent shale include unpyrolyzed organics and the unreleased oil.

3.2.3. Physical Properties Estimation

The oil samples collected from the pyrolysis process were characterized by measuring the physical properties such as wax appearance temperature (WAT), density and viscosity.

3.2.3.1. Fourier Transformed Infrared Spectrometry (FTIR)

The wax appearance temperature (WAT) for the sample was estimated using Fourier transform-infrared (FTIR) spectroscopy. FTIR analyses were conducted using a Perkin Elmer 1600 Spectrometer upgraded for control with the Perkin Elmer Spectrum v2.0 software. These experiments were based on the method developed for WAT measurement using FTIR by Roehner and Hanson [128]. This method is based on the hypothesis that measuring changes in integrated absorbance from 735 to 715Cm^{-1} would provide a measurement of sample (oil) WAT.

3.2.3.2. Densitometer

Density, specific gravity, or API gravity may be measured by means of a hydrometer (ASTM D 1298) [129], a pycnometer (ASTM D 1217) [130], or by a digital density analyzer (ASTM D 4052) [131]. API Gravity is a preferred parameter when discussing oils and is defined by the equation

$$\text{Degree API} = 141.5/\text{Sp gr @ } 60/60°\text{F} - 131.5 \qquad (3.1)$$

The densities of the samples were measured with an Anton-Parr DMA 512 high pressure external measuring cell (Anton Parr GmbH, Graz, Austria) connected to the mPDS 2000 evaluation unit with interface adapters based on the recommended ASTM D 5002 [132], for density measurement of crude oils. The densitometer uses the principle of oscillation of a U tube filled with sample liquid to measure the density of a sample. Room

air and doubly distilled water were used to calibrate the instrument. The density of the sample at that particular temperature was obtained from the calibrated time period of oscillation.

3.2.3.3. Rheometer

Viscosity measurements were made with a Brookfield programmable digital rheometer LVDV- III + model (Brookfield Engineering Laboratories Inc., Middleboro Massachusetts). The rheometer measures fluid shear stress and viscosity at given shear rates. The principle of operation of the DV-III is to drive a spindle (immersed in the test fluid) through a calibrated spring [133]. The viscosity drag of the fluid against the spindle is measured by the spring deflection. A cone and plate version was used for the measurement. A CPE-40 cone spindle was used for all measurements. The viscometer was set to the required temperature using Rheocalc software and the calibration was verified using different Brookfield viscosity standard fluids. After verifying the calibration the sample viscosity was estimated.

4. RAW MATERIAL CHARACTERIZATION

4.1. Elemental Analysis

The elemental analysis of raw materials was performed using CHNSO. Ten samples of each oil shale were analyzed. Table 4-1 lists the mean values along with the standard deviations for sample #1 and sample #2. The elemental analysis shows that the sample #1 (PO) retained H/C ratio of 1.1 and O/C ratio of 0.67. Sample #2 (CO) shows a slightly higher H/C ratio (1.17) and a lesser O/C ratio (0.57) than sample #1 (PO). Both the samples (sample #1 and sample #2) fall in Type-1 oil shale category on Van Krevelen classification diagram [134].

4.2. Thermal Gravimetric Analysis

The organic and decomposable mineral in the samples were estimated using the TGA. There was no significant buoyancy effect observed in the temperature range used in this study under ambient pressure.

Table 4- 1: Elemental analysis of oil shales.

CHNSO	Sample #1 (PO)		Sample #2 (CO)	
	wt %	Stdev	wt %	Stdev
Carbon	17.45	0.26	22.09	1.00
Hydrogen	1.60	0.08	2.14	0.12
Nitrogen	0.53	0.06	0.65	0.06
Sulfur	0.18	0.04	0.11	0.02
Oxygen	15.69	0.79	16.54	0.97
H/C (molar)	1.10	-----	1.17	-----
O/C (molar)	0.67	-----	0.56	-----

The TGA thermogram of the pyrolysis (N_2) of sample #1 (PO) at 20°C/min is shown in Figure 4-1. This figure also shows an example of the reproducibility achieved during pyrolysis of the powdered oil shale. Sample #2 (CO) samples did not show a uniform organic matter distribution. Different sections of the core sample were pyrolyzed in the TGA to estimate the organic content and decomposition rates. Samples from different section of the cylindrical core were subjected to pyrolysis in a TGA to estimate the organic content. Figure 4-2 shows the TGA thermograms at different ramp rates. The total organic weight loss is different while the total weight losses (1000°C) are identical for all the sections in the sample.

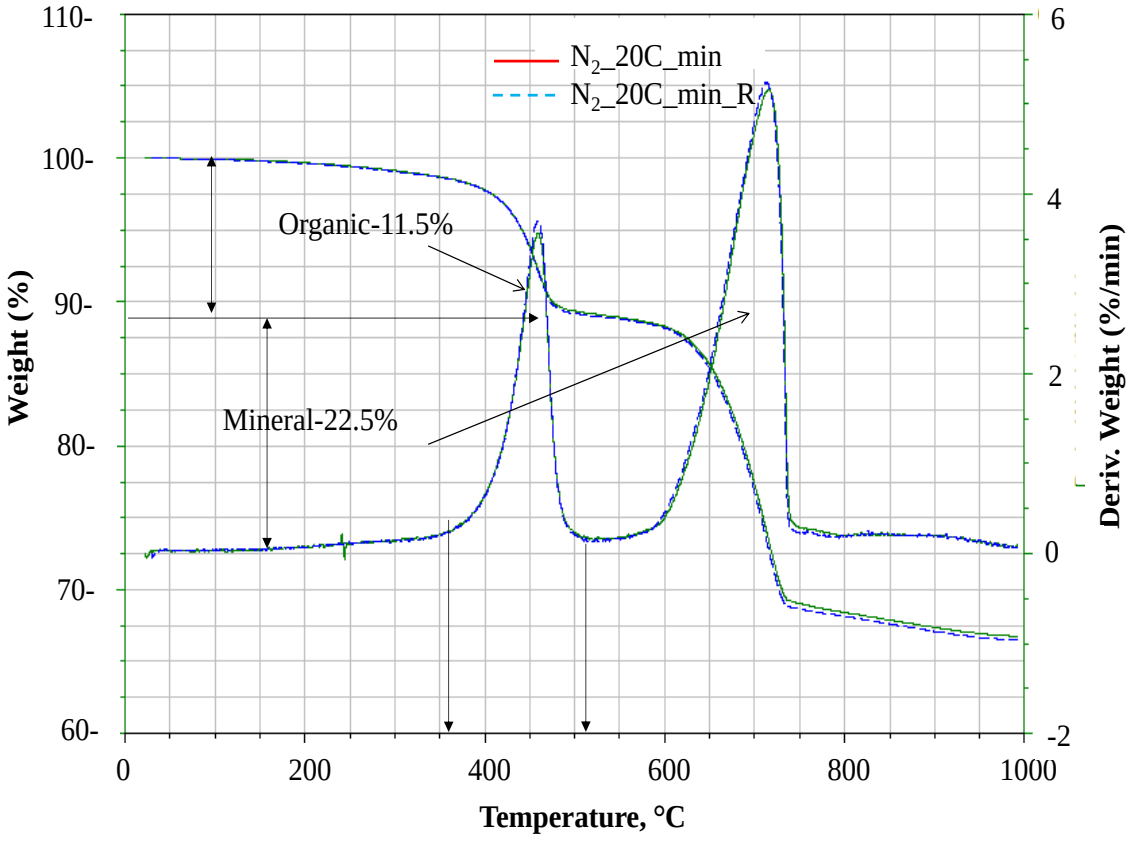

Figure 4-1: TGA pyrolysis of sample #1 (PO) at heating rate of 20°C/min. Data are quite reproducible

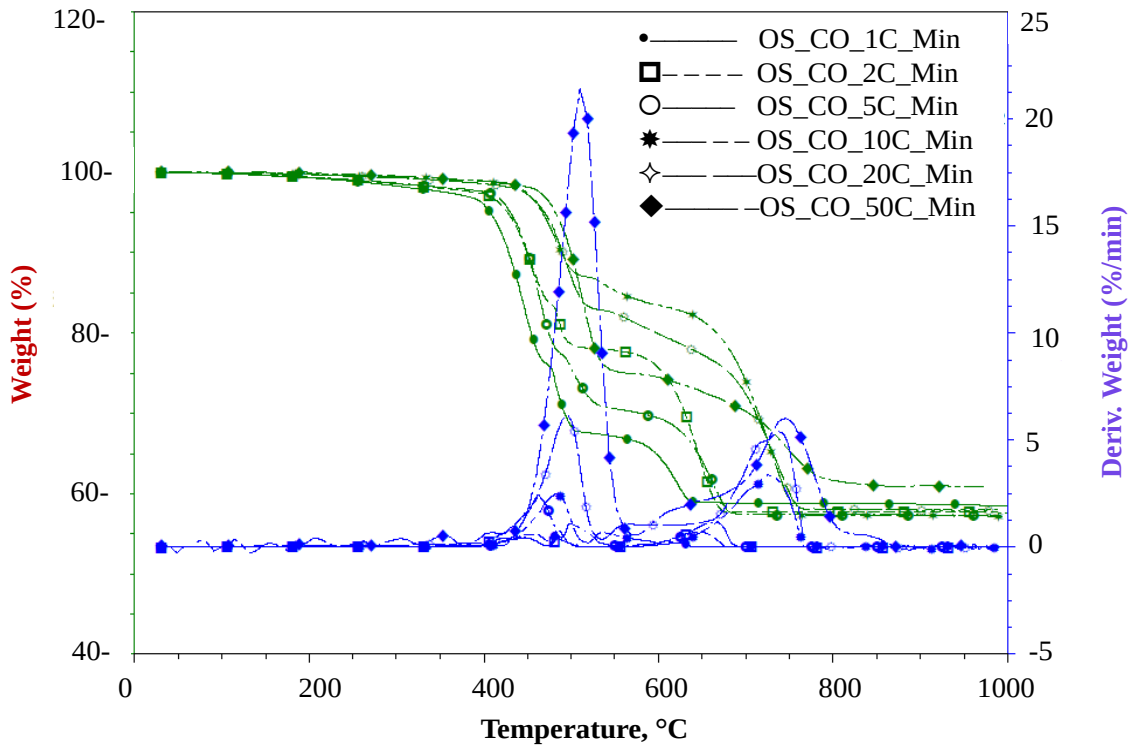

Figure 4- 2: Pyrolysis of different sections of core sample (sample #2) at different heating rates in N_2 environment.

The results suggest that the organic content varies within the core. To gain a representative average composition of the shale (core), the whole sample was crushed and mixed. This resultant sample was again pyrolyzed in TGA and the result is shown in Figure 4-3. There was no significant weight loss observed during preheating, confirming the absence of moisture in these samples. Two significant derivative peaks in the mass derivative curves in all nonisothermal experiments were observed, corresponding to organic and carbonate decompositions. The average organic matter in powdered and core oil shales were estimated to be 11.5% and 17.5% weight of the total oil shale respectively. The higher temperature reactions involve primarily the decomposition of minerals in samples. The decomposable minerals were observed to be 22.5% and 20.62% (average) in powdered and core oil shales respectively.

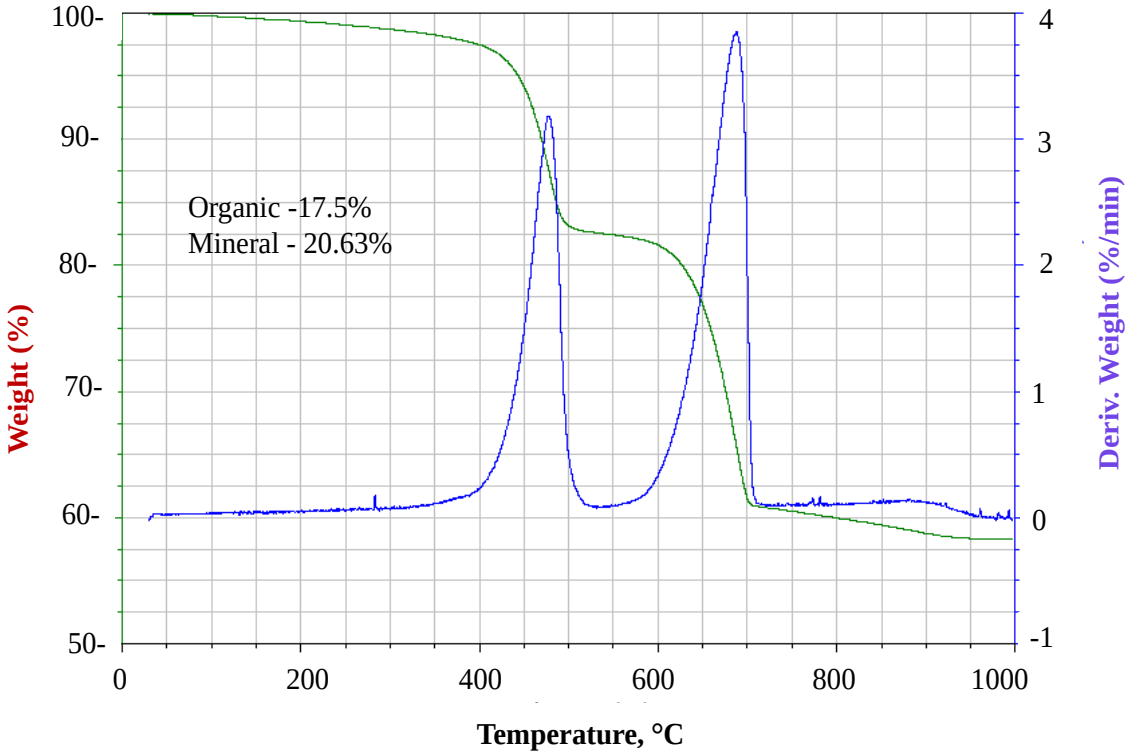

Figure 4- 3: Pyrolysis of the uniformly mixed powdered of core oil shale (sample #2) at 10°C/min in N_2 environment

TGA analyses were performed in a wide range of experimental conditions. The changes in the conditions of TGA analyses for different samples are described where the results are discussed. The initial set of TGA experiments were performed with different particle size and different flow rates of nitrogen. Sample #1 (PO) were also treated under different environments, helium, carbon-dioxide and air. The results are summarized in Appendix A. The powdered (sample #1) oil shale (100 mesh) and nitrogen at 100 ml/min were used to study the kinetics of organic matter decomposition. Nitrogen was selected as the inert gas because of its ready availability and reproducibility in the data. Appendix B summarizes the kinetic study of pyrolysis (N_2 environment) and combustion (air

environment) using the conventional methods. Application of the advanced isoconversional method on pyrolysis data is described in detail in section 4.2.

4.3. X- Ray Diffraction Analysis

The XRD signatures are shown in Figure 4-4 for sample #1 (PO) and in Figure 4-5 for sample #2 (CO) and the weight percentages of minerals identified are summarized in Table 4-2.

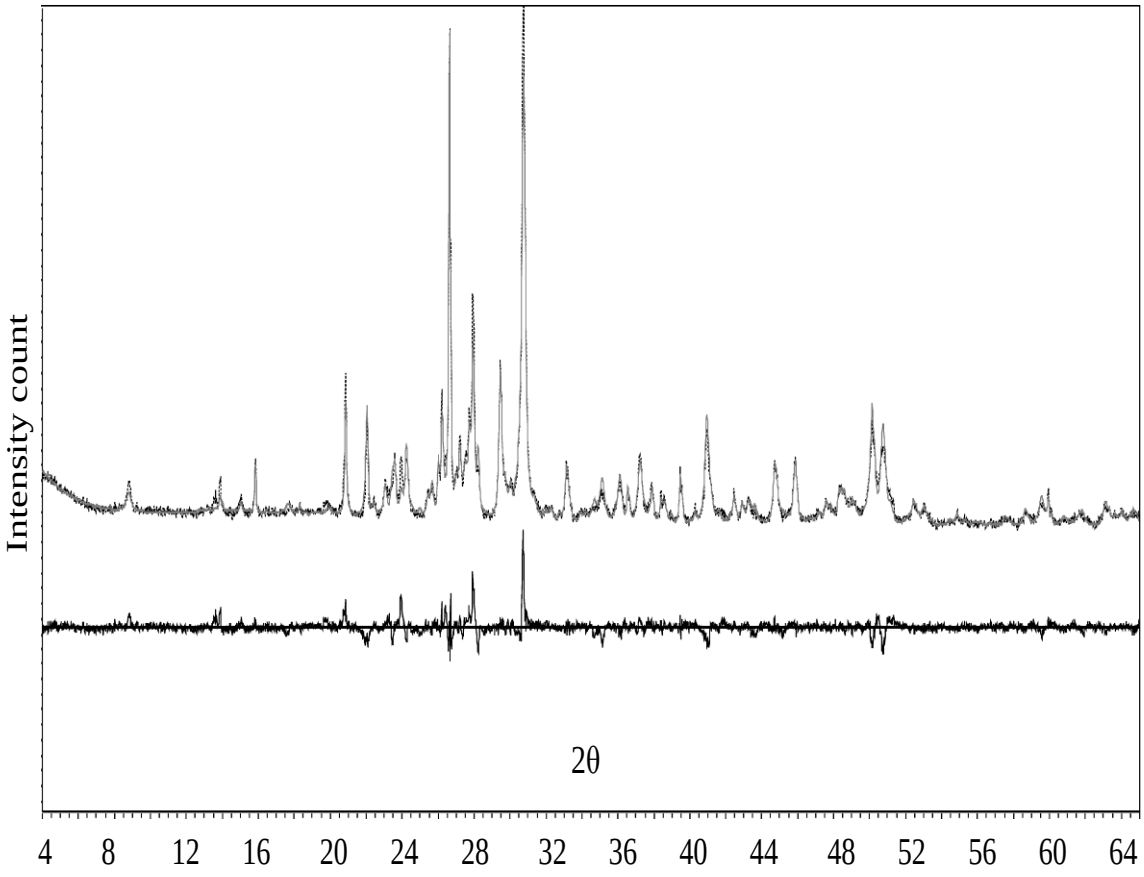

Figure 4- 4: Bulk XRD results of Green River oil shale (sample #1). Y-axis displays X-ray counts, and the X-axis degrees 2 theta. Figure shows, from top to bottom, observed (gray) and calculated (dots) bulk XRD patterns, the difference pattern (black). The peak location for each mineral is omitted from the graph for visual clarity.

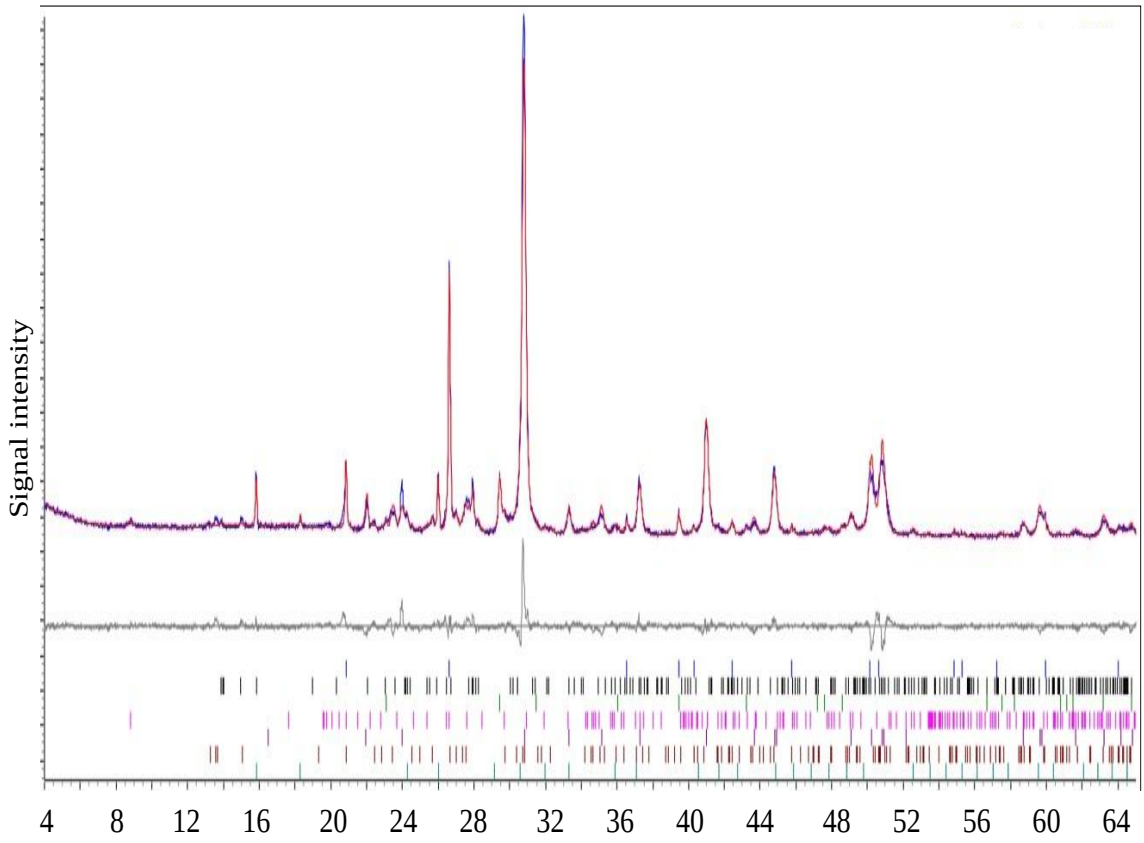

Figure 4- 5: Bulk XRD results of Green River oil shale (sample #2). The y-axis displays X-ray counts, and the x-axis degrees 2 theta. Figure shows, from top to bottom, observed (blue) and calculated (red) bulk XRD patterns, the difference pattern (grey), and peak locations for each mineral (color coded by mineral, see legend/results at upper right).

Table 4- 2: Minerals present in oil shales (weight percent of the total identified crystal minerals).

Minerals	Weight %		Chemical Formula
	Sample #1 (PO)	Sample #2 (CO)	
Quartz	7.7	7.7	SiO_2
Plagioclase	19.5	7.60	$CaAl_2Si_2O_8$
Calcite	6.9	3.95	$CaCO_3$
Illite	5.8	2.84	$(K,H_3O)(Al,Mg,Fe)_2(Si,Al)_4O_{10}[(OH)_2,(H_2O)]$
Dolomite	33.5	62.93	$Ca\ Mg\ (CO_3)_2$
Orthoclase	12.4	10.88	$KAlSi_3O_8$
Aragonite	11.7	--	$CaCO_3$
Analcime	2.4	4.13	$NaAlSi_2O_6.H_2O$

XRD analyses of the shale samples reveal a complex mineral signature. These shale samples are composed mainly of carbonates, quartz and feldspars. Small amounts of illite (5.8%) and analcime (2.4%) are present in the powdered oil shale sample. Core oil shale contains 2.84% illite and 4.13% analcime. Illite (12% water @ 110°C -140°C) [135] and Analcime (8% water @ 175°C -375°C) [136] are the hydrated minerals present in the raw material with the potential to release this water on thermal treatments. Around 470°C the hydroxyl group is released from illite. This continues up to 850^{o}C, which may interact with the organic portion of the shale [135]. Core oil shale was found to be dolomite (62.93%) rich and was free from aragonite.

4.4. TGA-DSC Analysis

A set of TGA runs was examined with powdered oil shale sample of 100 mesh size at different stages using the scheme mentioned in section (3.2.2.3). Figure 4-6 shows the schematic of coke test scheme and the percentages of weight losses, based on initial mass, at different stages. Intermediate samples were collected for elemental analyses. There was no significant coke formation with powdered (100 mesh) samples pyrolysis in TGA. This is because of the absence of mass resistance in TGA experiments under these conditions.

4.5. High Pressure TGA Pyrolysis

The effects of pressure on the decomposition of oil shale are of interest for the in-situ recovery of the organic material since the kerogen rich regions are often 500 to 1000 feet underground. The shale compositions and over-burden pressure vary with the depth. The high pressure TGA unit described in section 3.1.2.3 was used.

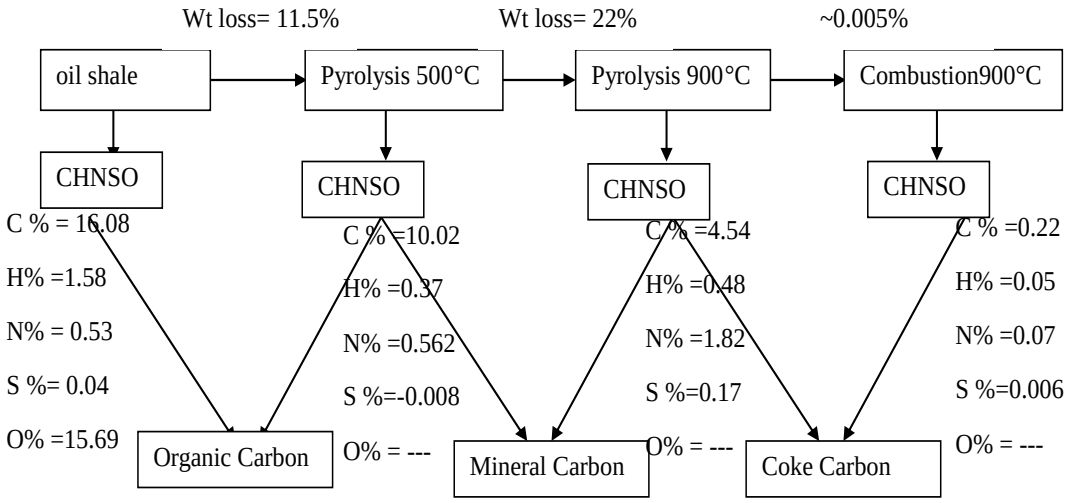

Figure 4- 6: Schematic of the different stage TGA analyses to estimate the organic and coke in the spent shale. The data show the TGA analyses performed with sample #1 (PO) and intermediate sampling was conducted to perform elemental analyses.

Sample #1 (PO) and sample # 2 (CO) were pyrolyzed at pressure of 500 psi.. The core sample (sample # 2) was crushed to 100 mesh size. The instrument configuration was modified as shown in Figure 4-7 to conduct the experiments. The original pressure control device was dismounted and a back pressure regulator was installed in the vent line. A condenser at -6°C was assembled to collect the liquid products. Two experiments with each sample (PO and CO) were conducted at ambient pressure and 500 psi under identical reactor configuration (Appendix C). The temperature was programmed with an initial hold at 30°C for 2 mins and was then ramped at 10°C/min to 800°C and then held isothermally for 10 mins. Nitrogen was used as flow gas to maintain the pressure. The balance gas flow (N_2) rate was 12.6 lit/min, purge gas (N_2) was 11.5 lit/min and reaction gas (N_2) was set at 0.5 lit/min. The weight loss profiles during pyrolysis are shown in Figure 4-8. Further, TGA-DSC analysis on spent shale was performed to estimate the unreacted organic matter left in the spent shale and the coke formed.

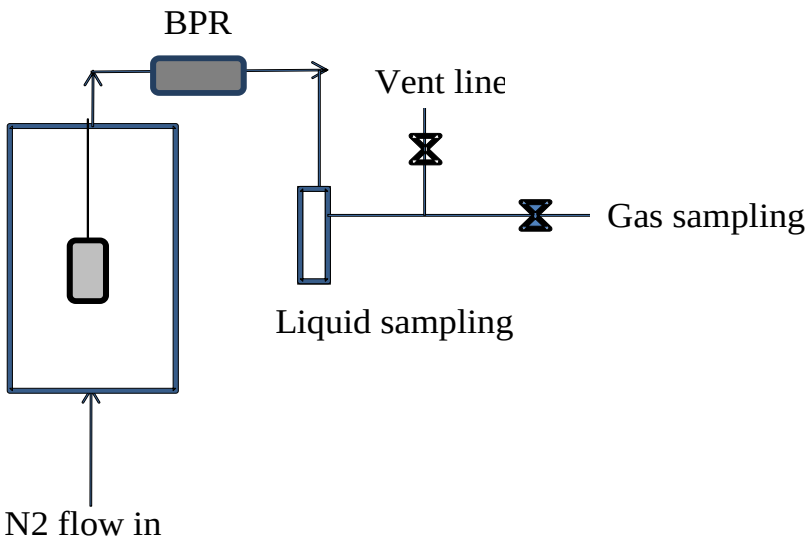

Figure 4- 7: Schematic diagram of high pressure TGA pyrolysis. Purge and balance gases were passed from the bottom and a back pressure regulator was used to maintain the high pressure environment in the furnace chamber.

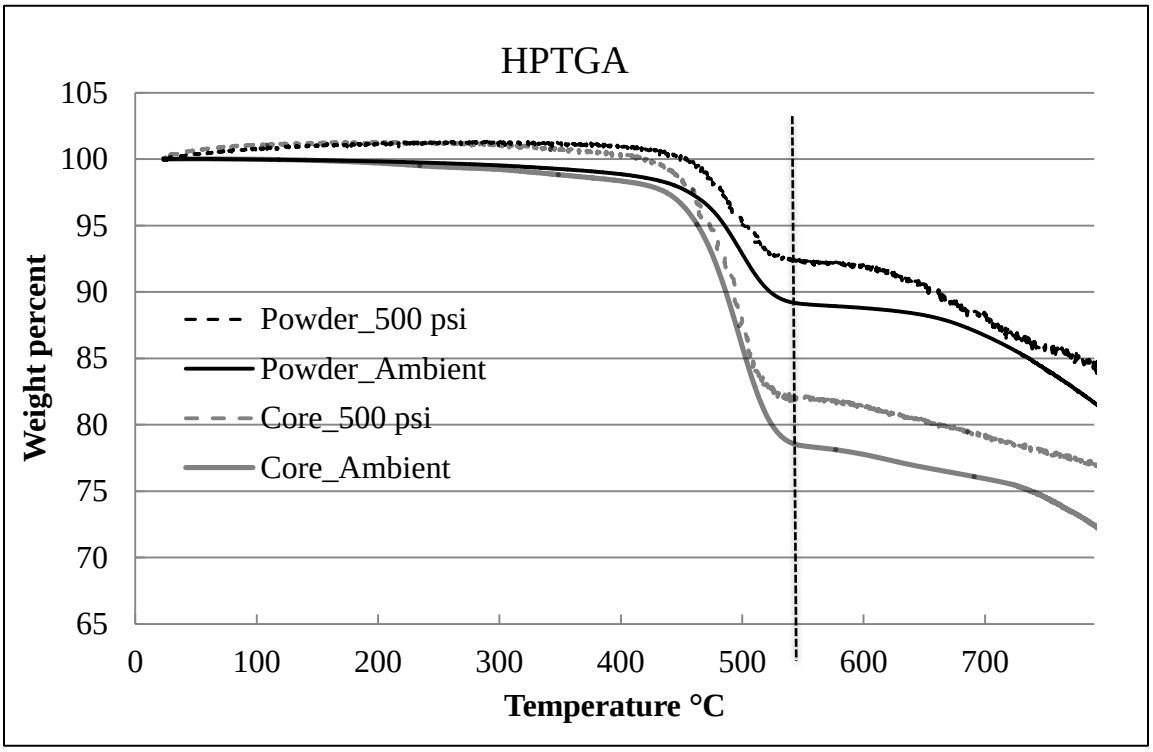

Figure 4- 8: Weight loss profiles at ambient and high pressure (500 psi) during HPTGA pyrolysis of sample #1 (PO) and crushed sample #2 (CO).

These results indicate that complete conversion of organic matter was achieved during the HPTGA experiments at around 530°C at the heating rate of 10°C/min. The weight loss values during pyrolysis under 500 psi were observed to be less than those during ambient TGA pyrolysis. Organic matter in pressurized pyrolysis was transformed to coke (around 3% of initial weight). However, the layer effect (greater initial amount in the sample pan) also contributed to the coke formation [48].

Sample #1 (PO) samples were also pyrolyzed at three different heating rates at 500 psi in a high pressure TGA at Brigham Young University (BYU) (Appendix C). Coke formation during the high pressure pyrolysis was also observed in these runs. The amount of coke formed was in the range of 0.6 to 1%. Less coke was formed due to small amount of raw materials used, which translates to no layer effect.

5. KINETIC ANALYSIS OF OIL SHALE PYROLYSIS TGA DATA

This section provides a complete TGA dataset for the pyrolysis of Green River oil shale. The performance of the different kinetic models in being able to match the data was compared. Advanced isoconversional models have not seen widespread use perhaps due to their relative computational complexity. The methodologies for implementation of these models allow computations of parameter uncertainties as well. The sophisticated parameter fitting methods are intuitive and easily implemented. However, selection of a unique model from a number of available choices is sometimes difficult. The root mean square errors between the experimental and modeling data are compared. Selection of a model has real consequences on process predictions – hence it is important to understand the advantages and disadvantages of using different models.

5.1. Nonisothermal TGA Pyrolysis of Oil Shale

Nonisothermal TGA experiments were performed at heating rates between 0.5°-50°C/min for the decomposition of the crushed and undried sample #1 oil shale (PO) samples (20-30 mg). Nonisothermal TGA offers certain advantages over the classical isothermal method because it eliminates the errors introduced by the thermal induction period. Nonisothermal analysis also permits a rapid and complete scan of the entire temperature range of interest in a single experiment. Weight loss data along with derivatives are shown in Figure 5-1 for seven heating rates. The mass and temperature measurements in the instrument were calibrated periodically and confirmed with a

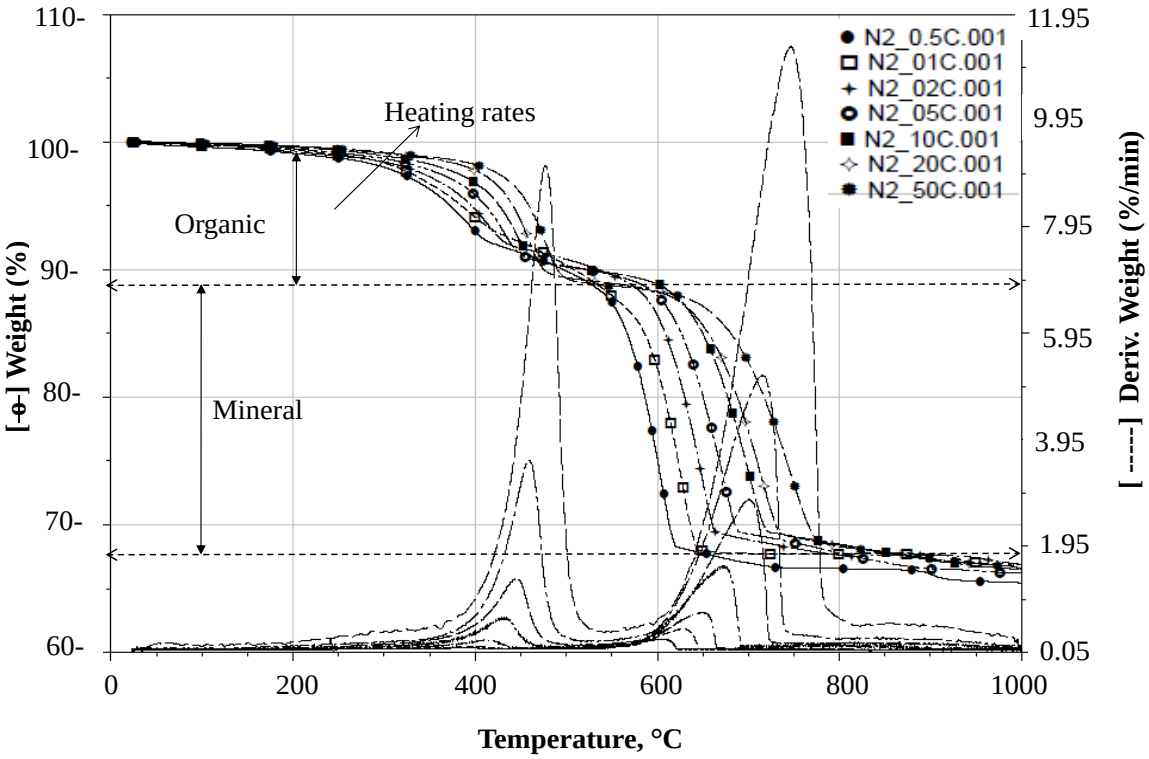

Figure 5- 1: Nonisothermal TGA pyrolysis thermograms: rates go from 0.5°C/min to 50°C/min. The solid lines are weight curves and the dashed lines are derivatives. The arrow indicates that the rates increase as we go from bottom to top. In the derivative curves, the highest peaks for the highest rate used. The second set of derivative peaks is due to mineral decomposition.

standard material, calcium oxalate. Excellent reproducibility was observed in the mass loss curves. The TGA kinetics could be affected by different process parameters; such as flow rate, particle size, etc. Galan and Smith [48] concluded that if the particle size was greater than about 4 $x10^{-4}$ m and if more than two to three layers of particles were present, transport of heat and mass influence the rate. Hence, the sizes of the particles used along with other conditions employed were specifically designed to eliminate heat and mass transfer effects during pyrolysis. The total flow rate of nitrogen gas was 100 ml/min, 60 ml/min as purge and 40 ml/min as balance gas.

The total extractable kerogen content in Mahogany oil shale was found to be about 10-12 % of the total weight. There was no significant weight loss observed during preheating, confirming the absence of moisture content in the sample. This result was confirmed in TGA experiments, where there was neither significant peak detection nor weight loss below 150°C. Two significant derivative peaks in all nonisothermal experiments were observed, corresponding to organic and carbonate decompositions. The carbonate decomposition commenced at 525°C or above, depending upon the heating rate, and resulted in a total weight loss of about 25-30%. It was also observed that the maximum rate shifts to higher temperatures and decomposition rate increases as the heating rate increases from 0.5° to 50°C/min. This difference is due to shorter exposure time to a particular temperature at faster heating rates (Figure 5-1). The organic decomposition occurs between 250°-550°C and depends on heating rate. The data show one single peak for organic decomposition, indicating that one distinguishable process occurs in this temperature range. Nonisothermal experimental conditions and onset analysis criteria such as start, maximum rate and end points are summarized in Table 5-1.

Table 5- 1: Analysis criteria for the nonisothermal TGA pyrolysis data.

Heating rate		Analysis Criteria					
		Start		End		Maximum	
β	Initial weight (mg)	T(°C)	wt % Loss	T(°C)	wt % Loss	T_{max} (°C)	wt % Loss
0.5	22.64	255.6	1.32	421.6	8.02	392.7	6.48
1	28.64	269.6	1.16	437.6	7.48	398.3	5.79
2	26.90	280.0	1.33	456.4	8.43	414.1	6.52
5	25.97	348.9	2.17	474	9.41	432.2	7.17
10	38.45	349.7	1.74	490	9.67	445.6	7.26
20	29.49	371.6	1.58	504	10.68	460.1	7.92
50	22.37	377.3	1.43	530.6	11.13	477.0	7.89

5.2. Kinetic Analysis – Advanced Isoconversional Methods

It has been noted in the earlier literature that kerogen is a cross-linked, high molecular weight solid [137, 138]. During pyrolysis, bonds are broken, leading to multiple reactions. As described earlier, one peak was observed in the organic decomposition temperature range. Consequently, globally single stage decomposition was assumed in deriving kinetic rate expressions.

Kerogen $\longrightarrow$ Decomposition Products

Advanced isoconversional methods or sophisticated parameter estimation methods would be appropriate for the analysis of kinetics of decomposition of complex materials like kerogen [63, 69]. The salient features of these methods are discussed here. The conversion of solid matter in shale (kerogen) to products from TGA weight loss data is defined as [139],

$$\alpha = \frac{W_o - W_t}{W_o - W_\infty} \tag{5.1}$$

In general, the rate of decomposition can be expressed using the non parametric kinetic equation

$$\frac{d\alpha}{dt} = f(T) \cdot f(\alpha) \tag{5.2}$$

Using the Arrhenius expression leads to the following,

$$\frac{d\alpha}{dt} = f(T) \cdot f(\alpha) = A \cdot e^{\frac{-E}{RT(t)}} \cdot f(\alpha) \tag{5.3a}$$

Isoconversional methods are specifically designed to address deficiencies in variable heating rate analyses [63]. Advanced model-free isoconversion method has been used in this study. The concepts of advanced isoconversional method and estimation of

uncertainty were adapted from a series of papers published by Vyzovkin, Wight, and their co-researchers [79-82, 140-142].

For a constant heating rate $\beta = dT/dt$, equation (5.3a) can be written as:

$$\beta \cdot \frac{d\alpha}{dT} = A \cdot e^{\frac{-E}{RT(t)}} \cdot f(\alpha) \tag{5.3b}$$

The direct solution of this equation requires numerical differentiation of the experimental measurements [79]. The integral form of this equation after separating variables is:

$$\int_0^{\alpha^*} \frac{d\alpha}{A \cdot f(\alpha)} = \frac{1}{\beta} \int_0^{T^*} e^{\frac{-E}{RT(t)}} dT = \frac{1}{\beta} [I(E_\alpha, T_\alpha)] \tag{5.4}$$

There is no known analytical solution to the integral in equation (5.4). Several approximations have been proposed [143, 144]. It would also be possible to perform numerical integration using well established procedures. The assumptions that reaction model does not depend on heating rates and is constant for a small conversion interval lead to the integral form of the rate law (5.5).

$$\frac{\alpha_{\text{end}} - \alpha_{\text{start}}}{Af(\alpha)} = \frac{I(E_\alpha, T_\alpha)}{\beta} \tag{5.5}$$

These assumptions suggest that the integral at any particular conversion should be the same for all heating programs and be a function of time-temperature relationship. According to this, for a set of N experiments carried out at different heating programs, the activation energy is determined at any particular level of conversion by minimizing the following function [79].

$$\chi^2(E) = \frac{1}{N(N-1)} \sum_{i=1}^{N} \sum_{j \neq i} \left(1 - \frac{I_i(E,T)}{I_j(E,T)} \right)^2 \tag{5.6}$$

Here the subscripts *i* and *j* represent two experiments performed under different heating programs. The trapezoidal rule is used to evaluate the integral numerically and the minimization procedure is repeated for each value of α to find the dependence of activation energy on the extent of conversion. The activation energy distribution obtained in equation (5.6) can be used to determine [$A \cdot f(\alpha)$] as a function of α. The confidence intervals for the activation energies and for the values of $A \cdot f(\alpha)$ can be calculated using the statistical approach described [79, 142]. The experimental rate and conversional data can be reconstructed based on the model parameters using equation (5.7) below.

$$\ln\left[\beta_i \left(\frac{d\alpha}{dT}\right)_{\alpha,i}\right] = \ln\left[A \cdot f(\alpha)\right] - \left(\frac{E_\alpha}{R \cdot T_{\alpha,i}}\right) \tag{5.7}$$

A *MATLAB* program utilizing the function *ODE45* was used to solve the above ordinary differential equation. $E(\alpha)$ and $A \cdot f(\alpha)$] which were inputs to the *MATLAB* program were obtained using the isoconversional analysis described above.

The kinetic models can be used to extrapolate to non experimental rates. Slow pyrolysis that is likely during in-situ oil shale production and high rates of flash pyrolysis are of interest. The assumptions of the isoconversion method (Equation (5.5) allow calculating the temperature to reach a level of conversion at extrapolated heating rates using the following mathematical equivalency [81],

$$\frac{I(E_\alpha, T_{\alpha,i})}{\beta_i} = \frac{I(E_\alpha, T_{\alpha,j})}{\beta_j} \tag{5.8}$$

The equation above was used to estimate the temperature at which the material starts to convert. The procedure for reconstruction was then used to obtain conversions and rates at extrapolated conditions. One of the advantages of using the advanced isoconversional approach is that uncertainties in *E* values can also be estimated.

5.2.1. Kinetic Analysis – Advanced Parameter Fitting Approaches

Results from other parametric fitting models were compared with those obtained with advanced isoconversional method. The *Kinetic05* package developed by Braun and Burnham at Lawrence Livermore National Laboratory and supplied by *GeoIsoChem* is capable of obtaining kinetic parameters of a variety of models. These include the power law and the distributed reactivity models. TGA or other thermal analysis data can be used. Distributed reactivity model options include the Friedman-based isoconversional method, Gaussian and Weibull distributions, and a few others. The application of these models were discussed by Burnham and Braun [68] for different complex materials. In *Kinetic05,* the model parameters are refined by minimizing the residual sum of squares between observed and calculated reaction data by using nonlinear regression. The details of mathematical formulas and solution procedures have been published previously [68].

5.3. Kinetic Analysis Results – Advanced Isoconversional Methods

The TGA data were normalized from zero to one prior to analysis. The temperature at which the derivative of weight loss starts to rise was chosen as the zero conversion point, and the temperature at which the weight derivative returned to the base line was the end point. *Isokin*, a package developed at the University of Utah [79] was used for the calculation of the distribution of activation energies and other kinetic parameters. Distributions in kinetic parameters, E and $A \cdot f(\alpha)$ were determined as functions of conversion.

The confidence interval estimation was performed by using different number of heating rates and/or different combinations of heating rates. Uncertainties were calculated for 10 conversion intervals for different cases (Figures 5-2, a-d). Uncertainty values

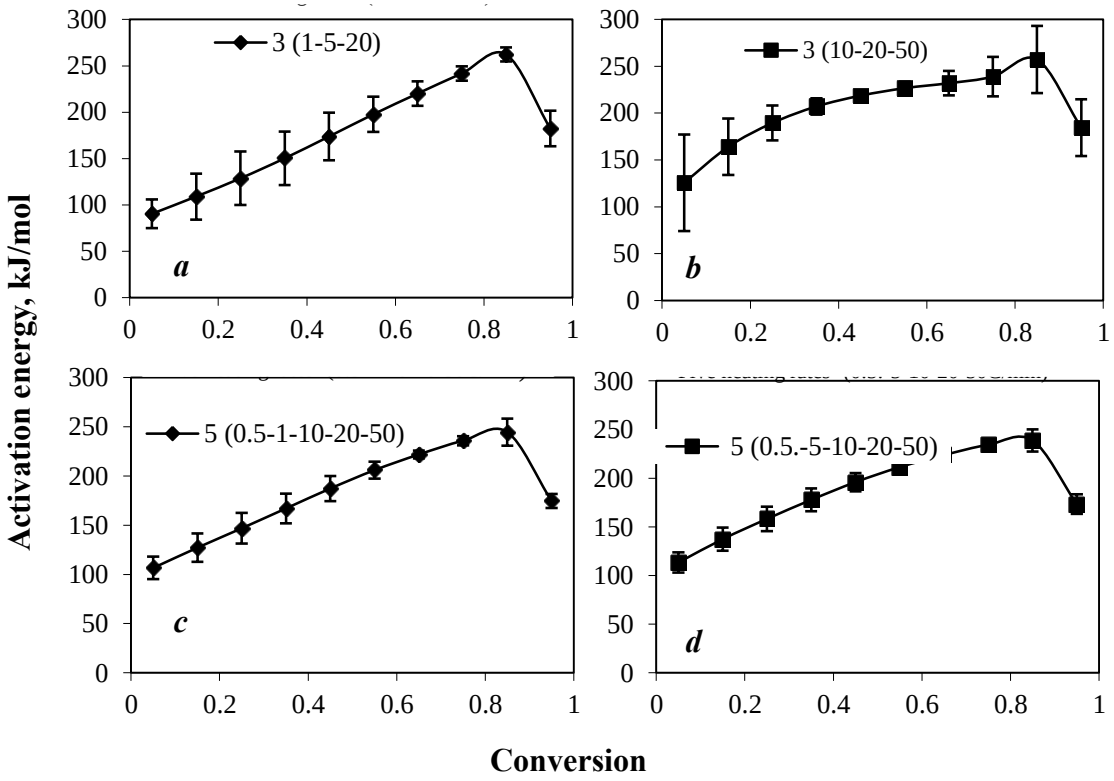

Figure 5- 2: Distribution of activation energies for pyrolysis of Green River oil shale (sample #1) calculated using the advanced isoconversional method. The uncertainties in activation energy values are shown for different number of heating rates considered and for different combinations. As all of the heating rates are used, uncertainties are reduced over the entire conversion range (d).

increased when fewer rates were used. When heating rates spanning the wider range (for example 50°C/min and 0.5°C/min) were included in sparse data sets, the uncertainties were generally lower. Figure 5-3(a) shows activation energy distribution (as a function of conversion) and associated uncertainties when all the seven heating rates were employed. Figure 5-3(b) shows $A \cdot f(\alpha)$ as a function of conversion. Activation energies ranged from 93 - 245 kJ/mol. The values of $A \cdot f(\alpha)$ varied from 1.42E6 - 4.46E16 min^{-1}. The kinetic parameters estimated in this work are consistent with those observed by others for Green River oil shale [60, 61]. For Kukersite shales, which was considered a "standard" because

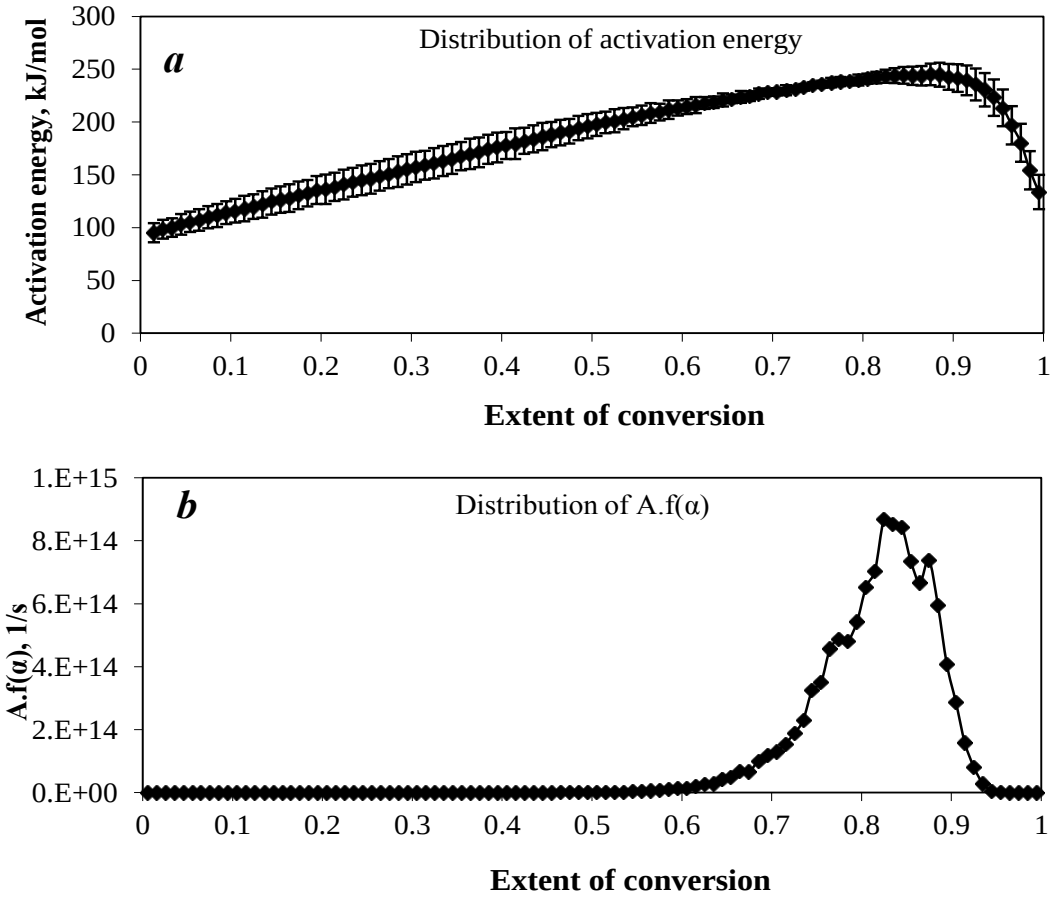

Figure 5- 3: Distribution of kinetic parameters with extent of conversion [(a) Activation energy (b) *A·f(α)*] determined using the advanced isoconversional method. All of the seven rates were used in calculating the kinetic parameters. Uncertainties in activation energy values are also shown.

of reproducibility, the activation energies ranged from 210 kJ/mol to 234 kJ/mol [68]. The values of activation energies reported in this work of about 93 kJ/mole to 245 kJ/mol are lower at lower conversions.

Advanced isoconversional method provides combined preexponential factor and reaction model as function of conversion. The values of preexponential factor *A* can be calculated after assuming a reaction model (order, functionality, etc.). For example, the Friedman method assumes a first-order reaction, and using the functionality of (1-α) for

f(α),A can be calculated. A graphical implementation of the Friedman approach also yields *E(α)* and *A* as functions of conversion. The comparison of kinetic parameters obtained from *Isokin* first-order model and Friedman graphical method are depicted in Figure 5-4. The agreement between kinetic parameters obtained using the two approaches is excellent. The results support that thermal decomposition pyrolysis of Mahogany oil shale is globally a first-order process. This is also confirmed by observing the Constable plot, that examines the relationship between logarithm of *A* and *E* [145]. The linear (or near-linear) profile in the Constable plot may be adequate [140] to confirm the order of the reaction. The Constable plots shown in Figure 5-5 are remarkably linear confirming the order to be unity for both approaches employed.

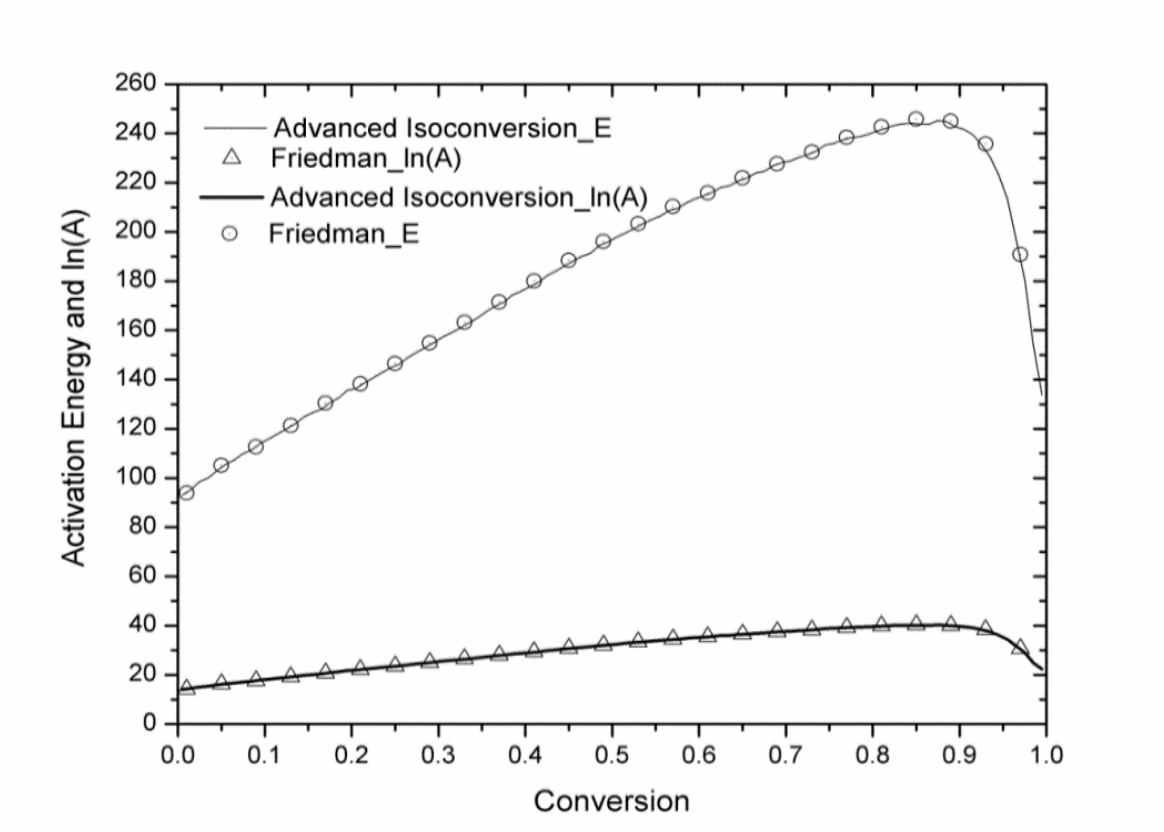

Figure 5- 4: Comparison of kinetic parameters from advanced isoconversional and the Friedman method. The kinetic model is assumed to be first order for this comparison.

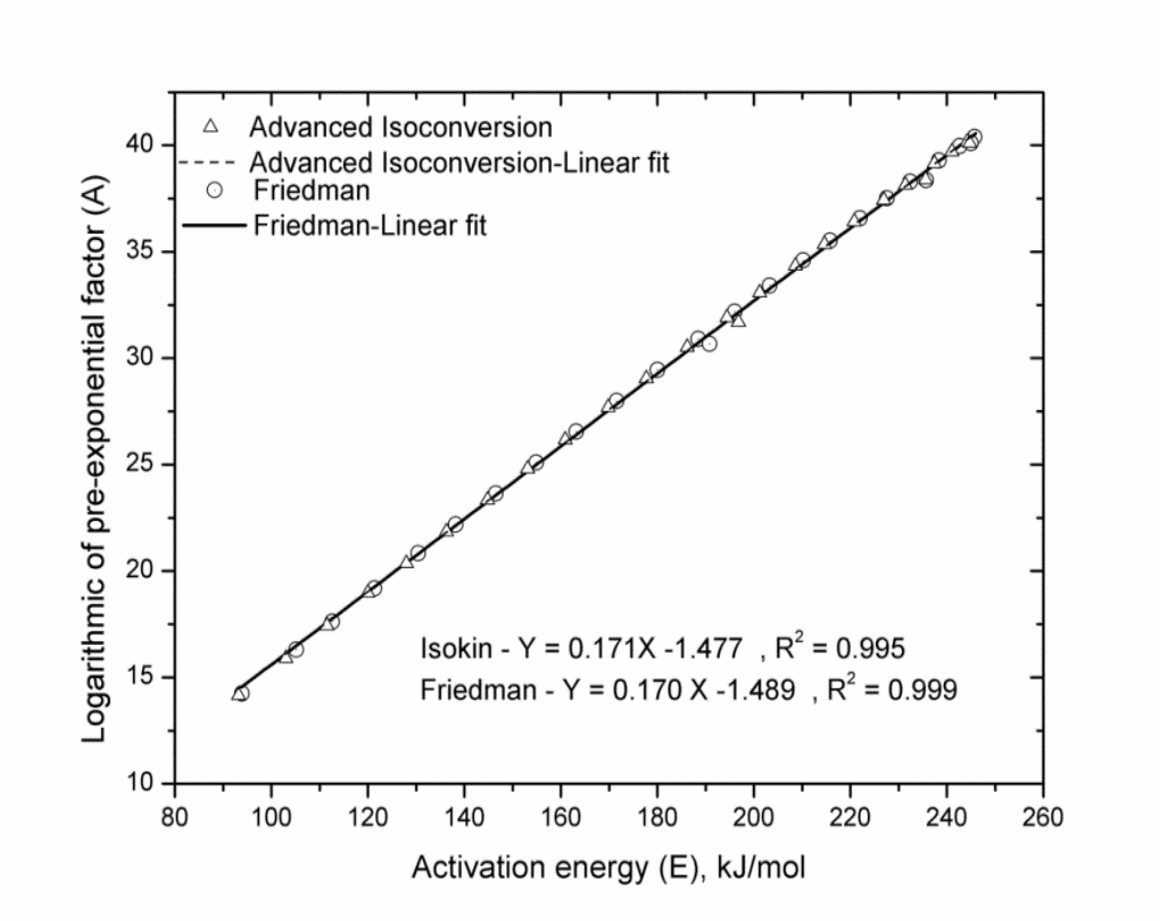

Figure 5- 5: Constable plots for Friedman and advanced isoconversional kinetic parameters.

The distributions of E and $A{\cdot}f(\alpha)$ were used in model equations to recreate the experimental data. A *MATLAB* code with the *ODE45* solver was used in the calculations. In the practical implementation of the code, temperature was the dependent variable. Results of the model comparisons with the experimental data are shown in Figure 5-6. The agreement between the model and the experimental data is good over most of the conversion range, and for all the rates. The experimental data at 10^{o}C/min were used as basis to calculate the conversion profiles for rates at which experimental data was not available. Extrapolated profiles at rates ranging from 0.01°C/min to 500°C/min are

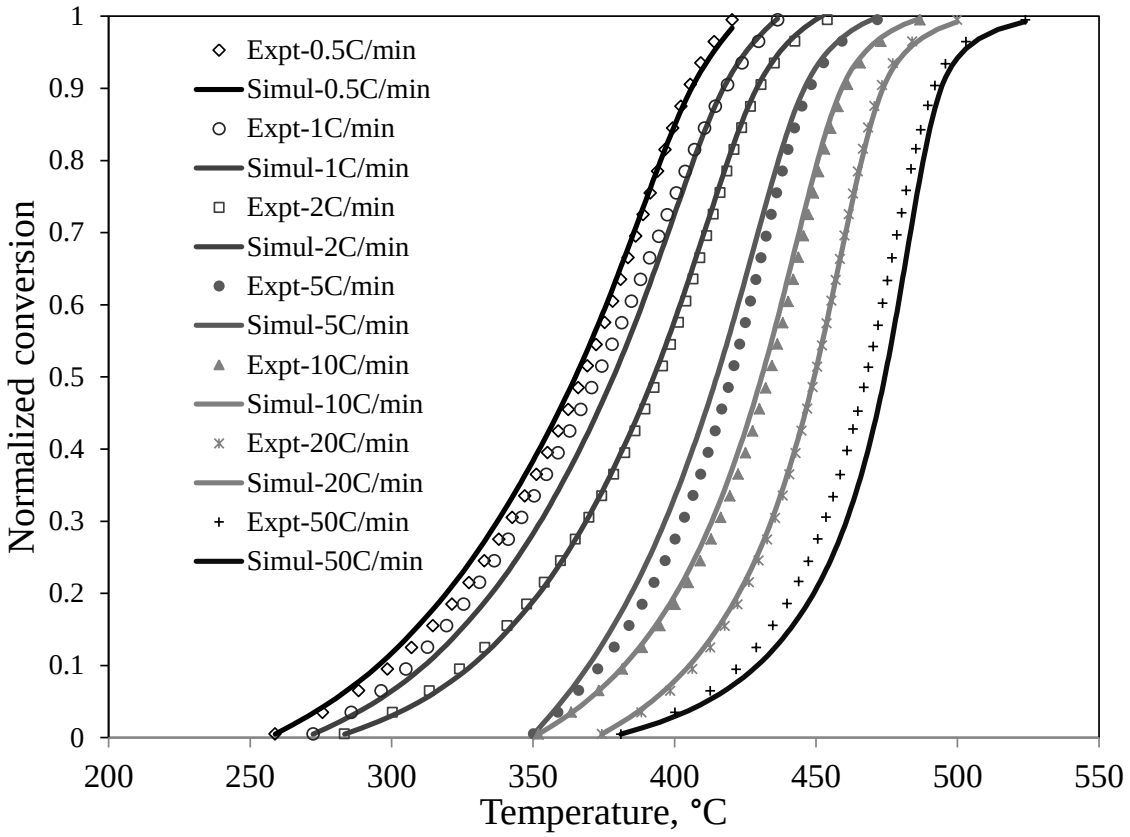

Figure 5- 6: Experimental and simulated conversion profiles at different heating rates using the advanced isoconversional method. *MATLAB* based computational method described in the text was used.

shown in Figure 5-7. At slow heating rates, decomposition begin at lower temperatures while in the fast pyrolysis, the products are released at higher temperatures. Simulated decomposition rates and onset temperatures shift to higher temperatures at higher heating rates. The extrapolated results are not all consistent with some experimental results. To explain all aspects of the extrapolated profiles, introduction of reaction initiation type mechanisms [13, 49] proposed by a few researchers may have to be considered.

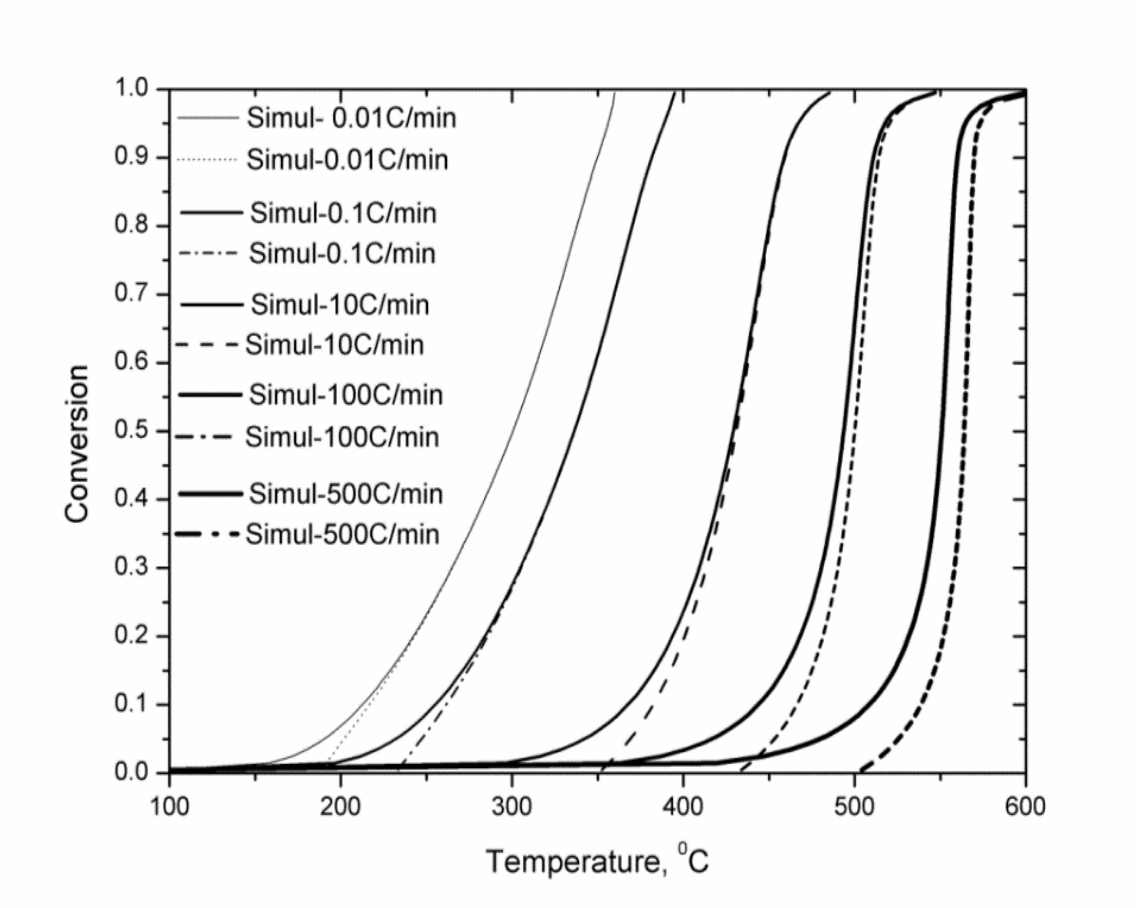

Figure 5- 7: Simulated conversion profiles at extrapolated constant heating rates using two different initial temperatures. Continuous lines show profiles with T_0 = 100°C and dotted lines depict extrapolation with T_0 calculated from Equation 5.8).

5.3.1. Kinetic Analysis Results– Advanced Parameter Fitting Models

The models from Kinetic05 used for comparison purposes are listed in Table 5-2. Table 5-2 also shows the parameters obtained. The power law model was applied in two cases; first-order and n^{th}-order. In the latter case, optimal values of n, E and A were obtained using nonlinear regression. The n^{th}-order reaction model is mathematically equivalent to Gamma distribution [146]. The Gaussian distribution approach used by Braun and Burnham [97] was also used with the first and the n^{th}-order models. Discrete reactivity distribution models are based on different combinations of A and E assuming

Table 5- 2: Parameters obtained using selected kinetic models available in kinetic05.

Kinetic models		*E* (kJ/mol)	*A* (1/s)	Order	Paremeter-1	Paremeter-2
Gaussian	n = n	180.061	8.12E+10	0.53	4.19E+00	
	n = 1	181.446	1.29E+11	1.00	3.78E+00	
Discrete	Case-1	Fig 8-(a)	5.72E+09	1.00		
	Case-2	Fig8-(b)	1.00E+14	1.00		
	Case-3	Fig8-(c)	$e^{(a+bE)}$	1.00		
Weibull		163.154	6.64E+09	1.00	1.04E+04	9.99E+00
1^{st} order		156.968	2.19E+09	1.00		
n^{th} order		160.735	5.80E+09	1.65	1.65	
Isoconversional		Figure-4		1	Friedman based	

the reaction to be first-order. Three different cases were used in this work and the results were compared;

1. Fixed *E*-spacing,
2. Initial *A*-range and fixed *E*-spacing
3. Constable relationship for A and E - ($ln(A) = a + b \cdot E$).

The distributions of activation energies from discrete models are shown in Figure 5-8. The three different approaches produced different kinetic parameters. Use of Weibull distribution is another parameter fitting method used extensively for petroleum source rocks by Lakshmanan et al. [147]. Isoconversional method in *Kinetic05* is based on the first-order Friedman-type of analysis. The distribution of activation energies obtained using this approach in *Kinetic05* is almost identical to the distribution obtained using the advanced isoconversional method (Figure 5-4). The reconstruction of conversion and rate experimental data using different *Kinetic05* models and *Isokin* were compared at all experimental heating rates. The results are shown for a heating rate of 10°C/min in Figure 5-9. The general trend is that the cumulative conversions are matched reasonably well while the rates have higher discrepancies.

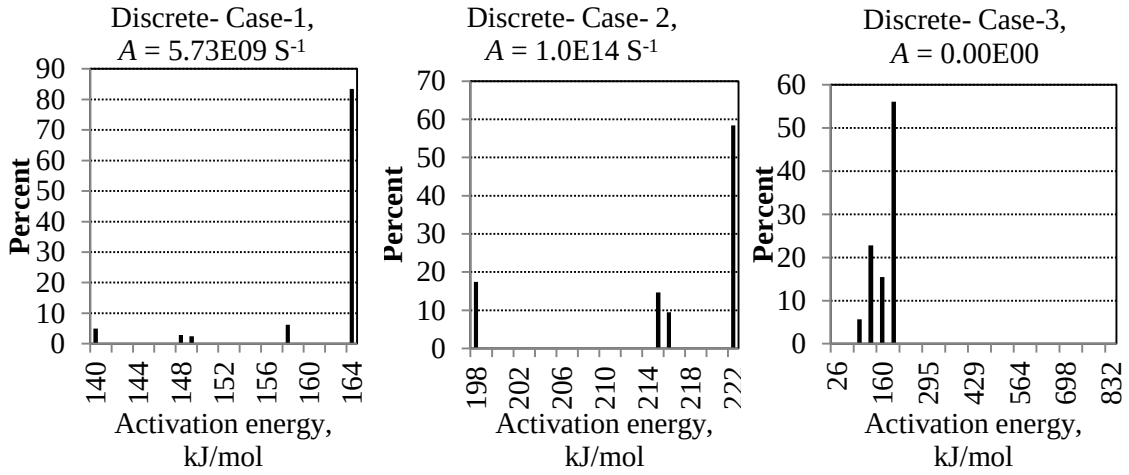

Figure 5- 8: Distribution of activation energies from discrete reactivity models (Case 1-3 as described in the text).

5.3.2. Comparison of the Different Kinetic Models Used

The comparison of the sum of the root mean square (RMS) errors (all 7 experimental heating rates) is shown in Figure 5-10 (a- for reaction rates and b- for conversions). The errors were calculated for 100 points of conversion at the same values of experimental temperatures. The RMS values are lower for the advanced isoconversional method compared to the parameter fitting and reactivity distribution models. The isoconversional approach from Kinetics05 also produced RMS values comparable to the ones shown for the advanced isoconversional method. The parameter fitting approaches, particular with discrete activation energies also result in reasonable RMS values. The parameter fitting approaches may result in determination of parameter sets that are non unique. For example, the first-order and n^{th}-order models with Gaussian distribution are characterized by different parameter sets (Table 5-2), but produce about the same goodness of fit (Figure 5-10). Similar discrepancy was observed with first order

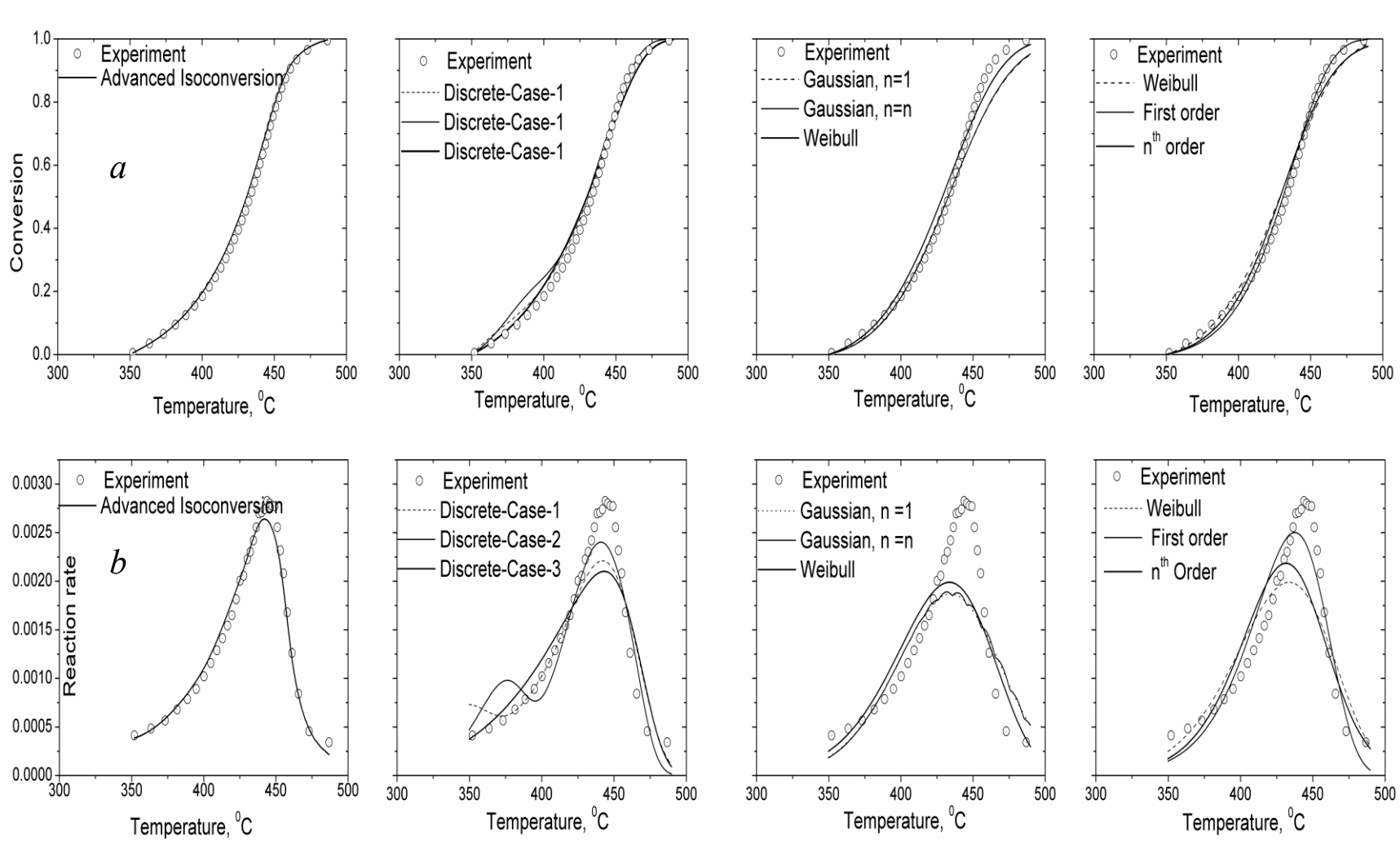

Figure 5- 9: Comparison of different kinetic models at 10°C/min [panel (a) conversion and panel (b) reaction rate].

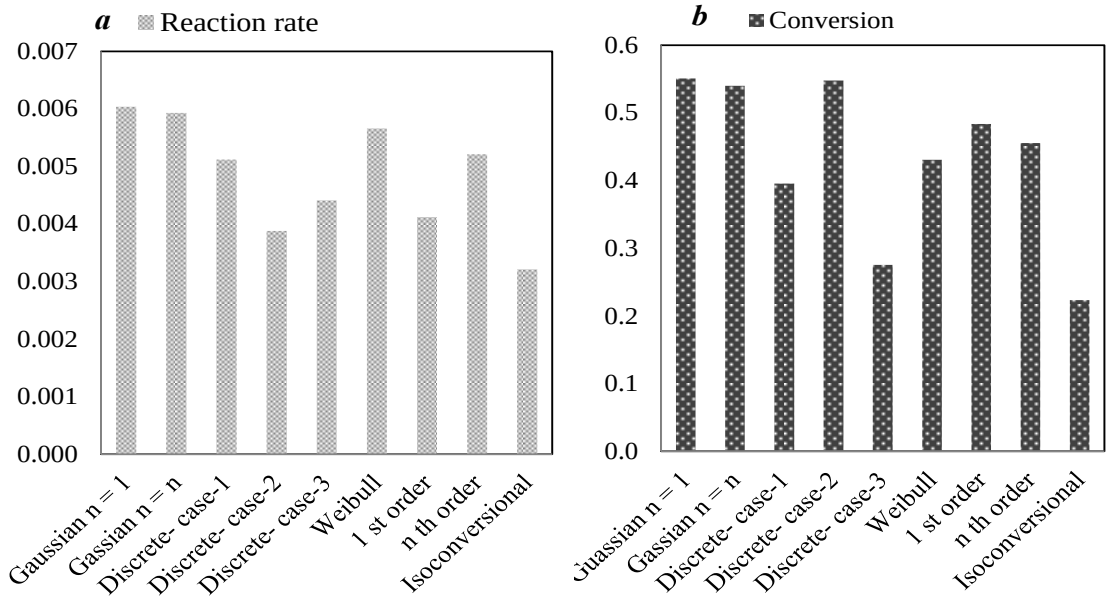

Figure 5- 10: Comparison of different kinetic models based on sum of root mean square (RMS) residues. In all these calculation, 100 experimental data points were used. RMS is summed over all of the seven experimental heating rates**.**

and n^{th} - model. The RMS values for conversion data is less with n^{th} order compare to first order while it reversed for rate data. When this happens, model discrimination becomes an issue. However, these models are flexible, and can be used with any reaction combinations (parallel, series, etc.). The isoconversion approach which does not consider a kinetic model apriori gets around this, but may not be as flexible as the parameter fitting methods. Burnham and Dinh [69] argue that isoconversion models are not suitable for modeling reactions in series.

The kinetic parameters obtained from different models were used to extrapolate the data outside of the experimental range. The resulting profiles are compared in Figure 5-11 for conversion and reaction rate at a heating rate of 100°C/min. Conversion profiles are also shown in Figure 5-12 for a heating rate of 0.01°C/min. The high heating rates would be applicable for a flash pyrolysis process, while the slow heating rates are likely

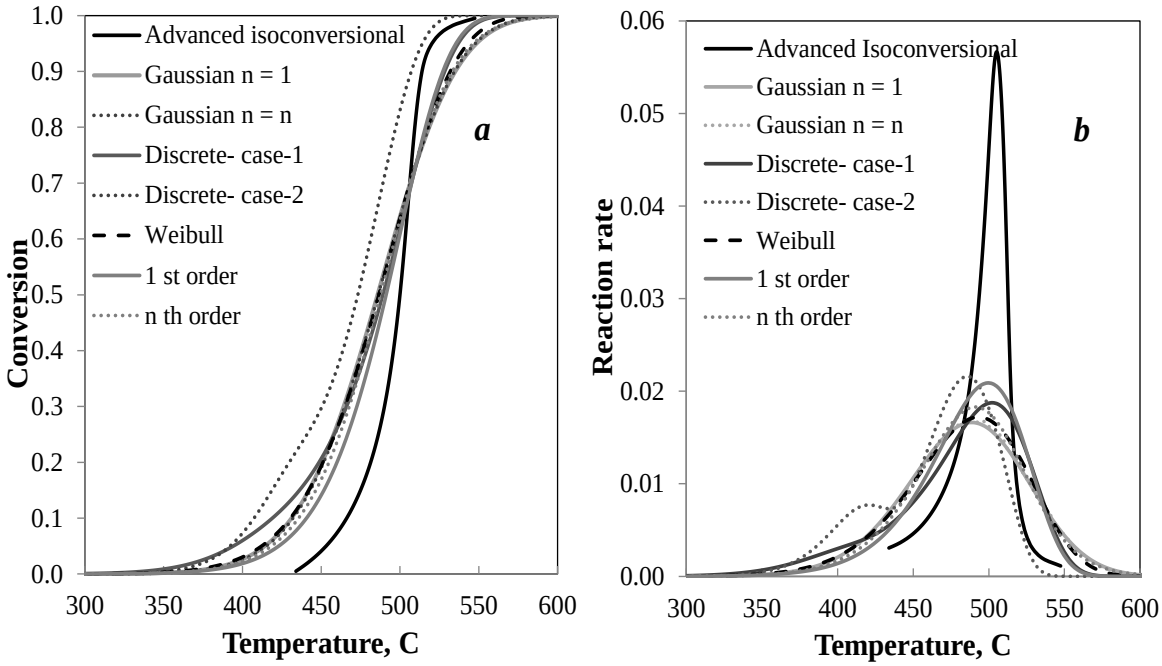

Figure 5- 11: Comparison of different kinetic models at a heating rate of 100°C/min [(a) conversion and (b) reaction rate]. It is seen that under fast pyrolysis conditions, model of choice does have significant impact on predictions.

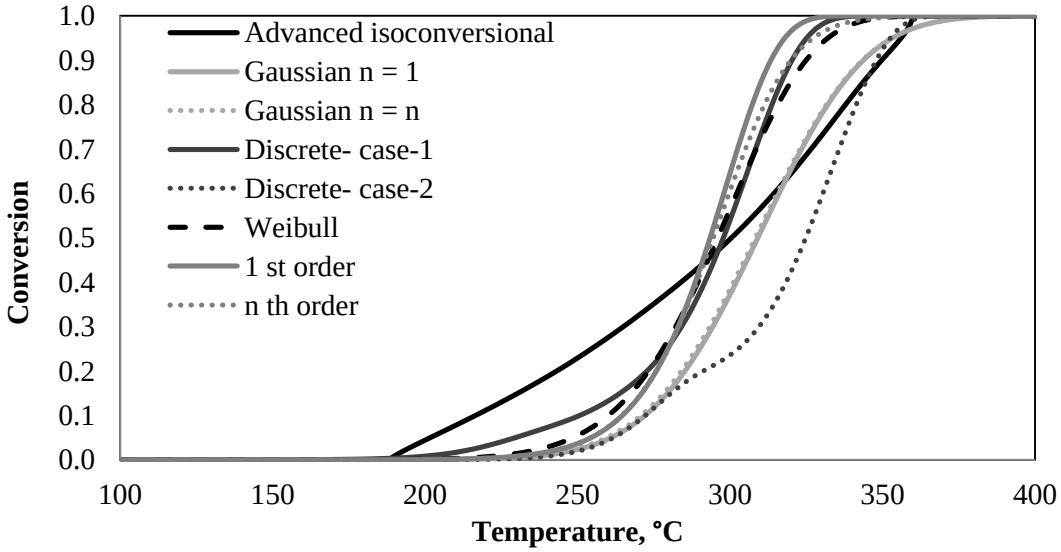

Figure 5- 12: Comparison of the conversion profiles from different kinetic models at a heating rate of 0.01°C/min. The rates for insitu operations are usually slower than 0.01°C/min. At these slow rates, also choice of the model used is important in understanding the rate of conversion of oil shale.

in insitu heating of oil shale deposits. These figures show that there are discernible consequences when the models are used to extrapolate the data. At high heating rates, decomposition begins at much higher temperatures when the isoconversional model is used. This trend is consistent with what is observed in the TGA. The peak rates and the temperature range over which the reactions occur (spread of the rate curve) are better reproduced when the isoconversion method is used. Similarly, at lower heating rates, conversion begins at a lower temperature when the isoconversional model is used. The better performance of the isoconversion model is attributed to the fact that it follows the progress of reactions on the relevant conversion intervals.

The advanced isoconversional method yielded activation energies as function of conversion in the range of 93 kJ/mol to 245 kJ/mol. The decomposition process can be viewed as consisting of multiple parallel reactions with individual activation energies. Maximum uncertainties in activation energies computed using the advanced isoconversion method were about 10% of the energy values calculated. The isoconversion approach produced the lowest RMS values in both rates and cumulative conversion (for all of the heating rates, combined), but the parameter fitting approaches also produced reasonable duplication of the data. The parameter fitting approaches using power law, activation energy distribution or discrete energy values in specific conversion intervals are intuitive and fast. However, model selection is difficult because numerous models produce equivalent results. Change in one parameter (for example order) is compensated by changes in activation energies or preexponential factors to produce comparable RMS values. Isoconversional models are in theory “kinetic model” free and their applicability to the decomposition of a complex material like kerogen is excellent.

However, their applicability in reproducing multi-step kinetics has been questioned. Application of these models to real life processes requires extending these models outside of the experimental data range from which they were derived. It is shown that the choice of the right model is of great consequence since model predictions outside of the experimental range vary considerably between the models chosen. Even though this analysis has been conducted with oil shale, the approach and conclusions are likely to be applicable to other complex materials.

5.4. Kinetics of Isothermal Decomposition

The isothermal pyrolysis (N_2 environment) experiments with sample #1 (PO) oil shale were conducted using TGA in the range of 300°C-600°C. The thermal induction time period was kept as low as possible (100^oC/min, the maximum ramp rate of TGA Q-500). Isothermal analyses cannot be performed at higher temperature (above 500°C), since most of the organic material decomposes before the temperature is attained. The total isothermal reaction time was fixed for 4 hrs. The experimental conditions and data obtained are summarized in Appendix B.

The distributions of kinetic parameters obtained from advanced model free method were simulated for isothermal pyrolysis. The thermal induction period was introduced in the kinetic model in a manner similar to that of the experiments performed. The simulated conversion profiles were generated first at 100°C/min heating rate to isothermal temperature. Once the isothermal temperature is achieved the conversion followed the isothermal pyrolysis. The TGA experimental and model simulated isothermal conversion profiles are compared in Figure 5-13. The true isothermal pyrolysis, achieving the isothermal condition with no thermal induction periods, was also

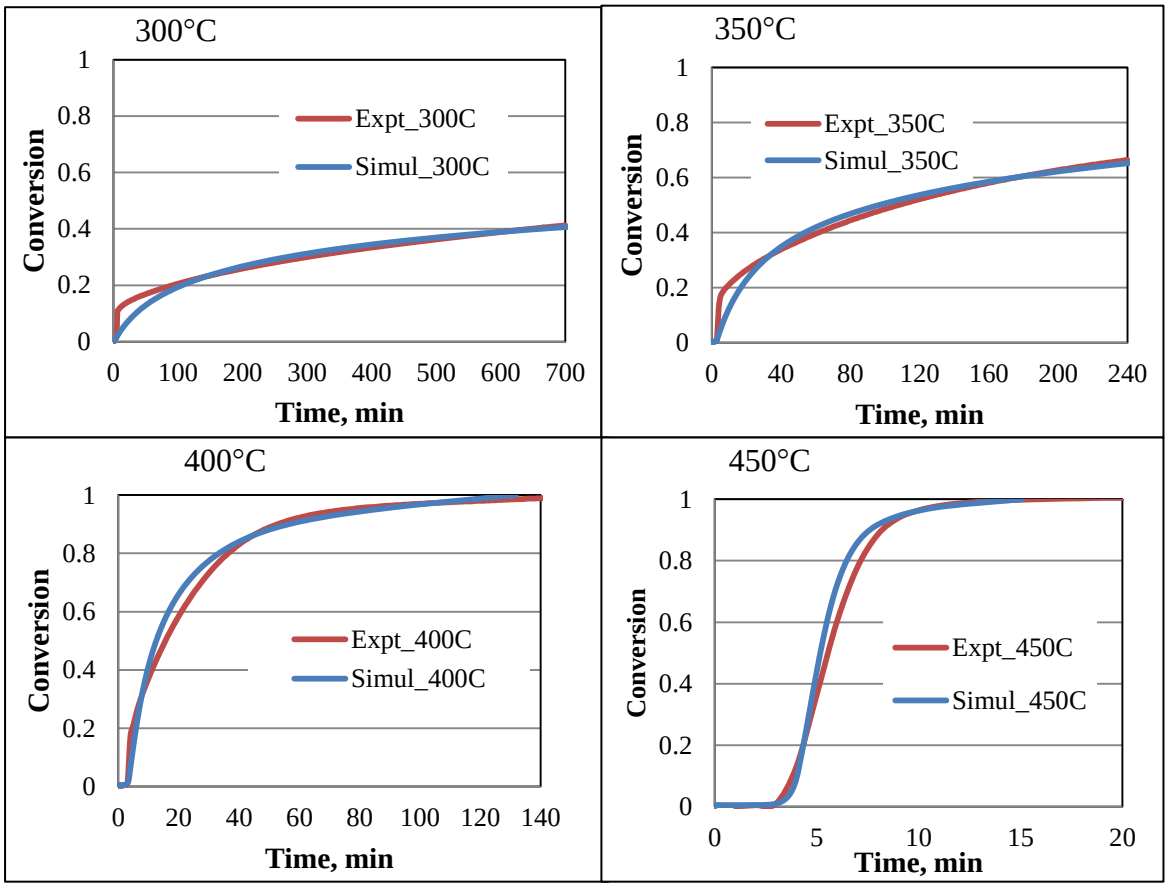

Figure 5- 13: Comparison of the experimental and simulated conversion profiles under isothermal pyrolysis.

simulated for a wide temperature range. Figure 5-14 shows the simulated conversions profiles for true isothermal pyrolysis.

The kinetic parameters of oil shale pyrolysis derived from nonisothermal pyrolysis are able to effectively simulate the isothermal pyrolysis. The experimental and simulation conversion profiles follow the same trend. A comparison of true isothermal and thermally induced time period (100°C/min) indicates that the thermal induction is more crucial at high temperature pyrolysis and must be taken into account (Table 5-3).

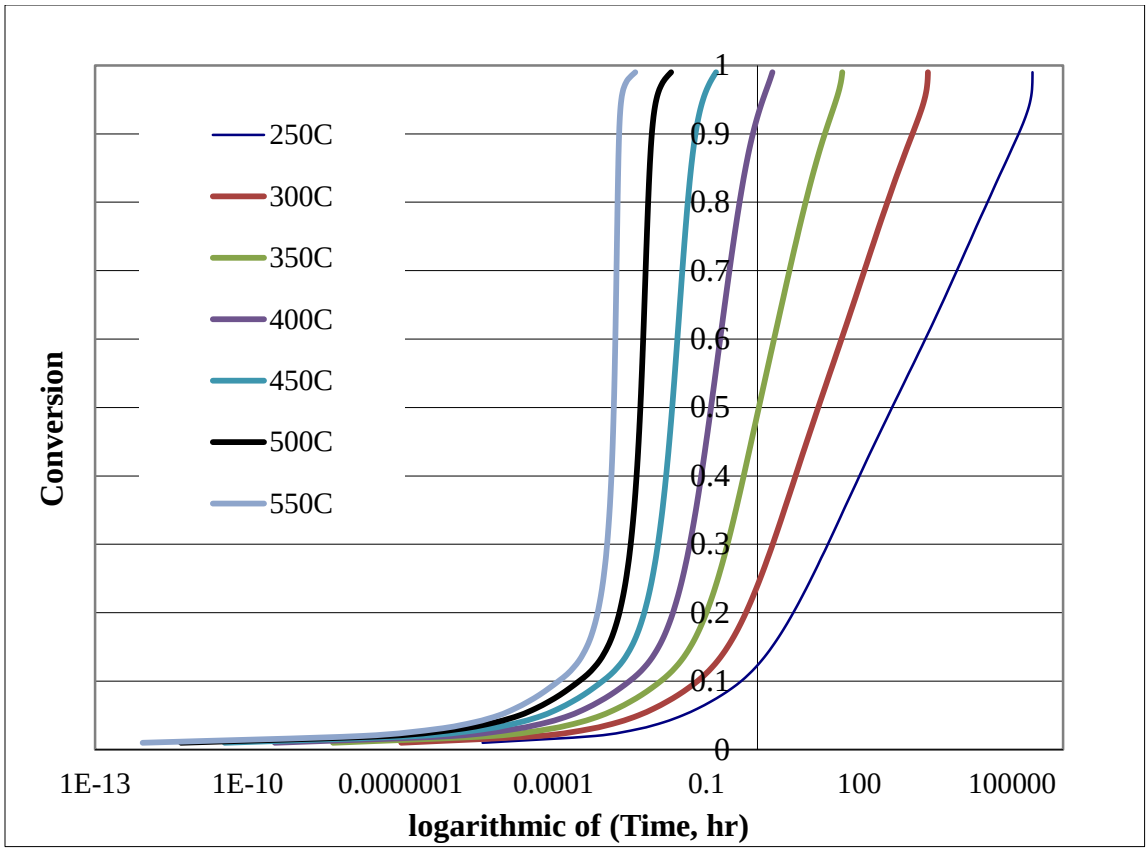

Figure 5- 14: Simulated conversion profiles under true isothermal pyrolysis.

Table 5- 3: Time required to achieve the complete conversion of the organic matter during true and thermal induction (100°C/min) isothermal pyrolysis

Temperature	Time, min	
Isothermal	True	Induction (100°C/min)
200°C	4.60E+09	4.60E+09
250°C	1.40E+07	1.42E+07
300°C	1.30E+05	1.30E+04
350°C	2800	2800
400°C	125	130
450°C	11	15
500°C	1.6	5.8
550°C	0.3	5.1

5.5. Pyrolysis Kinetics of Different Oil Shales

The oil shale samples used in this study contain varying amounts of the organic material. The decomposition profiles of the organic material in these samples were compared at different heating rates. Three heating rates 5°C/min, 10°C/min and 20°C/min were used to pyrolyze sample #1 and sample #2 of 100 mesh in TGA. The thermograms obtained are compared and shown in Appendix A. Figure 5-15 shows an example of the comparison at 20°C/min. The profiles show that the decomposition of the organic matter occurs in the same temperature span at certain heating rates for both samples. The kinetic parameters were also observed to be in the same range within the uncertainty. The results show that the kinetics of organic decomposition in oil shale do not depend a great on deal the organic matter present in the sample.

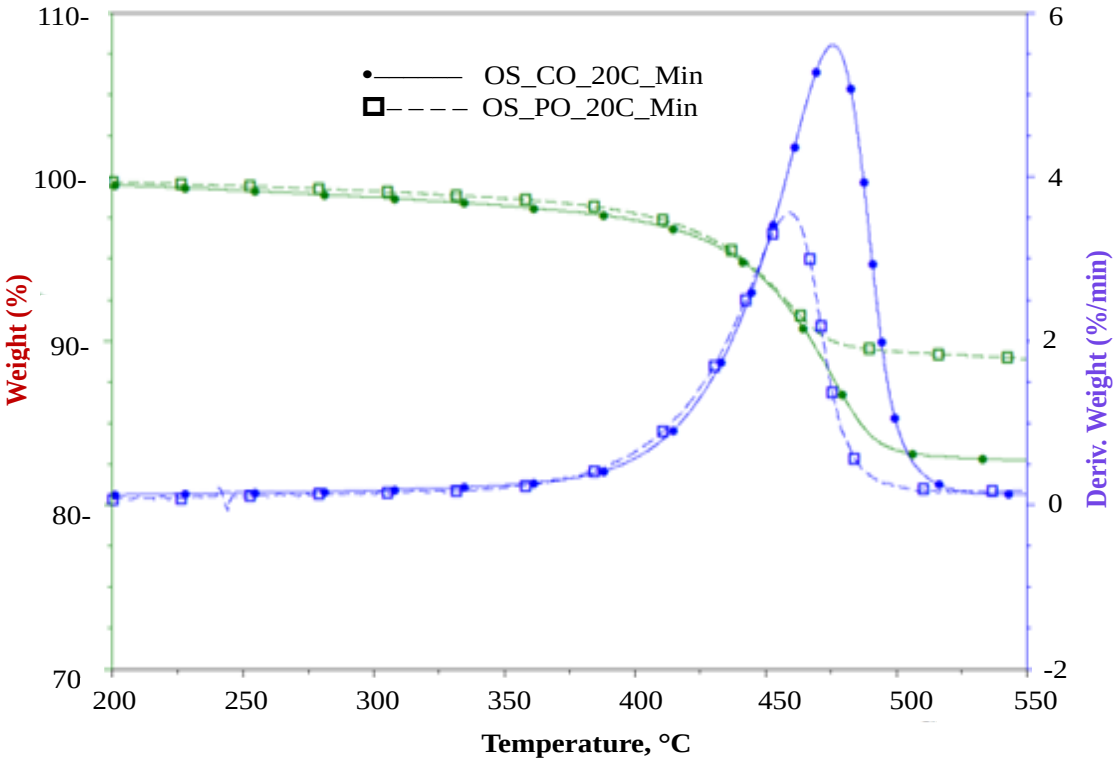

Figure 5- 15: Thermograms of sample #1 (PO) and sample #2 (CO) at heating rate of 20°C/min.

6. COMPOSITIONAL AND KINETIC ANALYSIS USING TGA-MS

Thermo gravimetric analysis (TGA) is an analytical device used for accurately measuring weight loss of a material subjected to a temperature history. The weight loss information can be used to construct kinetic models of the decomposition process. The method is efficient and very effective in developing sophisticated models. Detailed kinetic analysis of the decomposition of Green River oil shale was published by Tiwari and Deo [148]. The next logical step is to discern the composition of the evolving products and to construct kinetics of the formation of these products. The compositions of the products formed during pyrolysis not only depend on the fundamental chemistry of the organic matter decomposition in shale, but also on overall system or reactor configuration. The advantage of using TGA-MS is that the reaction products are identified as they go through the mass spectrometer. The measurements and data analysis were performed to achieve this objective. The compositional analyses of a large pool of inorganic and organic products of oil shale decomposition by TGA-MS were carried out. Four different heating rates were studied to understand the shift in the product distribution as the material is exposed to different time- temperature programs. Ratios of key components were studied. It is feasible to compute kinetics of the formation of either individual or lumped components (like naphtha) if the percentages of these products (as a fraction of the total weight loss) are known. Calculations to demonstrate this feasibility are included.

6.1. TGMS Analysis of Powdered Oil Shale (PO)

The crushed sample #1 (PO) of 100 mesh size was dried for 4 hrs at 100°C to remove moisture. There was no significant weight loss during drying, and hence the samples were used as received after screening to 100 mesh. A TGA instrument (TA Instruments Q500) coupled with a mass spectrometer (Thermostat model GSD 301 T3 from Pfeiffer Vacuum) was used over the entire temperature range.

The oil shale decomposition was studied in the nitrogen environment (pyrolysis). Total flow rate of nitrogen was 100 ml/min (90 ml/min as purge and 10 ml/min as balance gas). The particle size was less than 1.49×10^{-4} m. It has been reported that the decomposition is kinetically controlled under these conditions [149]. The products formed are swept into the mass spectrometer, eliminating or minimizing secondary reactions. It is assumed that the total sweep gas flow rate is high enough to carry the entire vapor out from the chamber and prevent any vapor phase cracking, condensation and further coking. The TGA-MS analysis was performed at four different heating rates (Table 6-1). TGA furnace chamber outlet was connected to the MS instrument through a hot capillary column heated to150°C. The total numbers of components targeted for analysis by single ion monitoring in mass spectrometry are shown for each of the experiments in Table 6-1. Experiment at 5°C/min heating rate was repeated; the first was conducted with 22 compounds as the target while the repeat experiment looked at 56 components. The compounds targeted for the analysis at different heating rates are shown in Table 6-2. The list includes very light hydrocarbon to heavier hydrocarbon of 20 carbon number compounds along with mineral gases.

Table 6- 1: TGA-MS experimental conditions, total compounds were analyzed and observations.

Heating-rate	Final Temp (°C)	Total compounds	Weight mg	%wt-loss @250°C	%wt-loss @500°C	%wt-loss @600°C	T_{max} (°C)
0.5°C/min	650	43	22.54	0.34	9.38	20.14	401.03
1°C/min	600	56	13.10	0.65	9.60	15.99	413.09
$5°C/min^{-1}$	960	22	13.34	0.59	10.76	13.20	442.61
$5°C/min-^{2}$	600	56	13.26	0.46	10.30	11.29	443.41
10°C/min	650	41	19.05	0.63	11.28	12.47	456.93

The total weight loss and derivative curves are shown in Figures 6-1 and 6-2. The lower heating rates are grouped into Figure 6-1 and the higher heating rates in Figure 6-2. The two distinct peaks correspond to organic decomposition at the lower temperature followed by inorganic decomposition at higher temperatures. The organic decomposition peak shifts to higher temperatures as the heating rate increases. The same trend was observed in TGA studies on this oil shale [148]. Most of the organic decomposition occurred before the temperature of 600°C was reached. The organic decomposition temperature scale was divided in the three sections, A_1 (30°C-250°C), A_2 (200°C -500°C) and A_3 (500°C- 600°C). The weight losses in these temperature ranges are shown in Table 6-1. There is no significant weight loss in the section A_1; this indicates that there is little or no water in the samples. Only the experiment at 1°C/min shows a small peak in section A_1. The weight loss is very small and this could be because of the molecular rearrangement or a noise in the signal. Section A_2 shows the most significant weight loss and this is attributed to the organic matter decomposition. The weight loss in third section (A_3) is greater at lower heating rates. In this temperature range, illite releases the

Table 6- 2: Compounds targeted in the mass spectroscopic analysis.

Compound	Molecular weight	Compound	Molecular weight
Hydrogen	2	Tetracene	228
Methane	16	Pentacene	278
Water	18	Pentene	70
CO_N_2	28	Hexene	84
H_2S	34	Hetene	98
CO_2_Propane	44	Octyene	110
Ethane	30	Decyelene	138
Butane	58	Heneicocene	294
Pentane	72	Propylbenzene	120
Benzene	78	Butylbenzene	134
Hexane	86	Penthylbenzene	148
Heptane	100	1-butyl-3-ethyl-1,3-cyclohexadiene	164
Octene	112	Hexyl benzene	162
Octane	114	Nanodecane	268
Nonane_Napthalene	128	Tetradecane	198
Decene	140	Tetradecene	196
Decane	142	Tetradecyne	194
Undecane	156	Pentadecene	210
Dodecane	170	Pentadecyne	208
Tridecane	184	Hexadecane	226
Pentadecane	212	Hexadecene	224
Octadecane	254	Hexadecyne	222
Unknown-1	260	Butene	56
Eicosene	280	Butyne	54
Eicosane	282	Heptadecane	240
Heneicosane	296	Heptadecene	238
Toluene	92	Heptadecyne	236
Xylene_Ethylebenzene	106	Unknown-2	298
Anthracene	178		

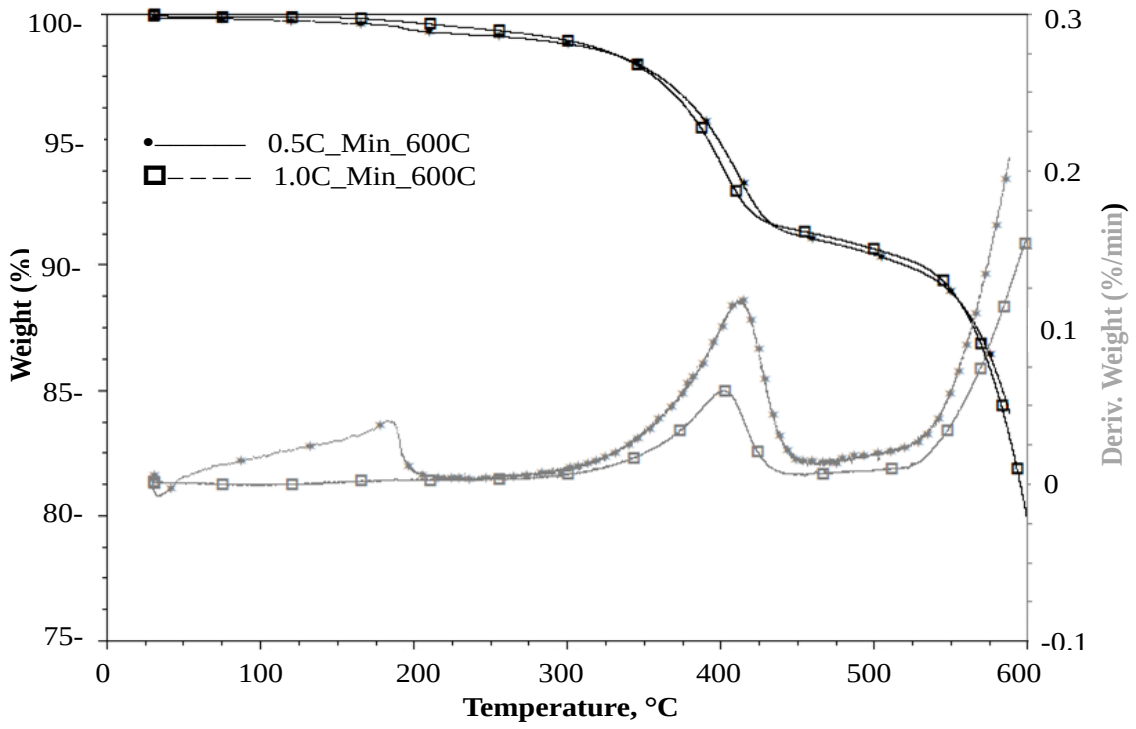

Figure 6- 1: TGA-MS weight loss and derivative curves for the two lower heating rates.

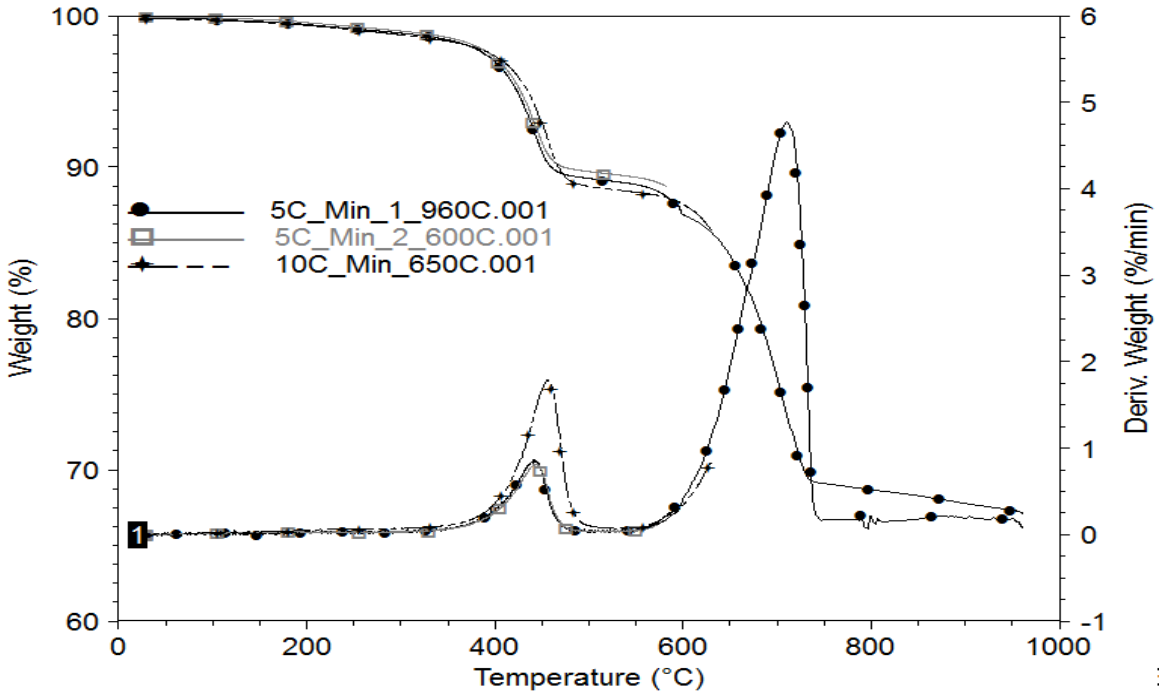

Figure 6- 2: TGA-MS weight loss and derivative curves for the two higher heating rates.

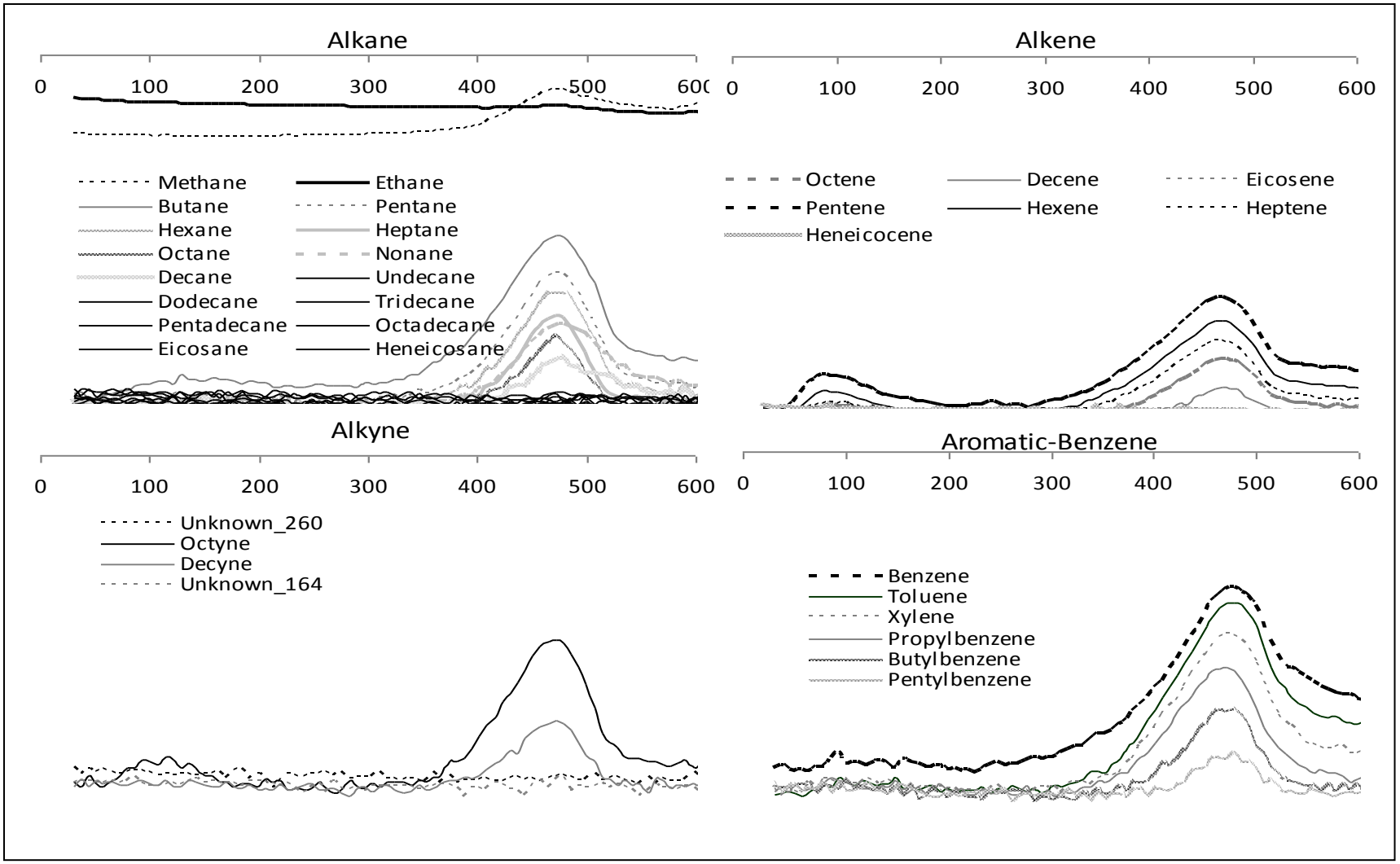

Figure 6- 3: Evolution signals of different types of compounds at a heating rate of 10°C/min.

hydroxyl group which may react with the organic matter. Evolution rates of different compounds were tracked using the ion current signal intensity. The signal intensities of various targeted compounds at a heating rate of 10°C/min are shown in Figure 6-3. Ionic signatures of different compound classes such as alkanes, olefins, alkenes, alkynes, alkyl benzenes and other polyaromatic compounds are shown. It is observed that the lighter hydrocarbons evolve slightly earlier, and their rates of formation are higher. This is consistent with the observation of Oh et al. [95]. The advantage of using the mass spectrometer coupled with the TGA is to be able to evaluate if different compounds found in the product are all being formed at the same time. Traces of different compounds of the same carbon number are superposed on the same plot in Figure 6-4. Benzene signal is compared to that of hexane, while the decane signal is plotted along with the trace for butyl benzene. Hexane arrives slightly ahead of benzene while no significant difference is observed in the evolution patterns of the C_{10} hydrocarbons.

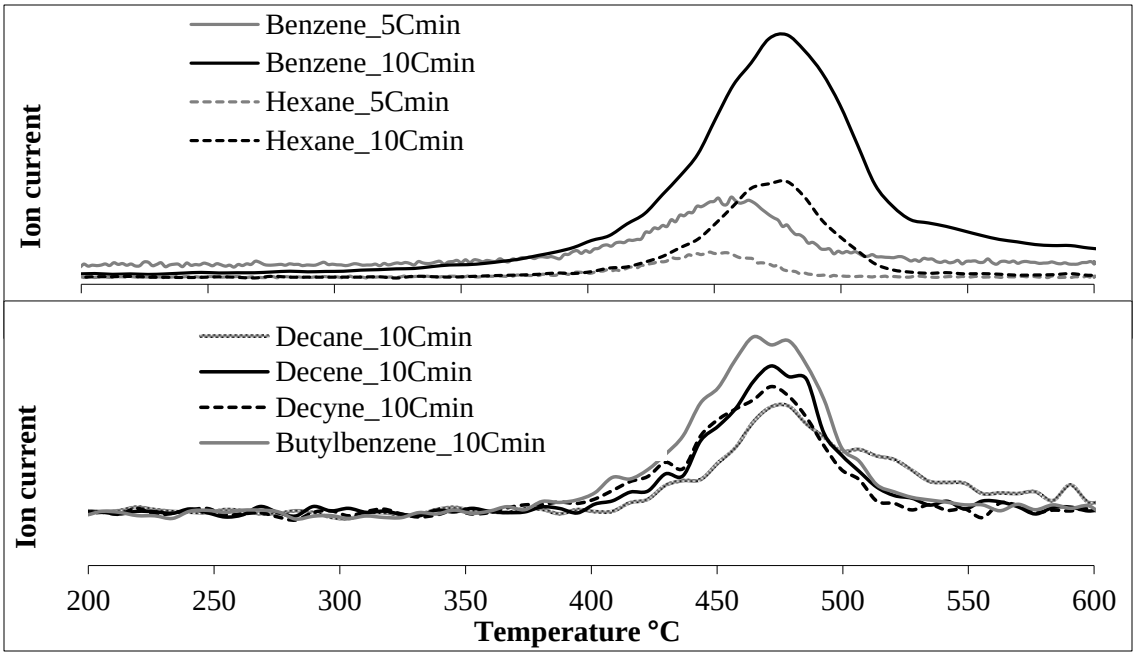

Figure 6- 4: Ion current signals for different compounds of the same carbon number.

Quantification of mass spectrometric signals is challenging because the response factors are not necessarily linear or well known. An approximate quantification approach can be used to compare compositions of the different organic compounds. The areas under each of ion density peaks were integrated to estimate the amounts of each of the constituents. Baseline adjustment was made before the integration was performed. The distribution of products for two heating rates – 5°C/min and 10°C/min are shown in Figures 6-5 and 6-6.

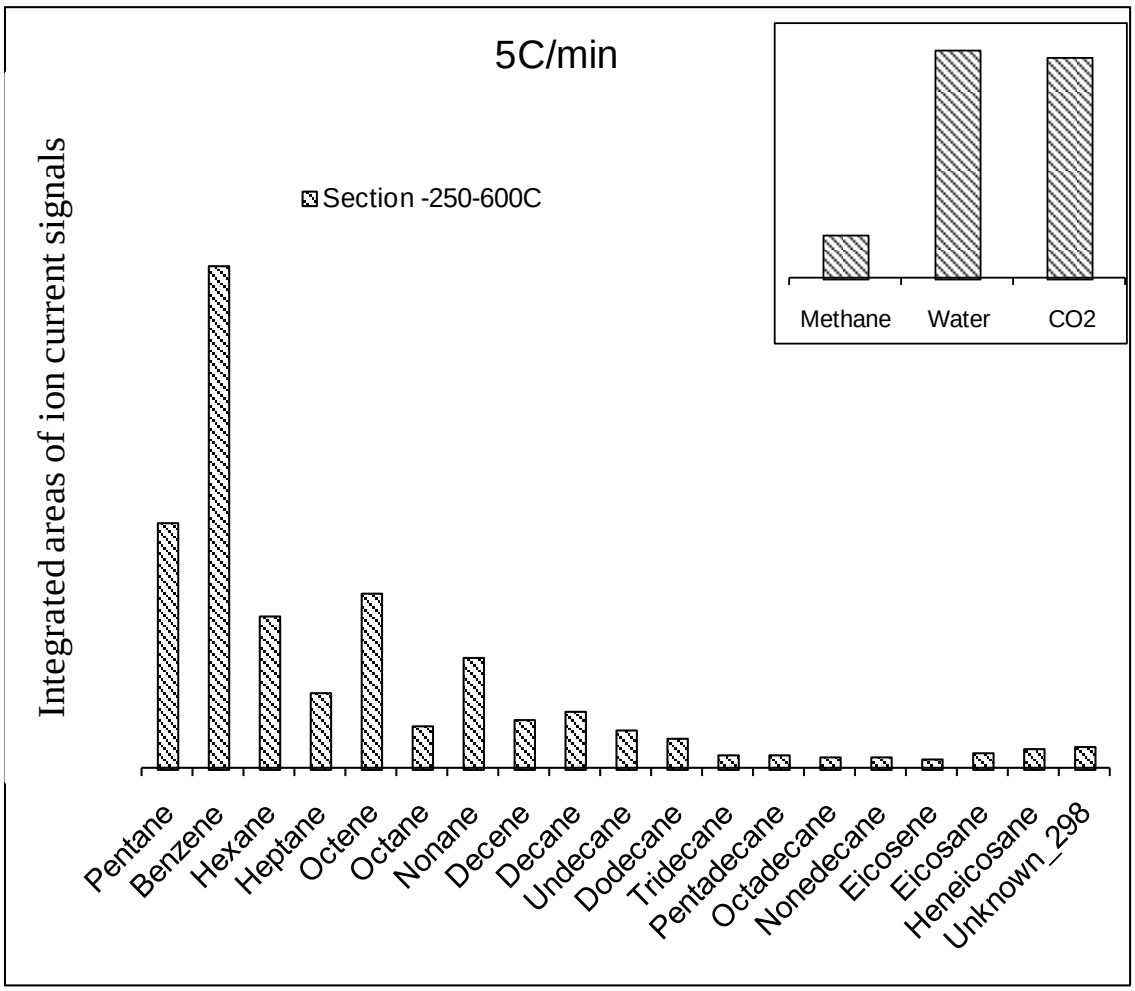

Figure 6- 5: Concentration indices of different species at 5°C/min as calculated from areas of the peaks. The areas cannot be directly related to true concentrations in a mass spectrometer.

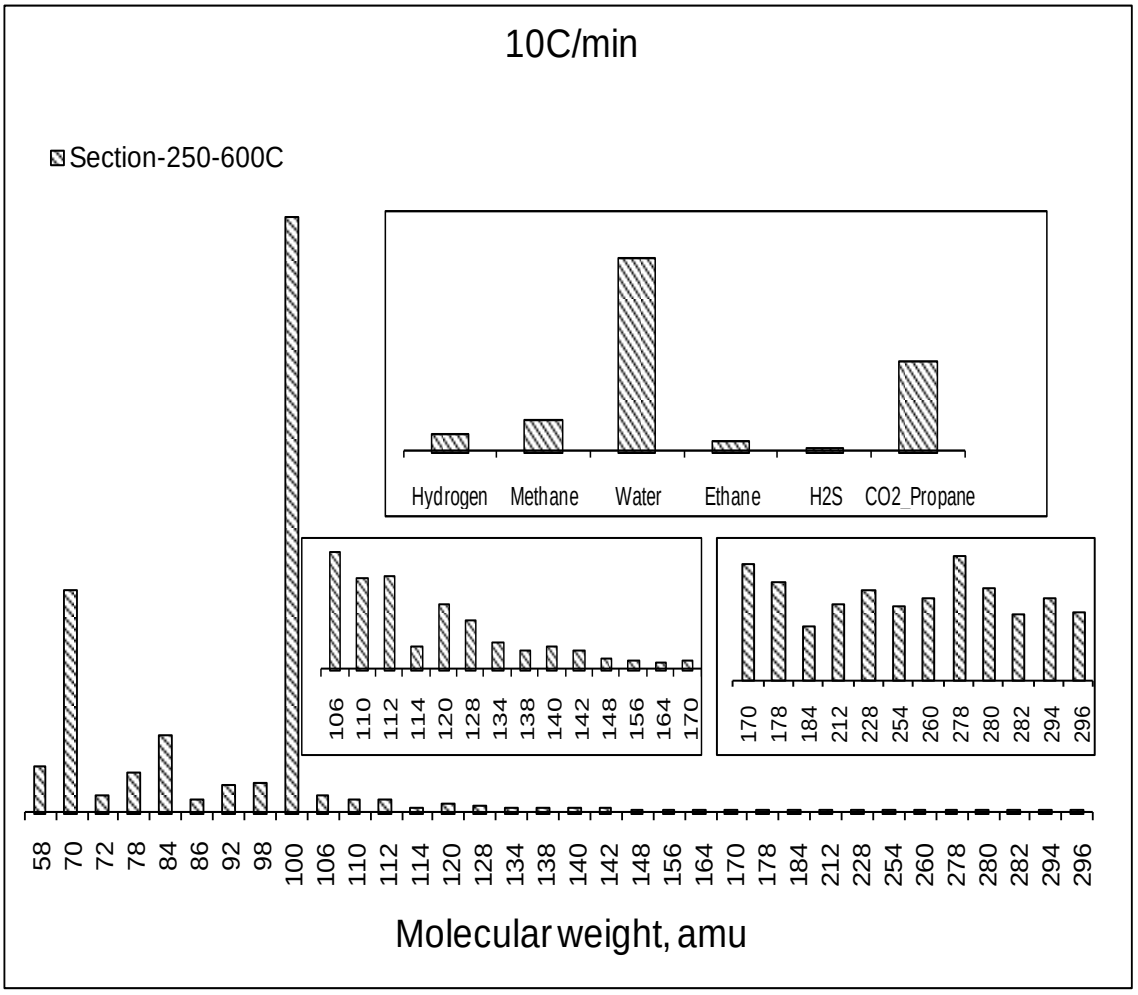

Figure 6- 6: Concentrations of different species at 10°C/min.

Lighter components dominate the distribution at the heating rate of 5°C/min and benzene is a significant portion of the products. In general, the amounts of alkyl aromatics are greater than the alkanes of the same carbon number. The amounts of alkenes are also greater than corresponding alkanes and this is consistent with observations based on gas chromatographic analyses.

In Figure 6-7 ratios of concentrations of different species are compared. The ratio of lighter alkanes to heavier alkanes decreases as the carbon number increases. More benzene is formed than hexane at each of the heating rates. The amount of benzene is

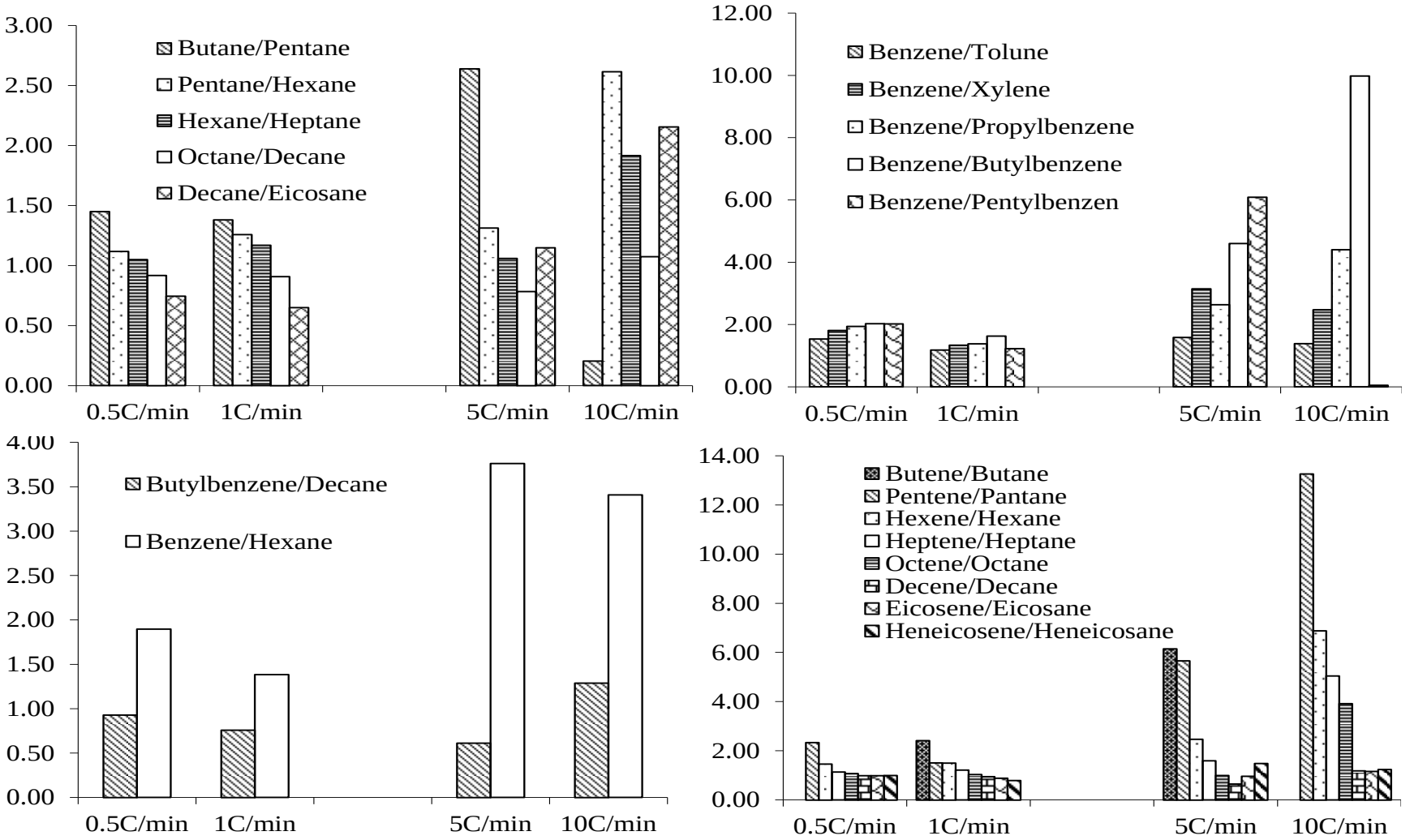

Figure 6- 7: The ratio of relative areas of ion current response for different products under different heating rates.

greater than alkyl aromatics and the ratio of benzene to alkyl aromatics increases with increase in heating rate and the length of the alkyl group. Higher heating rates generate more alkenes compared to respective alkanes and as the carbon number increases this ratio decreases. In general, increase in heating rate produces more light hydrocarbons, more aromatics and concentrations of alkenes increase.

6.2. Derivation of Kinetic Parameters

Advanced isoconversion methods would be appropriate for the analysis of kinetics of decomposition of complex materials like kerogen [69, 150]. This method allows for calculation of distribution of activation energies for multiple reactions involved in the decomposition of complex material like kerogen to products. Tiwari and Deo [148] discussed this method and obtained distributions of activation energies (with conversion) for the decomposition of the Green River oil shale using TGA data. The activation energies were in the range of 93 kJ/mol to 245 kJ/mol. The uncertainties in activation energies were about 10% over the entire conversion range. Identical approach was used to calculate the activation energies as function of conversion using all of the four heating rates. The plot is shown in Figure 6-8. Activation energies were in the range of 92 kJ/mol to 226 kJ/mol and are thus quite consistent with the analysis performed using only the TGA (and with many more heating rates). The uncertainties in the activation energies were in the 10-12% range and also consistent with previous observations [148]. The activation energy of 217 kJ/mole reported by Burnham [99] also falls within this range. The TGA-MS analysis allows estimating kinetics of the formation of the products since the product compositions are being measured as decomposition proceeds. Compounds in the carbon number range C_5-C_{12} were considered to belong to

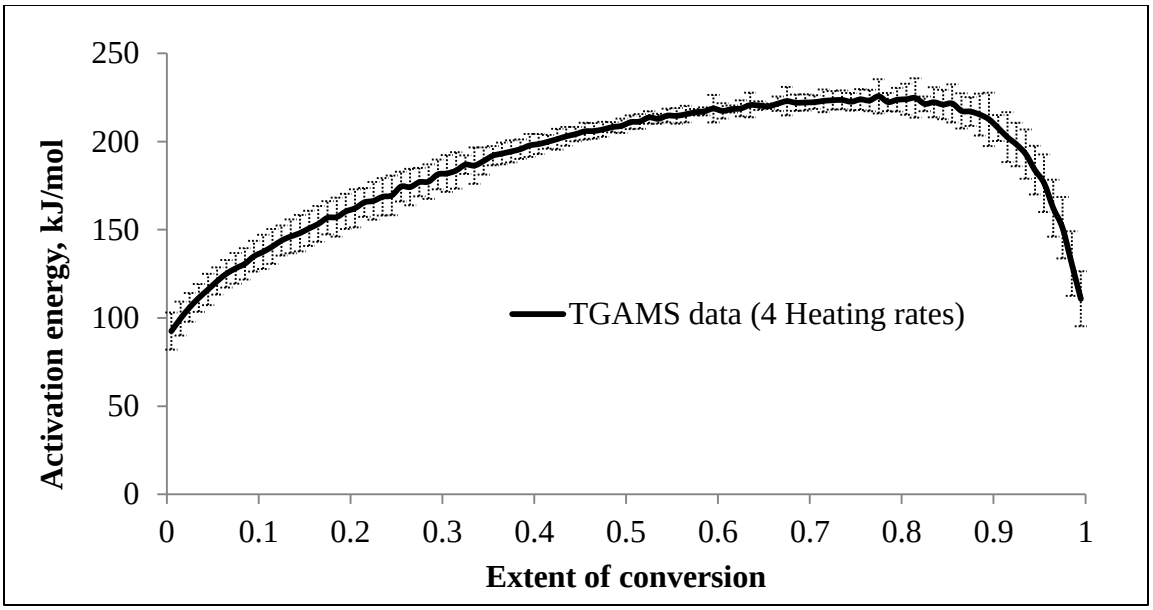

Figure 6- 8: Distribution of activation energy of overall organic weight loss with conversion determined using the TGA-MS data.

the naphtha fraction. The weight loss of shale attributable to naphtha formation is shown in Figure 6-9(a). The TGA-MS data do not provide direct information on the total amount of naphtha that is produced from oil shale pyrolysis. It is known from a number of pyrolysis experiments conducted in the laboratories that about 1.5% to 1.7% of the total weight loss in shale can be attributed to naphtha formation. The naphtha fraction decreases slightly as the heating rate increases. These factors were considered in assigning weight loss attributable to naphtha at the three heating rates considered in this analysis. Once the rate of evolution of naphtha at the three heating rates is established, activation energy of its formation can be derived as a function of conversion using the advanced isoconversional method. The activation energy plot is shown in Figure 6-9(b). The range of activation energies was 41 kJ/mol to 206 kJ/mol. The values over the entire range of conversion are lower in general than values for the overall decomposition. The uncertainty in the activation energy values is higher (~70%) at high conversion values,

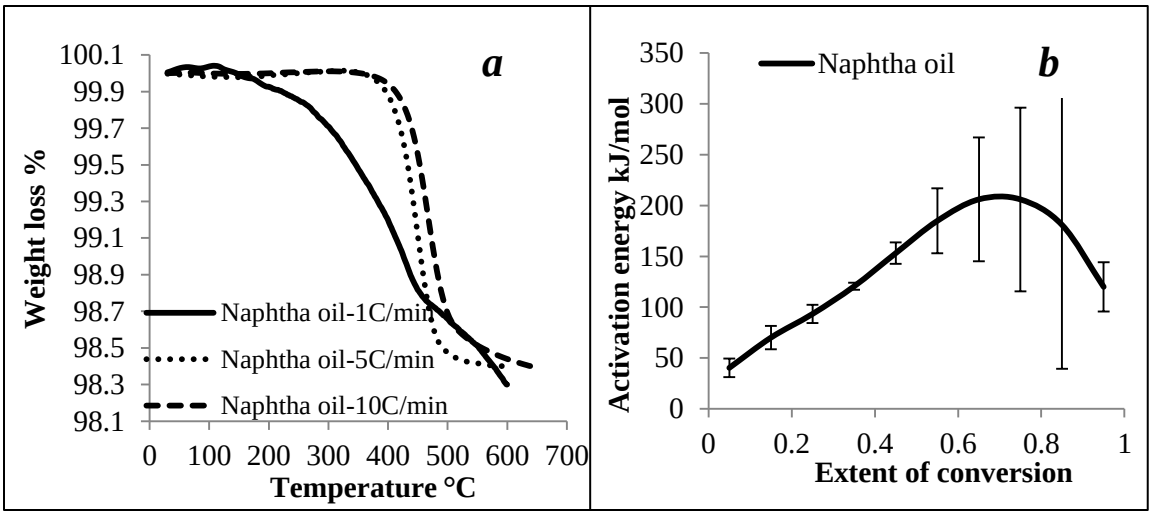

Figure 6- 9: Formation of naphtha, (a) weight loss curves of oil shale leading to the formation of the naphtha fraction and (b) distribution of activation energy for the formation of naphtha.

but below 40% over most of the conversion range. This is because the shape of the weight loss curve at the lower heating rate (1°C/min) is markedly different than the shapes at the other two heating rates. Similar approach was used to obtain kinetics of formation of individual compounds such as benzene (Figure 6-10(a)). The activation energies for benzene formation range from 65 to 175kJ/mol (Figure 6-10(b)). The uncertainty in the activation energy values is even higher for individual compounds due to the variability of their concentrations at the different heating rates. The uncertainty in activation energies is reduced as more than one component is lumped. For example, when the same analysis was performed with the lumped C_8 fraction (Figure 6-11(a)), the data noise decreased significantly (Figure 6-11(b)). The naphtha example shown improved the spread in the kinetic parameters further. When the entire weight loss curve(s) was used in analysis, the uncertainty in activation energies was in the same range as using TGA.

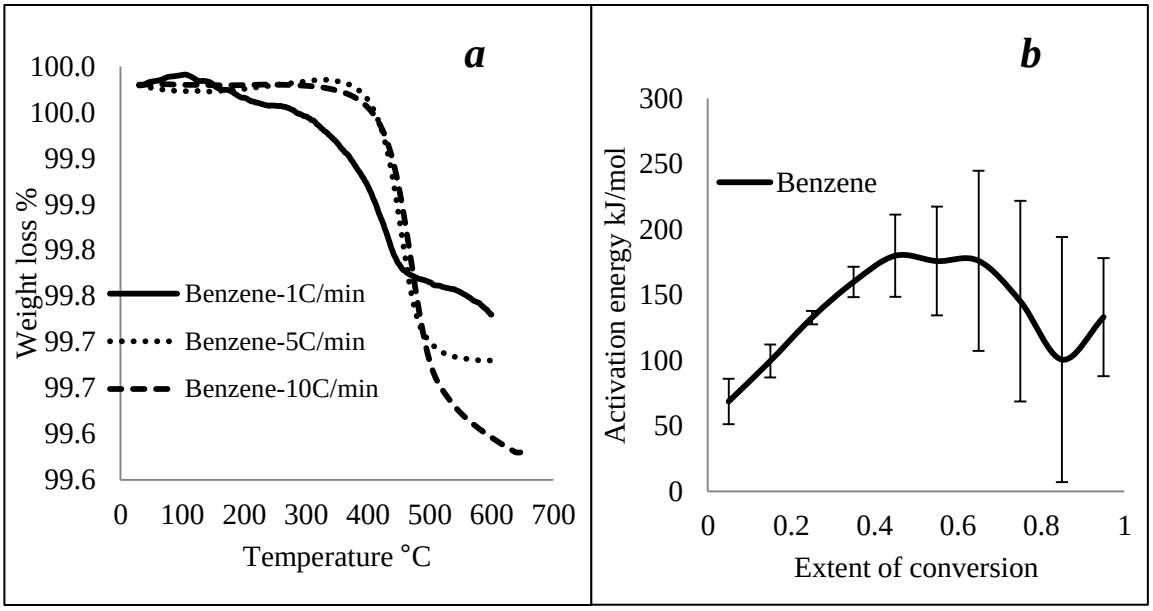

Figure 6- 10: Formation of benzene, (a) weight loss curves of oil shale leading to the formation of the benzene and (b) distribution of activation energy for the formation of benzene.

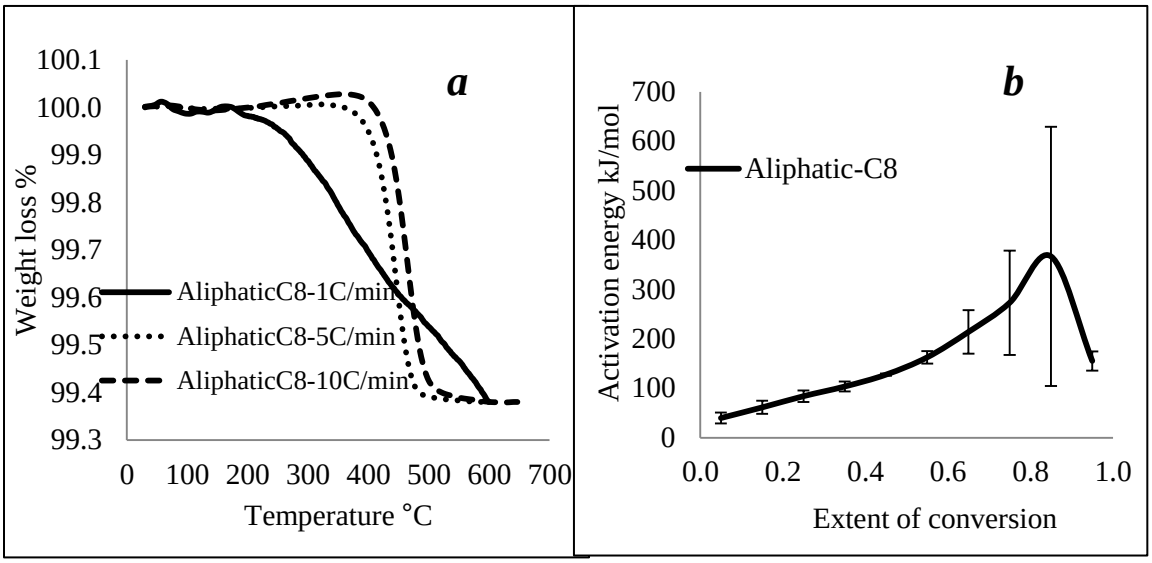

Figure 6- 11: Formation of aliphatic-C_8, (a) weight loss curves of oil shale leading to the formation of the aliphatic-C_8 and (b) distribution of activation energy for the formation of aliphatic-C_8.

7. MULTISCALE PYROLYSIS AND BULK PRODUCT ANALYSIS

The pyrolysis of the grain size samples with TGA provides the weight loss data. The total weight loss is because of the oil and gas formation. The absence of coke in the spent shale reveals that the mass resistance was negligible under ambient pressure pyrolysis of the grain size sample. The pyrolysis of large size sample is constrained due to temperature distribution in the sample. Heat and mass transport influence this process. A large volume of the sample was pyrolyzed to understand these effects and to collect the products for analyses.

7.1. Pyrolysis of Powdered Samples

To understand the effect of operating conditions on pyrolysis at a grain scale, the experiments with powdered oil shale were conducted in batch, pressurized batch, semi-batch, and continuous flow modes.

7.1.1. Batch Pyrolysis of Powdered Samples

Batch pyrolysis is a process in which the products remain in the closed system and participate in the secondary reactions. The batch pyrolysis experiments with sample #1 (PO) were conducted under isothermal conditions at 350°C, 425°C and 500°C in a Swagelok reactor of 1" diameter. The experiments at 500°C were conducted for 30 mins, 12 hrs and 18 hrs. The isothermal experiments at 350°C and 425°C were run for 6 hrs, 12 hrs and 18 hrs. The temperature was controlled from the reactor surface (TC-5) and

recorded (Appendix D). The results of these experiments are summarized in Figure 7-1 and in Appendix C.

Sample #1 (PO) was also pyrolyzed at an initial pressure of 500 psi. Nitrogen gas was used to pressurize the batch unit. The experiments at 350°C and 500°C were conducted for 6 hrs. To observe the effect of process time, two more experiments for 18 hrs at 425°C and 500°C were also conducted. The results from the pressurized batch pyrolysis of sample #1 are summarized in Figure 7-2 and Appendix C. The pressure in the batch reactor increased with temperature and time as a result of the formation of gaseous products. However, the nitrogen in the headspace also contributed for the pressure developed in the system. A large increase in the pressure (2300 psi) was observed in the experiment conducted at 500°C for 18 hrs with an initial pressure of 500 psi.

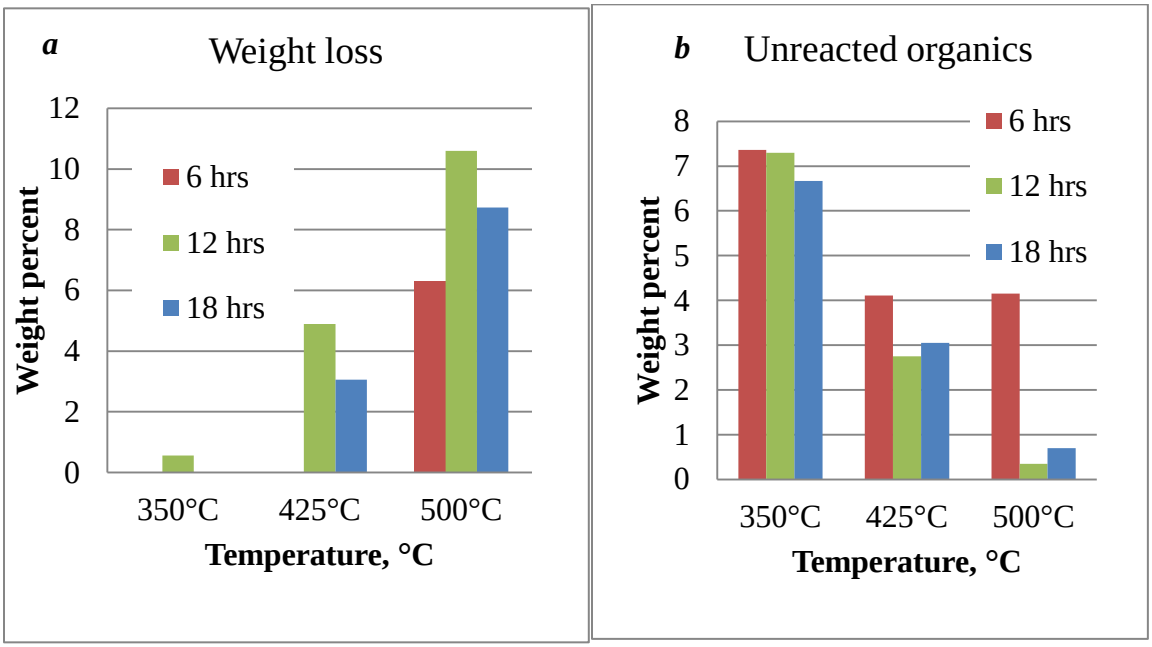

Figure 7- 1: Batch pyrolysis of sample #1, (a) weight loss and (b) unreacted organics during the process. 500°C data for 6 hrs is actually for 30 mins.

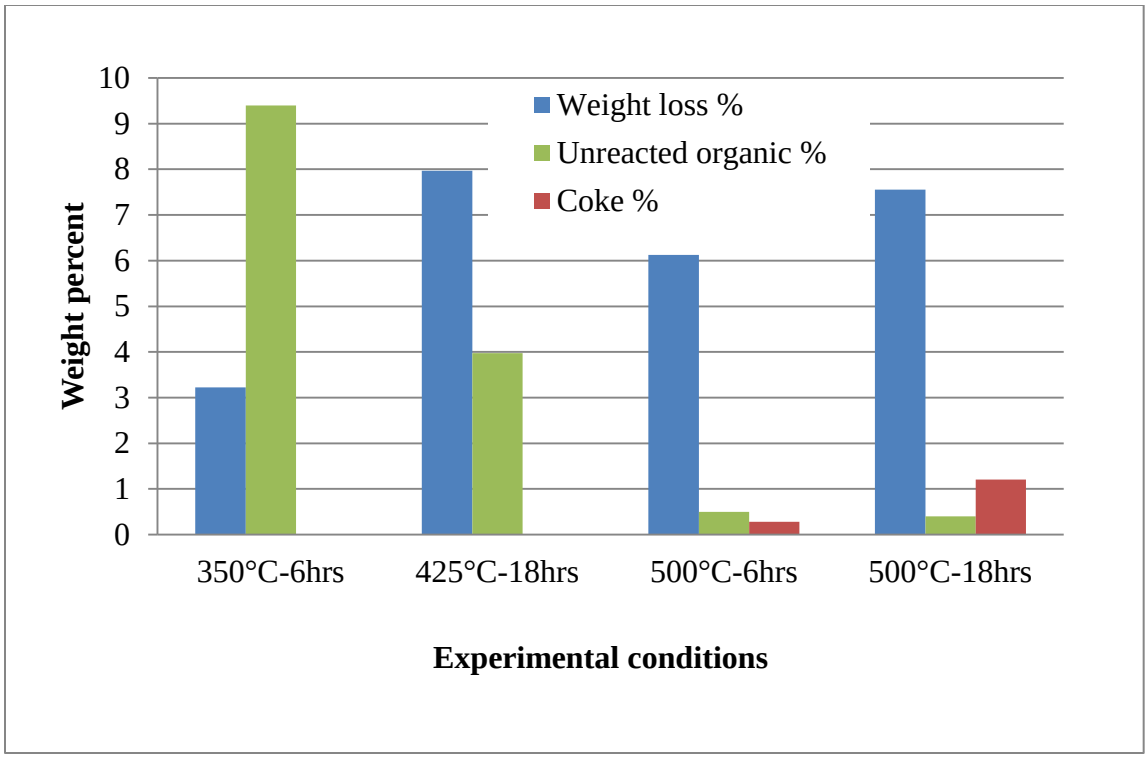

Figure 7- 2: Results from the batch pyrolysis of the sample #1 (PO) under initial pressure of 500 psi.

In batch experiments, the runs for 6 hrs did not yield any appreciable overall weight loss at 350°C and 425°C, while at 500°C a large weight loss (6.2%) was observed. As reaction time increased to 12 hrs, the weight loss increased with an increase in temperature. Further increase in the process time reduced the weight loss. No significant weight loss occurred at 350°C for 18 hrs experiments. However, a small amount of the gases were collected at the end of the experiment. This can be a result of condensation of the products formed at 12 hrs. This reflected in the analyses of unreacted organic portion of the spent shale. There was no amount of coke formed observed in the batch pyrolysis of sample #1 (PO).

In pressurized batch experiments at 350°C and 425°C, a slight drop in the pressure was observed after the temperature stabilized. Plausible reasons for this

observation can be the diffusion of the products into the raw material or condensation of the gases formed. The experiments at 500°C yielded the weight loss and the amount of coke formed. Increasing the reaction time at 500°C resulted in more coke, from 0.28 % for 6 hrs to 1.20 % in the 18 hrs experiments.

A comparison of batch and pressurized batch pyrolysis is shown in Figure 7-3. Weight loss was observed at 350°C for 6 hrs in a pressurized batch experiment. The relationship between weight loss and process conditions showed no definitive effect of the pressure. The results show that the pressurized system produced more coke under the same conditions at higher temperature pyrolysis. Increasing the time reduced the ratio of weight loss to the amount of coke formed during pressurized batch pyrolysis. This also suggests that pressure may also alter the decomposing mechanism rather than the degradation reaction in the oil.

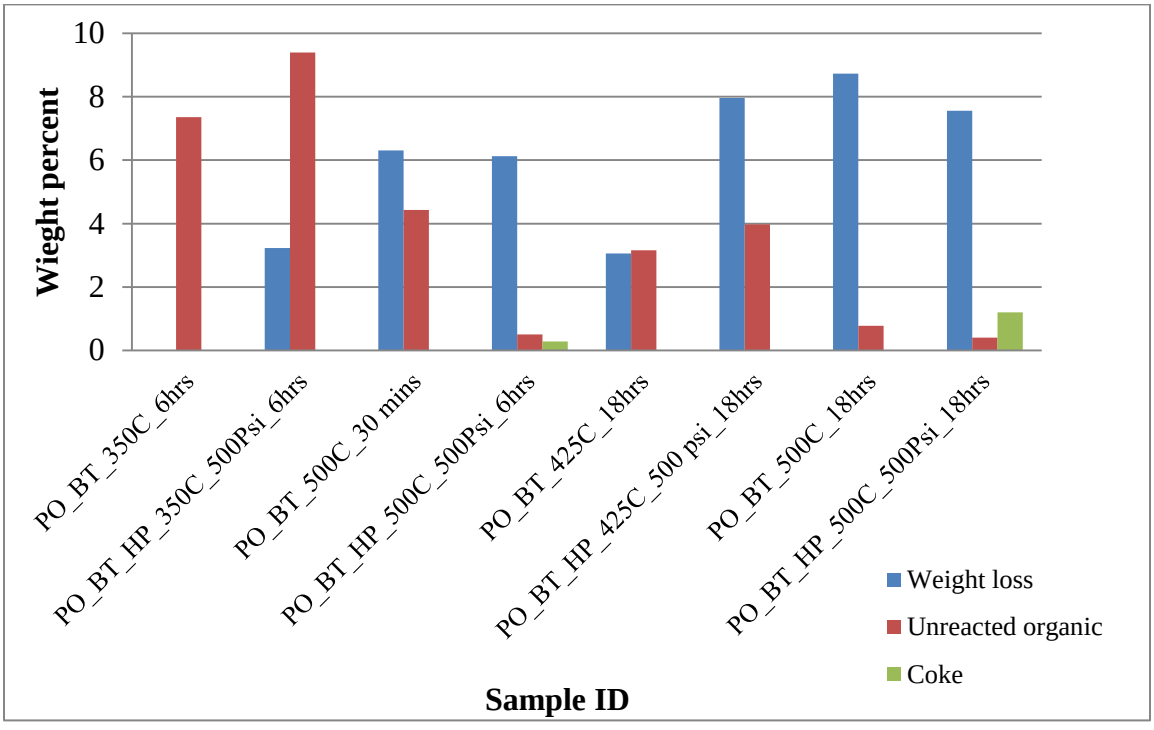

Figure 7- 3: Comparison of the ambient and pressurized batch pyrolysis of sample #1.

There was no free oil that could be collected from the batch pyrolysis of powdered oil shale. The oil produced might have mixed with the spent shale during cooling. The extraction of oil from spent shale was carried out by two methods. In the first method, the known amount of spent shale was mixed with toluene in a closed vial for a week. A ratio of 10:1 for toluene to spent shale was used. Then, the spent shale was filtered and liquid samples collected with toluene were analyzed using GC. The second method, soxhlet extraction procedure, with spent shales at 200°C for 16 hrs was used. The GC analyses on liquid samples collected from soxhlet and solvent extractions did not show any separable peaks. Coke formation was observed after the extraction process despite not observing it in the original experiments and it increased with increase in the pyrolysis temperature.

Pyrolysis temperature, time and pressure showed the significant effects on gaseous product distribution. The weight loss and the volume of gas produced increase with increases in temperature and process time. The distribution of the hydrocarbons in gaseous products depends on the process time and temperature. The batch pyrolysis at 500°C showed a large number of hydrocarbon gases that ranged from C_1 to C_{12}. In pressurized batch experiment at 350°C the distribution of gases shifted to condensable components, up to carbon number C_{14}. It was observed that an increase in the process temperature and time produced lighter gases.

7.1.2. Semibatch Pyrolysis of Powdered Samples

The objective of semibatch experiments was to understand the mechanism(s) of product evolution. An autogenous process in which the products leaves the pyrolysis environment by self-generating pressure [7] was studied.

Sample #1 was used to perform the semibatch pyrolysis. The semibatch pyrolysis experiments were conducted at isothermal temperatures of 350°C, 425°C and 500°C for various length of time. The 500°C experiment for 6 hrs was terminated after 30 min and 350°C experiment for 18 hrs was extended to 24 hrs. These experiments were conducted in a Swagelok reactor of 1" diameter and the evolved products were allowed to escape from the top of the reactor through a condenser into a tedlar bag. The results are summarized in Figure 7-4 and in Appendix C.

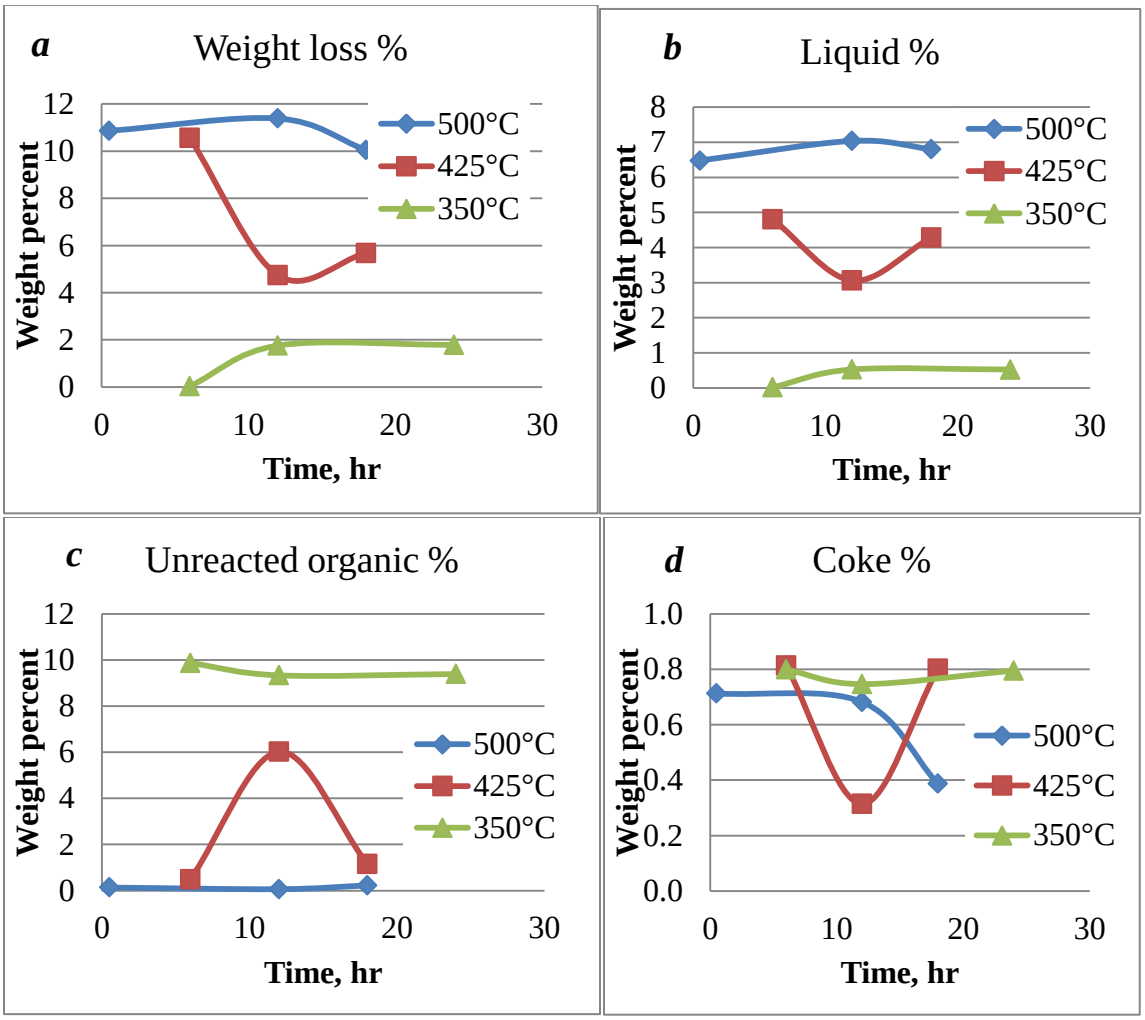

Figure 7- 4: Semibatch pyrolysis of sample #1 at different temperatures and durations, (a) weight loss, (b) oil yield, (c) unreacted organics and (d) amount of coke formed during the process.

The experiments at 350°C showed no significant weight loss after 6 hrs. Weight loss was observed during the 12 hrs experiment and a further increase in the process time (18 hrs) resulted in a drop in the weight loss. A similar trend was observed during the pyrolysis at 500°C when process time increased after 12 hrs to 18 hrs. The experiments at 425°C resulted in a large decrease in weight loss after 12 hrs when compared to the 6 hrs experiment. As the process time increased the weight loss increased but the final value was less than the 6 hrs experiment. The effect of weight loss behavior at 425°C reflected in oil yield and unreacted organics. This may be a result of autogeneous pressure at 425°C which is not enough to sweep the products out of the heated zone and the products were mixed with the spent shale. The percentage of unreacted organics was observed to be higher for 12 hrs pyrolysis at 425°C. An increase in the weight loss increased the oil yield and coke formation. Increase in the temperature reduced the percentage of coke formed. However, these values are within the range of instrument error. The ratio of oil to coke increased with temperature and process time (Figure 7-5). It was observed that at low temperatures the amount of coke formed is higher than the yield of oil. A trace amount of water was also produced in these experiments. The gases produced at 425°C or 6 hrs showed light fractions (C_1 to C_8) while in the experiment at 500°C for 12 hrs it ranged up to carbon number C_{14}.

The results form batch and semibatch pyrolysis of grain size sample suggest that the pyrolysis temperature and process time change the product distribution. Based on these results, it can be hypothesized that the rate of product formation is lesser at low temperature and it increases with temperature. The loosely bound components are released first and then the increase in heat input or time decomposes the tightly bound

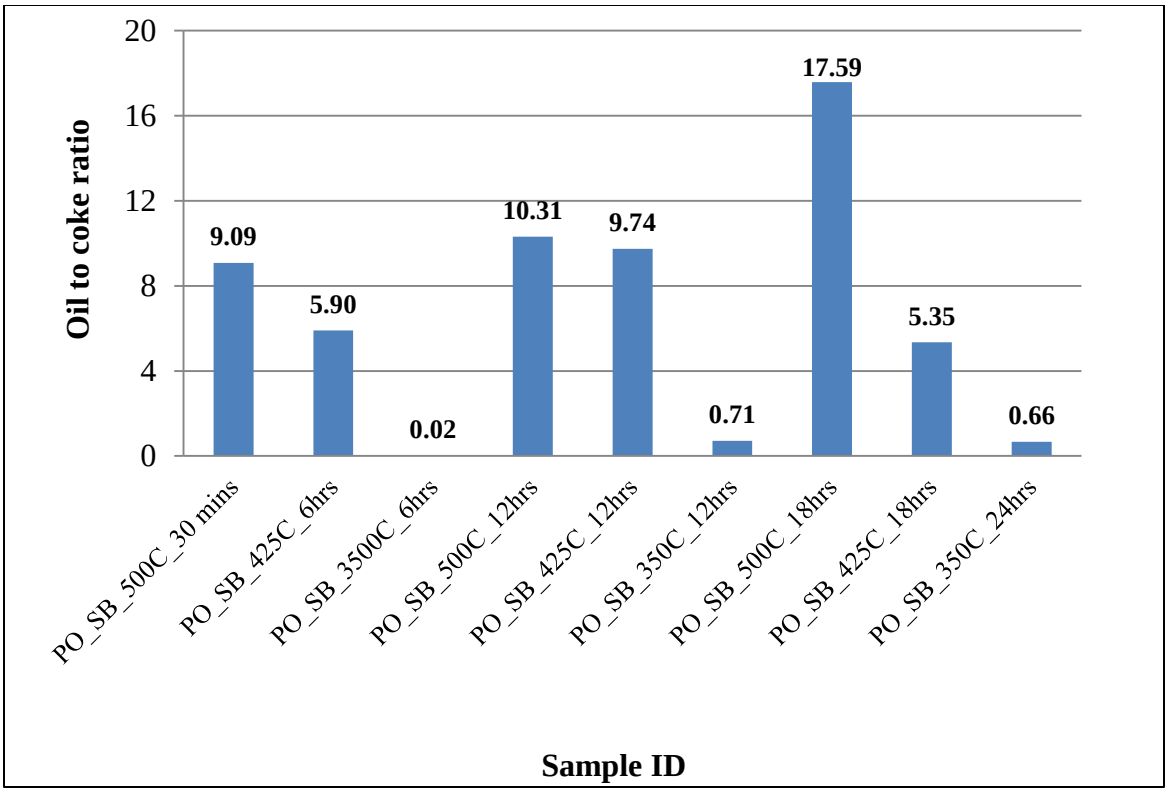

Figure 7- 5: Oil to coke ratio (weight %) during the semibatch pyrolysis of sample #1.

compounds. If the products are not allowed to escape the oil degradation starts. A competitive reaction environment is created and the rate at which the products are formed and their participation in the secondary reactions become important. In the batch experiment for 12 hrs, the weight loss was high while after 18 hrs the weight loss decreased. This may be attributed to the fact that the higher boiling point products were released at 12 hrs and contributed to the weight loss. Since the products remain in the closed system the condensation of the oil during cooling occurred that decreased the weight loss. In the case of the semi batch pyrolysis, the product removal depends on self-generated pressure due to product formation. At low temperature the rate of product formation is low and the products undergo secondary reactions and yield coke and lighter gases.

7.1.3. Continuous Flow Pyrolysis of Powdered Samples

The oil shale sample #1 (PO) was pyrolyzed in a continuous flow environment at heating rates of 1°C/min, 5°C/min and 10°C/min from ambient temperature to 500°C and held at the final temperature isothermally for 2 hrs. The temperature at the center of the sample (TC-1) was used as the mode for controlling the heat input. The products were removed through a constant flow rate of sweep gas from the top of the reactor and were collected at different time intervals. The oil yield during higher heating rate, 10°C/min (12.17%) was more than 5°C/min (5.67%) and 1°C/min (2.85%) experiments (Table 7-1). The distribution of the oil yield produced at different temperature during the heating rate of 10°C/min is shown in Figure 7-6. Maximum amount of oil (6.24%) was produced around 400°C. During the experiment at 5°C/min oil yields of 2.94% and 1.02% were achieved at the process temperatures of 300°C and 400°C, respectively. At lower heating rate the sample was collected at the end of the experiment. The oil yield is higher at higher heating rate as a result of higher product formation rate. At lower heating rate the material/product remains in the heated zone for a longer time which results in higher weight loss and lesser oil yield.

Table 7- 1: Experimental conditions and summary of the results during continuous flow pyrolysis of sample #1 (PO). UO represents unreacted organics and Min denotes minerals in the spent shale analysis.

Sample ID	HR C/min	OS gm	Wt Loss %	Oil Yield	Gas Loss %	UO %	Min %	Coke %
PO_CF_10C/min_500C_2 hrs	10	30.82	12.49	12.17	0.32	1.55	19.23	0.89
PO_CF_5C/min_500C_2hrs_	5	29.29	13.49	5.67	7.81	---	---	---
PO_CF_1C/min_500C_2 hrs	1	28.02	16.63	2.85	13.79	0.42	19.07	---

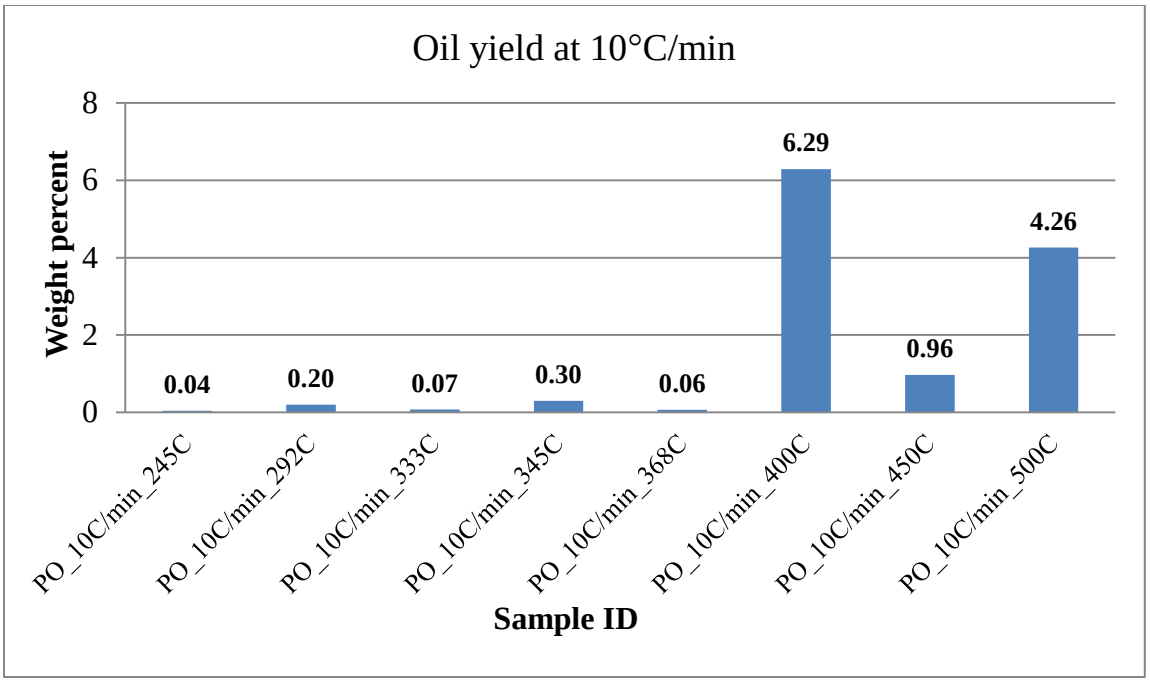

Figure 7- 6: The oil yield at different temperatures during the continious flow pyrolysis of sample #1 (PO) at heating rate of 10°C/min.

7.2. Pyrolysis of 3/4" Core Samples

7.2.1. Continuous Flow Pyrolysis of ¾" Core – Effect of Temperature

The pyrolysis experiments of oil shale core samples (sample #2) of 3/4" diameter at isothermal temperatures, 300°C, 350°C and 400°C, and ambient pressure were conducted. An autoclave Swagelok reactor of 1" internal diameter was used. These experiments were performed for 24 hrs. The temperature at the center of the sample (TC-1) was used as the controlling parameter for pyrolysis. Hence, the temperature across the core was higher than the pyrolysis temperature. The temperature offset was around 50°C-120°C and was higher at high temperature pyrolysis. The liquid samples were collected in two condensers in series at an average temperature of -6°C. The experimental conditions and obtained results are summarized in Appendix C. The effect of the

pyrolysis temperature on weight loss and oil yield is shown in Figure 7-7. The weight loss and oil yield increased with an increase in temperature. The second set of experiments showed relatively lesser weight loss.

Chromatograms of the shale oils are shown in Figure 7-8. The oil produced under the same conditions exhibited reasonable reproducibility in GC chromatograms. The signature of the chromatograms suggested that the oil compositions shift toward lighter carbon numbers as the isothermal pyrolysis temperature increased. The chromatograms were classified and quantified in terms of normal alkanes, non normal alkanes and residue. C_{10} is the sum of up to C_{10} hydrocarbons. C_{50} measures C_{45} to C_{50}, and the last column is a sum of C_{51} to C_{60} hydrocarbons. Figure 7-9 shows the distribution of oil compositions for the first set of the isothermal experiments. The total percentages of both types of alkanes and of residues for shale oils are shown in Figure 7-10.

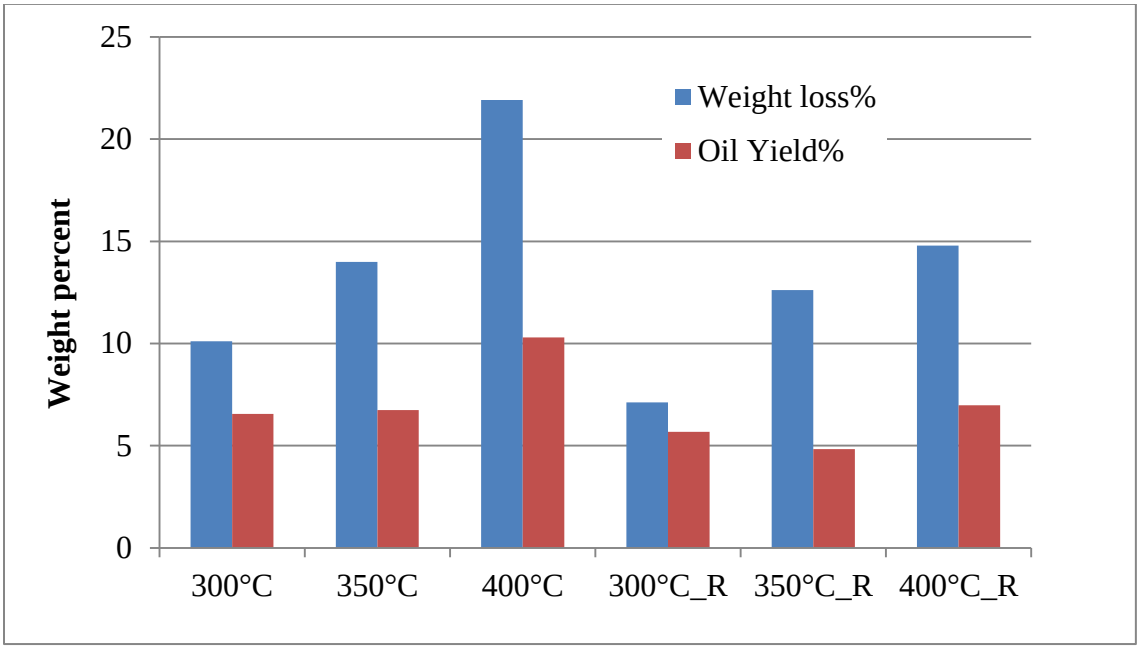

Figure 7- 7: The weight loss percent and oil yield from the isothermal pyrolysis of ¾" core samples. Second set is repeated experiments under the same conditions and denoted as Temperature _R.

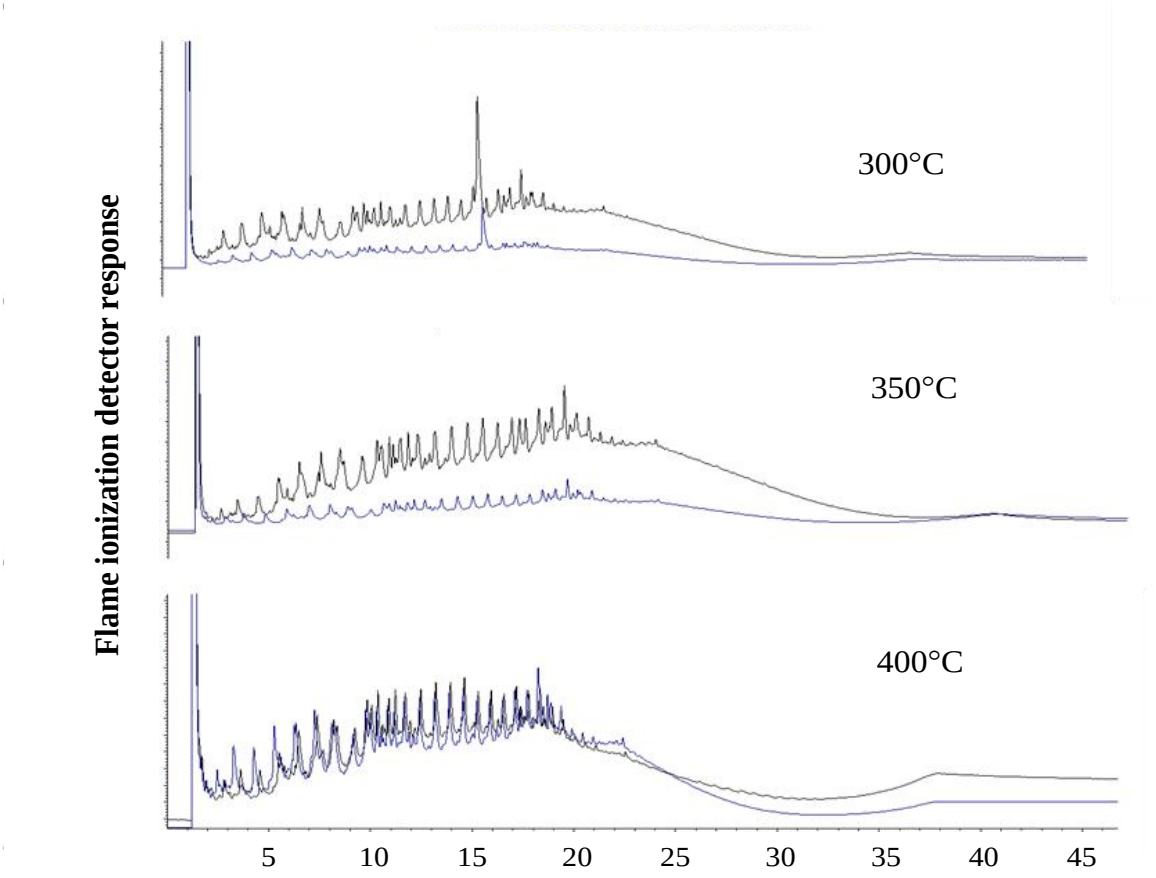

Figure 7- 8: Comparison of the chromatographs for produced oil from pyrolysis of ¾" core samples at isothermal temperatures.

It was observed that alkane to non alkane ratios decreased as temperature increased. This indicates possible secondary cracking and polymerization in the oil phase. The second data set (Temperature_R) shows this trend clearly, while no clear trend was observed in the first set. The second data set also showed that more residue (C60+) was formed with an increase in temperature (13.87%@300^{o}C and 18.07%@400^{o}C). The second set is expected to be a more accurate representation of the compositional trends. The analyses were repeated to verify the trends. It can be concluded that the weight loss and oil yields increase with temperature but producing more residue in the oils. The GC-MS analysis conducted on the shale oils produced from these experiments revealed the

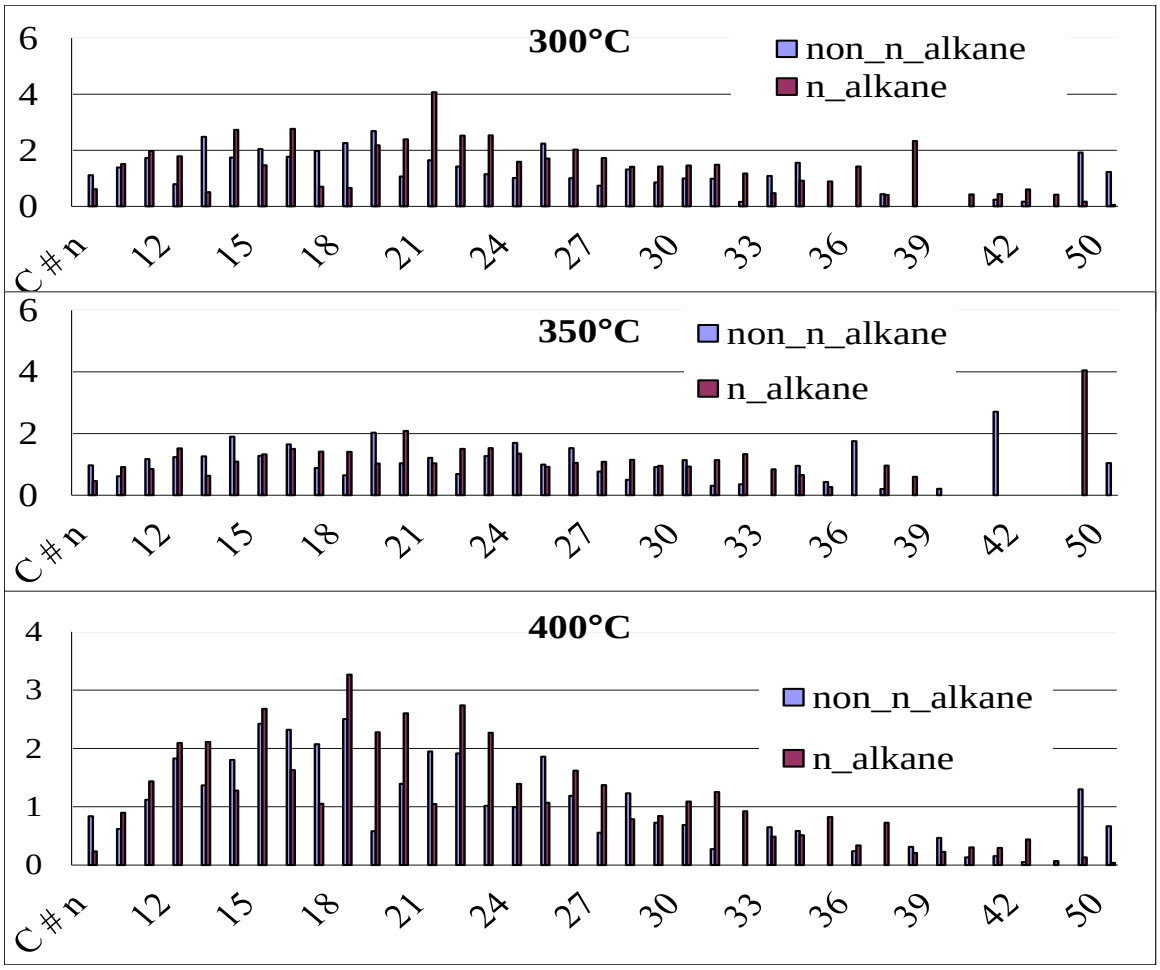

Figure 7- 9: Normal alkanes and non normal alkanes distribution the oil samples. The y axis is weight percent and the x axis is carbon number.

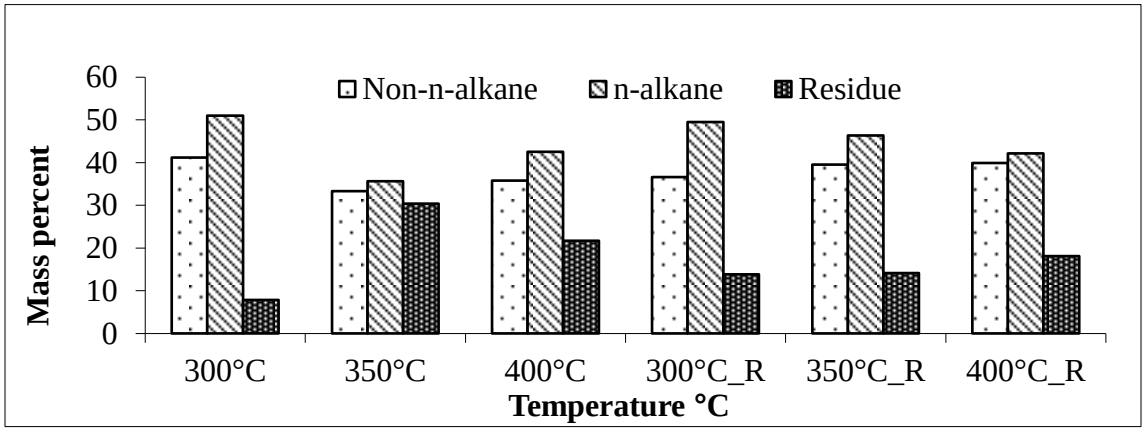

Figure 7- 10: Percent of the total n-alkane, non n-alkane and residue in shale oil samples. The second set is the repeated experiments and denoted by _R.

presence of several hundred components. The components with significant presence in the oil produced at 400°C are listed in the Table 7-2. These analyses showed that the individual alkene to alkane ratio depends on the pyrolysis temperature and no definitive trend was observed with increase in the carbon number and pyrolysis temperature.

The first set of the samples were analyzed in detail. The spent shale analyses of the first set of the experiments are summarized in Table 7-3. TGA pyrolysis followed by the combustion of spent shale showed a significant weight of the organics in the spent shales. This indicates the trapping of the organic matter and shale oil, in the oil shale matrix. The amount of the coke increased with the temperature (6.87% at 400°C). The weight loss at 400°C was higher. This might a result of mineral decompositions during high temperature pyrolysis.

Elemental analyses of spent shales and shale oils are summarized in Table 7-4. The values of the CHNSO elements in spent shales and shale oils of pyrolysis at different temperature were observed to be in the same range (within the range of instrument error). The carbon and hydrogen in shale oils were 80% and 11% respectively. The hydrogen to carbon molar ratio (H/C) shifted from about 1.2 for oil shale to 1.6 for shale oil. The nitrogen content of shale oil was higher than the raw shale. Nitrogen was used as a sweep gas that might have contributed to the amount of nitrogen observed in the oils. The hydrogen to carbon ratio in spent shale had more variability in the range of about 0.2 to 0.7. The percentage of the oxygen increased in spent shale. The possibility of the spent shale oxidation might have contributed to the high oxygen content.

Table 7- 2: Significant compounds identified using GCMS in the oil produced at 400°C.

Library/ID	Area %	Library/ID	Area %
1-Heptene	0.67	2-Decanone	0.37
Heptane	0.80	1-Dodecene	1.64
Toluene	0.40	Dodecane	2.47
Heptane, 2-methyl-	0.35	Undecane, 2,6-dimethyl-	0.99
1-Octene	0.94	Cyclohexane, 2-butyl-1,1,3-trimethyl-	0.60
Octane	1.33	Octane, 2,3,7-trimethyl-	0.97
Cyclohexane, 1,1,3-trimethyl-	1.19	1-Tridecene	1.46
1-Heptene, 2,6-dimethyl-	0.36	1-Octene, 3,7-dimethyl-	1.02
6,6-Dimethylhepta-2,4-diene	1.49	Tridecane	1.96
Benzene, 1,3-dimethyl-	0.36	1H-Indene, 2,3-dihydro-1,1,3-trimethyl-	0.31
1-Nonene	1.23	Naphthalene, 1,2,3,4-tetrahydro-1,1,6-trimethyl-	1.18
Nonane	1.56	Decane, 2-methyl-	0.97
Octane, 2,6-dimethyl-	0.35	2-Tetradecene, (E)-	1.67
Heptane, 3-ethyl-2-methyl-	0.33	Naphthalene, 2,7-dimethyl-	0.76
Benzene, 1-ethyl-2-methyl-	0.30	Tetradecane	2.27
Benzene, 1-ethyl-2-methyl-	0.35	Dodecane, 4-methyl-	2.60
2-Octene, 2,6-dimethyl-	0.65	1-Pentadecene	1.22
Benzene, 1,2,3-trimethyl-	0.32	Pentadecane	2.02
Nonane, 4-methyl-	0.33	1-Hexadecene	1.27
Cyclohexane, 1,2,3-trimethyl-	0.54	Hexadecane	2.76
Benzene, 1,3,5-trimethyl-	0.50	Pentadecane, 2,6,10-trimethyl-	2.06
Cyclopentene, 1,2,3,4,5-pentamethyl-	0.44	Heptadecane	4.07
1-Decene	1.64	1-Octadecene	1.34
1H-Pyrrole, 2,3,5-trimethyl-	0.46	Octadecane	3.12
Decane	2.12	Hexadecane, 2,6,10,14-tetramethyl-	5.34
Benzene, 1,3,5-trimethyl-	1.11	Nonadecane	3.24
1-Decene, 4-methyl-	0.44	Eicosane	3.33
Decane, 4-methyl-	0.53	Heneicosane	3.54
2-Decene, 4-methyl-, (Z)-	0.40	Docosane	3.35
Benzene, 1-methyl-4-(1-methylethyl)-	0.48	Heneicosane	3.34
2-Nonanone	0.36	Tetracosane	2.46
1-Undecene	1.90	Pentacosane	2.62
Undecane	2.35	Hexacosane	2.39
1H-Pyrrole, 3-ethyl-2,4,5-trimethyl-	0.30	Heptacosane	2.64

Table 7- 3: TGA analysis of spent shales from the pyrolysis of ¾" cores (First set).

Temperature	Oil yield %	Weight loss %		
		Pyrolysis_Reactor	Unreacted Organics%	Coke%
300°C	6.56	10.11	3.80	3.77
350°C	6.75	14.00	1.76	3.65
400°C	10.29	21.92	7.54	6.87

Table 7- 4: CHNSO analysis of raw oil shale (OS), spent shale (SS) and shale oil (SO).

Samples	C %	H %	N %	S %	O %	Total	H/C (molar)	O/C (molar)
OS_Core	22.09	2.14	0.65	0.11	16.54	41.53	1.17	0.56
SS_CO_3/4"_400C	13.06	0.21	0.27	0.01	27.99	41.54	0.19	1.61
SS_CO_3/4"_350C	14.10	0.82	0.47	0.02	20.87	36.28	0.70	1.11
SS_CO_3/4"_300C	14.12	0.44	0.26	0.01	25.42	40.24	0.38	1.35
SO_CO_3/4"_400C	80.89	11.10	2.05	0.65	2.13	96.82	1.65	0.02
SO_CO_3/4"_350C	79.91	10.91	2.34	0.62	1.93	95.71	1.64	0.02
SO_CO_3/4"_300C	79.72	10.72	2.34	0.65	2.36	95.79	1.61	0.02

7.2.2. Continuous Flow Pyrolysis of ¾" Core – Effect of Process Conditions

Reactor configurations may interfere with the process parameters. A schematic diagram of simplified setup with less dead volume used for these experiments is shown in Figure 7-11. Core samples (sample #2) of ¾" diameter and ~ 3.5" long were used to study the effects of temperature, pressure and heating rates on the pyrolysis process. Three temperatures, 300°C, 400°C and 500°C, and two heating rates, 1°C/min and 10°C/min, were applied for ambient and 500 psi pyrolysis. The surface temperature (TC-5) was used as a controlling probe for all the experiments. Isothermal experiments were maintained at the final temperature for 24 hrs while nonisothermal experiments were terminated when the temperature reached 500°C. Two temperature measurements, at the reactor surface (TC-5) and at the center of core (TC-1) were recorded (Appendix D).

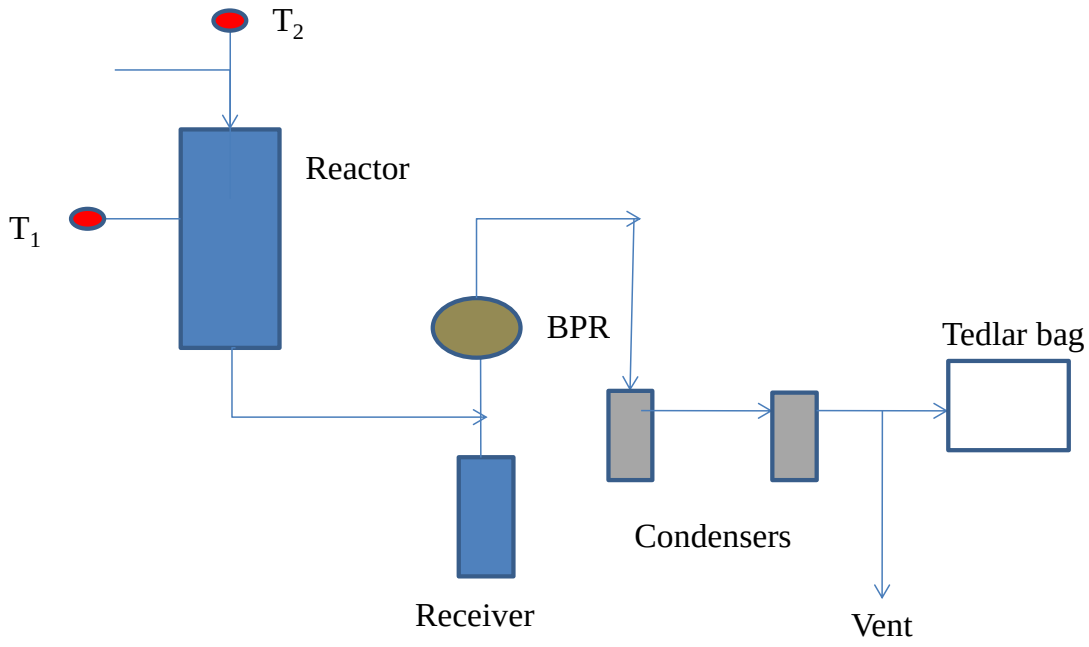

Figure 7- 11: Schematic of the experimental setup for ¾" core pyrolysis.

The liquid product was collected in the metal receiver and vapor products were allowed to escape through the Back Pressure Regulator (BPR) in to a series of condensers. The total liquid collected from the metal receiver and two condensers was used to calculate the oil yield and to analyze the oil composition. The gas samples were collected twice in the same bag to calculate the average gas composition. In the isothermal experiment, gas sampling was done when the temperature reached isothermal conditions and at the end of the experiment. At high pressure, second gas sampling was carried out while depressurizing the system. Gas sampling during nonisothermal conditions was conducted at the end of the experiments, at 1°C/min when the temperature was in the range of 490-500°C, and at 10°C/min when temperature was 450°C-500°C.

Figure 7-12 shows the weight loss (a) and oil yield (b) during isothermal pyrolysis. Figure 7-12 also shows that unreacted organics (c) in the spent shale and the amount of coke formed (b) during the pyrolysis. A similar data set is summarized for

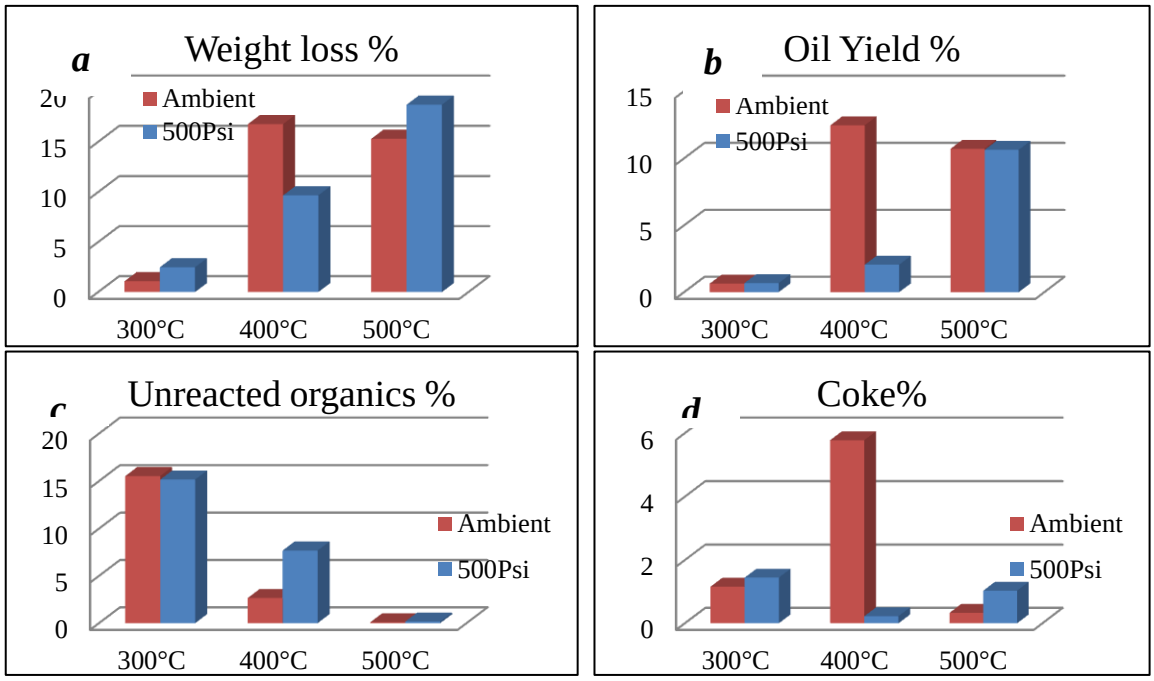

Figure 7- 12: Effect of temperature and pressure: (a) weight loss, (b) oil yield, (c) unreacted organics and (d) amount of coke formed during isothermal pyrolysis of ¾" core.

nonisothermal pyrolysis in Figure 7-13. These results showed that as the temperature increased, the weight loss and oil yield increased. The weight loss and oil yield were lesser and more coke was formed under high pressure compared to ambient pressure at the same temperature. Nonisothermal experiments at heating rates of 1°C/min (~8 hrs) and 10°C/min (~1 hr) generated similar results. The three process factors, temperature, pressure and heating rate, (the fourth is process time) are not additive. Two primary reasons, heterogeneity in the raw material and the effect of the operational parameters influence the results. Within the assumption of homogeneous samples the data showed that 300°C is not high enough to accelerate the reactions, very slow rate of organic decomposition occurred. As the temperature increased to 400°C, organics started decomposing, but do not achieve the complete conversion within 24 hrs. The decomposition of organic matter was complete at 500°C and the products were released.

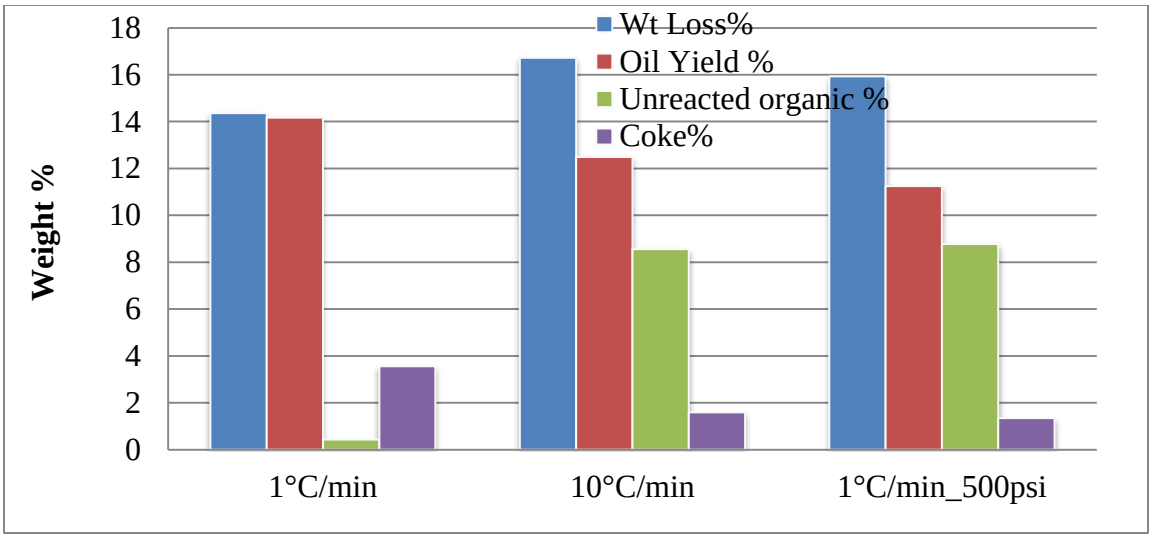

Figure 7- 13: Effect of temperature and pressure on weight loss, oil yield, unreacted organics and formation of coke under nonisothermal conditions.

The oil yield and the amount of coke formed on the basis of weight loss calculations are shown in Figure 7-14. The results showed that the maximum oil yield under high pressure was lesser than the minimum oil yield in ambient pressure during isothermal pyrolysis. The pyrolysis at 300°C and ambient pressure produced more coke than weight loss (fluid products). A clear trend emerges when the data were interpreted in the form of oil to coke ratio. This ratio does not depend on the initial amounts of the organic matter in the sample. Figure 7-15 shows the ratio of the oil to coke produced during the pyrolysis of oil shale at different conditions. This ratio increases as the temperature increased in both ambient and pressurized experiments. Increase in the heating rates also increased this ratio. The effect of heating rate and pressure exhibited a reverse trend. It was also observed that at 400°C (both, ambient and high pressure pyrolysis) the unreacted organic material in the spent shale decomposes at a faster rate and at a lower temperature. This indicates that the organic matters become softer during pyrolysis at 400°C but could not be released from the core matrix (Figure 7-16).

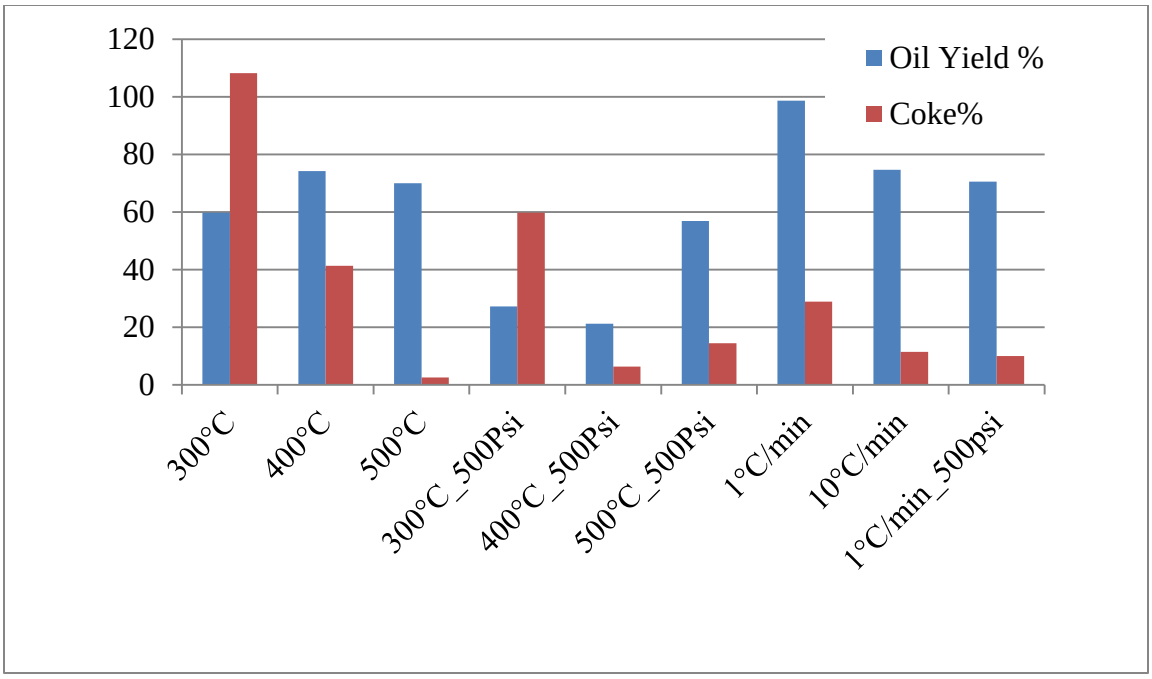

Figure 7- 14: Effect of temperature, heating rate and pressure on distribution of organic matter in oil yield and coke. The calculation is based on weight loss.

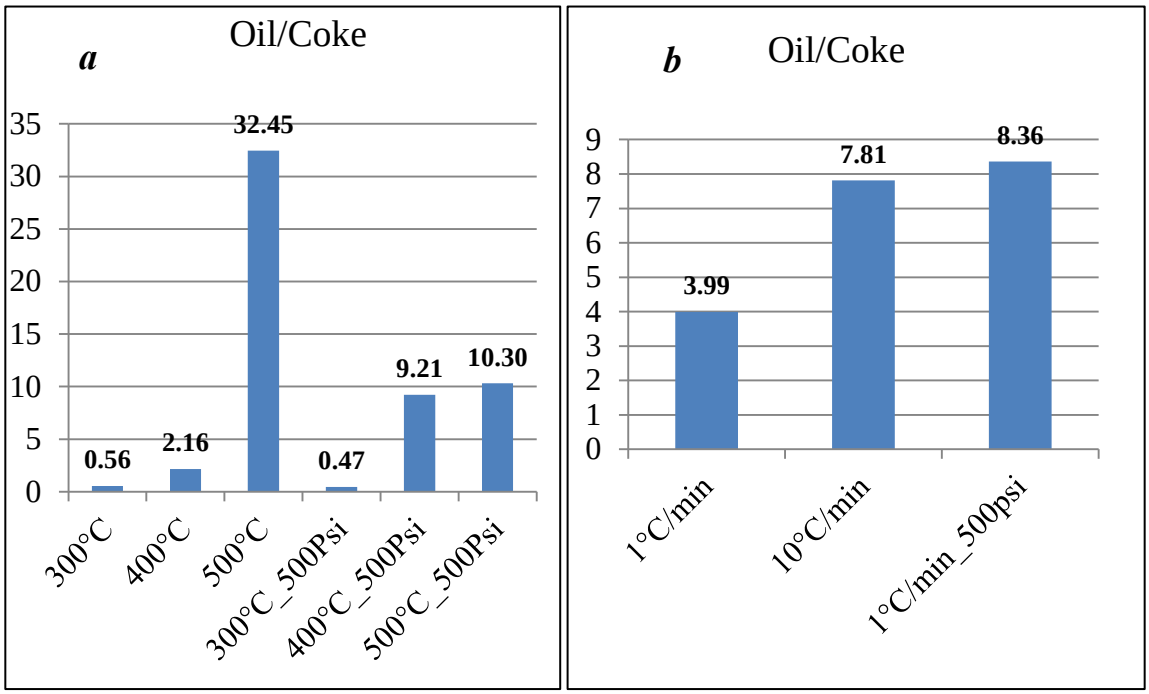

Figure 7- 15: The ratio of oil to coke during core pyrolysis (a) isothermal and (b) nonisothermal conditions. The y axis is ratio of oil to coke and the x axis is sample ID.

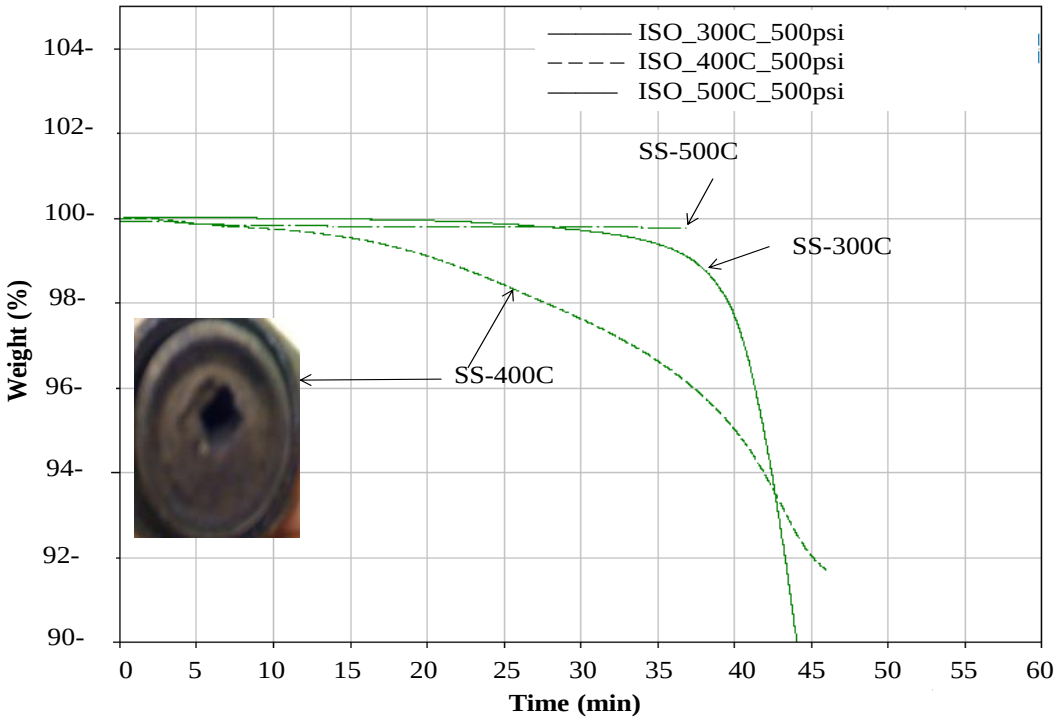

Figure 7- 16: TGA analysis of the spent shale from the pyrolysis of ¾" core under isothermal temperatures, 300°C, 400°C and 500°C, and 500 psi pressure.

Overall, the results suggest that high temperature, higher heating rate and lower pressure favor more oil yield. High pressure may alter the reaction mechanism and also increases the residence time of the products in the heated zone. At low heating rates and high pressure, the sample spends more time in the heated zone and the products participate in secondary reactions-coking and cracking. Cracking produces lighter products, while high temperatures generate more coke. In isothermal conditions the oil yield is higher in ambient pyrolysis compared to elevated pressure at the same temperature and increase in temperature increases oil to coke ratio. Lower heating rates produce less oil compared to coke than higher heating rates. A counterintuitive trend was observed under high pressure in nonisothermal heating; the ratio is higher under pressure than ambient conditions at heating rate of 1°C/min.

Figure 7-17 shows the gas chromatograms for the oil produced at two different conditions. The chromatograms showed that though the signature of the peaks coincide, the relative amount changes. An assumption that the entire injected sample was eluted out from the GC column was applied and the peak area of different hydrocarbons was used to produce single carbon number (SCN) distribution for the oil samples. The SCN of the oil samples are shown in Figure 7-18. The oils produced from different conditions ranged from hydrocarbon number C_9 to C_{40} and the compositional variation is large. Increase in pyrolysis temperature produces lighter products and the carbon numbers also shift towards higher boiling point hydrocarbons. Similar SCN distribution was found in elevated pressure experiments under isothermal and nonisothermal conditions. High pressure increases the residence time of the evolved products and secondary reaction are responsible for this shift in SCN distribution. Increase in the heating rate produces heavier hydrocarbons. The product evolution rate is higher under high temperature pyrolysis. Further, the SCN distribution was classified in three grades of fuel, naphtha (C_7-C_{12}), middle distillate (C_{13}-C_{20}) and fuel oil (C_{21}-C_{47}). The classified grades of hydrocarbons in oil sample are shown in Figure 7-19. The combined effect of the parameters on oil quality showed that higher temperature and higher pressure produce more naphtha grade oil and the lower heating rate and higher pressure produce more middle distillate. The amounts of the grades of oil sample may change slightly depending on the residue present in each oil sample.

Gas samples were analyzed with two detectors TCD and FID in series. The chromatograms response of TCD and FID showed the presence of different hydrocarbons and nonhydrocarbons in the gas samples collected during pyrolysis.

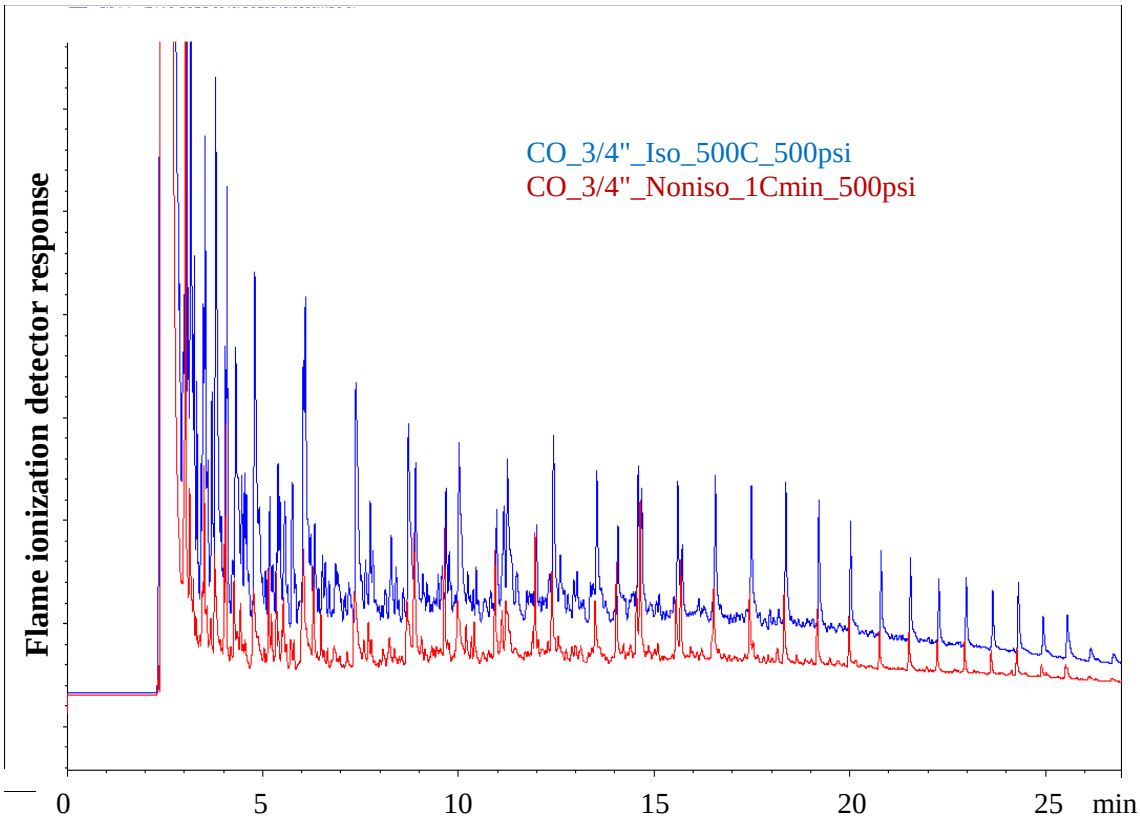

Figure 7- 17: Chromatograms of the oil produced at pressure of 500 psi during isothermal at 500°C (Blue) and nonisothermal at 1°C/min experiments.

The ratio of condensable (C_4+) and noncondensable (C_1-C_3) gases were used to compare the results. Figure 7-20 shows the ratio of the hydrocarbon gases. Higher temperatures and ambient pressure produce more noncondensable gases while higher pressure, higher heating rate and high temperature produce more condensable gases. During the nonisothermal experiments, the gas samples were collected over different temperature segments and that affects the compositions. A large peak for CO_2 was observed in all the gas samples.

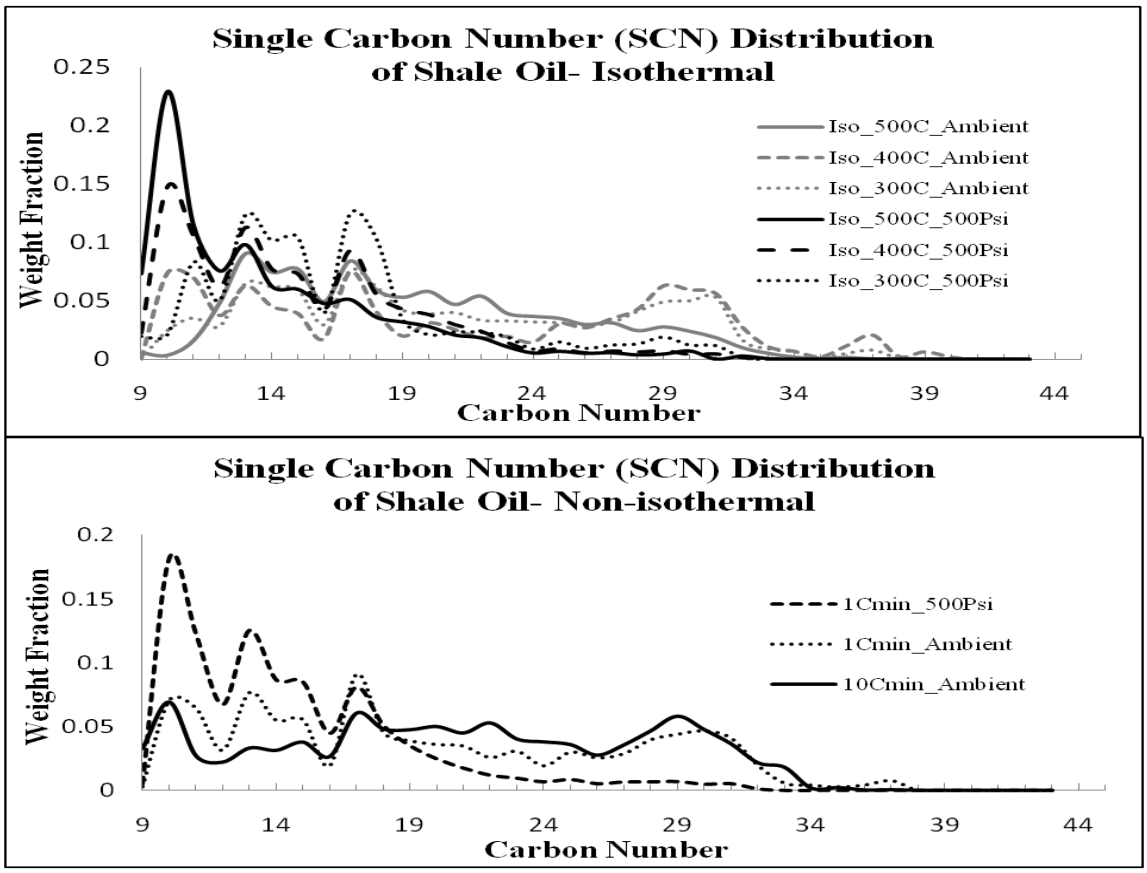

Figure 7- 18: Single carbon number distribution of the shale oils produced under different conditions.

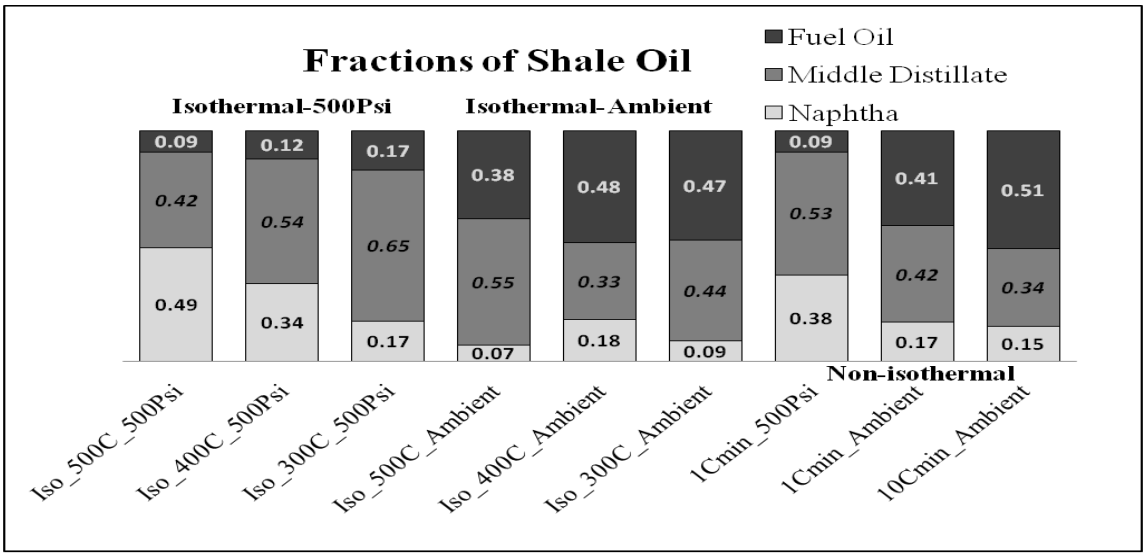

Figure 7- 19: The representation of SCN distribution in oil fractions. It is assumed that 100 % oil eluted from GC (pseudo SIMDIS analysis).

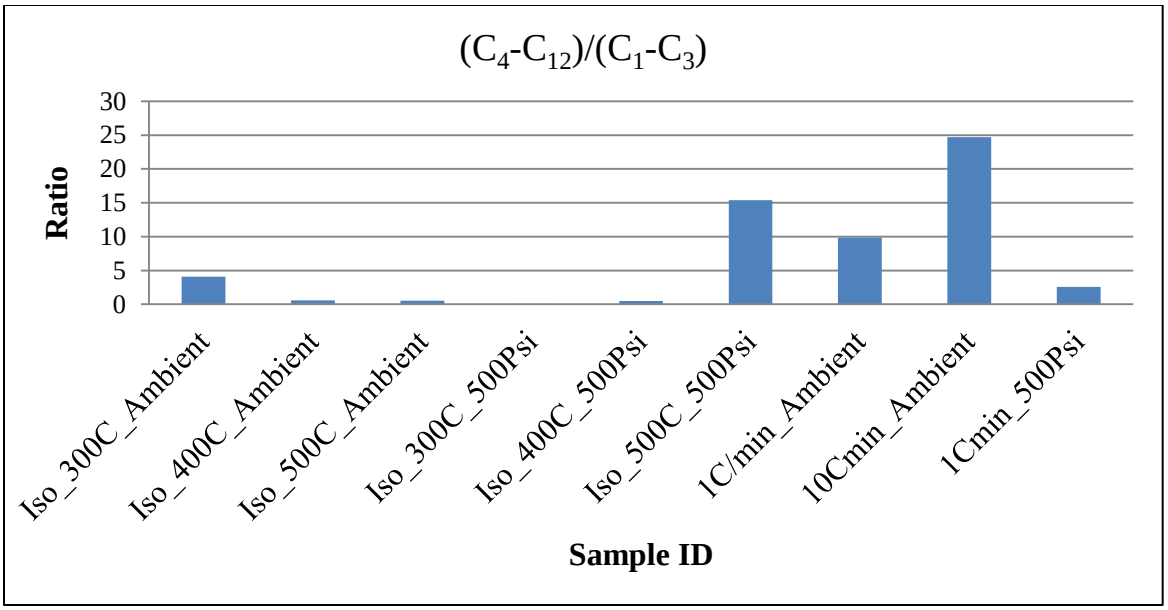

Figure 7- 20: Ratio of the amount of condensable and noncondensable gases evolved at different experimental conditions.

7.3. Pyrolysis of 1" Core Samples

Nonisothermal pyrolysis experiments of 1" core (Sample #2) were performed in a Flange reactor of 1.25" internal diameter under ambient pressure. The reactor surface was heated at rates of 1°C/min, 5°C/min and 10°C/min to 500°C and held isothermally for 2 hrs. The experimental conditions and results are summarized in Table 7-5. The temperature difference between the core center (TC-1) and the reactor surface (TC-5) increased with the heating rates (Appendix D). At 1°C/min the difference was 30°C and at 10°C/min it was 120°C.

Table 7- 5: Summary of the nonisothermal pyrolysis of 1" core oil shale samples.

Sample ID	HR °C/min	OS gm	Wt. Loss %	Oil Yield	Oil Yield/Wt. Loss%
CO_1"_1C/min_500C_Ambient_2hrs	1	145.08	15.34	8.76	0.57
CO_1"_5C/min_500C_Ambient_2hrs	5	144.46	13.50	8.20	0.60
CO_1"_10C/min_500C_Ambient_2hrs	10	145.32	10.41	7.66	0.73

The liquid samples were collected in the receiver and in the condenser. The amount of the liquid collected in the condenser was higher than the amount in the receiver at the same temperature. The distribution of oil yield at 1°C/min with temperature is shown in Figure 7-21. The oil yield was maximum at 450°C. The experiment at heating rate of 5°C/min produced the oil at 480°C. While in the experiment at 10°C/min the oil formation occurred at the end of the experiment where the reactor was held at 500°C for 2 hrs. Oil amount of 1.37% and 4.29% were collected in the receiver and condenser during the experiment at 5°C/min. At 10°C/min the oil yield in the condenser was 5.12% and 0.94 % in the receiver.

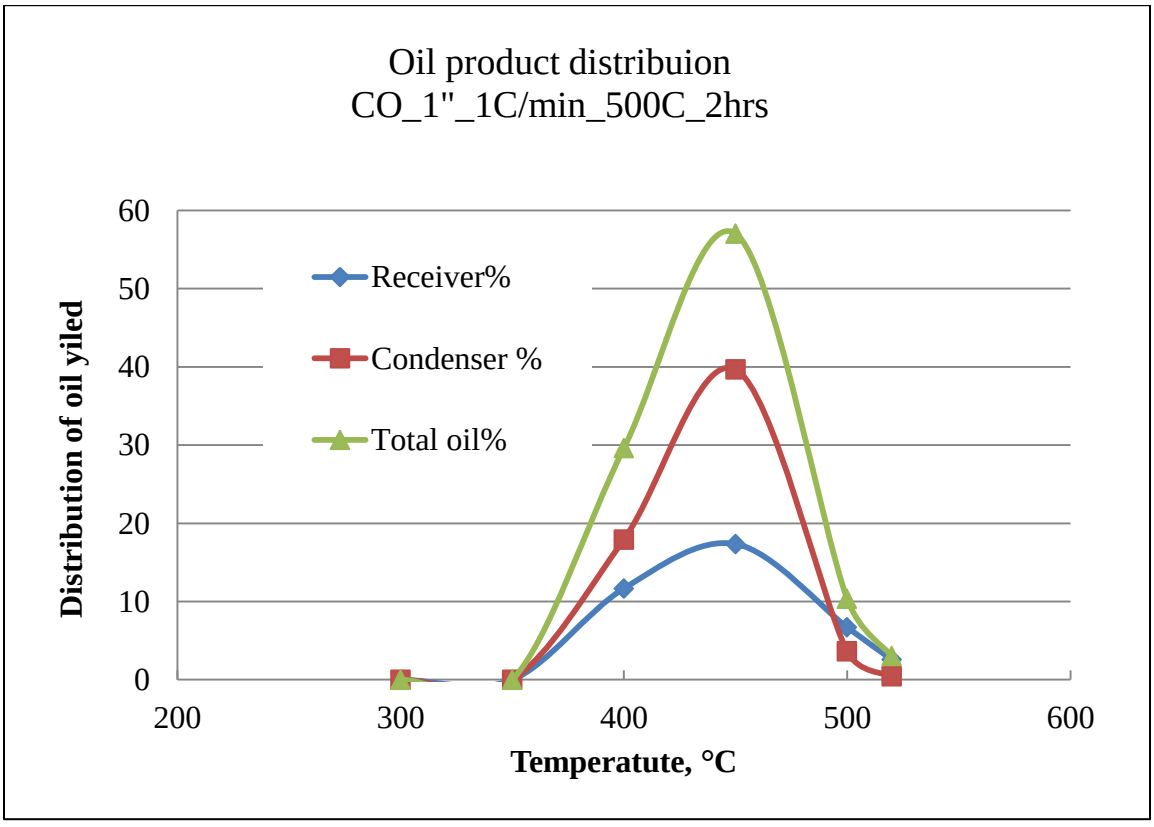

Figure 7- 21: The yield of the oil produced at different temperatures during the pyrolysis of 1" core (sample# 2) at 1°C/min. The data after 500°C point are for isothermal hold time (2 hrs).

The results from these experiments indicate that the temperature of oil formation increases with an increase in the heating rate. This is in agreement with the TGA analyses. However, some gaseous products were observed in the samples collected at 300°C during different heating rates. It was observed that increasing the heating rate reduces the weight loss and correspondingly the oil yield. Less process time at higher heating rates would be a plausible reason for this. The ratio of oil yield to weight loss increased with an increase in heating rate. At higher heating rates, the product formation rate is higher, which favors higher oil yields. Similar trend was also observed with powdered oil shale (section 7.1.3) and ¾" core sample (section 7.2.2).

Gas chromatograms of the oil samples collected at different time intervals in the condenser and receiver showed a large variation in the carbon number distribution. Chromatogram signatures for the hydrocarbon compounds in the oil samples were translated into single carbon number (SCN) distribution. The SCN distribution was further classified into oil grades. Figure 7-22 shows the distribution of oil grades for the liquid products collected at different temperatures (conditions) during the experiments at the heating rate of 1°C/min. A similar representation for the experiments at heating rates of 5°C/min and 10°C/min is shown in Figure 7-23 and 7-24, respectively. The oil samples collected at low temperatures (early in the process) were lighter than the oil samples collected at higher temperature. The oil collected in the receiver was thick and composed of higher hydrocarbon compounds. The oil produced at heating rate of 1°C/min was naphtha grade dominant. At the heating rates of 5°C/min and 10°C/min the distribution shifted to heavier hydrocarbons and the results at these heating rates showed no major difference. Small amount of fuel grade oil was found inside the reactor.

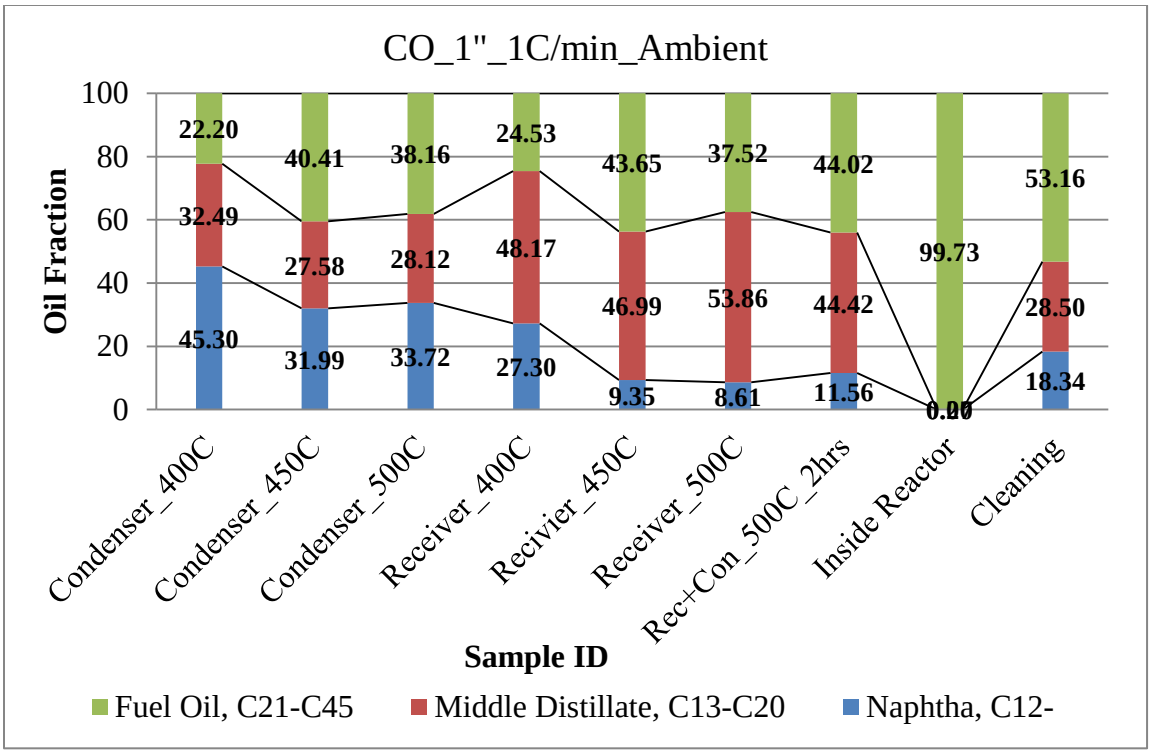

Figure 7- 22 : Grade of the oil samples collected during the pyrolysis of 1" core (sample #2) at heating rate of 1°C/min.

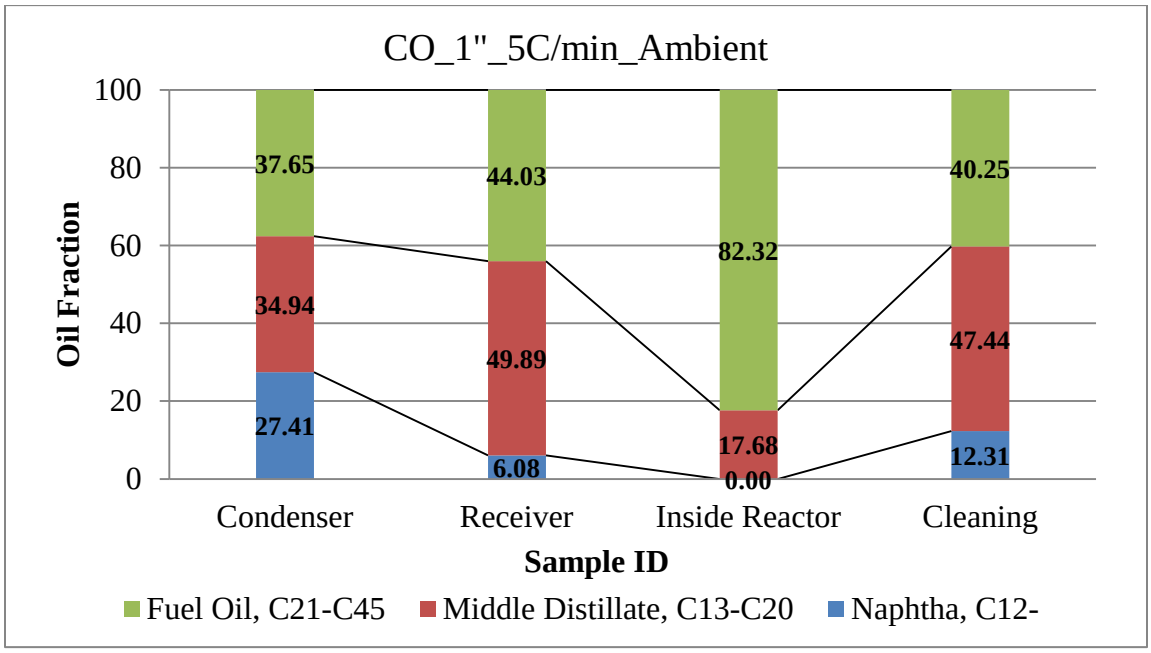

Figure 7- 23: Grade of the oil samples collected during the pyrolysis of 1" core (sample #2) at heating rate of 5°C/min.

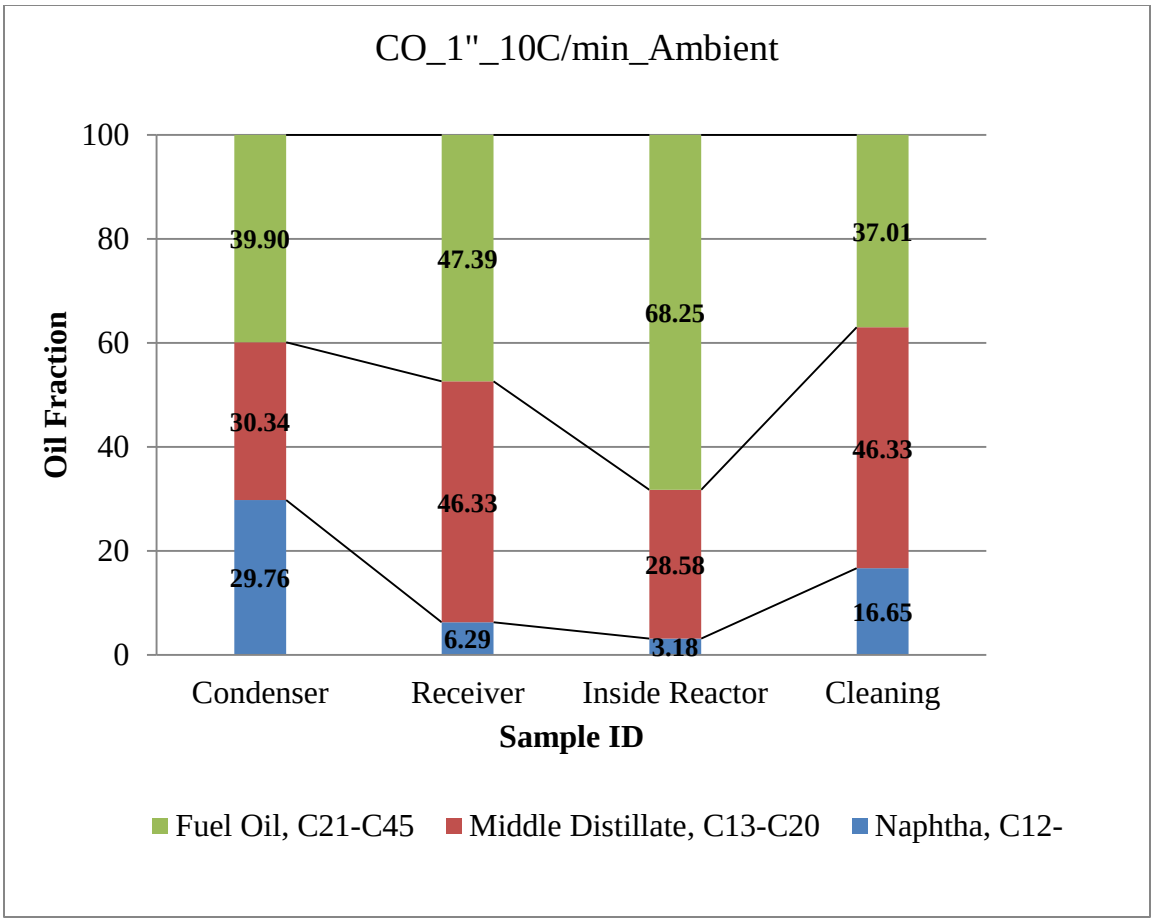

Figure 7- 24: Grade of the oil samples collected during the pyrolysis of 1" core (sample #2) at heating rate of 10°C/min.

Figure 7-25 shows the distribution of the gaseous products produced at different temperatures during the experiment conducted at 5°C/min. The distribution of the hydrocarbon gases over temperature did not show a uniform trend. The potential hydrocarbon gases were formed at 300°C and continued to be released from the pyrolysis process. It was observed that the gaseous products continued to evolve even when the experiments were terminated. Similar results were observed for the experiment at 1°C/min and 10°C/min.

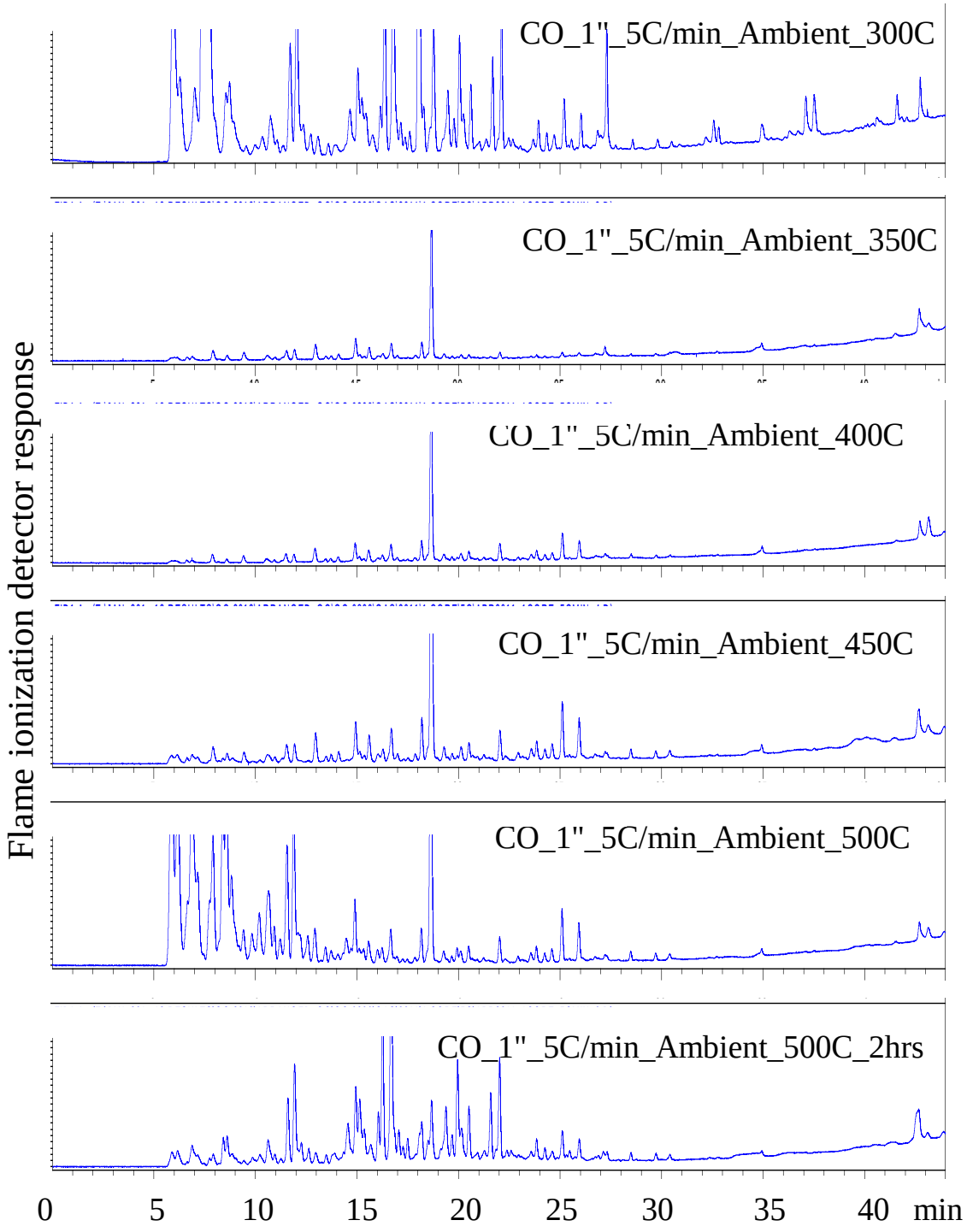

Figure 7- 25: The distribution of gaseous hydrocarbons in the samples collected at different temperatures during the experiment of 1" core at heating rate of 5°C/min. The chromatograms for 500°C_2hrs is for the sample at the end of the experiment.

7.4. Pyrolysis of 2.5” Core Samples

Cores of 2.5” diameter (sample #2) were pyrolyzed under isothermal conditions at two temperatures, 350°C and 500°C, and two pressures, ambient and 500 psi. The temperature at the surface of the reactor (T-5) was the pyrolysis temperature. A receiver was used before the condensers to collect the heavy fractions of the oil produced. The results are summarized in Table 7-6.

The temperature distribution across the core was large and increased with decreasing temperature. Higher weight loss was observed in high pressure experiments compared to the ambient experiments when the temperature was constant. This may be a result of better heat transport in a high pressure system (Appendix D). The oil yield increased with pressure in the experiments conducted at 350°C. However, the weight loss was higher in the pressurized experiments and thus the oil yields. The trend reversed at high temperature (500°C) pyrolysis experiments. The ratio of oil yield to weight loss decreased with an increase in the pressure and temperature. This suggests that under elevated pressure and temperature the amount of gaseous products increased. A complete decomposition of organic matter was achieved during the experiment conducted at 500°C. There were no unreacted organics observed in the spent shale while the amount of coke formed was found to be 6.06% in the high pressure experiment.

Table 7- 6: Experimental conditions and results from the pyrolysis of 2.5” core samples.

Sample ID	Temp	Pressure	OS, gm	Wt Loss%	Oil Yield	Oil Yield/Wt loss%
CO_2.5"_350C_Ambient_48hrs	350°C	Ambient	493.58	3.67	2.77	0.75
CO_2.5"_350C_500psi_48hrs	350°C	500psi	695.15	14.44	8.32	0.57
CO_2.5"_500C_Ambient_48hrs	500°C	Ambient	961.99	21.58	11.71	0.54
CO_2.5"_500C_500psi_24hrs	500°C	500psi	760.00	24.52	7.97	0.32

The experiment at 350°C and ambient pressure produced an oil yield of 2.77%. The liquid sample was collected in the receiver (with an ice bath). During the early stage of the experiment around 5ml (0.6%) water was produced. And with an increase in the process time oil was produced. The oil yields at different durations during the experiment conducted at 350°C and 500 psi are shown in Figure 7-26. The experiment yielded 5.66% oil in the condenser within the first 6 hrs. Figure 7-27 shows the distribution of the overall yield obtained during the pyrolysis at 500°C under ambient pressure. An oil yield of 7.20% was achieved with in 1 hr time the reactor was isothermal. The heavy fraction in the receiver accumulated over the entire pyrolysis process and at the end the oil in the receiver was 1.66%. An approximately 1 ml of water was also produced in about 16 mins and collected in the receiver. The experiment at 500°C and pressure of 500 psi yielded 7.86% oil within an isothermal time of 2 hrs. There was no significant oil produced at later stages during this experiment.

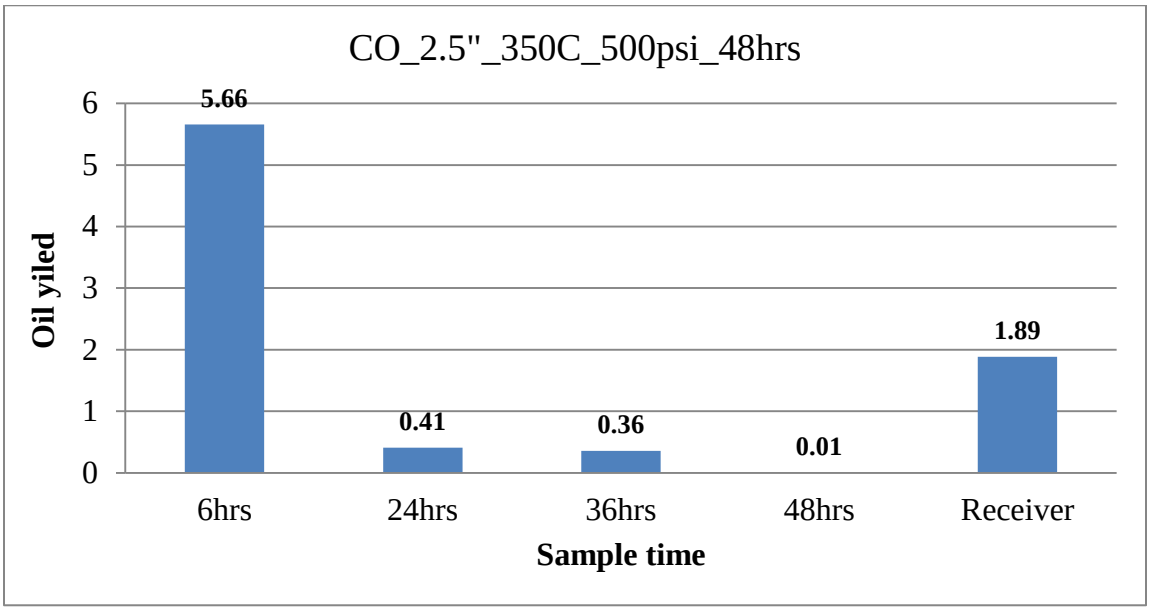

Figure 7- 26: The amount of the oil (yield) produced at different times during the pyrolysis of 2.5" core at 350°C and 500 psi.

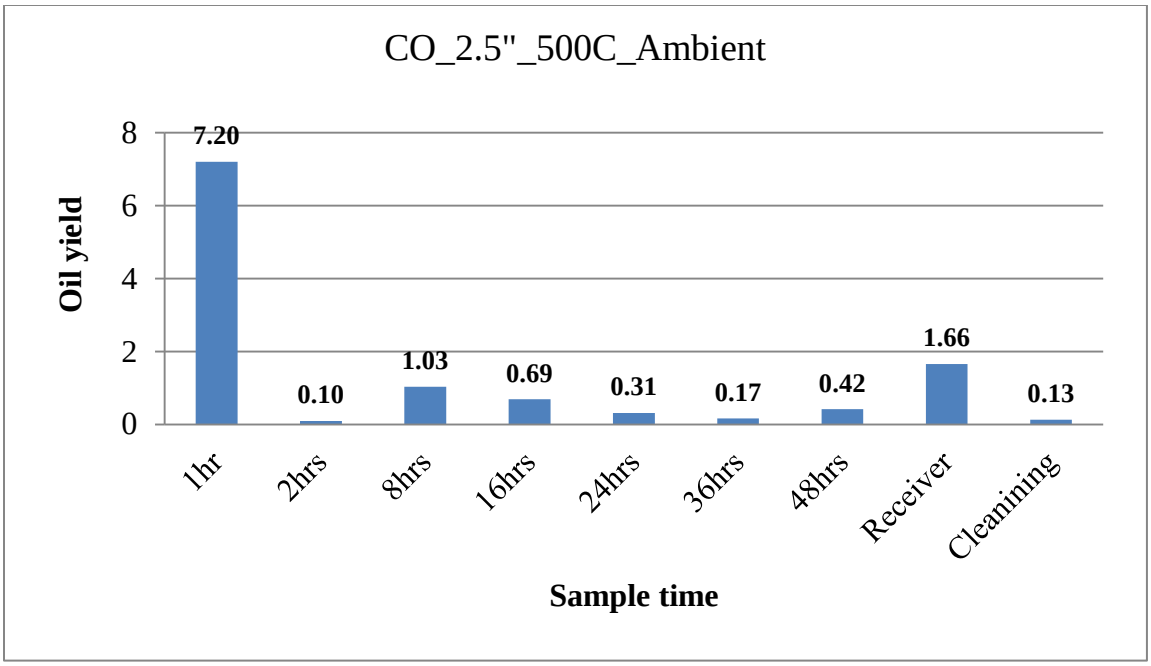

Figure 7- 27: The amount of the oil (yield) produced at different times during the pyrolysis of 2.5" core at 500°C and ambient pressure.

The gas and liquid samples, collected at different time intervals during these experiments showed a large distribution in the compositions. These compositions of the oil produced in the pyrolysis of ambient pressure are shown in Figure 7-28. The oil produced during early stages is lighter in composition (naphtha to middle distillate) while the compositions shifted to the heavier oil grades as the process time increased. Gaseous products were formed before the oil was collected in the condenser or receiver. Gaseous products were also observed in the samples collected at the end of the experiments (Figure 7-29). It should be noted that the condensation of higher hydrocarbon gases can increase the oil yield.

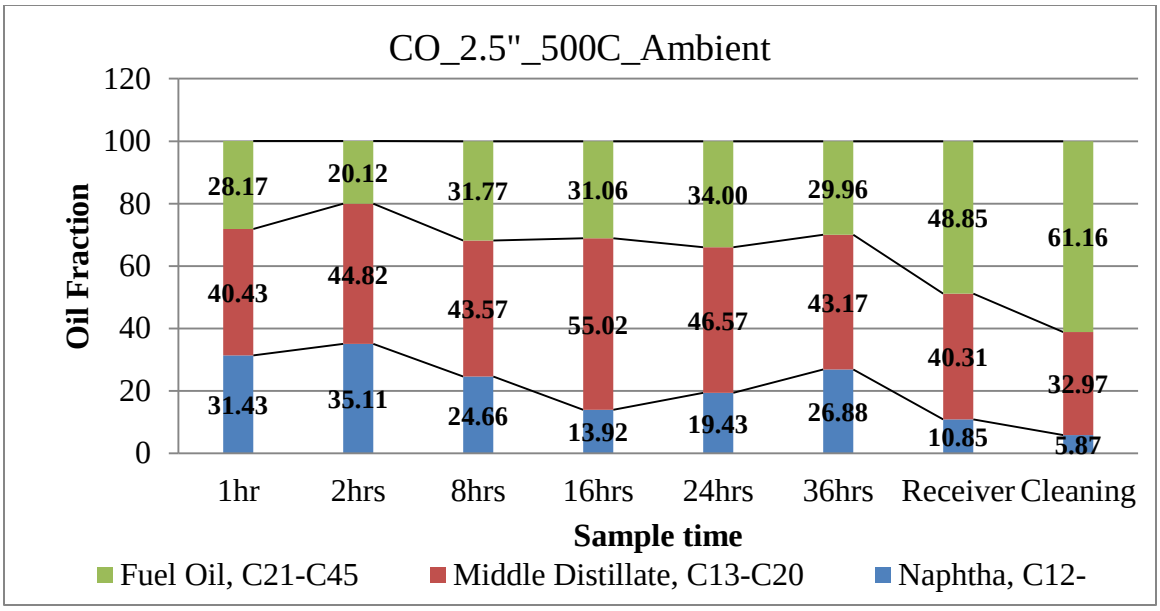

Figure 7- 28: Classification of the oil samples into oil grades.

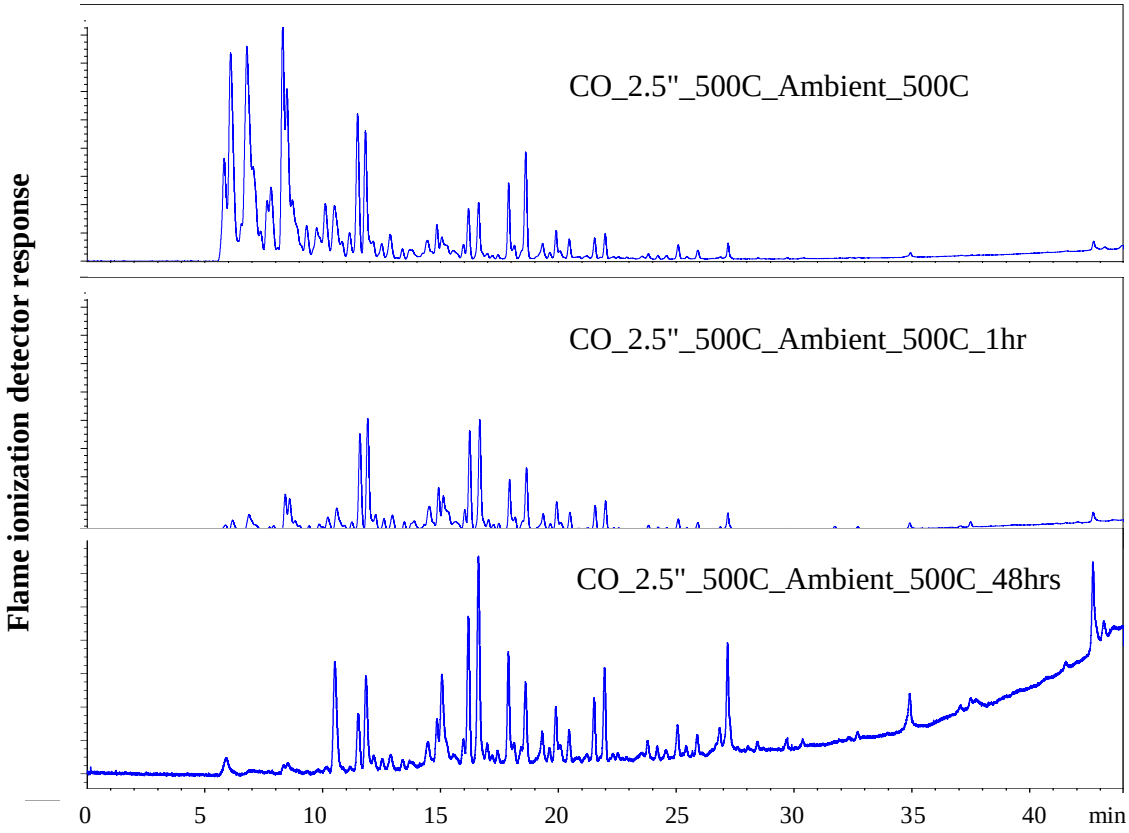

Figure 7- 29: The distribution of the hydrocarbon gases produced at different times during the pyrolysis of 2.5" core at 500°C and ambient pressure.

7.5. Summary of Multiscale (benchscale) Pyrolysis

Organic decomposition in oil shale occurs when enough heat is supplied to the material. Pyrolysis of oil shale samples of different sizes at low temperature, 200°C were conducted for a week and a month. There was no sign of hydrocarbon production in these experiments. At laboratory scale, significant organic portion of the shale pyrolyzed at 300°C or higher temperature. The rate of product formation is low at lower temperature and lower heating rate and it increases with an increase in temperature and heating rate. TGA analyses of isothermal experiments revealed that a small amount of powdered oil shale decomposes before 300°C. This weight loss may be due to loosely bound molecules in the kerogen. The formation of gaseous products when there is no oil production, confirmed the decomposition of organic matter to lower molecular compounds. An increase in temperature accelerates the decomposition reactions. At higher temperature, weight loss occurs at a faster rate and a wide range of products is generated.

Increase in the temperature increased the weight loss and completed the organic conversion in a lesser time and produces more oil, but also increases the amount of coke. The oil yield was higher at higher temperature and higher heating rates due to complete and faster decomposition of the organic matter in the shale. Increase in pressure favored the formation of coke and gaseous products when the pyrolysis temperature and time were constant. The primary reasons for these phenomena are secondary reactions, coking and cracking. These secondary reactions depend on temperature and residence time in heated zones, and control the quality of the products. Overall, high temperature, higher heating rate and low pressure favor higher oil yield compared to coke formation. These results are consistent with the reported literature [9, 41, 52]. Higher temperature and

pressure produce more naphtha grade oil. Higher temperature results in more noncondensable gases while higher pressure produces more condensable gases. Lower temperature and higher pressure produces oil of better quality oil but lesser yield and more coke.

Increase in the size of the sample offers more heat and mass resistance. The temperature propagates to the inner section and the products are formed, generating pressure in the system. The generated pressure allows the fluid products to flow out of the sample. The products formed in bigger cores encountered the situations similar to those with the powdered samples in batch and semibatch modes. The products are trapped in the impermeable and nonporous zones. When enough pore pressure is generated and/or the porosity is increased owing to pyrolysis of the sample, the products leave the system. Different sections of the cores experience different temperatures at different times. The product generation rates depend on time-temperature history, which varies across the core. Hence the overall decomposition temperature increases with increase in the size of the sample. The effect of the heating rate also changes with the size of the sample. The samples of 1" diameter showed no oil yield at 500°C in the experiment conducted at the heating rate of 10°C/min. However, holding the system isothermally at 500°C yielded oil.

The material balance from the pyrolysis of the core samples, 2.5" and ¾" diameters, under identical conditions is summarized in Table 7-7. The total weight loss observed during 2.5" core pyrolysis experiment was higher when compared to ¾" core. The reason for this could be either the presence of more organic matter in 2.5" sample or mineralogical changes which contributed to the weight loss. The ratio of oil yield to weight loss also decreased, which indicate the formation of large amount of gases. The

Table 7- 7: Overall mass balance of the pyrolysis process at two scales, ¾" core and 2.5" core. The experiments were performed under isothermal conditions for 24 hrs.

Material Balance	2.5" core CO_2.5"_500C_500psi_24hrs	3/4" core CO_3/4"_500C_500psi_24hrs
Wt. loss %	24.52 %	18.69 %
Oil yield %	7.96 %	10.63 %
Coke %	6.06 %	1.03 %
Gas %	16.56 %	8.06 %
Unreacted organics%	0.05 %	0.43 %

overall oil yield decreases and amount of coke increases as the sample size increases; mainly because of the secondary reactions in the oil/vapor produced and intraparticle mass resistance. The single carbon number distribution of the oil samples showed that the quality of the oil produced with these two different scales is not dissimilar in composition. The peak differences reveal that, ¾" sample had relatively more C_{10}-C_{14} compounds while the distribution shifted to C_{24}-C_{26} carbon compounds in the 2.5" sample experiment (Figure 7-30). The oil produced from the 2.5" core pyrolysis was found to be lighter (less than C_{10} hydrocarbons) in composition. More fractures were observed in the reacted 2.5" sample (Figure 7-31). This may be because of higher pressure generated inside the core. The analyses of gas samples showed that the pyrolysis of 2.5" sample produced hydrocarbons with relatively lighter gases. The presence of heavier compounds in the samples also depends on the condenser capacity/performance. The TCD response showed the presence of carbon dioxide in both the samples.

Shale oil collected from different experiments was used for the physical property analysis to measure the quality of oil produced. Only a few experiments produced a significant amount of oil which can be used for the density, viscosity and wax appearance temperature (WAT) estimations.

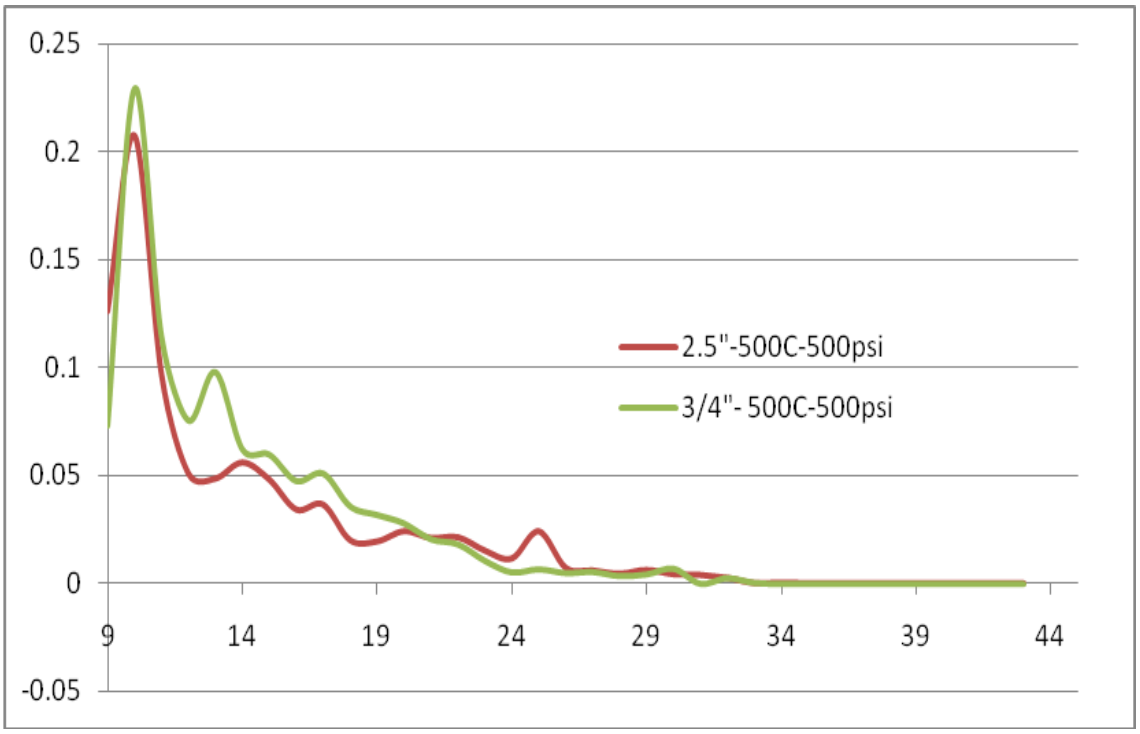

Figure 7- 30: Single carbon number distribution of the chromatograms obtained for oils of two different scales pyrolysis. The x axis is carbon number and the y axis is weight percent of SCN.

Figure 7- 31: Images of the spent shale from the pyrolysis of two different scales under same condition

The physical properties of the shale oils are summarized in the Appendix E. The density of the oil was of 25.30^{o}API (range of middle distillate crude oil) and increase in pressure produced lower WAT and less viscous oil. Lower heating rate and high temperature produced oil of lower WAT. Density of the oil was found to be independent of the size of the sample while WAT was observed to increase with the sample size. The viscosity of the oil produced from ¾" core is lesser (3.21centi poise (cp)) than 2.5" core (4.19 cp) under high pressure and 500°C. However, these values are within the error range of the viscometer used. The oil collected in the receiver in the experiment with 2.5" at 500^{o}C and ambient pressure was thick and showed higher WAT (30.72^{o}C) than the oil collected in the condenser (26.30^{o}C).

8. OIL SHALE PYROLYSIS: HYDROUS TREATMENT

When water is associated with the organic matter and minerals in the shale, the pyrolysis process has the potential of producing additional water [124]. The solubilities of different organic substances produced in the process may contaminate the water and cause environmental and health issues. Previous studies in the literature have focused on oil compositions in hydrous pyrolysis [14, 16]. The specific objectives of this study include determining the types and concentrations of organic compounds that may end up in the produced water and the effect of the presence of water on the yield and composition of oil. To accomplish these objectives, an experimental matrix was designed which included water soaked, hydrous and nonhydrous pyrolysis of oil shale.

8.1. Pyrolysis of Water-Soaked Oil Shale Samples

Deionized (DI) fresh water was added to the batch (closed system) with sample #1 (PO). The shale sample was soaked in deionized water for 5 months. Then, the water was filtered from the solids. No appreciable weight gain was observed. Pyrolysis experiments with TGA were performed with the water-soaked powdered oil shale sample to observe the effect of soaking on the decomposition temperature as well as the organic weight loss. TGA runs were conducted at two heating rates (5°C/min and 10°C/min). The results were compared with the anhydrous TGA pyrolysis experiments under the same conditions in Figure 8-1.

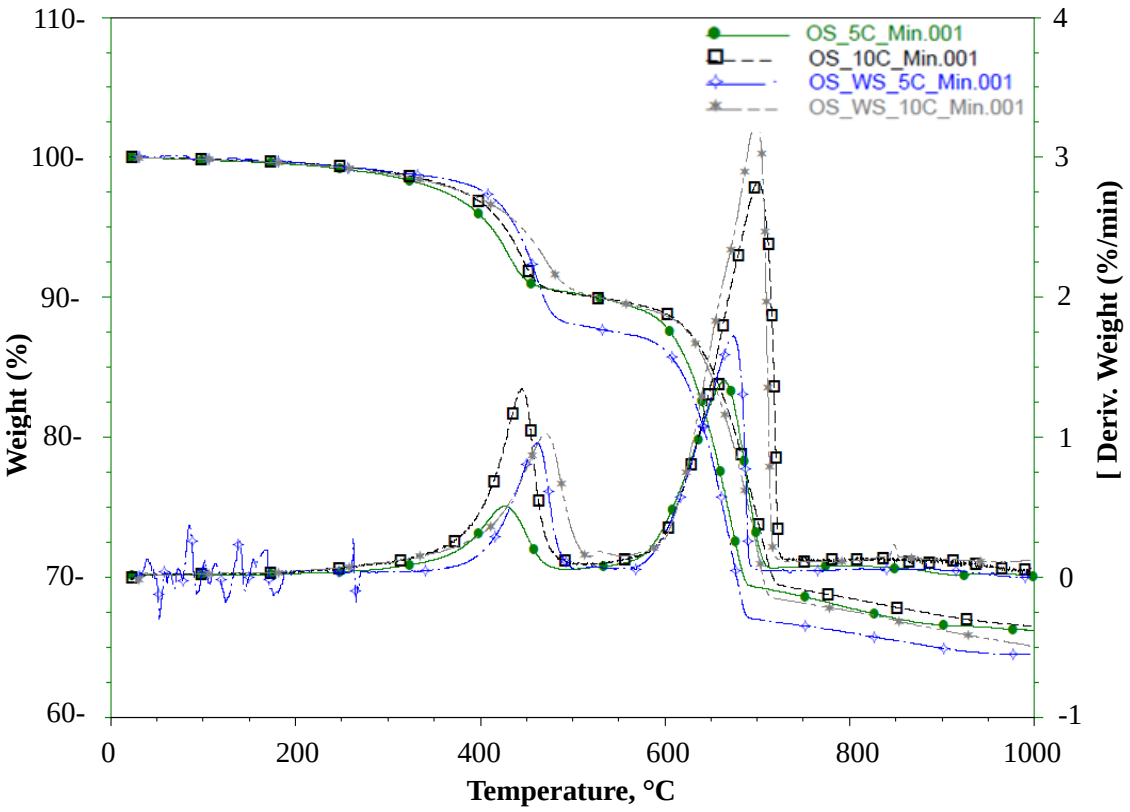

Figure 8- 1: Effect of water soaking on TGA onset points and comparison of water soaked (5 months) pyrolysis with anhydrous pyrolysis at two heating rates, 5°C/min and 10°C/min.

The run at 5°C/min with a water soaked sample showed some disturbance at an early stage, which may be a result of either instrument noise or signs of free and bound water present. The organic peak shifted towards higher temperature as the heating rate increased. This occurred in a manner similar to the anhydrous pyrolysis experiments. The comparison of water-soaked sample pyrolysis to anhydrous pyrolysis at a specific heating rate showed no significant difference. The pyrolysis of the water-soaked oil shale at heating rate of 5°C/min displayed a relatively higher organic weight loss when compared to anhydrous pyrolysis. TGA pyrolysis at 10°C/min showed identical weight loss in both the cases. The decomposition of the soaked sample started at a lower temperature than

the pyrolysis at 5°C/min. The trend reversed in the experiments at 10°C/min. However, these results are within the experimental error (2-3%) as observed in TGA analyses of anhydrous pyrolysis.

To estimate the effect of water soaking on oil composition, two shale (sample #2) core (CO) of ¾" diameter were soaked in deionized water. The core samples from 10 days and 142 days water soaking were subjected to pyrolysis. There was no significant weight gain in these samples during soaking. The water soaked samples were pyrolyzed at 400°C (142 days) and 450°C (10days) for 24 hrs. The temperature at the center of the core (T-1) was used to control the heat supply, hence higher temperature than the process condition was recorded around the core.

The GC and GC-MS analyses of the oil produced from water soaked pyrolysis and anhydrous oil shale pyrolysis were conducted and compared. Figure 8-2 shows the FID chromatogram of the liquid product produced from the pyrolysis of the core sample which was soaked in water for 142 days. Expanded chromatograms, beginning at carbon number 13, of the products from water soaked and anhydrous pyrolysis (identical conditions) experiments at 400°C are shown in Figure 8-3. The alkene-alkane pairs showed no discernible difference in the composition of the two samples. GC-MS analysis (Figure 8-4) revealed the presence of a number of aromatic series in the oils produced from water-soaked sample pyrolysis. Alkene peaks were associated with alkane and significant amounts of aromatic compounds were present in the oil produced. The presence of alkene and aromatic was observed to be slightly higher in the oil produced from the water soaked experiments as compared to anhydrous pyrolysis.

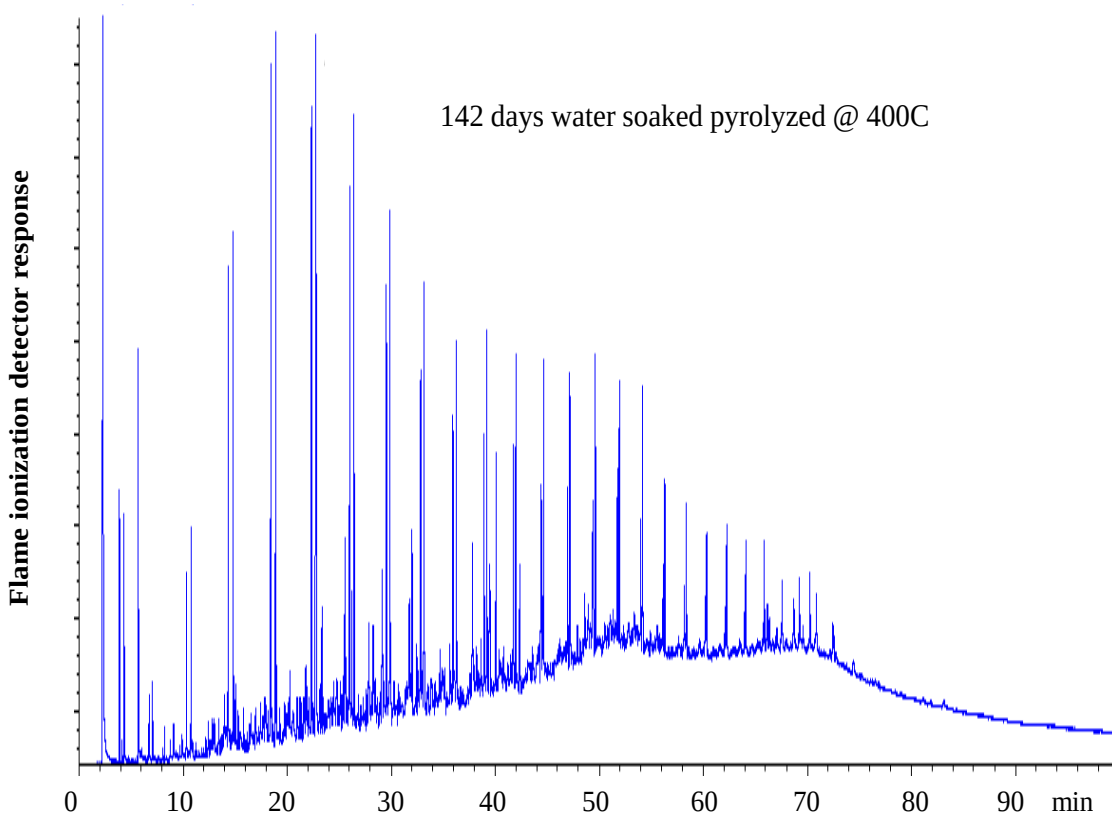

Figure 8- 2: Flame ionization detector chromatogram of a product from hydrous (142 days water soaked) pyrolysis at 400°C for 24 hrs.

8.2. Hydrous and Anhydrous Pyrolysis

Presence of water during pyrolysis increases the pressure due to steam formation and may provide a source of hydrogen [16]. Hydrous pyrolysis may alter the composition of oil produced during the process. Oil shale cores of 3/4" diameter were subjected for the hydrous and anhydrous experiments under identical conditions. Hydrous pyrolysis experiments were conducted with 20 ml with DI water in a closed system. Isothermal experiments at temperatures, 300°C, 400°C and 500°C for 72 hrs were designed and conducted (Appendix C). A similar experimental study was reported by Lewan [151] at lower temperatures with gravel size (0.5-2 cm) samples.

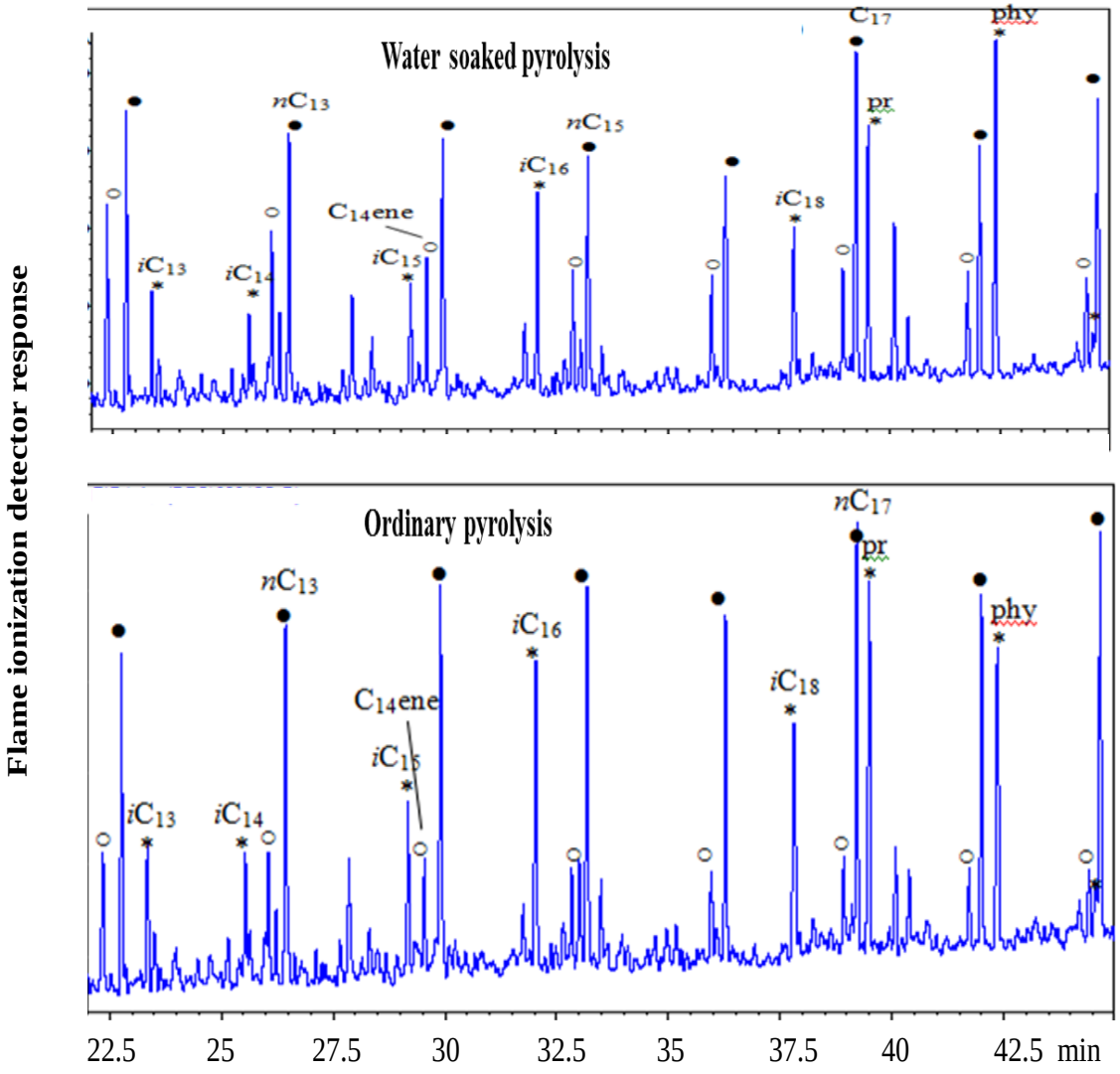

Figure 8- 3: Comparison of expanded chromatograms of products from water soaked (142 days) and nonhydrous pyrolysis at 400°C for 24 hrs.

During anhydrous pyrolysis (Figure 8-5) at 300°C, there was no significant weight loss (0.90 %) and no coke formation was observed. As the temperature increased, the weight loss and amount of coke formed increased. The spent shale from 400°C pyrolysis showed the presence of the organics which begin to decompose at lower temperature. At higher temperature the weight loss was higher. This might be because of mineral decompositions. No free liquid product was observed during the pyrolysis. This

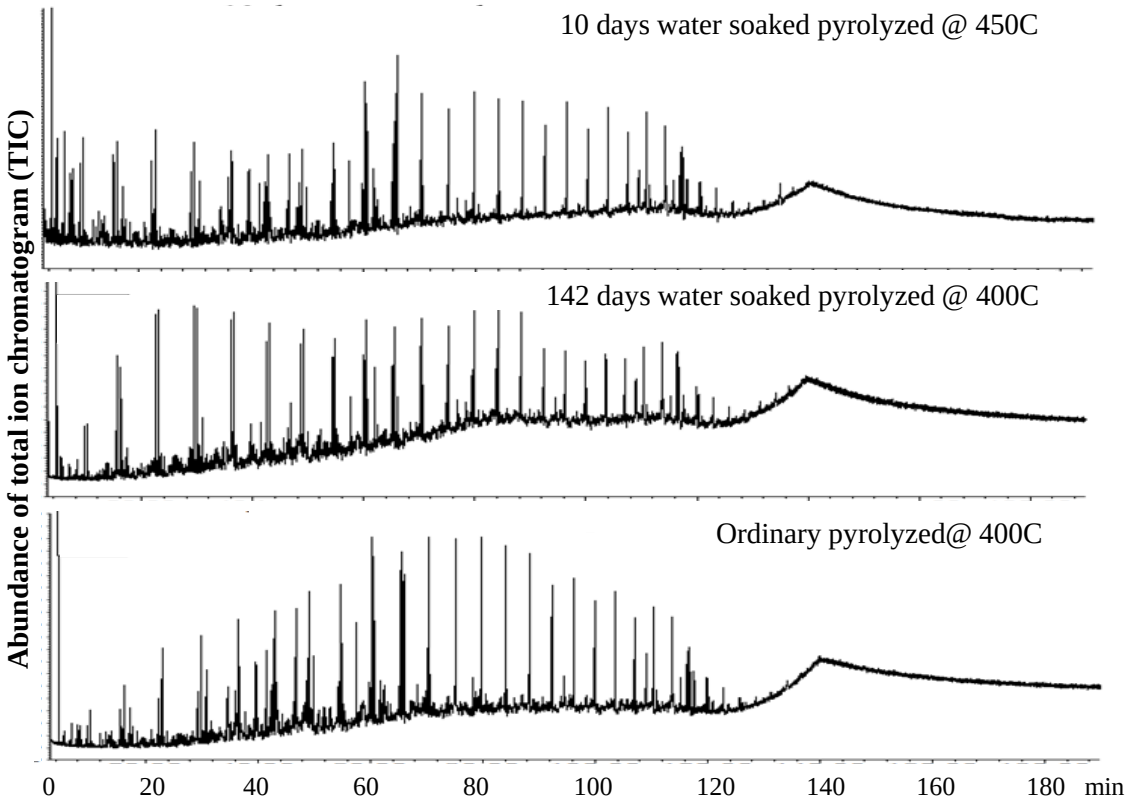

Figure 8- 4: Total ion spectra of the liquid products using GCMS. (a) 10 days water soaked sample pyrolyzed at 450°C. (b) 142 days water soaked sample pyrolyzed at 400°C. (c) Ordinary pyrolysis at 400°C.

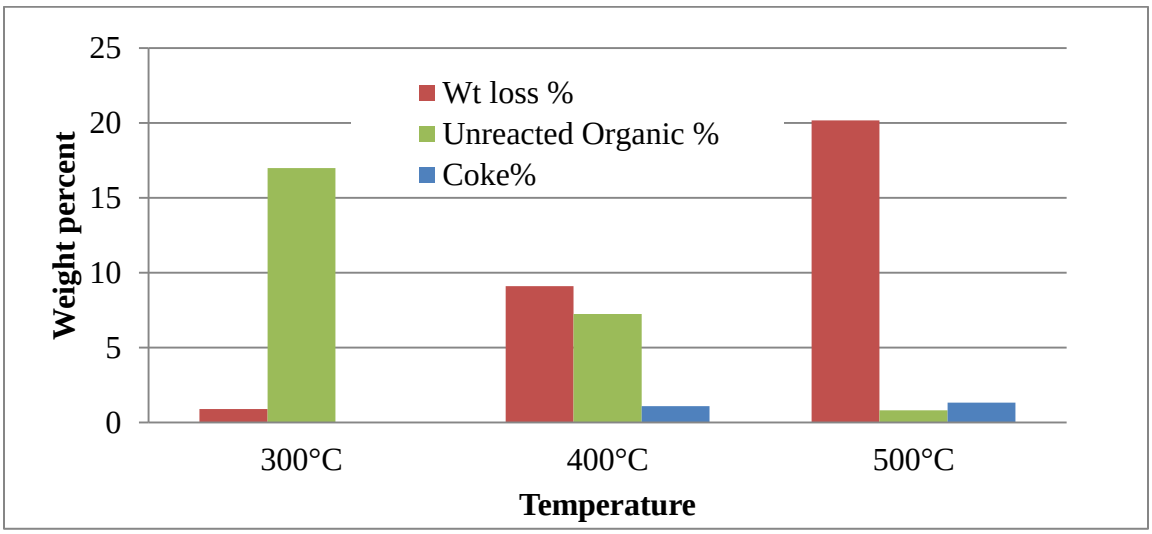

Figure 8- 5: Weight loss, unreacted organic and coke percent from the pyrolysis of ¾" core samples.

is consistent with the finding of Lewan [151]. The gas analyses showed that at 300°C a distribution of gases were in the range of C_1- C_{12}, while at 400°C the gases were dominated by methane and heptane.

In hydrous experiments the pressure increased rapidly with an increase in temperature. There was a large pressure (6000 psi) increase in the experiment at 500°C (Appendix D). Hence, for safety reasons the experiments with water were conducted at 300°C and 350°C. The pressure developed in the reactor due to formation of water vapor and a mixture of produced hydrocarbons was recorded. After pyrolysis, the condensed aqueous phase was analyzed to measure the alteration in the water phase composition because of the solubility of organics produced during pyrolysis.

Batch hydrous pyrolysis at 300°C and 350°C showed 4.5% and 7.1% weight losses respectively. No significant amounts of hydrocarbons from GC analyses were detected in water phase in the 300°C and 350°C experiments. The gas sample analysis of the experiment at 350°C showed a distribution of hydrocarbon gases higher than C_7 hydrocarbon. The spent shales from hydrous pyrolysis were found fractured in the form of slice (horizontal pieces). The TGA-DSC data revealed that there was a significant amount of unreacted organics (8% of spent shale) remaining in the 300°C experiment. The spent shale from the experiments at 350°C carried a large amount of mixed water with organics (6 % in spent shale).

Compared to anhydrous pyrolysis, the hydrous pyrolysis at 300°C showed significant increase in weight loss (4.46%) and the coke formed (1.05%). Large volume of hydrocarbon gases were produced that ranged from C_1 to C_{10} hydrocarbons in the hydrous experiment at 350°C (Figure 8-6). The oil collected from the aqueous phase

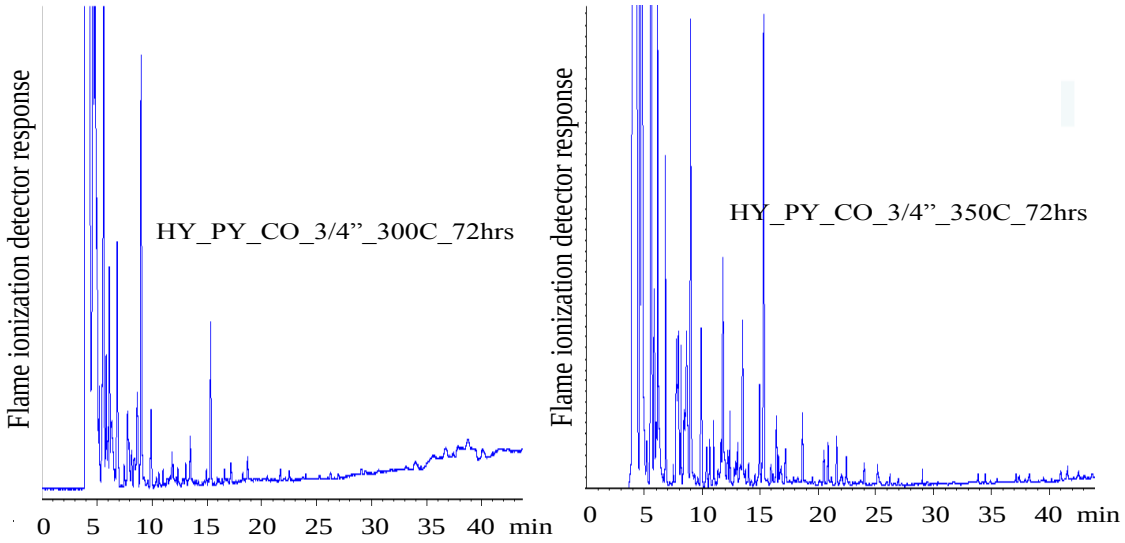

Figure 8- 6: FID chromatograms of the gaseous products produced from hydrous pyrolysis.

during the hydrous pyrolysis at 350°C showed a wide range of hydrocarbons. These results indicate that during the hydrous pyrolysis, the pressure generated accelerates the decomposition process producing a wide range of condensable gases.

8.3. Analyses of Water Phase

There is little or no water associated with the core shale samples from the Mahogany zone of the Green River formation used in this study. Hence, the core samples of 2.5" diameter were pyrolyzed (anhydrous pyrolysis) to produce a sufficient amount of water for analysis. The water produced from continuous flow isothermal pyrolysis of 2.5" core at 350°C under ambient pressure (CO_2.5"_350C_Ambient_48hrs) and at 500°C temperature under 500 psi pressure (CO_2.5"_500C_500psi_24hrs) were selected for analyses. Water was produced during the initial stage of the experiments. The water phase was carefully separated from the oil (using a pipette) and analyzed. The target of most analyses were dissolved aliphatic, aromatic and poly-aromatic hydrocarbons (PAH).

To understand the hydrocarbon contamination in water phase during hydrous and anhydrous pyrolysis of oil shale, the following analyses were performed at American West Analytical Laboratory (AWAL) located in Salt Lake City, Utah.

- Total organic carbon (TOC) in water phase, (Method: A5310B).
- Oil and Grease (OnG) in the water phase, (Method: E1664A).
- Volatile organic in the water phase using GCMS, (Method: 8468260C/5030C)
- Semivolatile organic in the water phase using GCMS, (8468270D/3510C)
- Oil phase organic using GCMS, (Semivolatile- 8270D/3580A, volatile-SW8260W)

Five samples from batch hydrous pyrolysis and continuous flow anhydrous pyrolysis were analyzed. The samples had four water phase and one oil phase sample.

1. HY_PY_CO_3/4”_300C-72 hrs : water phase
2. HY_PY_CO_3/4”_350C-72 hrs : water phase
3. CO_2.5"_350C_Ambient_48hrs : water phase
4. CO_2.5"_500C_500psi_24hrs : water phase
5. CO_2.5"_500C_500psi_24hrs : oil phase

The TOC and OnG results are shown in Table 8-1. The water produced from the pyrolysis of 2.5” core at 350°C (CO_2.5"_350C_Ambient_48hrs) was analyzed in detail. The TOC was about 15,500 mg/L in water phase. The oil and grease concentration was

Table 8- 1: Analytical results for total organic carbon (TOC) and oil and grease (OnG).

Sample ID	TOC (mg/L)	OnG (mg/L)
1.HY_PY_CO_3/4”_300C-72 hrs: water phase	13	<3
2.HY_PY_CO_3/4”_350C-72 hrs : water phase	<1	3.11
3.CO_2.5"_350C_Ambient_48hrs : water phase	15,500	3,070
4.CO_2.5"_500C_500psi_24hrs : water phase	<1	---
5.CO_2.5"_500C_500psi_24hrs : oil phase	------	696,000 (mg/kg)

about 3000 mg/L. It should be noted that the TOC was rather high. Determination of the origin of this organic carbon was found to be challenging.

The GC-MS data were obtained for volatile and semivolatile hydrocarbons for these samples and compared. There were no easily identifiable peaks in both the volatile and semivolatile categories, including the potential aromatics in the water phase samples. Results for volatile hydrocarbons are summarized in Table 8-2. Concentration of the compounds were below detection limits indicating that even though the water sample contains some organics, specific species cannot be identified. Results of the analysis of the semivolatile compounds are summarized in Table 8-3. The C_{22}-C_{35} aliphatic hydrocarbons were present in all the water phase samples and their amount increases with an increase in the pyrolysis temperature. The analyses of the water phase maximum concentration of 220 µl/g with possible compounds being oxygen containing aromatics–

Table 8- 2: Volatile hydrocarbon compounds targeted using GC-MS.

Compounds	1. Hydrous300°C water phase (ul/L)	2. Hydrous350°C water phase (ul/L)	3. Pyrolysis 500°C-500 psi water phase (ul/L)	4. Pyrolysis 350°C water phase (ul/L)	5. Pyrolysis 500°C-500psi oil phase (ug/Kg)
Benzene	< 200	< 1,000	< 2,000	< 2,000	943,000
Ethylbenzene	< 200	< 1,000	< 2,000	< 2,000	1,730,000
Methyl-tert-butyl ether	< 200	< 1,000	< 2,000	< 2,000	< 50,000
Naphthalene	< 200	< 1,000	< 2,000	< 2,000	766,000
Toluene	< 200	< 1,000	< 2,000	< 2,000	5,030,000
Xylenes,Total	< 200	< 1,000	< 2,000	< 2,000	8,500,000
C_6 Apliphatic hydrocarbons	< 200	< 1,000	< 20,000	< 20,000	4,540,000
C_7&C_8 Aliphatic hydrocarbons	*15,700*	*42,100*	*< 20,000*	*< 20,000*	*34,500,000*
C_9&C_{10} Aliphatic hydrocarbons	< 2,000	< 10,000	< 20,000	< 20,000	23,300,000
C_9&C_{10} Alkyl Benzenes	< 2,000	< 10,000	< 20,000	< 20,000	6,540,000

Table 8- 3: Semivolatile hydrocarbon compounds targeted using GC-MS.

Compounds	1.Hydrous- 300C water phase (ul/L)	2. Hydrous - 350C water phase (ul/L)	3. Pyrolysis 500C-500 psi- water phase (ul/L)	4. Pyrolysis- 350C- water phase (ul/L)	5. Pyrolysis 500C-500psi Oil phase (mg/Kg)
Acenaphthelen	< 20	< 20	< 23.5	< 37	< 50
Acenaphthylene	< 20	< 20	< 23.5	< 37	< 50
Anthracene	*< 20*	*< 20*	*< 23.5*	*< 37*	*108*
Benz(a) anthracene	< 20	< 20	< 23.5	< 37	< 50
Benzo(a) pyrene	< 20	< 20	< 23.5	< 37	< 50
Benzo(b)fluroranthene	< 20	< 20	< 23.5	< 37	< 50
Benzo (g.h.i)perylene	< 20	< 20	< 23.5	< 37	< 50
Benzo(k)fluoranthene	< 20	< 20	< 23.5	< 37	< 50
Chrysene	< 20	< 20	< 23.5	< 37	< 50
Dibenz(a,h) anthracene	< 20	< 20	< 23.5	< 37	< 50
Floranthene	< 20	< 20	< 23.5	< 37	< 50
Indeno(1,2,3-cd) pyrene	< 20	< 20	< 23.5	< 37	< 50
Phenanthrene	< 20	< 20	< 23.5	< 37	217
Pyrene	< 20	< 20	< 23.5	< 37	170
C_{11}-C_{12} Aliphatic hydrocarbons	*26*	*< 20*	*< 23.5*	*< 37*	*23,100*
C_{13}-C_{16} Aliphatic hydrocarbons	*< 20*	*< 20*	*< 23.5*	*52*	*46,200*
C_{17}-C_{21} Aliphatic hydrocarbons	*66*	*< 20*	*< 23.5*	*< 37*	*13,800*
C_{22}-C_{35} Aliphatic hydrocarbons	*64*	*77*	*< 23.5*	*120*	*338,000*
C_{11}-C_{13} Alkyl Naphthalenes	*< 20*	*< 20*	*< 23.5*	*< 37*	*3,130*
Total C_{12}-C_{22} PAH	< 20	< 20	< 23.5	< 37	494

phenols, alcohols, etc. The oil phase sample showed a wide range of hydrocarbons (including the aromatics, PAH) and can be a potential source of contamination.

These analyses show that the water phase sample from the hydrous pyrolysis contained some hydrocarbons close to the detection limits. However, the water produced during pyrolysis remains clean. In hydrous pyrolysis the water phase contamination may be due to longer contact time at higher temperature. The analyses of the oil sample showed the presence of potential hydrocarbons. This can lead to water contamination with longer contact times.

9. HETEROGENITY IN THE RAW MATERIAL

The composition of oil shale varies with geological environment. To address this variability in the compositions and its effect on the pyrolysis process and product distribution, the Utah Geological Survey (UGS) and the University of Utah drilled core samples at the Uinta Skyline 16 location. Cores of 4" diameter from a depth of 1000 feet drilled. Three fresh organic rich (Mahogany zone) samples from depth of 461.1 to 548.9 (~90 feet interval) were used in this study. These samples were titled as GR-1 (461.1-462.1 feet), GR-2 (485.9- 486.9 feet) and GR-3 (548.1- 549.1 feet).

9.1. Material Characterization

TGA and CHNS analyses were conducted on uniformly mixed powdered (100 mesh) shale samples of GR-1, GR-2 and GR-3. The powdered GR samples had different color and were suspected to contain different amounts of organic matter. The results from TGA analysis of the samples are summarized in Table 9-1. TGA experiments were performed at heating rate of 10°C/min. Elemental analysis for each sample was repeated three times and the average values with standard deviation are reported in Table 9-2.

Table 9- 1: TGA analysis (weight loss) of Skyline 16 (GR) samples.

Samples ID	OS, mg	Organic %	Mineral %	Coke %
GR-1	18.16	21.13	17.86	1.63
GR-2	17.00	7.20	29.85	0.0
GR-3	23.11	11.16	20.43	0.34

Table 9- 2: Elemental analysis (CHNS) of Skyline 16 (GR) samples.

Sample ID	C %	H %	N %	S %
GR-1	33.93 ±5.76	3.21 ±0.21	1.17 ±0.27	0.56 ±0.68
GR-2	19.80 ±5.23	1.40 ±0.64	0.47 ±0.19	0.13 ±0.17
GR-3	20.44 ±1.00	1.84 ±0.05	0.71 ±0.11	0.18 ±0.15

The samples analyzed reflect considerable variation in compositions of organic and mineral portions as well as in elemental weight percent. GR-1 had 21.13 wt% organic matter (highest) while GR-2 had only 7.2% organics. The amount of coke formed during pyrolysis corresponds to the amount of the organic matter in the sample. Relatively more coke was formed in the organic rich sample while there was no coke formation during the GR-2 pyrolysis. GR-2 had the highest decomposable minerals (29 %). A similar trend was observed in the elemental analysis. The percent of elements (C, H, N and S) was observed higher in the organic rich samples compared to the organic lean samples. GR-1 had 34% carbon, 3.2 % hydrogen, 1.8 % nitrogen and 0.56% sulfur. GR-2, which had an intermediate composition, had the least organic constituent and the smallest percent of elements (CHNS) among the samples.

9.2. Pyrolysis of GR Core Samples

The cores from GR-1(461.2-461.7 feet), GR-2 (485.9-486.4 feet) and GR-3(548.2 -548.7 feet), 1" diameter each were used for pyrolysis. Each core was dissected into three sections (Figure 9-1) to perform the isothermal pyrolysis for 24 hrs. Continuous flow isothermal experiments at 350°C, 425°C and 500°C were conducted with hot N_2 flow (~100 ml/min). The temperature of the reactor surface (T-5) was used to control the pyrolysis temperature. Temperature profiles were recorded at three points; reactor surface

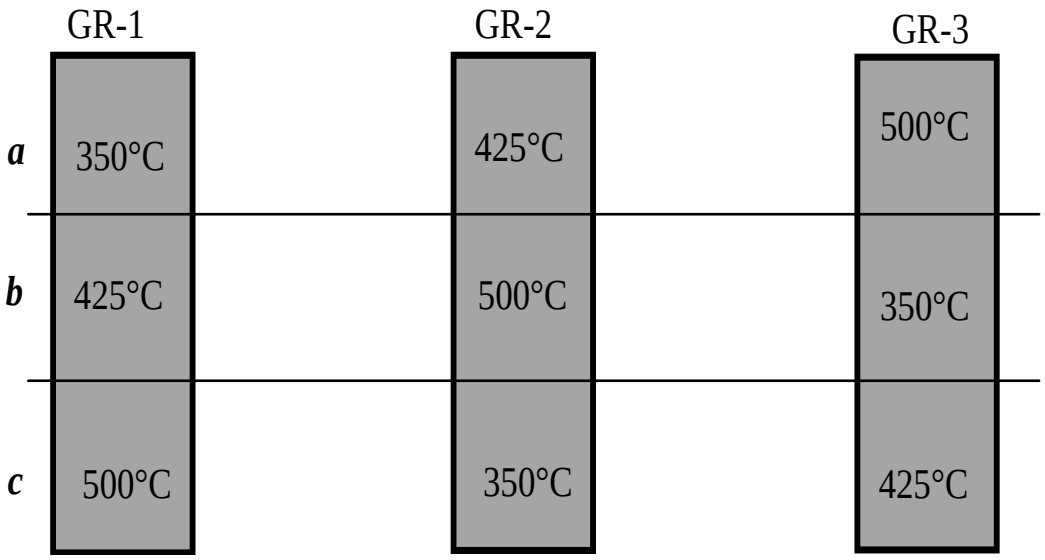

Figure 9- 1: GR core sections subjected to isothermal pyrolysis under different temperatures.

(TC-5), core surface (TC-4), and at the center of the core (TC-1). The steady state temperature difference between reactor surface and center of the core was about 50°C. The difference in temperature of core surface and center of the core was steady at 20°C. After the pyrolysis, oil and gas samples were collected for compositional analyses. The weight loss and oil yield were measured and gas losses were calculated by material balance. The results are shown in Figure 9-2 and Appendix C.

Increase in temperature increases the weight loss and oil yield. GR-1 the organic rich sample showed more weight loss and oil yield when compared to GR-2 and GR-3. A small amount of spent shale was further pyrolyzed and combusted to estimate the unreacted organic remains in the shale and coke formed during the pyrolysis respectively. The results from the spent shale TGA analyses are shown in Figure 9-3. The images of the spent shales from isothermal pyrolysis of the different sections of the three cores are shown in Figure 9-4. The cores of higher organic content (GR-1) during high temperature

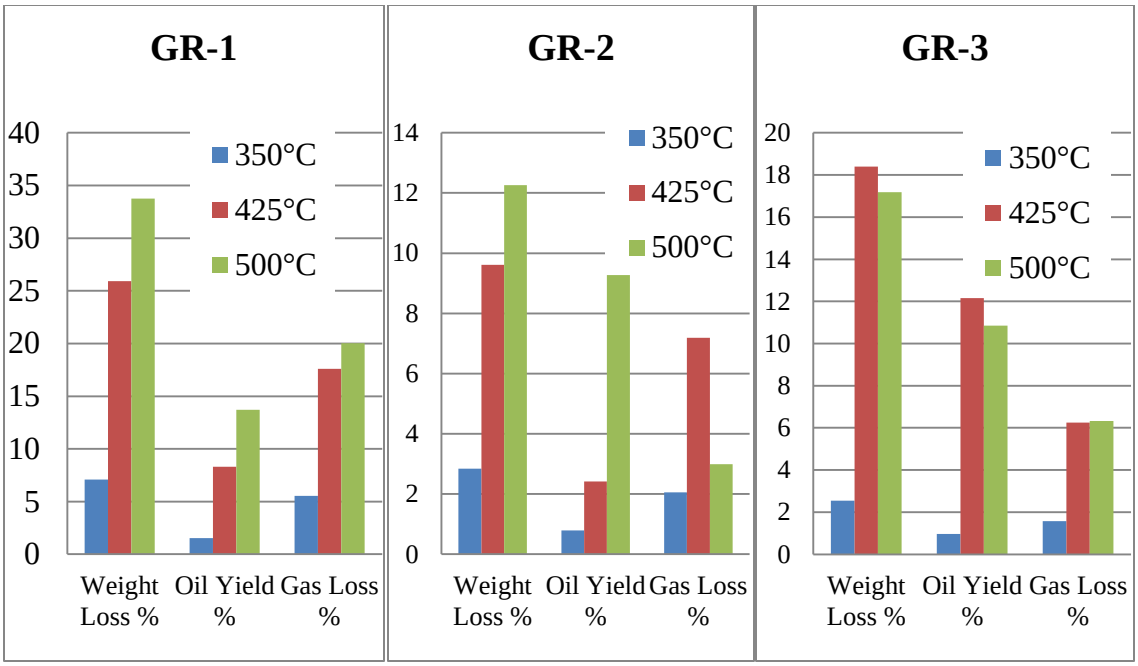

Figure 9- 2: The percent of weight loss, oil yield and gas loss during isothermal pyrolysis of GR core sections. Y axis represents the data in weight percent.

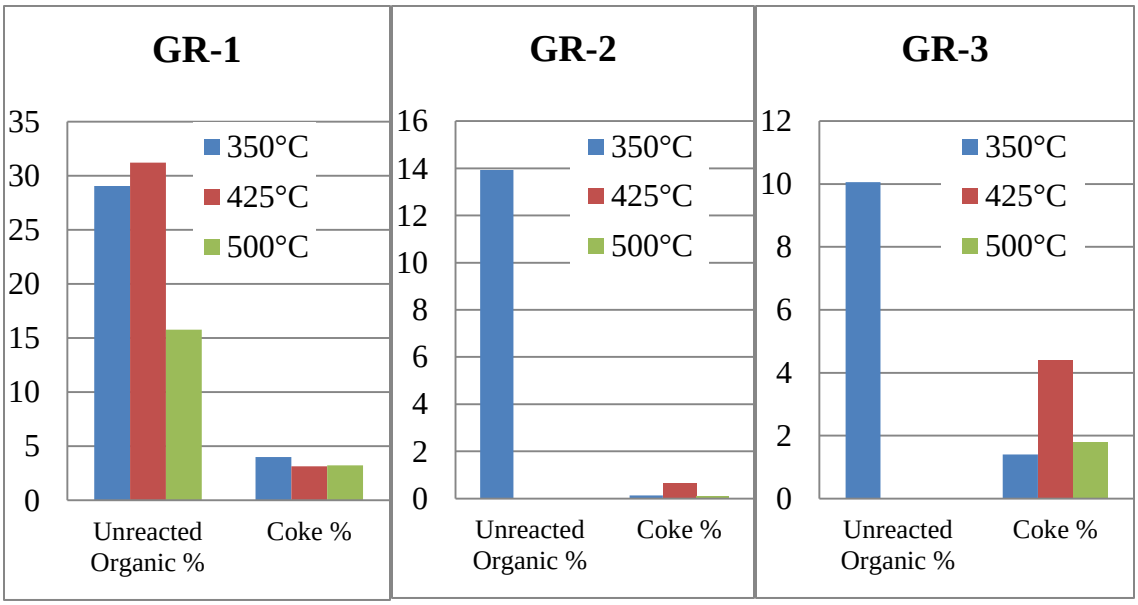

Figure 9- 3: The weight percent of unreacted organic and coke in the spent shales from isothermal pyrolysis of GR core sections. Y axis represents the data in weight percent.

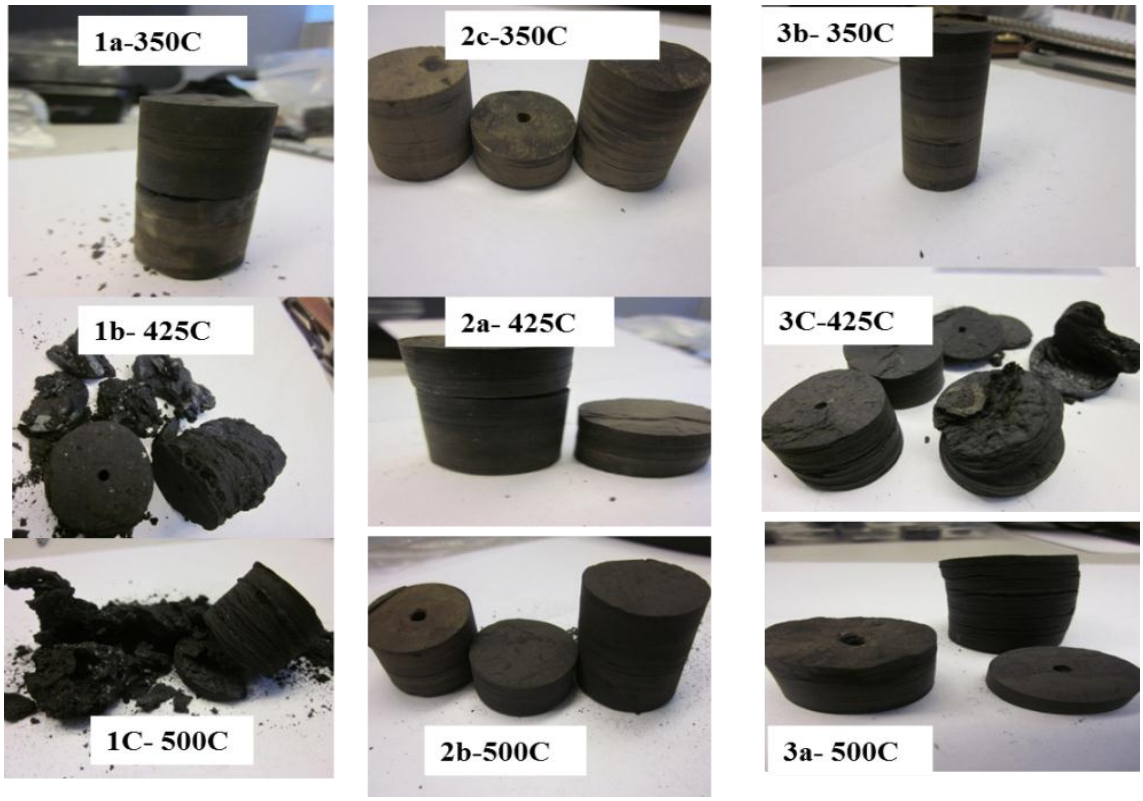

Figure 9- 4: Images of the spent shales from the pyrolysis of GR core samples.

(500°C) pyrolysis showed more deformation than lower temperature pyrolysis (350°C) and organic lean cores (GR-2). It was observed that at 350°C the organic decomposition was slow. Pyrolysis experiments at 350°C resulted in less weight loss and correspondingly low oil yield.

The pyrolysis of GR cores showed a trend similar to the powdered TGA and CHNS analyses of the same sections. GR-1 samples showed a greater weight loss at higher temperatures, but the oil yield did not correspond to the weight loss (maximum 13.7 % from GR-1 core at 500°C). During high temperature isothermal pyrolysis (24 hrs), mineral decomposition may also contribute to the weight loss. The TGA analysis of spent shale showed the presence of significant organic material in pyrolyzed GR-1 samples. This organic matter could either be unreacted organics or heavy oil produced

during pyrolysis. Pyrolysis of GR-1 cores also produced more coke relative to organic lean samples (GR-2 and GR-3). The results suggest that it is not only the temperature which influences coke formation, but the percent of the organic matter in shale is also important. The oil and gas samples collected were analyzed using gas chromatography. The chromatograms of oils from GR samples pyrolysis at 500°C are shown in Figure 9-5. The distribution of hydrocarbons (Figure 9-6) shows that the oils produced from different shales under identical conditions differ in the composition. A similar trend was seen in the gaseous products.

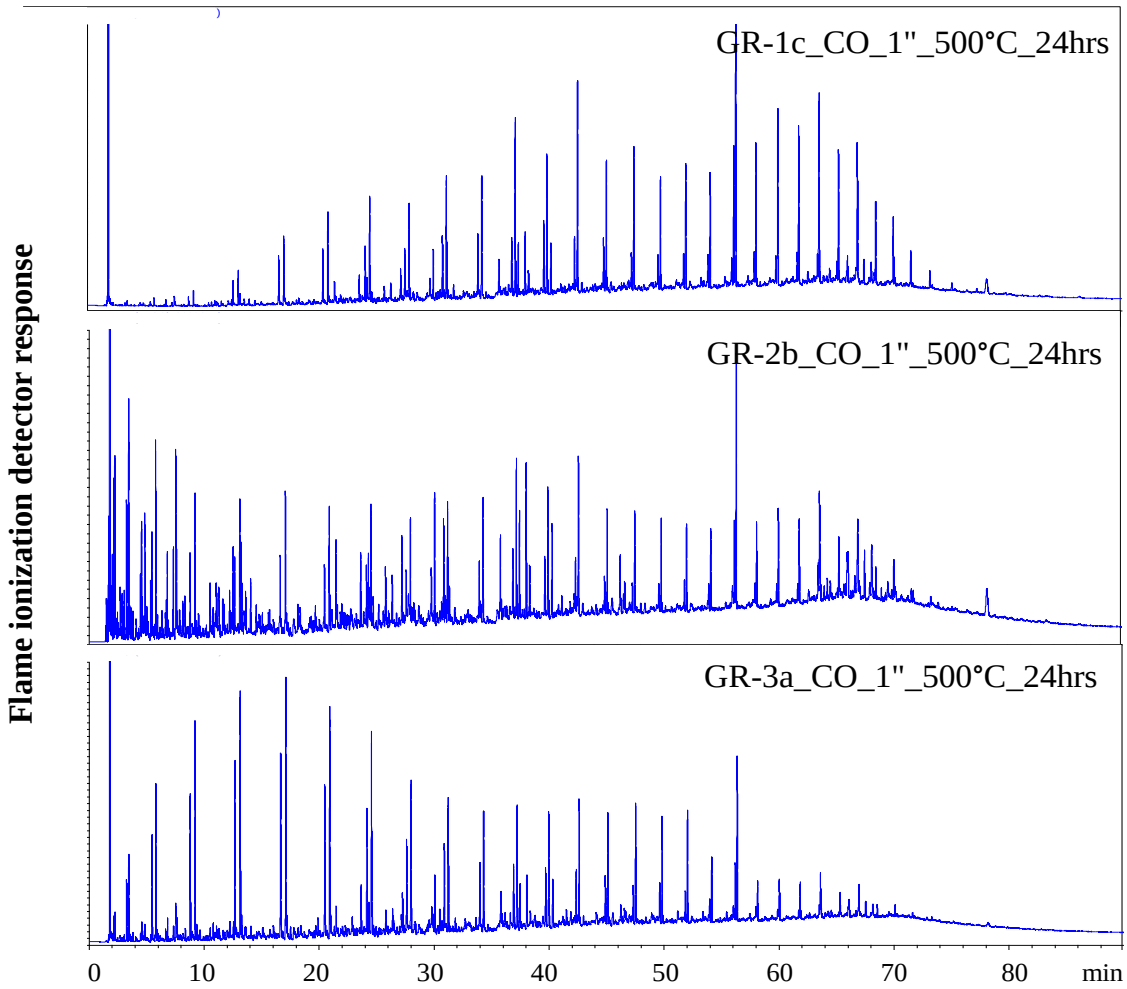

Figure 9- 5: Gas chromatograms of the oil produced at 500°C from GR-1, GR-2 and GR-3 oil shales.

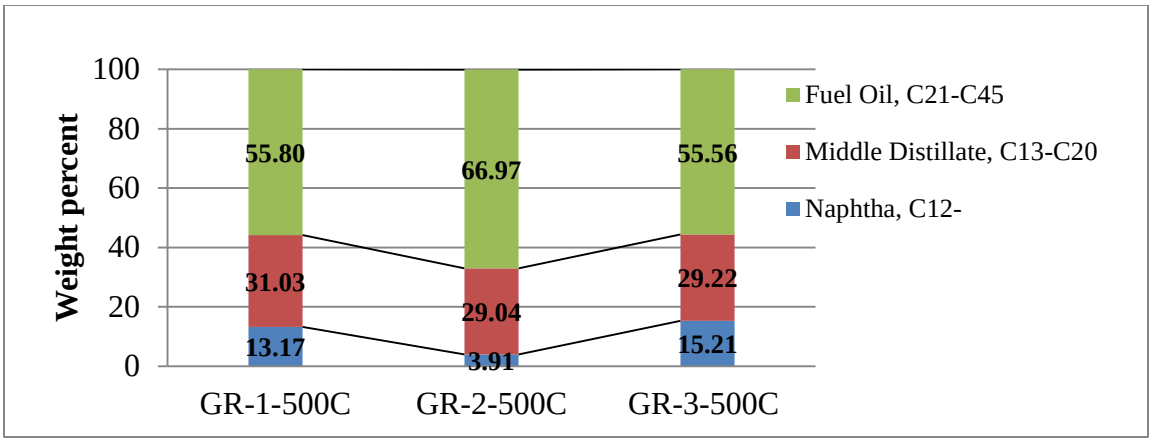

Figure 9- 6: Oil fractions based on single carbon distribution of the shale oils produced from GR samples at 500°C.

The computed tomography (CT) scan analysis of core samples before and after pyrolysis was conducted using Xradia high resolution (~42 Micron voxel) MicroXCT in the Metallurgical Engineering Department at the University of Utah. Figures 9-7 and 9-8 show the effect of pyrolysis on GR-1 samples at two different temperatures. The results show that these samples had huge variation in mineral signatures. During pyrolysis different sections of cores released different amounts of organic matter and created voids. The associated mineral compounds and channels formed during the pyrolysis also affect the product formation and distribution.

9.3. TGA Pyrolysis of Isolated Kerogen

The kerogens from the homogenous powdered samples of GR-1, GR-2 and GR-3 shales were extracted at the Chemistry Department at the University of Utah using a series of strong acids (demineralization process) [152]. TGA experiments, pyrolysis followed by combustion, of the isolated kerogens from GR samples were conducted. The experiments were performed at three heating rates 5°C/min, 10°C/min and 20°C/min to 1000°C in a nitrogen environment and the spent materials were combusted from 400°C

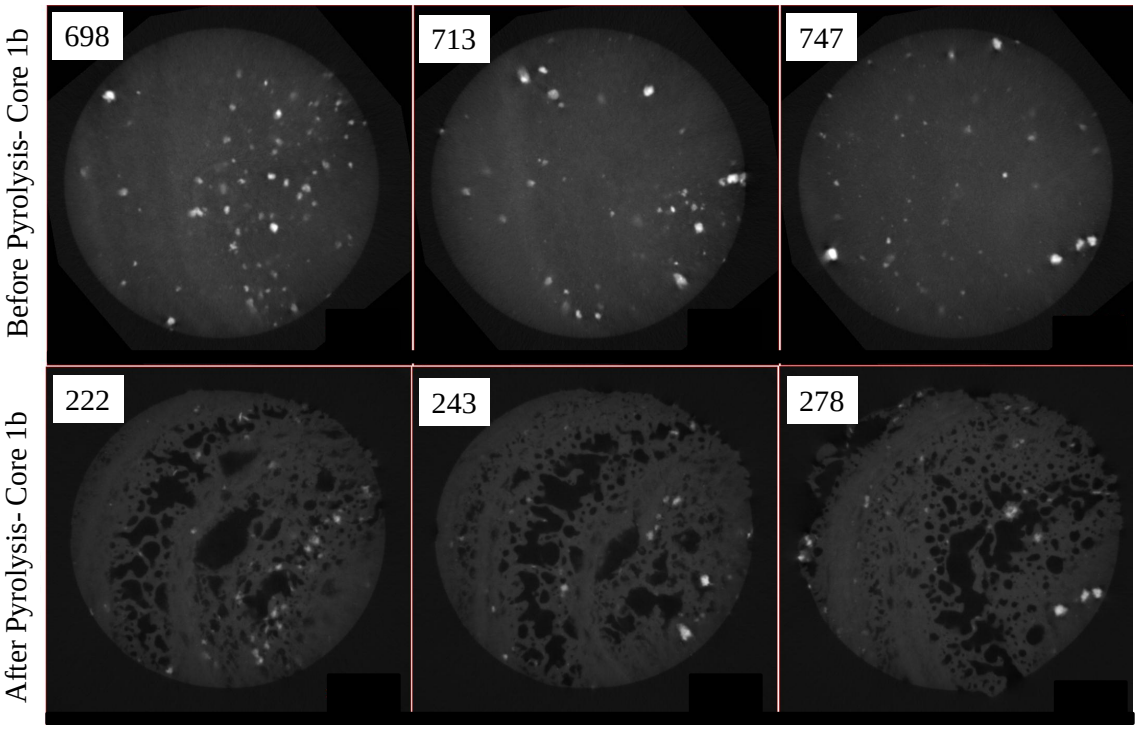

Figure 9- 7: Effect of the pyrolysis (425°C) on GR-1 sample.

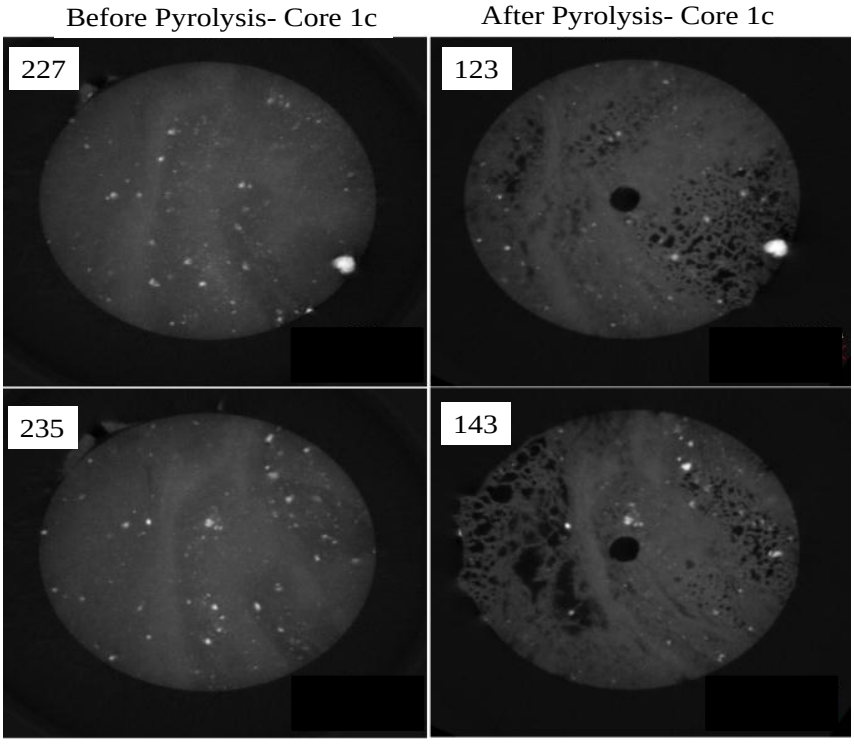

Figure 9- 8: Effect of the pyrolysis (500°C) on GR-1 sample.

to 600°C (10°C/min) and held for 10 mins at 600°C without opening the furnace chamber. The results are shown in Appendix A. The results show that the onset points (start and end) in the pyrolysis zone of all three kerogens were identical. The onset points of kerogen (extracted) decomposition also coincided with those of organic matter of the shale under identical conditions as shown in Figure 9-9. The distribution of kerogen decomposition over temperature suggested that the kinetics is independent of raw material. The kerogen (extracted) weight losses differ and correspondingly the final weight loss. The difference in the final weight loss depends on the extent of demineralization achieved. The coke formed during pyrolysis varies in the range of 10-15 % of initial kerogen weight and was relatively higher for GR-1. This trend was also observed during the TGA pyrolysis of GR-1 shale sample.

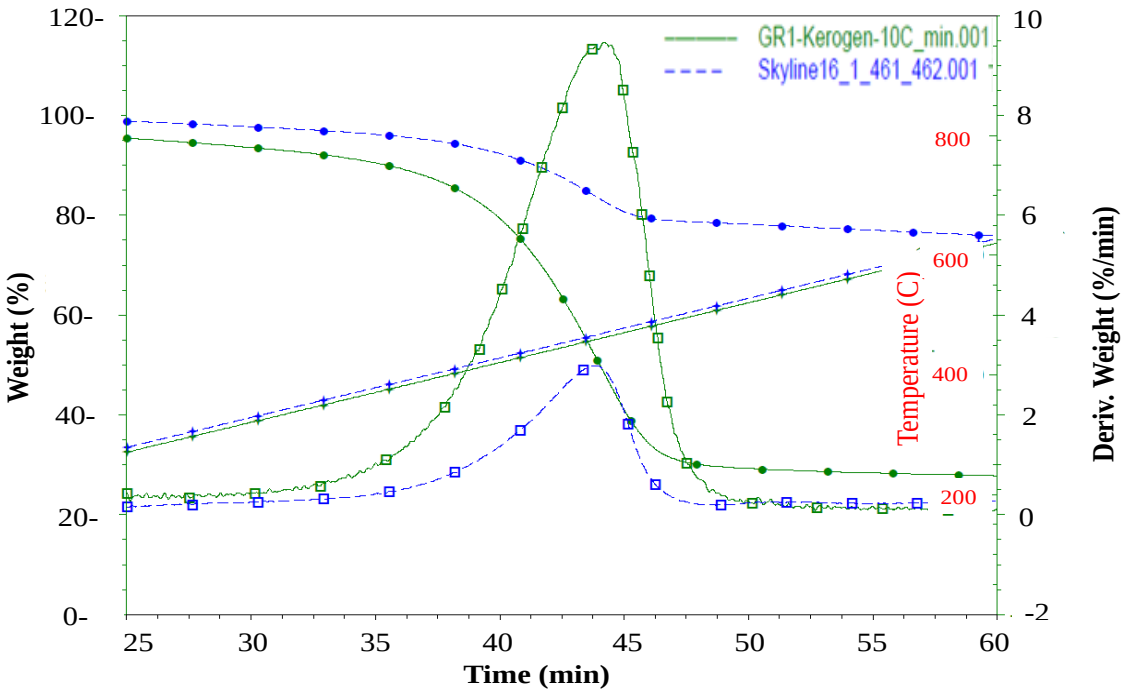

Figure 9- 9: Comparison of the organic matter decomposition onset points during the pyrolysis (10°C/min in N_2 environment) of isolated kerogen (extracted) and original raw oil shale from the same source (GR-1).

10. MATHEMATICAL MODELING OF OIL SHALE PYROLYSIS

The process of transforming solid kerogen to liquid and gaseous products is complex. Several interrelated physical and chemical phenomena occur simultaneously. Products are formed and exit the mineral matrix at definitive velocities through permeable paths. A pore network is created and the pressure changes during the gaseous product formation due to decomposition of the organic matter. A model created with COMSOL multiphysics for oil shale thermal retorting has been developed. The general kinetic model was integrated with some of the important physical processes which occur during pyrolysis. The effect of the process conditions was also investigated.

10.1. Modeling Framework

The main components of the oil shale pyrolysis process, in a logical sequence are depicted in Figure 10-1. A mathematical representation of the physical phenomena during oil shale pyrolysis is modeled in COMSOL multiphysics simulation suite. COSMOL multiphyics uses finite element method to solve the coupled equations simultaneously. The data visualization is relatively simple. It has the capability to include problem specific equation with existing simulation modules. The purpose of developing this model was to understand the coupling of various phenomena in oil shale pyrolysis and to estimate the effect of operational parameters on product distribution. The model developed in this study includes heat transfer due to conduction and mass transformation due to reaction kinetics. Further, porosity and permeability models were included in the

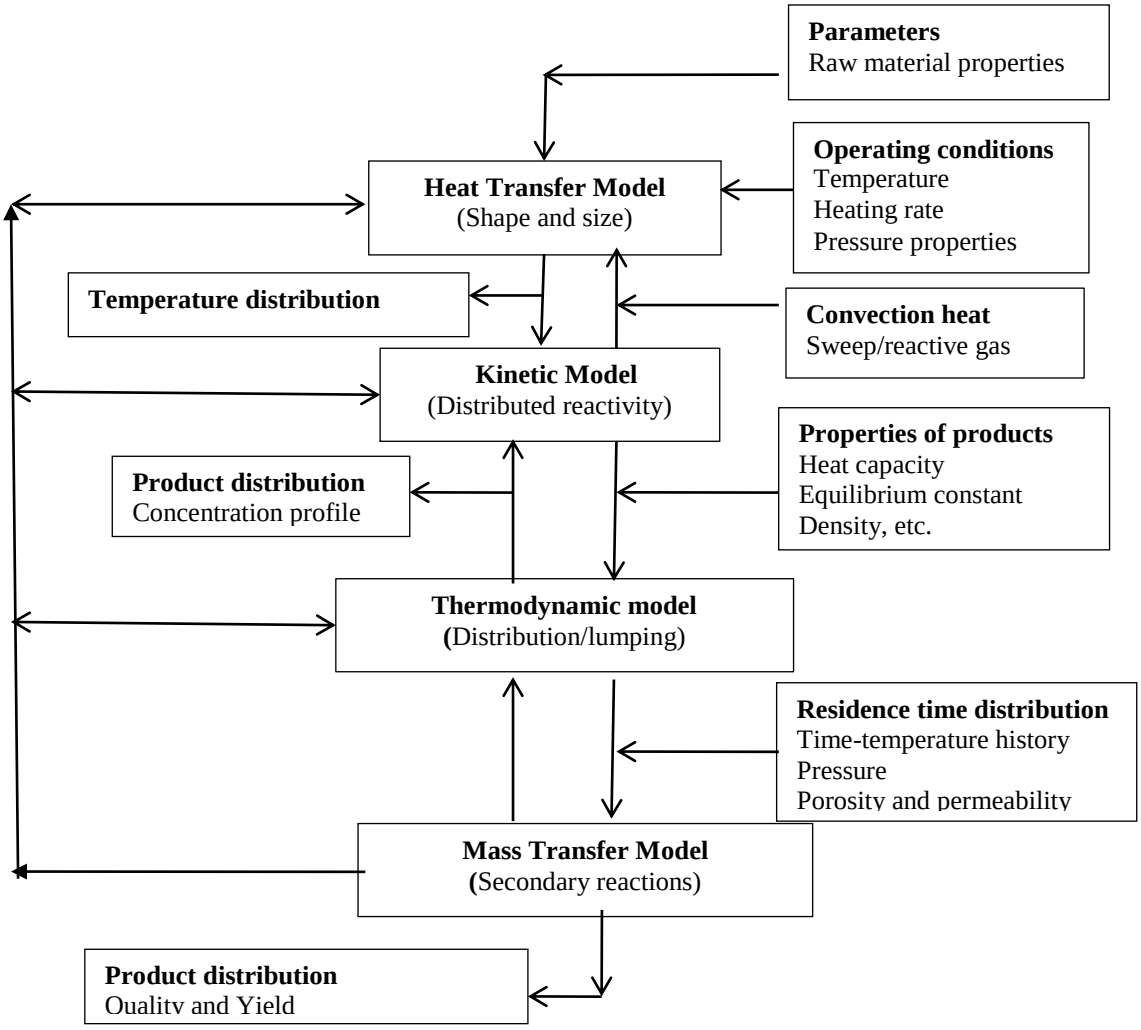

Figure 10- 1: Schematic of the model design to simulate the coupled multiphysics involved in the thermal treatment of oil shale.

framework and convective phenomena in heat and mass balance equations were included. In a shrinking core model, the particle size changes. Hence a grain model concept was applied. It was assumed that the physics vary only in the radial direction. Figure 10-2 shows the geometric representation of simplified simulation scheme adopted in this study. The coupled governing equations were solved simultaneously. Appropriate changes in the physical properties of the material were taken into account as the decomposition process evolved. For example, the propagation of heat conduction within

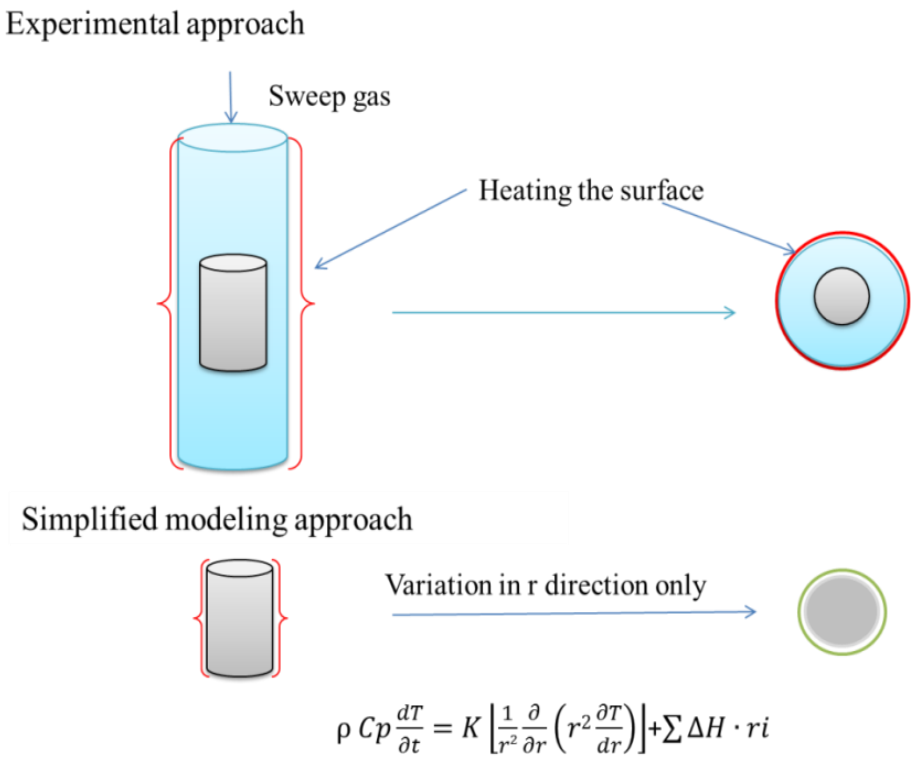

Figure 10- 2: Schematic of experimental approach and identical simulation environment. The variation is in the r direction only.

10.2. Governing Equations and Solution Methodology

The governing equations included in the basic model are shown below.

- Heat transfer equation

$$\rho \cdot Cp\frac{\partial T}{\partial t} + \nabla\left(-k\nabla T\right) = Q - \rho \cdot Cp \cdot \vec{u}\nabla T \qquad (10.1)$$

- Mass transfer equation

$$\frac{\partial c_i}{\partial t} + \nabla\left(-D_{AB}\nabla c_i\right) = r_i - \vec{u}\nabla c_i \qquad (10.2)$$

- Rate equation

$$ri = -A \times e^{\left(-\frac{E}{R\times T}\right)} \times Ci \qquad (10.3)$$

the particle changes the basic physical properties such as density, thermal conductivity, and heat capacity used in the heat transport governing equation. The changes in the physical properties ρ_{OS}, *Cp* and *K* of raw material were adopted from the literature [37, 52] and allowed to be changed as the reaction progressed using the following expressions;

- Density of the raw material- function of organic composition (org)

$$\rho os = \frac{\text{Rho\_org} \times \text{Rho\_rock}}{(\text{Org} \times (\text{Rho\_rock} - \text{Rho\_org}) + \text{Rho\_org})} \quad (10.4)$$

- Heat capacity of the raw material- function of oil yield and temperature

$$\text{Cp} = 4186.8383 \times [0.172 + (0.067 + 0.00162 \times \text{Grade\_OS} \times \text{cO}) \times (10^{-3} \times \frac{9}{5} \times \text{T})] \quad (10.5)$$

- Thermal conductivity of the raw material –function of oil yield and temperature

$$K = 1.73074 \times [(a'_1 \times (1 - b'_1 \times \left(\frac{9}{5} \times (T - 273.15) - 53\right) - b'_2 \times \left(\frac{9}{5} \times (T - 273.15) - 53\right)^2 \times \exp(a'_2 \times \text{Grade\_OS} \times \text{cO})] \quad (10.6)$$

a_1', b_1, a_2` and $b_2$` are constants. Three reaction mechanisms were examined- a single step mechanism which does not account for the secondary reactions and a two-step mechanism in which oil produced during the process participates in the secondary reaction. The mass coefficients in the reactions were adopted from the literature and were modified based on the observation in the laboratory [121]. The third mechanism is a multistep mechanism proposed by Burnham and Braun [121] and modified by Bauman and Deo [153] for mass stoichiometric coefficients as to match the mass and elemental balances. The mass coefficients (equation 10-7 to 10-9) are assumed constant, though reaction temperature affects the distribution of product.

Table 10-1 shows the molecular weight (MW) and elements, carbon and hydrogen data for the multistep mechanism. The data up to three decimal points are required to conserve the mass balance. The mass coefficients were calculated balancing the elements and conserving the mass. The products of the primary reaction from kerogen decomposition are classified as HO (heavy oil), LO (light oil), Gas, Char and Methane. Methane is not included in the Gas fraction and does not go through the secondary processes. All other products participate in further pyrolysis and produce solid and fluid products by cracking or coking.

- Single step mechanism

$$\text{Kerogen} \longrightarrow 0.63\ \text{Oil} + 0.24\ \text{Gas} + 0.13\ \text{Coke} \tag{10.7}$$

- Two step mechanism

$$\begin{aligned} \text{Kerogen} &\longrightarrow 0.63\ \text{Oil} + 0.24\ \text{Gas} + 0.13\ \text{Coke} \\ \text{Oil} &\longrightarrow 0.80\ \text{Gas} + 0.20\ \text{Coke} \end{aligned} \tag{10.8}$$

- Multistep mechanism

$$\begin{aligned} \text{Kerogen} &\longrightarrow a_1\cdot\text{HO} + a_2\cdot\text{LO} + a_3\cdot\text{Gas} + a_4\cdot\text{Char} + a_5\cdot\text{CH}_4 \\ \text{HO} &\longrightarrow b_2\cdot\text{LO} + b_3\cdot\text{Gas} + b_4\cdot\text{Char} + b_5\cdot\text{CH}_4 \\ \text{LO} &\longrightarrow c_3\cdot\text{Gas} + c_4\cdot\text{Char} + c_5\cdot\text{CH}_4 \\ \text{Gas} &\longrightarrow d_4\cdot\text{Char} + d_5\cdot\text{CH}_4 \\ \text{Char} &\longrightarrow e_3\cdot\text{Gas} + e_5\cdot\text{CH}_4 + e_6\cdot\text{Coke} \end{aligned} \tag{10.9}$$

Table 10- 1: Elements and molecular weight data used in constructing the multistep step reaction mechanism.

Component	Kerogen	HO	LO	Gas	Char	Methane	Coke
C	1479.000	31.751	11.189	3.354	1.004	1.000	1.185
H	2220.000	42.818	17.510	11.634	0.546	4.000	0.316
Ratio	1.501	1.349	1.565	3.468	0.544	4.000	0.267
MW	20000.550	424.492	152.034	52.011	12.604	16.042	14.552

The kinetic parameters for kerogen decomposition were taken from Tiwari and Deo [148]. The distributions of activation energy and preexponential factor as decomposition reaction progresses were used for the first step. The kinetic expressions for secondary reactions were fixed, E =200 kJ/mol and A = 1E10 S^{-1}. The heat of the reaction was assigned a value of 370 kJ/kg [154]. All the species concentrations were converted to mass units and the equations were solved keeping the overall mass conserved.

The model was simulated first for a single particle, TGA analysis of a fine powder. The convection terms from heat and mass equations were omitted. To understand the effect of the scale (large size) the model was modified by including flow. Convective heat transfer as well as convective flow of the products was introduced in the governing equations using Darcy's law and the continuity equation assuming fluid follows the ideal gas law. Continuity equations coupled with the Darcy flow generates the velocity data. Ideal gas law was used to account for the change in pressure because of density (ρ) variation. Velocity field (u) is determined by the pressure gradient (∇p), the fluid viscosity (μ), and the structure of the porous medium permeability (K_p).

- Darcy law $$u = \frac{Kp}{\mu} \nabla p \quad (10.10)$$

- Continuity equation $$\frac{\partial}{\partial t}(\rho\varepsilon) + \nabla \cdot (\rho u) = Q_m \quad (10.11)$$

- Ideal gas law $$\rho = \frac{pM}{RT} \quad (10.12)$$

An empirical formula for the porosity generated due to kerogen conversion was used [155]. The relationship of porosity and permeability was established using standard Kozney-Carman equation by assuming the average pore diameter of 50×10^{-6} meter.

- Porosity of oil shale as a function of conversion

$$\varepsilon = 0.003+(0.0146+0.0129\times (Grade\_OS\times xK)-0.000046 \times (Grade\_OS \times xK)^2) \quad (10.13)$$

- Permeability of oil shale

$$K_p = D_p^2 \times \varepsilon^3/(150 \times (1- \varepsilon)^2) \quad (10.14)$$

The model was calculated with the physical and chemical conditions mentioned above. The initial and boundary conditions were assigned according to the geometry and simulation conditions. For temperature, the initial condition was room temperature and boundary conditions were the pyrolysis temperatures (isothermal and nonisothermal). The boundary was set at atmospheric pressure. The mesh size in the geometry was generated and optimized for each simulation to achieve fast and reliable results.

Following assumptions were applied to develop the model

- It is assumed that the material was a 30 gal/ton grade oil shale contains 18% organic matter that was uniformly distributed. The physical properties expressions (*ρos, Cp , K*) were reported for this grade in the literature.

- The material was heated in the radial direction and it was assumed that the system is symmetrical with respect to z and theta direction.
- Mass transfer through diffusion was not considered. A very small value 10^{-50} [m^2/s] was used for all the species
- Mass transfer equation was solved for each species involved in the reaction network. Kerogen, char and coke were considered as the solid phase, while the oils and gases were the fluid phase.
- Single phase fluid behavior was applied assuming propane as a model fluid to compute the flux of each species. Model built follows the ideal gas law.

10.3. Model Results and Observations

The model developed was simulated with several conditions. A single particle model was examined for all three mechanisms to understand the kinetics and product distribution. This simulation scheme did not include the convective terms and it used the intrinsic kinetics parameters like in the TGA experiments and in a closed system. Figure 10-3 shows the kerogen decomposition and product formation for a single step mechanism for isothermal (400°C) and nonisothermal (10°C/min) boundary conditions. The two step and multistep mechanisms were simulated for the identical conditions and the results are shown in Figure 10-4 and Figure 10-5, respectively.

It can be observed from the results of single particle simulation that the kinetics used for the kerogen decomposition is able to simulate the process effectively. The kerogen decomposition followed the similar trend as TGA analysis. The products formed are in accordance with the mechanisms and associated mass stoichiometry. The results also suggest the effects of the secondary reactions on the final products. To achieve the

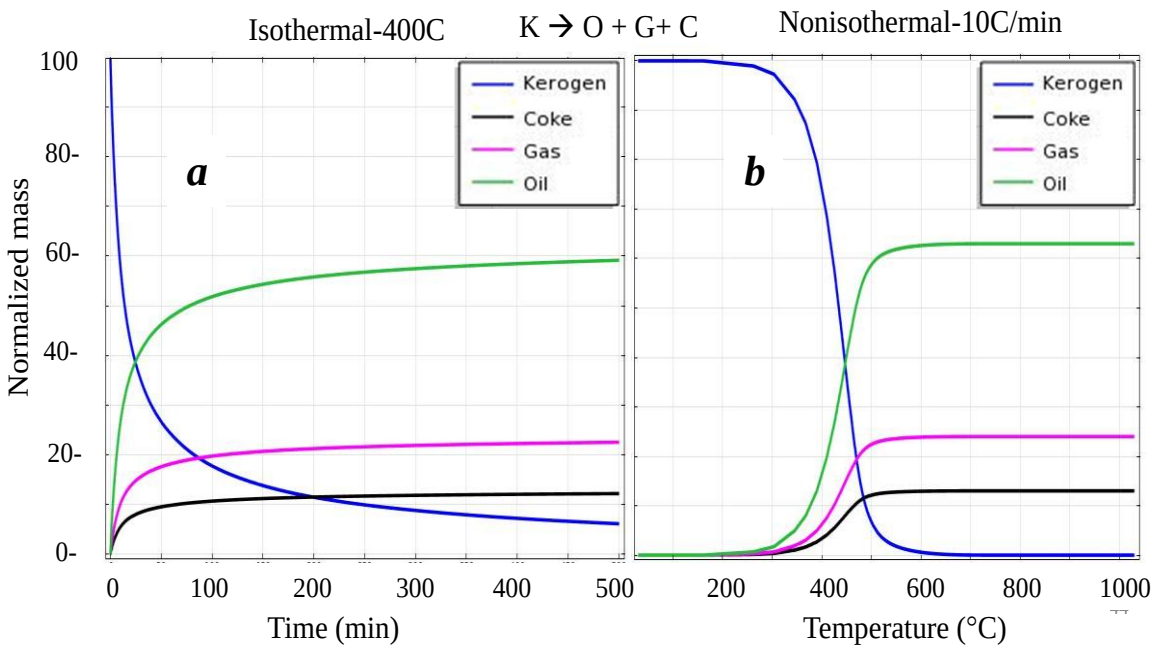

Figure 10- 3: Kerogen decomposition (single particle) and product formation profiles using single step mechanism under (a) isothermal (400°C) and (b) nonisothermal (10°C/min).

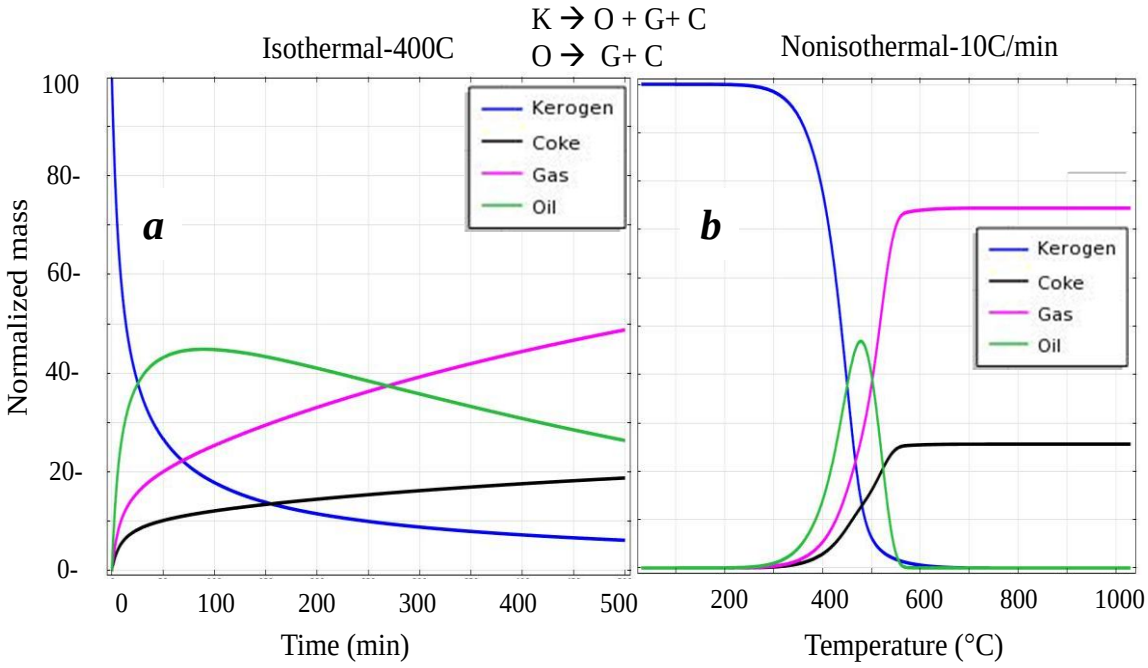

Figure 10- 4: Kerogen decomsposition (single particle) and product formation profiles using two step mechanism under (a) isothermal (400°C) and (b) nonisothermal (10°C/min).

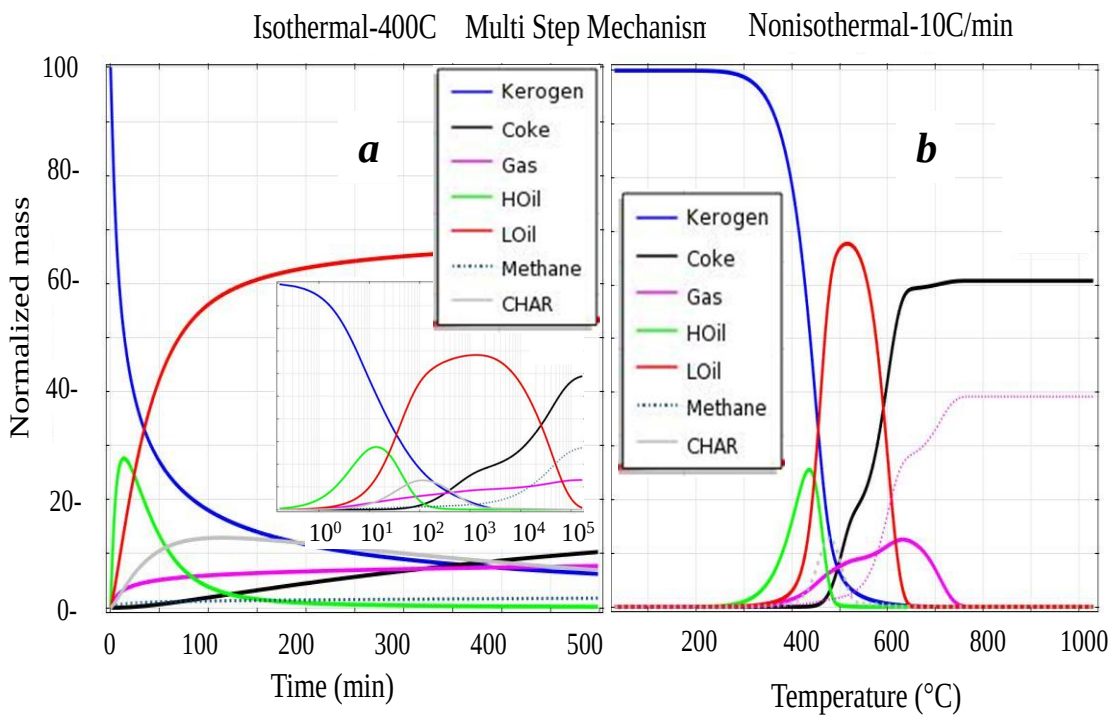

Figure 10- 5: Single particle (TGA scheme in batch mode) of kerogen decomposes to different products using multiple step reactions mechanism under (a) isothermal (400°C) and (b) nonisothermal (10°C/min) pyrolysis. The small window shows the material profiles at long time scale (a log scale).

maximum yield of the desired products, the material needs to be in a pyrolysis environment for a certain time and temperature. Increasing the temperature and heating rate reduced the optimal time. However, it is clear from the results that if the products are heated for a longer time (isothermal) or to higher temperatures (nonisothermal) the final result will be coke and gases. Thus, it is important to sweep the products out.

The reaction mechanism is an important factor to control the product distribution. The multistep mechanisms showed that products are dominated by light oil fractions if the process is shutdown when kerogen decomposition is about 90% at 400°C (isothermal) and 10°C/min (nonisothermal) cases. This value was observed to decrease with an increase in temperature and heating rate for the maximum production of light oil. These

are results of the secondary reactions. The two step mechanism which describes oil degradation as secondary reaction shows that maximum oil yield occurs at 80% and 95% kerogen conversion at 400°C isothermal and 10°C/min nonisothermal conditions respectively.

The next logical step in understanding the product formation rates and distributions was simulating the process with open boundary conditions with a large sample size. The fluid products generated were allowed to travel within the sample by the pressure gradient generated due to gas and methane formation. Core geometry of 10 cm radius was selected. The material was heated in two different configurations which were surface heating and heating from the center of the core. The schematic of the geometries for this simulation scheme is shown in Figure 10-6. In case of heat source at the center of the core a boundary with a radius of 1cm was created inside to act as a heater. There is a temperature distribution across the material in heating schemes. Temperature distribution

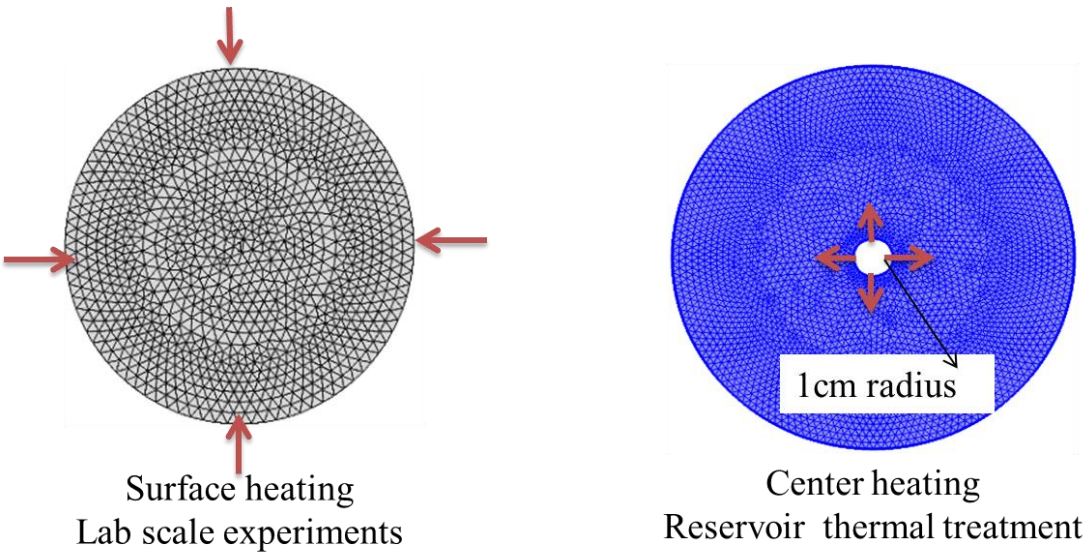

Figure 10- 6: Schematic of the application of the heat to the source material via surface heating and center heating.

controls the kinetics, and hence the product distribution. The temperature distribution across the sample due to heat conduction and resulting rates of heavy oil formation in different sections in case of isothermal (400°C) surface heating are shown in Figure 10-7. The formation and degradation of products occur in a manner similar to single particle simulations. The temperature at the surface is higher thus the formation and degradation of heavy oil occur earlier. And, if the desired products (oils) are not collected at specific time/temperature they participate in the secondary reaction network resulting in formation of more coke and gases.

Further, other physical processes such as convective heat, convective mass transport, and creation of porous media to flow were included in the model. The simulations were carried out when the pressure generated due to the product formation regulated the flow behavior of the fluid products.

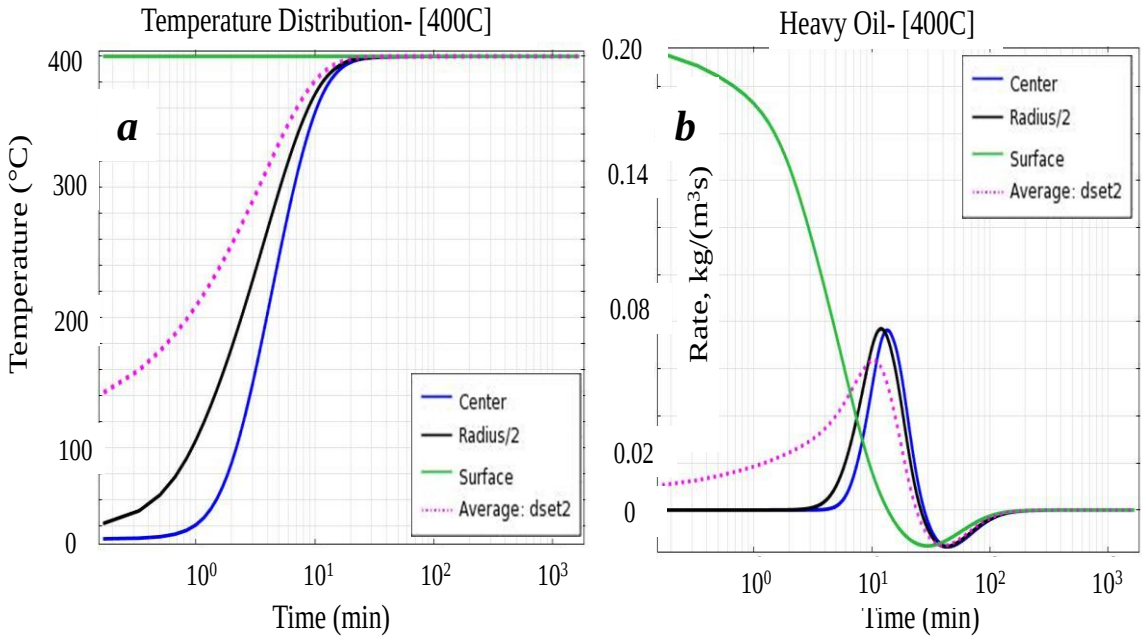

Figure 10- 7: Isothermal (400°C) surface heating, (a) distribution of temperature and (b) rate of heavy oil formation in different sections of the core.

A single phase flow by using propane as a model fluid, for gas and methane fractions with Darcy's law was incorporated in the model. The convection terms in heat and mass equations were included. All fluid products were assumed to follow the velocity of model fluid. The comparison of the rates of product formation at the surface with convection and no convection under nonisothermal heat input at the surface (10°C/min) is shown in Figure 10-8. The rates of fluid products are comparatively higher with convection. This indicates that the convective source in heat and mass transport equations influences the product rates.

When the material is heated from surface, the products form faster at the outer zone and are released. Temperature propagates from the outer surface to inner zone. The product formation creates a porous network. The products at the inner zone form and are transported from a cold to a hot zone. The high temperature in this path favors the secondary reactions, but fluid spends less time due to high porosity. In the case of central

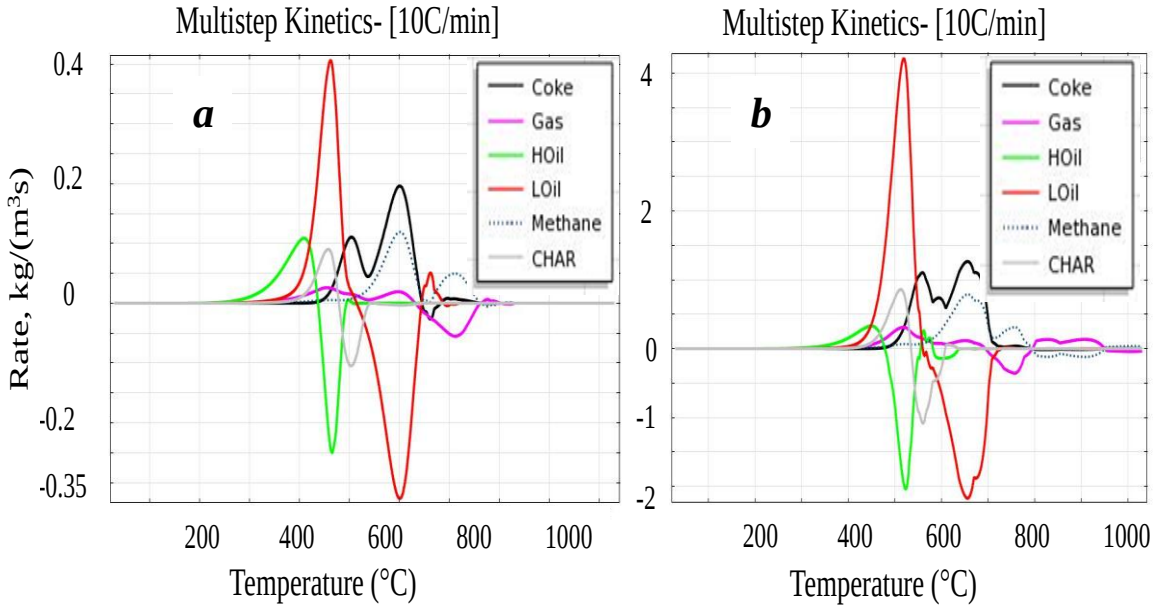

Figure 10- 8: Effect of convection on product formation rates.

heating, the products hit the low temperature and less permeable zone. These conditions restrict the flow and products spend more time within the sample. The condensation reactions due to local thermodynamic conditions may occur. The thermodynamic behavior of the fluid products is not taken into consideration in this model. In both the cases, kinetic conversion experienced a combined isothermal and nonisothermal temperature history. Figure 10-9 shows the average total flux (kg/m^2.s) of the fluid products from the surface of 10cm radius core samples in the surface heating and center heating schemes under isothermal (400°C) heat supply to the material. The comparison of these two plots shows that due to different time/temperate history the material is exposed, average outward fluxes of the products from the surface varies significantly in the distribution. In case of the center heating products come out with a time delay and lighter oil is produced.

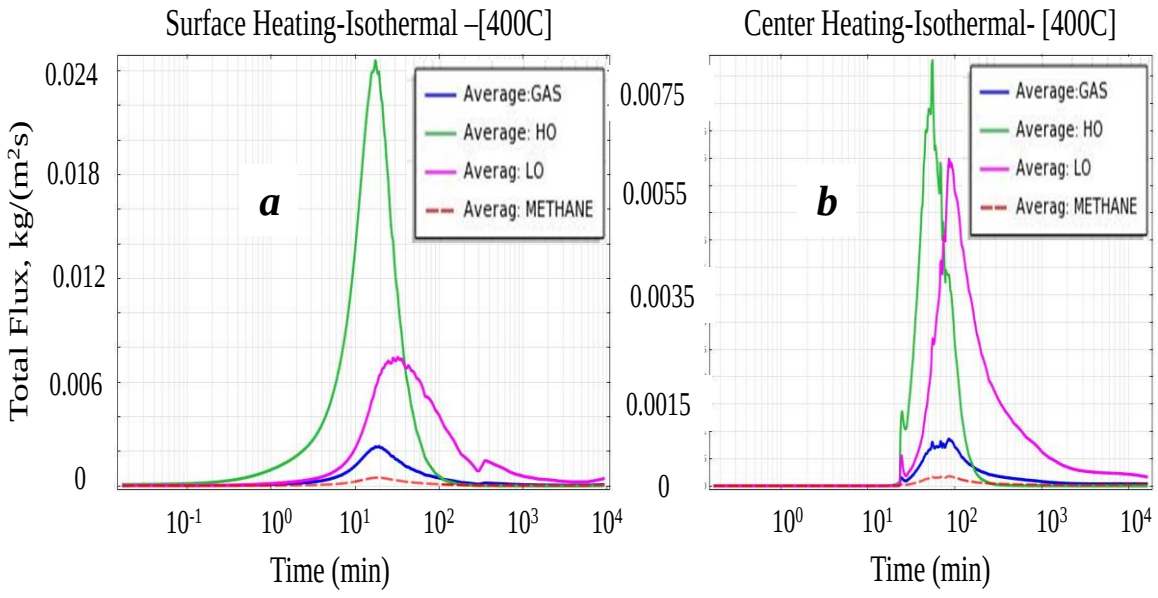

Figure 10- 9: Average total flux of the fluid products from the surface of the core during (a) surface heating and (b) center heating schemes.

10.4. Summary of the Model Results

The model is able to capture the effect of operation conditions and influence of secondary reactions on the distribution of products. The secondary reactions of coking and cracking in the product phase were addressed and their formation kinetics were included. The product distribution is constrained by elemental and product mass balances. The model is capable of predicting compositional information for generated and collected products at different scales. The simulation was designed to understand the effects of the temperature and heating rate on product distribution when additional physics involved in the process are applied. Surface and center heating schemes replicate two different boundary conditions of the core. The heat transfer through a large block experienced both isothermal and nonisothermal behavior simultaneously. The heat distribution regulates the kerogen conversion to product and formation rates. The secondary reactions in the process control the final product distribution. Each physical and chemical process included in this study influences the results. Additional processes which are not considered in this model may alter the product distribution such as thermodynamics of the phase equilibria, multiphase flow behavior, contributions of mineral reactions to the reaction network and the gas pressure generation, etc. The measurement study of the fracture and expansion during the pyrolysis at various temperature and compressive loads was reported [156-158]. These physical processes may also be important in developing a model. The model needs validation against experimental data.

11. CONCLUSIONS AND FUTURE WORK

The study carried out in this research indicates that oil shale pyrolysis is a complex process and that the distribution of the products depends on the raw materials and process conditions. Pertinent conclusions from each part of the study are listed. Limitations and some considerations for future work are described following the conclusions.

11.1. Conclusions

11.1.1 TGA Pyrolysis-Kinetic Study of Organic Decomposition

Thermal gravimetry analyses (TGA) on the samples were performed under different conditions and in different environments. The overall weight loss decomposition profile depended on the operational environment (N_2, Air and CO_2). The decomposition of Mahogany oil shale during pyrolysis using TGA revealed the distribution of the kinetic parameters on the conversion scale. The absence of coke in the spent shale reveals that the mass resistance was negligible at this scale. The activation energy derived from the advanced isoconversional method ranged from 93 to 245kJ/mol with an uncertainty of about 10%. A simulated kinetic model (advanced isoconversional method) that does not include transport effects was extrapolated. The distributions of kinetic parameters over conversion scales simulated isothermal pyrolysis. The intrinsic kinetics was found to be the same for the samples used in this study. The pyrolysis of kerogen from different oil shales also shows similar trends. This indicates that the intrinsic kinetic of organic

decomposition does not depend on the presence of organic matter and mineral matrix in oil shale. However, the amount of coke formed was observed to be higher in organic rich samples, especially when pure kerogen was pyrolyzed. A significant amount of coke was also observed under high pressure even with 100 mesh size particles (High pressure TGA analyses).

11.1.2 TGAMS Pyrolysis-Compositional and Kinetic Analysis

Single ion monitoring of mass spectra from combined TGAMS analysis was used to reveal the inflections in TGA thermograms during the continuous pyrolysis of powdered samples at different thermal ramps. The identification, quantification, and thermal behavior of many hydrocarbon products and mineral gases were studied. The feasibility of obtaining kinetic parameters of individual and lumped components using the advanced isoconversional method was demonstrated with examples of benzene and lumped components, C_8 and naphtha. However, because the compound evolution signals as detected by mass spectrometry were noisier than the overall weight loss data, the uncertainties in these measurements were much greater in certain conversion ranges. Similar principles can be used to derive single component evolution kinetics.

11.1.3 Multiscale (Benchscale) Pyrolysis Experiments

Experiments with different core sizes were performed under batch and continuous flow conditions and at isothermal and nonisothermal conditions for different heating rates. A few experiments were conducted at 500 psi. It was observed from GC and GCMS analyses that the variation in the composition of the products was large. With an increase in the size of the sample and pressure, the heat and mass resistances increase, producing more coke. This may be due to an increase in the residence time of the evolved

products in the heated section. The products at higher temperature participated in secondary reactions namely coking and cracking. Secondary reactions produce light products as well as coke in significant amounts. The increase in the coke formation with pressure was confirmed with high pressure TGA pyrolysis.

Increasing the pyrolysis temperature and heating rate, increased weight loss, oil yield and the amount of gas produced. Low temperature and low heating rate yielded more coke than weight loss. High temperature, higher heating rate and low pressure favored more oil yield. Oil yield decreased and the amount of coke formed increased as the sample size and/or pressure increased. However, the relationship between these parameters was not linear. It was also observed that increase in the temperature, pressure and size of the sample improved the quality of the oil produced.

11.1.4 Hydrous Treatment of Oil Shale Pyrolysis

TGA analyses of water soaked oil shale samples reveal no effect on decomposition temperatures. The oil produced from water soaked oil shale pyrolysis contains relatively more alkenes and aromatics. Organic species with a potential to be in the water phase are produced during pyrolysis. The water solubility of these compounds vary over a wide range depending on pyrolysis conditions and on sorption coefficients. The analyses in this study showed a very low to nondetectable range of the organic species concentration in the water phase in most of the samples analyzed. If a potential source exists, aquifer contamination possibilities are very high. Depending on the type of interaction with the aquifer, concentration of dissolved constituents in water may persist over long periods of time.

11.1.5 Heterogeneity in the Raw Material

The results in this research indicated that there is a significant heterogeneity present in the raw shale. The sample from the specific location (Skyline-16) showed considerable variations in the amount of organics present. The yields of oil depend on the organic matter present and the complex mineral matrix associated with the sample. Pore scale analyses of the core sample before and after pyrolysis showed that the sample with less organic matter and thermally stable mineral matrix did not show any significant deformation during pyrolysis. Pyrolysis of organic rich core produced large pore space during the thermal treatment.

It was also observed that at grain size the thermal decomposition of the organic matter in different shales and of isolated kerogen extracted from these samples followed the same thermal history. The kinetic parameters of thermal decomposition of the organic matter in shale and extracted kerogen were identical and do not depend on source material. However, the amount of the coke depends on the amount of organic material and it increases with an increase in organic matter.

11.1.6 Mathematical Modeling of Oil Shale Pyrolysis

The model developed in COMSOL multiphysics uses advanced model free kinetic parameters of calculating decomposition reaction rate for the primary product formation. Secondary decomposition reactions are included to account for compositional changes at different time, length and temperature scales. The model is simulated for isothermal and nonisothermal cases. The yield and quality of the products are strongly dependent on the heat supply rate and product transformation path. The mechanisms and associated kinetic parameters are also important. The model captures the basic physical and chemical

phenomena involved in the progress of process. The heating mode and sample size are vital factors in achieving a desired quality as well as yield of the pyrolysis products. This model can be used as a tool to predict the pyrolysis products and transport in oil shale. This helps in designing oil shale pyrolysis processes to optimize the yield and quality of the desired product based on resource characteristics. The study conducted can be used to scale up experimental data from resource samples to rubble or field scales. However, variations between resources may make this computational tool resource specific. Computational efficiency and numerical stability are not well known for this problem.

The data generated experimentally and the model developed provide an understanding of the simultaneous effects of the operational parameters and physical and chemical processes on oil quality and yields. The results may be useful to put forward a reaction mechanism, and to derive a composition based kinetic model which are useful in optimizing the operating conditions for practical applications (retort modeling or reservoir modeling).

The conclusions described above must be kept in perspective because of the complexity and heterogeneity of the material and the process. Some of the experimental and modeling challenges are listed below.

- The total amount of organic matter during thermal treatment is distributed among liquid, gas, coke and unreacted organic material. There is a wide range of heterogeneity in oil shale in both organic and mineral compositions.
- The structure and composition of the organic matter (kerogen) are not yet well established.
- Accurate isothermal and nonisothermal operations at large scale are not possible.

- The heterogeneity in the raw material makes the analyses complicated.
- The product distribution shows a uniform trend that is not quantitative.
- Secondary reactions occur during the process through complicated mechanisms.
- The products exhibit competitive reaction mechanisms of formation, but the source of this irregularity is unknown.
- Many mechanisms could be postulated. Parameters in mathematical models can force a good fit, but this does not mean that the model is unique.

11.2. Future Work

The TGA kinetic model needs to be integrated with large size samples. This information should be combined with a heat and mass transfer model to create a model for pyrolysis in the core. The combined analysis may permit the absolute quantification with temperature distribution of the products and may be used in the development of a comprehensive kinetic model. The study of mineralogy suggests that additional reactions, dehydration and dehydroxylations need to be included in the complete pyrolysis mechanism. The mathematical model developed in this study needs to be improved to account for the thermodynamic behavior of the products formed.

The experiments with homogeneous material, and known and variable porosity, hence residence time, would be helpful in developing a kinetic model which treat the effects of pyrolysis conditions on oil evaporation and its relationship to oil cracking and coking. The chemical mechanisms affecting oil yield and compositions may differ at high pressure. Experiments are required to be performed when no mass and heat resistances are present (powdered sample) and keeping the same residence time of evolved product in ambient and high pressure conditions to understand the effect of the pressure on

decomposition mechanism. The effect of the pressure is not considered in kinetic expression for organic decomposition used in this study. More large scale pyrolysis experiments need to be conducted to confirm that the water phase remains free of oil components.

APPENDIX A

TGA ANALYSES OF OIL SHALE

A.1. Effect of Particle Size on Oil Shale Pyrolysis

Sample #1 (PO) was crushed and screened for different mesh size. The samples were pyrolyzed (N_2) and further combusted (Air) in a TGA-DSC unit. The flow rate of sweep gas was fixed at 50 ml/min and the heating rate of 10°C/min was used. The thermograms at three particle sizes are compared in Figure A-1. No significant difference was observed on organic decomposition temperature scale with the size of the particle used. There was also no sign of coke observed in these runs. However, there was a slightly difference in the overall weight loss.

A.2. Effect of Sweep Gas Flow Rate on Oil Shale Pyrolysis

The crushed powder oil shale (sample #1) of -100 to +140 mesh size was pyrolyzed and further combusted under different flow rates of sweep gas, nitrogen. The flow rate used ranges from no flow to maximum flow rate of 100 ml/min. The experiments were performed at heating rate of 10°C/min. The thermograms are shown in Figure A-2. The thermograms reveal that there was no uniform trend in organic decomposition profile with the flow rates. The flow rate at 100°C/min provided better and sharp peaks for the decomposition rate profiles. This may be because the instrument was calibrated for 100 ml/min flow rate.

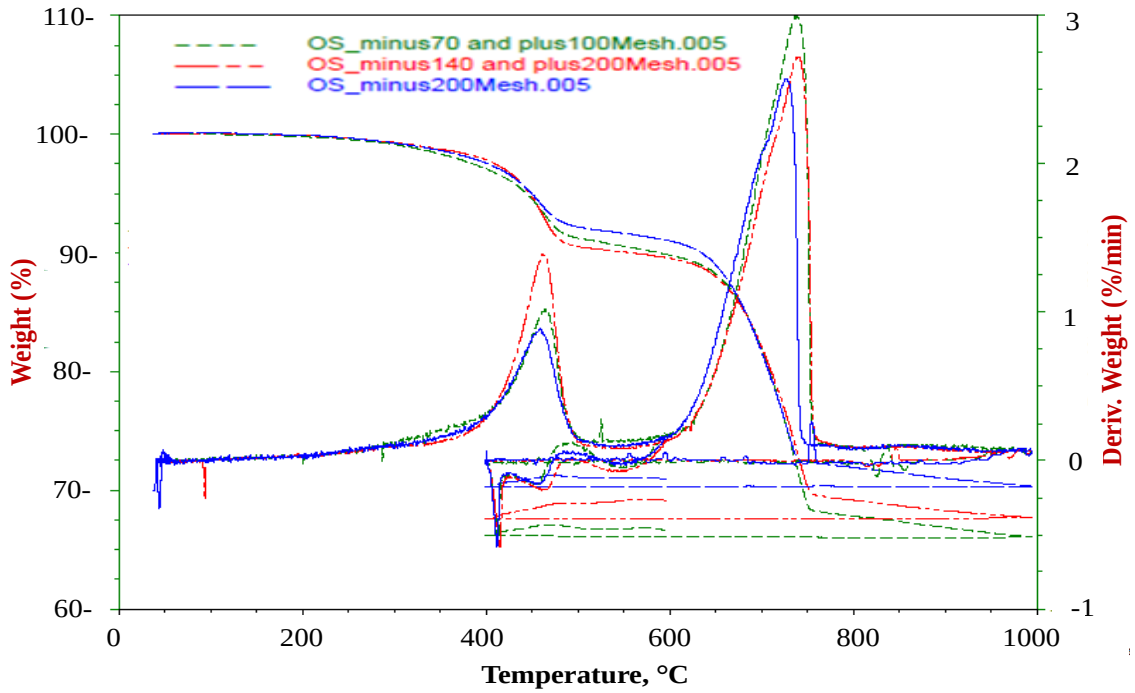

Figure A- 1: Pyrolysis (N_2) of powdered oil shale with different particle size ranges from minus 70 mesh to plus 200 mesh.

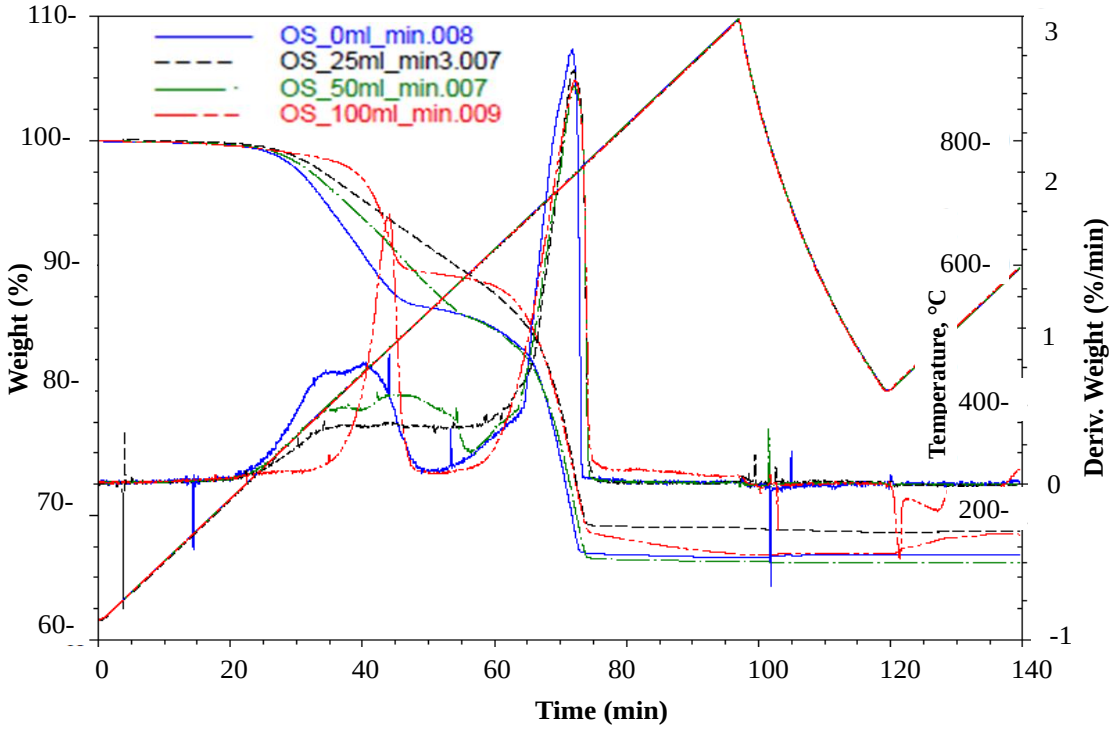

Figure A- 2: Pyrolysis (N_2) of powdered oil shale with different flow rates of nitrogen.

A.3. Oil shale (PO) Retorting in Different Environments

Kinetics of the organic decomposition of oil shale in different gas environments may be relevant in different types of in-situ processes. The powdered oil shale (sample #1) samples were subjected to thermo gravimetric analysis under different environments and heating rates (Table A-1). The powdered oil shale (sample #1) of 100 mesh size was used along with 100 ml/min flow rate of sweep gas. The TGA data (onset points, weight loss and temperature) were compared for pyrolysis (N2), combustion (Air) and CO_2 (50% with N_2) environments at two heating rates (5°C/min and 20°C/min). The comparative TGA thermograms are shown in Figure A-3. The results are summarized in Table A-2 for organic decomposition window. The thermograms in N_2 and CO_2 environments showed only one peak while air had two peaks in organic decomposition section. The range of decomposition temperature shifted to higher temperature as the heating rate increased in all the experiments. The total organic weight loss was observed more in combustion (air) compared both N_2 and CO_2 experiments. Comparatively, the temperature span in CO_2 experiments was larger than with N_2 and the total organic weight losses were not significantly different. Helium and nitrogen experiments did not did not show significant differences.

Table A- 1: List of the experiments performed with TGA in different environments.

TGA Nonisothermal Experiments, °C/min			
N_2	Air	CO_2-N_2-50%	He
0.5	0.5		
1	1	1	1
2	2	5	2
5	5		10
10	10	10	
20	20	20	
50	50		50

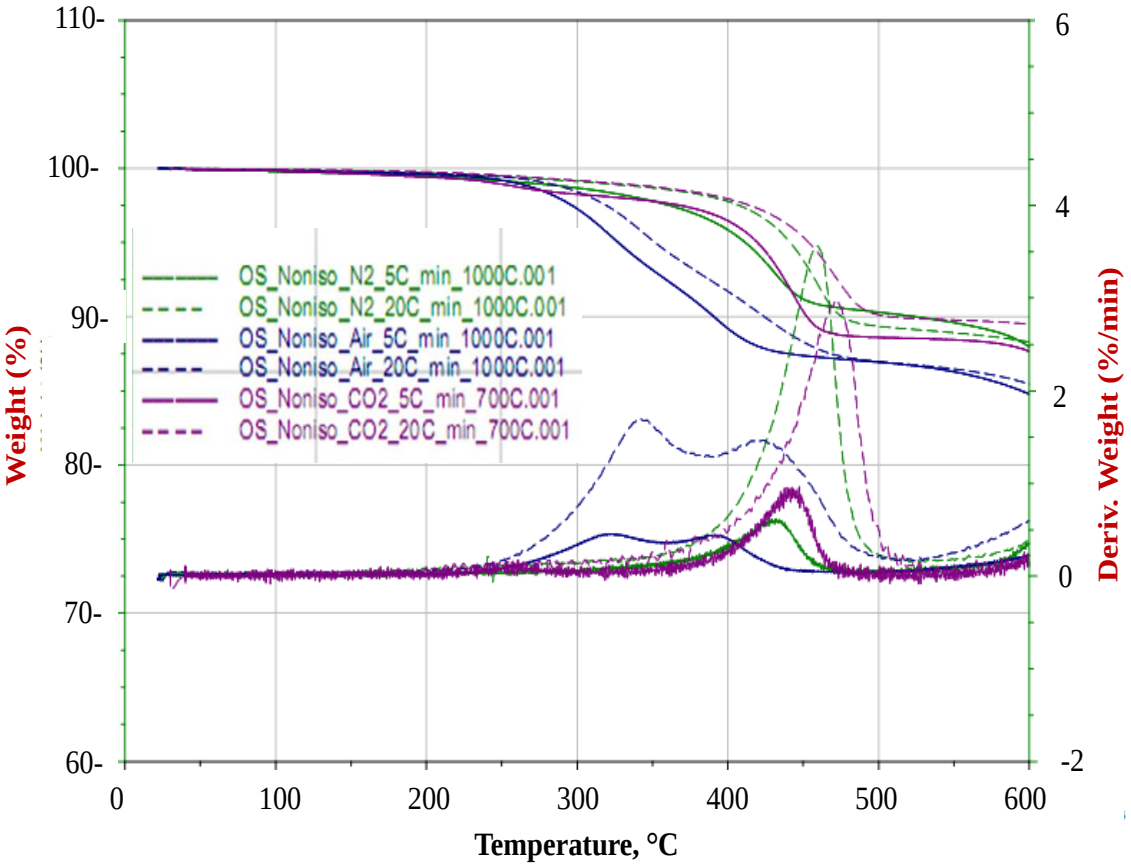

Figure A- 3: The TGA curves for organic decomposition of oil shale in three different environments (N_2, Air, and CO_2) and at two different heating rates, 5°C/min and 20°C/min.

Table A- 2: The TGA onset points (weight loss and temperatures) for organic decomposition of oil shale in three different environments (N_2, Air, and CO_2).

Organic decomposition		N_2	Air		CO_2
			1St peak	2nd peak	(50% N2)
5C/min	Start T, C	348.93	211.6	358.5	336.31
	End T,C	474	358.5	459.65	496.12
	Wt loss %	9.41	7.46	12.72	10.98
20C/min	Start T, C	371.61	215.5	389.2	351.32
	End T,C	504	389.2	504	530.56
	Wt loss %	10.68	7.58	13.07	10.15

A.4. Comparison of the Pyrolysis of Sample #1 (PO) and Sample#2 (CO)

The TGA thermograms of sample #1 and sample #2 at three heating rates are compared in Figure A-4. Samples of 100 mesh size and flow rate of nitrogen at 100 ml/min were used. The weigh derivative profiles for both the samples follow the same temperature window.

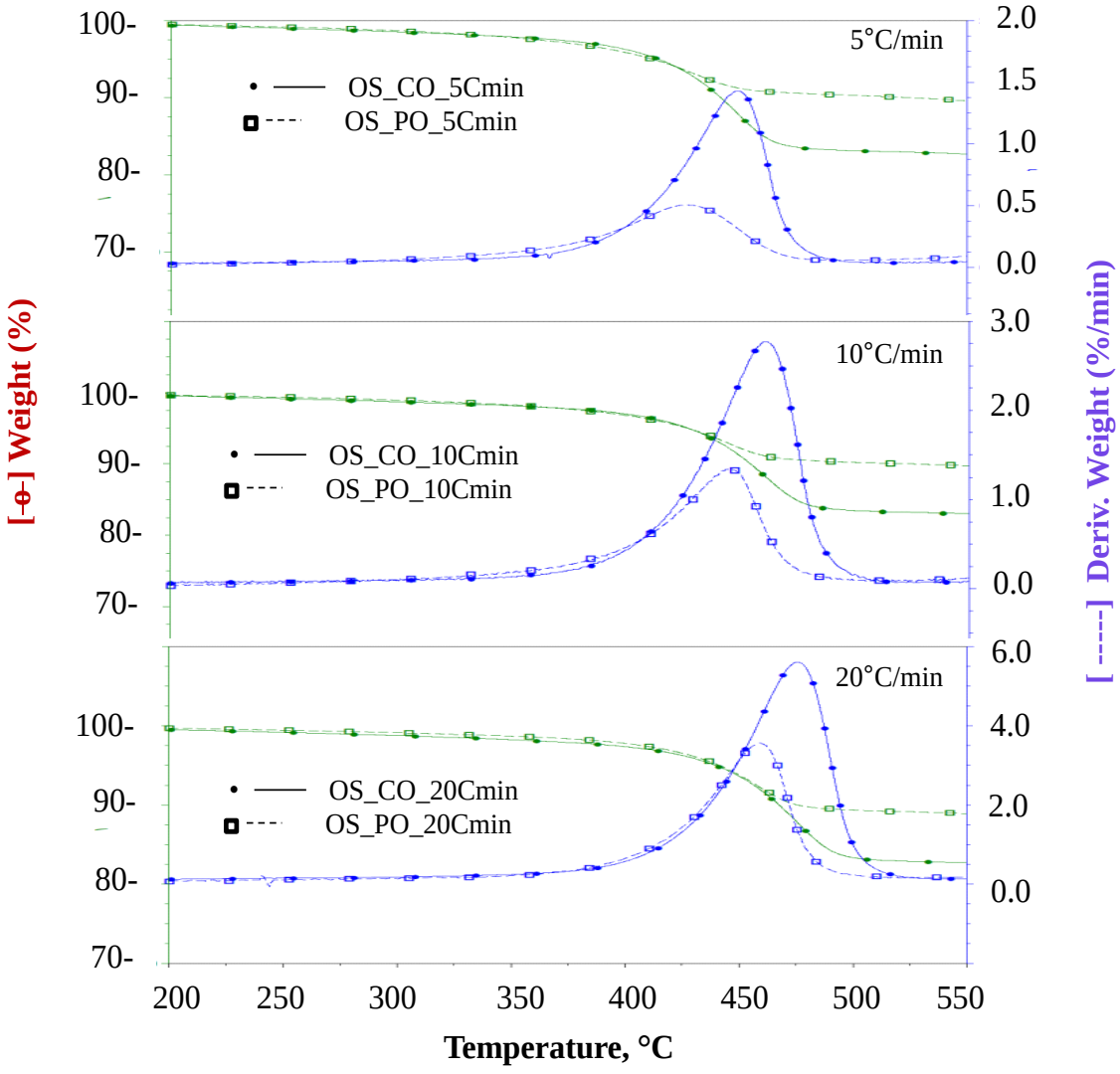

Figure A- 4: Comparison of the pyrolysis of sample #1 (PO) and sample #2 (CO) at three heating rates.

A.5. TGA of the GR Kerogen Pyrolysis Followed by Combustion

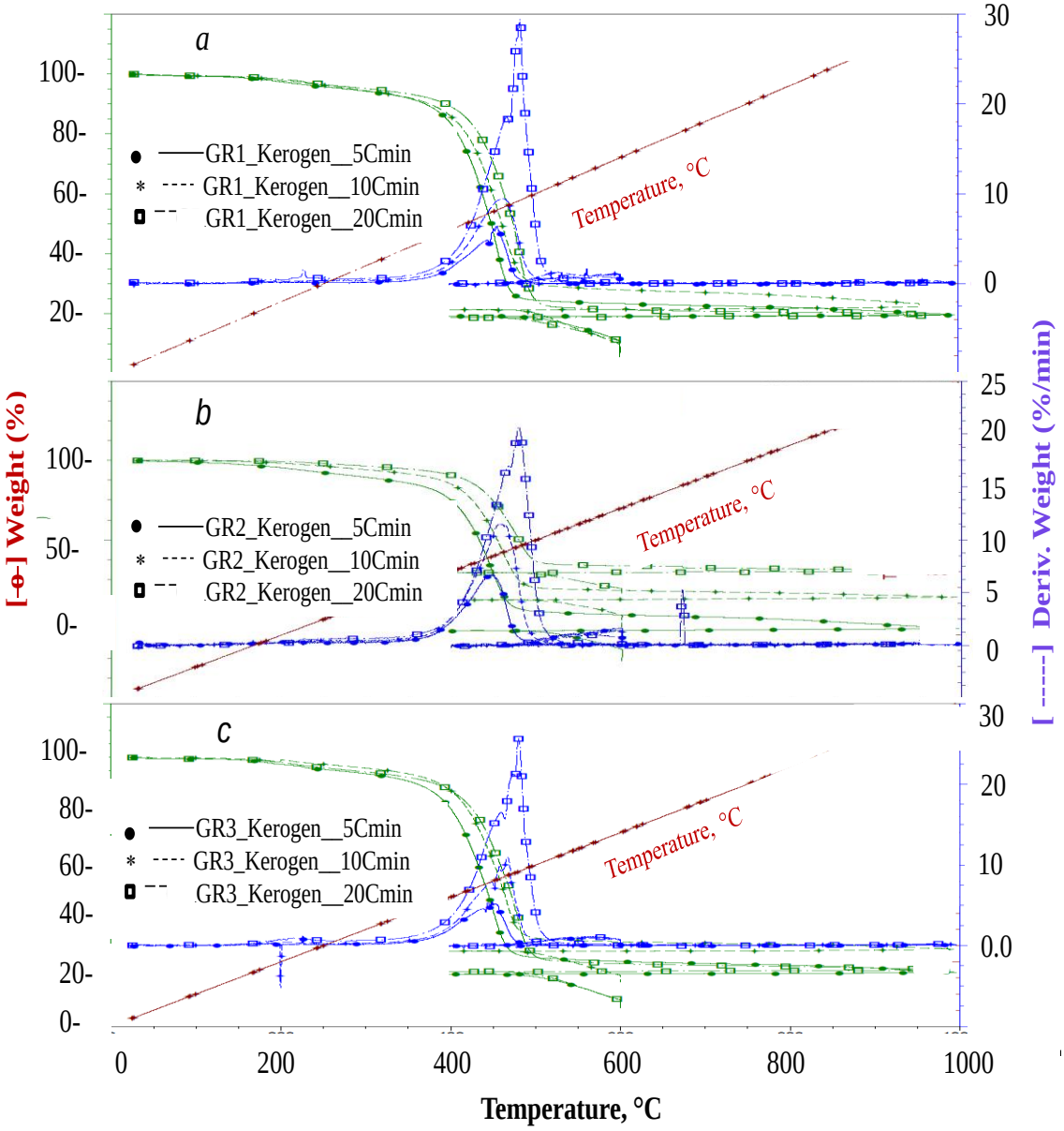

Figure A- 5: Pyrolysis of GR kerogens at heating rates of 5°C/min, 10°C/min and 20°C/min. (a) GR-1 kerogen, (b) GR-2 Kerogen and (c) GR-3 kerogen. Pyrolysis was followed by combustion at 10°C/min.

APPENDIX B

KINETIC EXPRESSION: CONVENTIONAL MODELS

A single particle size (100 meshes) of Mahogany oil shale (sample #1, PO) was used to study the kinetics of the organic decomposition with thermal gravimetric analysis (TGA, Q-500). Isothermal (300-600^{o}C) and nonisothermal (0.5 to 50^{o}C/min) experiments in N_2 and air environments were conducted. Different conventional mathematical approaches for both the cases were applied to determine the kinetic parameters activation energy, *E* and preexponential factor, *A* with the assumption of first order reaction.

The TGA operating conditions such as purging time, 10 mins and total flow rate of sweep gas, 100 ml/min were kept fixed for all the experiments. In isothermal experiments, the thermal induction time period was kept as low as possible using 100^{o}C/min heating rate. Correction factor was included in the analysis of data to account for induction period. The nonisothermal experiments were performed from ambient to 1000^{o}C. TGA data were analyzed in the range of organic weight loss (10-12%) and conversion profiles were normalized from zero to one to derive the kinetic parameters.

B.1. Kinetic Expressions: Conventional Mathematical Methods

Only one peak was observed in the organic decomposition temperature range for the N_2 environment in both isothermal (Figure B-1) and nonisothermal (Figure 5-1) cases. Consequently, single stage decomposition was assumed in deriving kinetic rate expressions. In contrast, for TGA experiments conducted in the air environment, two

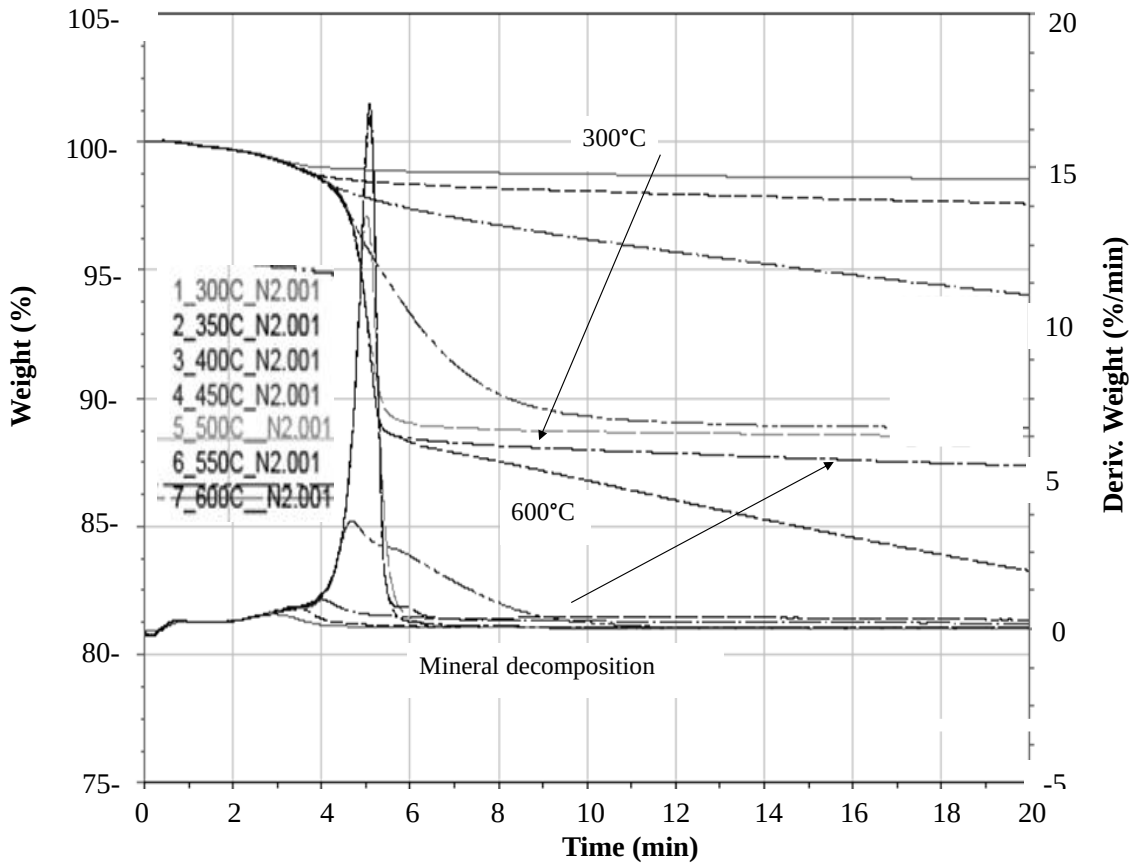

Figure B- 1: Isothermal TGA curves in the N_2 environment (pyrolysis).

peaks were detected in organic decomposition temperature regions for all isothermal (Figure B-2) and nonisothermal (Figure B-3) experiments, indicating that there may be two reactions occurring simultaneously. The mechanism of the formation of intermediates may be significantly different in the two environments, with the intermediate in pyrolysis being formed relatively fast. Thus, both the single stage and two stage decomposition mechanisms were examined in deriving the combustion kinetic parameters.

The weight loss were transformed to conversion using the following expressions

$$\alpha = \frac{W_0 - W_t}{W_0 - W_\infty} \qquad \text{(B-1a)}$$

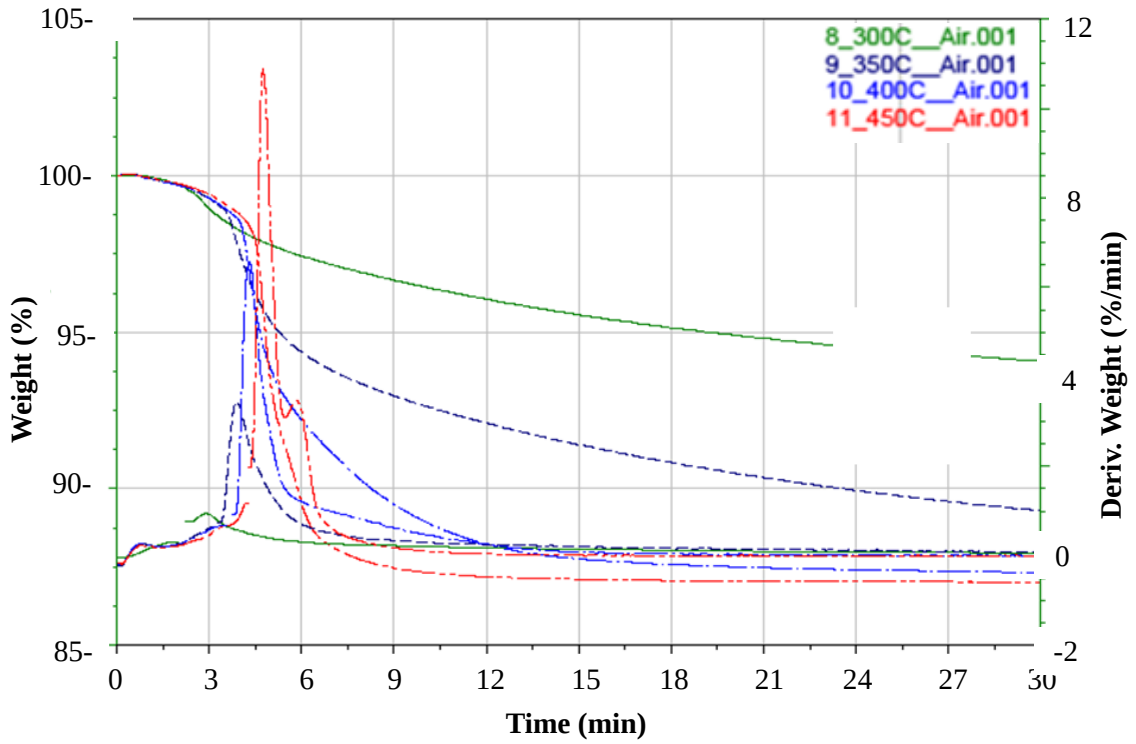

Figure B- 2: Isothermal TGA curves in air environment (combustion).

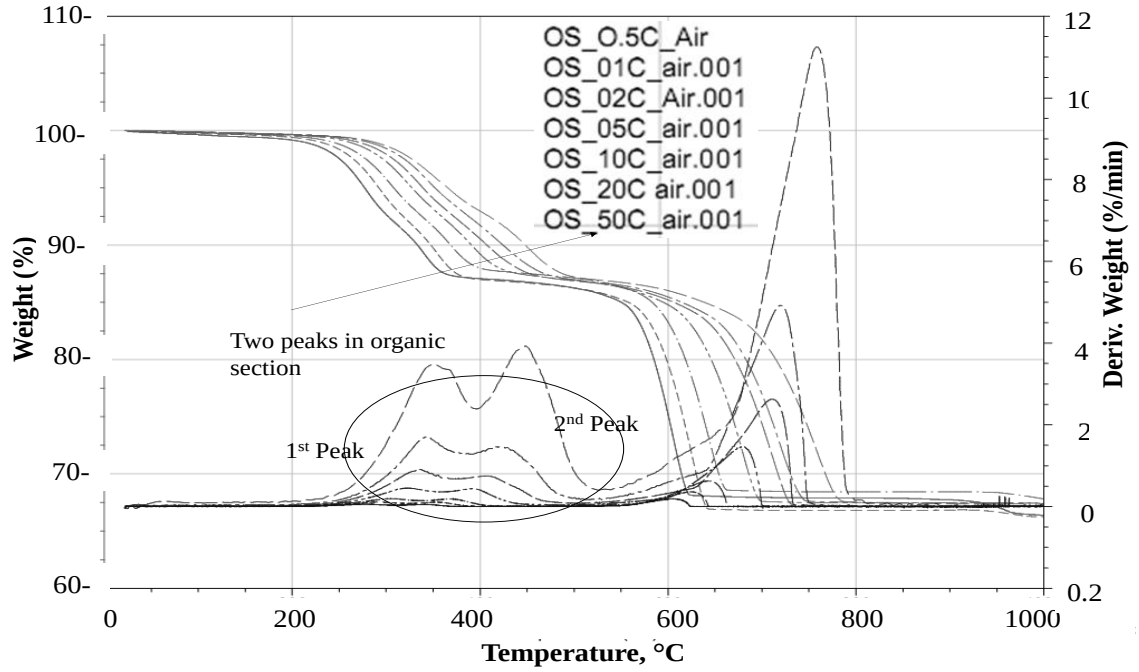

Figure B- 3: Nonisothermal TGA combustion. Rates go from 0.5°C/min to 50°C/min.

'or'

$$\alpha = \frac{W_0 - W_t}{W_0 \cdot X} \qquad \text{(B-1b)}$$

Equation (B-1a) was used for the calculation of nonisothermal conversions. The conversions for the isothermal experiments were calculated using equation (B-1b). The correction factor (*X*) was calculated based on the assumption of 10% of the organic material in the oil shale samples and the values are mentioned in Tables B-1 and B-2. The analysis criteria for nonisothermal experiments are summarized in Tables B-3 and B-4.

Assuming first order reaction, the rate law model equation can be combined with an Arrhenius dependency on temperature, leading to the general expression for the decomposition of a solid.

$$\frac{d\alpha}{dt} = A \cdot \exp\left[\frac{-E_a}{R \cdot T}\right] \cdot (1-\alpha) \qquad \text{(B-2)}$$

Table B- 1: Isothermal TGA data for N_2 environment (pyrolysis) and data analysis using the integral method.

Temp	Time	Initial weight	Isothermal condition		Corre-ction factor	Integral Method			
°C	min	mg	time min	wt loss %	X	1/T kelvin	R^2	*k*	ln *k*
300	720	26.75	3.33	0.83	0.091	0.0017	0.51	0.009	-7.13
350	240	26.69	3.82	1.25	0.087	0.0016	0.88	0.005	-5.40
400	240	22.64	4.36	1.79	0.082	0.0015	0.96	0.031	-3.47
450	240	24.68	4.96	3.99	0.060	0.0014	0.81	0.297	-1.21
500*	240	25.00	5.59	10.71					
550*	180	23.95	6.3	11.62					
600*	30	24.10	6.96	12.11					

*Isothermal analyses cannot be performed at these temperatures, since most of the organic material decomposes before this temperature is attained.

Table B- 2: Isothermal TGA data for air environment (combustion) and data analysis using the integral method.

Temp	Total time	Initial weight	Isothermal condition		Corre-ction factor	Integral Method			
^oC	min	mg	time min	wt loss %	X	1/T kelvin	R^2	*k*	ln *k*
300	240	23.64	2.70	0.73	0.093	0.0017	0.87	0.036	-3.31
350	240	23.39	3.82	1.86	0.081	0.0016	0.87	0.191	-1.65
400	240	23.24	4.31	3.15	0.068	0.0015	0.84	0.873	-0.14
450	180	32.16	4.88	5.68	0.043	0.0014	0.86	2.801	1.03

Table B- 3: Analysis of the nonisothermal TGA pyrolysis data using the differential method.

	Initial weight	Analysis Criteria						Differential Method				
		Start		End		Maximum						
β	*mg*	*T* ^oC	*wt % Loss*	*T* ^oC	*wt % Loss*	T_{max}, ^oC	*wt % Loss*	R^2	*slope*	*I**	E_a *kJ/mol*	*A* min^{-1}
0.5	22.64	255.6	1.32	421.6	8.02	392.7	6.48	0.96	9351	10.8	77.74	24510
1	28.64	269.6	1.16	437.6	7.48	398.3	5.79	0.95	9002	10.07	74.84	23624
2	26.90	280.0	1.33	456.4	8.43	414.1	6.52	0.96	10379	11.8	86.29	266505
5	25.97	348.9	2.17	474	9.41	432.2	7.17	0.97	14873	17.93	123.65	3E+08
10	38.45	349.7	1.74	490	9.67	445.6	7.26	0.97	14905	17.54	123.92	4E+08
20	29.49	371.6	1.58	504	10.68	460.1	7.92	0.97	17757	21	147.63	3E+10
50	22.37	377.3	1.43	530.6	11.13	477.0	7.89	0.96	17218	19.56	143.15	2E+10

Table B- 4: Nonisothermal TGA data for air environment (combustion).

Heating rate	Initial weight	First Peak						Second Peak			
		Start		End		Maximum		End		Maximum	
β	*mg*	*T* ^oC	*wt % Loss*	*T* ^oC	*wt % Loss*	T_{max} ^oC	*wt % Loss*	*T* ^oC	*wt % Loss*	T_{max} ^oC	*wt % Loss*
0.5	18.68	179	0.67	311.3	8.16	279.9	5.20	396.4	12.91	340.2	10.80
1	20.26	199.1	0.59	323.8	7.95	294.1	5.29	400.3	13.02	354.4	10.74
2	19.98	201.9	0.49	339.1	7.56	305.9	4.80	421.5	12.29	367.1	9.93
5	30.56	211.4	0.44	358.5	7.46	323.8	4.68	459.6	12.72	392.2	10.13
10	34.98	216.5	0.02	374.9	7.69	337.1	4.82	499.4	13.13	409.5	10.18
20	21.69	215.5	0.38	389.2	7.58	341.1	4.10	504.6	13.07	425.9	10.13
50	30.22	227.7	0.42	395.3	6.81	351.4	4.03	522.9	13.03	450.4	10.20

B.2. Isothermal Kinetic Analysis- Integral method

The integral form of equation (2) can be written as

$$\ln(1-\alpha) = -k \cdot (t - t_o) \qquad \text{(B-3)}$$

where k is the specific rate constant and t_o is the time at the start of the constant-temperature period (when the isothermal condition reached). The thermal induction period was eliminated from the kinetic analysis and correspondingly, the W_∞ was corrected by X. Application of the integral method to the isothermal data and the corresponding Arrhenius plots can be used to obtain frequency factors and activation energies for both the pyrolysis (N_2), and combustion (air) experiments. The kinetic data obtained are summarized in Tables B-1 and B-2 .The values for E_a and A in the N_2 environment were 134.78 kJ/mol and 1.2×10^9 min^{-1} respectively, while in the air environment these values were 100.47 kJ/mol and 5.1×10^7 min^{-1}.

B.3. Nonisothermal Kinetic Analysis

The experimental conditions and analysis criteria to obtain kinetic parameters such as start time, maximum point, and end point are summarized in Tables B-3 and B-4 for N_2 and air environments. On the basis of criteria chosen for the analysis, the conversion data were normalized from zero to one with respect to temperature. Nonisothermal kinetic data were derived with four different methods, namely, Direct Arrhenius plot, Integral method, Friedman approach and Maximum Rate method.

B.3.1 Differential Method- Direct Arrhenius Plot

The kinetic rate expression for nonisothermal experiments with Arrhenius dependency can be derived by introducing heating rate (β = dT/dt) in equation (B-2)

$$\frac{d\alpha}{dT} = \frac{A}{\beta} \cdot \exp\left[\frac{-E_a}{R \cdot T}\right] \cdot (1-\alpha) \qquad \text{(B-4a)}$$

Rearranging the above equation yields,

$$\ln\left[\frac{1}{(1-\alpha)}\right] \cdot \frac{d\alpha}{dT} = \ln\left[\frac{A}{\beta}\right] - \left[\frac{-E_a}{R \cdot T}\right] \qquad \text{(B-4b)}$$

If the model is correct, the plot of LHS versus 1/T results a straight line, and values of E_a and A can be obtained. Table B-3 shows the kinetic data obtained for N_2 data. Similarly, the air environment data were fit to both the single step and two step mechanisms (Table B-5).

B.3.2. Integral Method

The nonisothermal kinetic equation (B-2) can be separated in the terms of overall conversion and temperature for particular constant heating rate (β) and constant frequency (preexponential) factor.

$$\int_0^{\alpha} \frac{d\alpha}{(1-\alpha)} = \frac{A}{\beta} \cdot \int_{T_o}^{T} \exp\left[\frac{-E_a}{R \cdot T}\right] dT \qquad \text{(B-5)}$$

Table B- 5: Kinetic parameters for nonisothermal combustion data for single step and two step (first peak and second peak) mechanisms using the differential method.

	Single step		First peak		Second peak	
β	E_a	A	E_a	A	E_a	A
$^oC/min$	*kJ/mol*	min^{-1}	*kJ/mol*	min^{-1}	*kJ/mol*	min^{-1}
0.5	62.76	4876	64.53	7581	80.14	1.00E+05
1	66.38	15553	63.93	8997	101.6	3.00E+07
2	64.34	13850	63.52	11668	90.08	1.00E+06
5	62.99	14692	65.46	25958	79.95	3.00E+05
10	58.04	7107	64.82	31958	65.19	22064
20	60.95	19935	63.97	39353	79.94	9.00E+05
50	60.31	33201	62.56	56107	96.5	1.00E+07

Equation B-5 can be rearranged as,

$$\ln\left[\frac{-\beta\cdot\ln(1-\alpha)}{R\cdot T^2}\right]-\ln\left[1-\frac{2R\cdot T}{E_a}\right]=\ln\left[\frac{A}{E_a}\right]-\left[\frac{-E_a}{R\cdot T}\right] \qquad \text{(B-6a)}$$

This approach was developed by Chen and Nuttall [159]. The value of E_a and A can be obtained by repeated least square fits of the equation to the experimental data using iteration over the kinetic parameters. A simpler form of the integral method, known as the Coats and Redfern [160] method was used in this study that does not require any iteration (Table B-6).

$$\ln\left[\frac{-\ln(1-\alpha)}{T^2}\right]=\ln\left[\frac{A\cdot R}{E_a\cdot\beta}\right]-\left[\frac{-E_a}{R\cdot T}\right] \qquad \text{(B-6b)}$$

If the model is correct, fitting the conversion data along with temperature versus 1/T results in a straight line from which E_a and A can be obtained for different heating rates used in the calculation.

Table B- 6: Kinetic parameters using the integral method.

	Pyrolysis- Nitrogen		Combustion-Air					
	Single stage		Single stage		First peak		Second peak	
β	E_a kJ/mol	A ,min^{-1}	E_a, kJ/mol	A, min^{-1}	E_a kJ/mol	A ,min^{-1}	E_a kJ/mol	A ,min^{-1}
0.5	90.09	222253.59	75.73	71408.3	89.48	2.00E+06	70.97	22955
1	89.02	290903.36	79.86	228658	93.54	6.00E+06	77.8	1.00E+05
2	98.25	2044218.8	77.41	182669	88.32	3.00E+06	86.08	9.00E+05
5	153.31	4.98E+10	74.89	136058	89.08	4.00E+06	64.04	14891
10	143.63	1.12E+10	70.36	66892.6	88.23	4.00E+06	53.3	2441
20	189.39	3.05E+13	70.91	115150	84.05	2.00E+06	59.05	18305
50	176.94	4.04E+12	70.79	199596	88.86	1.00E+07	63.8	48544

B.3.3.Friedman Method

The Friedman [78] procedure assumes successive first order reactions and is based on the conversion data rather than on heating rates.

$$\ln\left[\frac{d\alpha}{dt}\right] = \ln\left[A \cdot (1-\alpha)\right] - \left[\frac{E_a}{R \cdot T}\right] \qquad \text{(B-7)}$$

Nonisothermal data can be analyzed at a specific conversion point (α) for all heating rates. If the data agrees with the model, the plot for log of conversion derivative versus 1/T results in a straight line. The slope and intercept provides E_a and A respectively. The results from Friedman approach on pyrolysis and combustion data are summarized in Table B-7. In both the cases single step mechanism with first order reaction was applied to drive the kinetic parameter.

Table B- 7: Kinetic parameters – distribution of activation energies as a function of conversion obtained using the Friedman approach.

Conversion	Pyrolysis-Nitrogen			*Combustion-Air*		
α	E_a, *kJ/mol*	*A, min*$^{-1}$	*lnA*	E_a, *kJ/mol*	*A, min*$^{-1}$	*lnA*
0.05	106.14	15283636	16.54	161.77	7.10E+13	31.89
0.1	118.03	1.30E+08	18.68	154.52	8.00E+12	29.7
0.2	140.6	7.10E+09	22.68	159.44	1.20E+13	30.13
0.3	161.43	2.62E+11	26.29	140.6	1.50E+11	25.76
0.4	180.17	6.55E+12	29.5	123.21	2.90E+09	21.78
0.5	202.24	2.75E+14	33.248	127.9	3.90E+09	22.08
0.6	217.08	3.34E+15	35.74	130.97	4.20E+09	22.15
0.7	232.95	4.33E+16	38.31	131.64	3.80E+09	22.06
0.8	230.63	2.53E+16	37.77	131.27	3.10E+09	21.86
0.9	214.85	1.13E+15	34.66	121.51	4.70E+08	19.96
0.95	225.32	5.09E+15	36.17	120.11	2.50E+08	19.35

B.3.4. Kissinger Method- Maximum Rate

The maximum rate method uses the maximum rate data [161]. The maximum rate is obtained by ensuring that the following condition is satisfied.

$$\frac{d\alpha^2}{dT^2} = 0$$

For a first order reaction (n = 1), equation (B-4) leads to the following form,

$$\ln\left[\frac{\beta}{T_{\max}^{\ 2}}\right] = \ln\left[\frac{A \cdot R}{E_a}\right] - \left[\frac{E_a}{R \cdot T_m}\right] \qquad \text{(B-8)}$$

Here, T_{max} is the temperature at the maximum reaction rate and α_m is the conversion at that condition. The apparent E_a and apparent A were determined by linear slope and intercept respectively (Table B-8). It was observed that the goodness of the fit and the values of the kinetic parameters differ depending on the mathematical method used. For example, the activation energies derived from four different methods in the N_2 environment were: 74-147 kJ/mol from the differential method, 89-189 kJ/mol from the integral method, 106-233 kJ/mol from the Friedman approach and 204 kJ/mol from the maximum rate method. The activation energies at different heating rates from differential and integral methods (Figure B-4) increased with heating rate from 0.5^{o}C/min to 20^{o}C/min with a slight decreased at 50^{o}C/min.

Table B- 8: Kinetic parameters using maximum rate method.

Kinetic parameters	Pyrolysis -Nitrogen	Combustion- Air	
		First peak	Second peak
E_a, *kJ/mol*	204.22	182.47	142.84
A, min^{-1}	3.34E+14	3.51E+15	3.23E+10

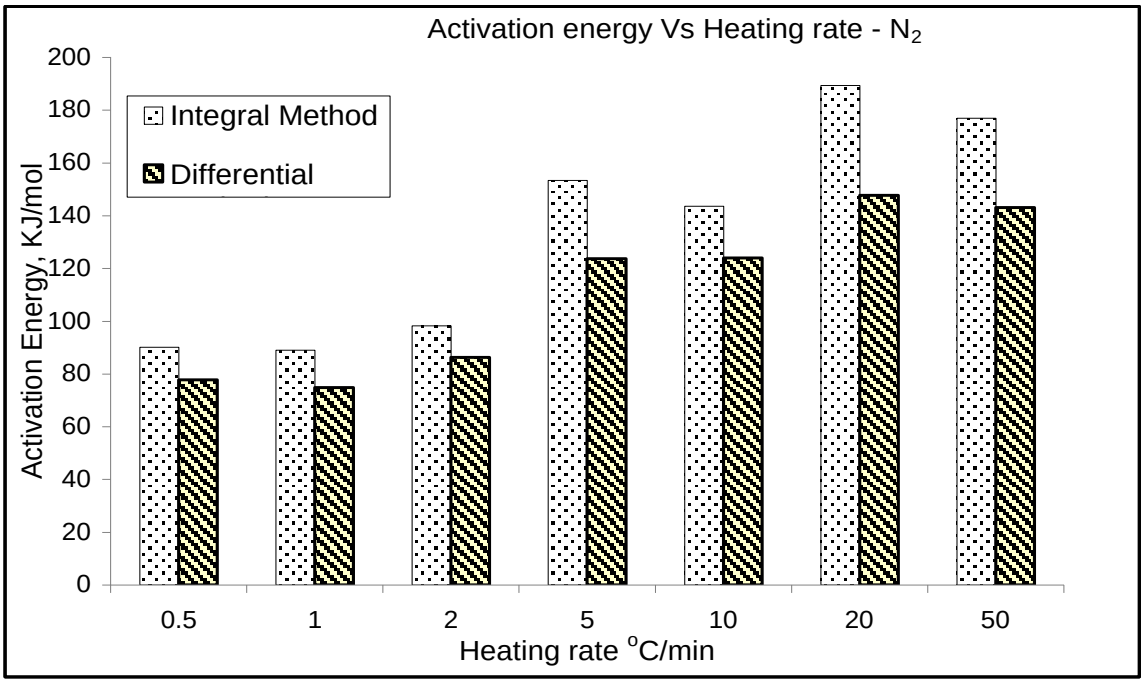

Figure B- 4: Activation energies for the pyrolysis of oil shale using conventional methods.

The activation energies for single step mechanism from differential and integral methods were 58.04-66.38 kJ/mol and 70.36-79.86 kJ/mol respectively for combustion process. While with two step mechanism, differential method derived 62.56-65.46 kJ/mol and 65.19-101.6 kJ/mol for first and second steps respectively. The activation energies obtained from integral method were 84.05-93.54 kJ/mol for first step and 53.30-86.06 kJ/mol for second step with two step mechanism. The choice of the mechanism depends on the method of analysis employed. The differential method showed a better fit than the integral method for the two step concept, while the opposite trend was observed for the single step mechanism. The distribution of activation energies with Friedman method for combustion data was found in the range of 120.11-161.77kJ/mol. The maximum rate method showed that the activation energy is greater for the first step (182.5 kJ/mol) than

the second (143 kJ/mol) in combustion process. These analyses also suggest that the combustion of oil shale needs less energy than pyrolysis.

The goodness of the kinetic parameters obtained from differential and integral methods were examined by re-plotting *ln* (*k*) versus 1/T data. Differential and integral (Figure B-5) methods both appeared to fit the pyrolysis data well and both support the concept of a single step mechanism. However, the slope of the linear fit differ for different heating rates, which creates a fundamental question regarding the application of these concepts to deriving kinetic parameters for complex reactions like kerogen decomposition. It has been argued in the literature that these conventional approaches are not appropriate for finalizing the activation energies for the intrinsic decomposition of complex materials. The isoconversion methods are specifically designed to address deficiencies in variable heating rate analyses. The conversion-based Friedman approach, which falls within the general category of isoconversion methods, showed an increase in activation energy with conversion followed by a decrease after 70 % conversion for pyrolysis process.

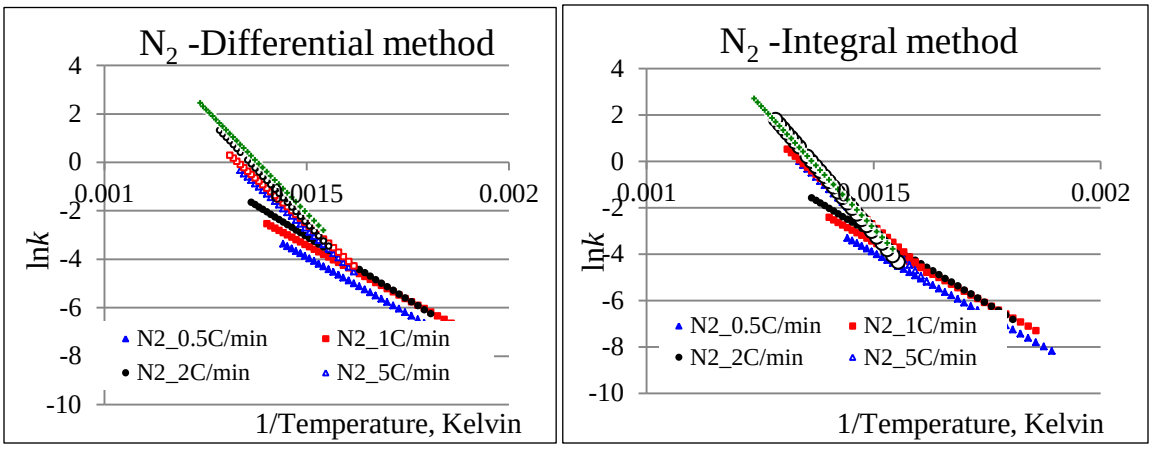

Figure B- 5: Goodness of the fit using (a) the differential method and (b) integral method on pyrolysis data.

APPENDIX C

EXPERIMENTAL DATA

C.1. HPTGA Pyrolysis

Table C- 1: Summary of HPTGA (ambient and high pressure) pyrolysis of sample #1 (PO) and sample #2 (CO).

Sample ID	Temp	Pressure	HR	Hold Time	OS, gm	Wt. loss %	Unreacted Organics %	Coke %
HPTGA_1_PO_Ambient	850°C	Ambient	10°C/min	10 mins	3.42	10.43	0.02	0.00
HPTGA_2_CO_Ambient	850°C	Ambient	10°C/min	10 mins	3.57	20.70	0.50	0.00
HPTGA_3_PO_ 500psi	850°C	500psi	10°C/min	10 mins	3.26	7.35	0.41	3.35
HPTGA_4_CO_500psi	850°C	500psi	10°C/min	10 mins	3.66	17.65	0.38	3.20

Table C- 2: Summary of the high pressure TGA experiments performed with sample #1 oil shale at BYU.

Sample ID	Temp	HR	Wt. loss %	Unreacted organics %	Coke %
HPTGA-BYU_1C/min_500C_500psi	500°C	1°C/min	8.56	~0.2%	~0.5%
HPTGA-BYU_10C/min_850C_500psi	500°C	10°C/min	7.47	~0.2%	~1%
HPTGA-BYU_20C/min_550C_500psi	550°C	20°C/min	8.39	~0.2%	~0.6%

C.2. Batch Pyrolysis of Powdered Oil Shale

Table C- 3: Summary of the batch pyrolysis of sample #1 (PO) samples and TGA analysis of spent shales.

			Reactor Pyrolysis				TGA pyrolysis and combustion of SS			
Sample ID	Temp	Duration	OS, gm	wt loss %	Liquid	Gas	Unreacted Organics %	Mineral %	Coke %	@ 350C
PO_BT_350C_6hrs	350°C	6 hrs	29.65	0.00	No	No	7.36	21.97	0.00	1.60
PO_BT_425C_6hrs	425°C	6 hrs	29.37	0.00	No	No	4.11	22.41	0.00	1.89
PO_BT_500C_30 mins	500°C	0.5 hrs	25.81	6.30	No	Yes	4.43	26.11	0.00	0.97
PO_BT_350C_12hrs	350°C	12 hrs	28.34	0.56	No	Yes	7.34	22.29	0.00	1.65
PO_BT_425C_12hrs	425°C	12 hrs	28.40	4.89	No	Yes	2.89	23.75	0.00	1.57
PO_BT_500C_12hrs	500°C	12 hrs	28.31	10.60	No	Yes	0.39	23.56	0.00	0.00
PO_BT_350C_18hrs	350°C	18 hrs	29.70	0.00	No	Yes	6.67	22.49	0.00	1.22
PO_BT_425C_18hrs	425°C	18 hrs	29.77	3.06	No	Yes	3.15	25.17	0.00	1.26
PO_BT_500C_18hrs	500°C	18 hrs	30.35	8.73	No	Yes	0.77	25.15	0.00	0.45

Table C- 4: Summary of the pressurized (500 psi) batch pyrolysis of sample #1 (PO) samples and TGA analysis of spent shales.

			Reactor Pyrolysis				TGA pyrolysis and combustion of SS		
Sample ID	Temp	Hold Time	OS	Wt. loss %	Liquid	Gas	Unreacted Organics %	Mineral %	Coke %
PO_BT_HP_500C_500psi_18hrs	500°C	18hrs	24.88	7.56	No	Yes	0.40	22.18	1.20
PO_BT_HP_425C_500 psi_18hrs	425°C	18hrs	25.6	7.97	No	Yes	3.98	20.12	0.00
PO_BT_HP_350C_500psi_6hrs	350°C	6hrs	25.44	3.22	No	Yes	9.40	21.78	0.00
PO_BT_HP_500C_500psi_6hrs	500°C	6hrs	24.48	6.13	No	Yes	0.50	23.28	0.28

C.3. Semi-batch Pyrolysis of Powdered Oil Shale

Table C- 5: Summary of the semibatch pyrolysis of sample #1 (PO) samples.

			Reactor Pyrolysis				TGA pyrolysis and combustion of SS		
Sample ID	Temp	Duration	OS, gm	Wt. Loss %	Oil Yield	Gas loss %	Unreacted Organics %	Mineral %	Coke %
PO_SB_500C_30 mins	500°C	0.5 hrs	30.01	10.86	6.48	4.38	0.13	22.35	0.71
PO_SB_425C_6hrs	425°C	6 hrs	31.99	10.57	4.80	5.76	0.49	21.58	0.81
PO_SB_3500C_6hrs	350°C	6 hrs	28.85	0.03	0.02	0.02	9.87	20.73	0.80
PO_SB_500C_12hrs	500°C	12 hrs	31.00	11.39	7.04	4.35	0.06	21.21	0.68
PO_SB_425C_12hrs	425°C	12 hrs	29.95	4.74	3.06	1.68	6.02	21.62	0.31
PO_SB_350C_12hrs	350°C	12 hrs	30.72	1.76	0.53	1.23	9.33	21.38	0.75
PO_SB_500C_18hrs	500°C	18 hrs	30.05	10.05	6.80	3.25	0.22	22.02	0.39
PO_SB_425C_18hrs	425°C	18 hrs	29.75	5.68	4.29	1.39	1.15	23.52	0.80
PO_SB_350C_24hrs	350°C	24 hrs	30.19	1.79	0.53	1.26	9.39	21.75	0.80

C.4. Continuous Pyrolysis of Core Samples

Table C- 6: Summary of the isothermal pyrolysis of ¾" core (sample #2) experiments under ambient pressure. Temperature of the center of the core was used as controlling probe to supply the heat.

			Reactor Pyrolysis			TGA pyrolysis and combustion of SS		
Sample ID	Temp	OS, gm	Wt loss %	Oil Yiled	Gas loss	Unreacted Organics %	Mineral %	Coke %
CO_3/4"_Iso_300C_24hrs_TCC	300°C	51.36	10.11	6.56	3.54	3.8	29.74	3.77
CO_3/4"_Iso_350C_24hrs_TCC	350°C	47.44	14.00	6.75	7.25	1.76	28.42	3.65
CO_3/4"_Iso_400C_24hrs_TCC	400°C	58.12	21.92	10.29	11.63	7.54	26.23	6.87
CO_3/4"_Iso_300C_24hrs_TCC_R	300°C	57.76	7.12	5.68	1.44			
CO_3/4"_Iso_350C_24hrs_TCC_R	350°C	55.41	12.62	4.84	7.78			
CO_3/4"_Iso_400C_24hrs_TCC_R	400°C	52.47	14.79	6.98	7.81			

Table C- 7: Summary of the experimental conditions and results of ambient and pressure pyrolysis of ¾" core (sample #2) samples.

	Pyrolysis Conditions				Reactor Pyrolysis				TGA pyrolysis and combustion of SS		
Sample-ID	Temp	Pressure	HR, °C/min	Hold Time	OS	Wt loss %	Oil Yield %	Gas loss%	UO %	Mineral %	Coke %
CO_3/4"_Iso_500C_Ambient	500°C	Ambient	100	24hrs	47.71	15.30	10.71	4.59	0.08	8.17	0.33
CO_3/4"_Iso_400C_Ambient	400°C	Ambient	100	24hrs	41.39	16.77	12.46	4.31	2.66	19.29	5.78
CO_3/4"_Iso_300C_Ambient	300°C	Ambient	100	24hrs	50.88	1.08	0.64	0.44	15.52	22.90	1.16
CO_3/4"_Iso_500C_500psi	500°C	500psi	100	24hrs	38.5	18.70	10.63	8.07	0.16	2.79	1.03
CO_3/4"_Iso_400C_500psi	400°C	500psi	100	24hrs	39.09	9.67	2.06	7.61	7.68	2.49	0.22
CO_3/4"_Iso_300C_500psi	300°C	500psi	100	24hrs	44.47	2.46	0.67	1.79	15.16	28.71	1.44
CO_3/4"_Noniso_1C/min_Ambient	500°C	Ambient	1	0hrs	34.6	14.36	14.17	0.19	0.43	20.55	3.55
CO_3/4"_Noniso_10Cmin_Ambient	500°C	Ambient	10	0hrs	42.04	16.72	12.50	4.23	8.55	6.61	1.6
CO_3/4"_Noniso_1Cmin_500psi	500°C	500psi	1	0hrs	42.51	15.93	11.25	4.68	8.78	11.2	1.35

Isothermal experiments were conducted for 24 hrs and nonisothermal were terminated when the temperature, 500C achieved. UO denotes unreacted organics.

C.5. Batch Pyrolysis of Core (3/4”) Oil Shale

Table C- 8: Summry of the batch pyrolysis of ¾” core oil shale.

Sample ID	Reactor Pyrolysis					TGA pyrolysis and combustion of SS		
	Temp	OS, gm	Wt loss %	Oil	Gas	Unreacted organics %	Mineral %	Coke%
CO_3/4"_BT_300C_72hrs	300°C	18.86	0.90	NO	Yes	17	23.89	0
CO_3/4"_BT_400C_72hrs	400°C	25.7	9.11	NO	Yes	7.25	23.47	1.10
CO_3/4"_BT_500C_72hrs	500°C	29.65	20.17	NO	Yes	0.80	16.99	1.31

Table C- 9: Summry of the hydoys batch pyrolysis of ¾” core oil shale.

Sample ID	Reactor Pyrolysis			TGA pyrolysis and combustion of SS		
	Temp	OS, gm	Wt loss %	Unreacted organics %	Mineral	Coke%
HY_PY_CO_3/4"_300C_72hrs	300°C	18.1711	4.46	8.45	18.30	1.05
HY_PY_CO_3/4"_350C_72hrs	350°C	25.6417	7.10	10.67	20.02	0.23
HY_PY_CO_3/4"_400C_72hrs	400°C	23.8354	--	1.68	18.95	0.17

C.6. Pyrolysis of Skyline 16 (GR) samples

Table C- 10: Summary of the GR core samples pyrolysis.

				Reactor Pyrolysis				TGA pyrolysis and combustion of SS		
	Sample ID	Temp	Hold Time	OS, gm	Wt. loss %	Oil yield %	Gas loss %	UO %	Mineral %	Coke %
GR-1	GR-1a_CO_1"_350C_24hrs	350°C	24 hrs	40.32	7.08	1.53	5.55	29.04	13.21	4.00
	GR-1b_CO_1"_425C_24hrs	425°C	24 hrs	40.49	25.91	8.31	17.60	31.21	7.92	3.15
	GR-1c_CO_1"_500C_24hrs	500°C	24 hrs	41.63	33.74	13.72	20.02	15.76	8.41	3.23
GR-2	GR-2c_CO_1"_350C_24hrs	350°C	24 hrs	50.78	2.84	0.79	2.05	13.92	27.04	0.14
	GR-2a_CO_1"_425C_24hrs	425°C	24 hrs	61.82	9.61	2.42	7.20	0.00	33.86	0.65
	GR-2b_CO_1"_500C_24hrs	500°C	24 hrs	52.93	12.26	9.27	2.99	0.00	23.53	0.10
GR-3	GR-3b_CO_1"_350C_24hrs	350°C	24 hrs	51.75	2.54	0.97	1.58	10.06	20.00	1.40
	GR-3c_CO_1"_425C_24hrs	425°C	24 hrs	47.88	18.40	12.15	6.25	0.00	24.36	4.41
	GR-3a_CO_1"_500C_24hrs	500°C	24 hrs	51.20	17.17	10.84	6.33	0.00	23.27	1.80

Table includes results from reactor pyrolysis of GR core samples followed by TGA analysis of spent shales. The results were normalized based on initial weight. UO represents unreacted organics.

Table C- 11: TGA analyses of isolated kerogen pyrolysis at three heating rates followed by combustion.

Sample ID	HR	Initial mass, mg	Pyrolysis end T	Pyrolysis Wt. loss %	Coke %
GR1-Kerogen-5°C_min	5°C/min	8.41	505°C	80.77	12.78
GR2-Kerogen-5°C_min		2.99	505°C	85.68	12.80
GR3-Kerogen-5°C_min		5.67	507°C	74.57	12.37
GR1-Kerogen-10°C_min	10°C/min	4.32	514°C	70.58	15.57
GR2-Kerogen-10°C_min		2.3	513°C	80.81	11.98
GR3-Kerogen-10°C_min		6.77	515°C	67.58	10.92
GR1-Kerogen-20°C_min	20°C/min	7.12	538°C	81.2	12.15
GR2-Kerogen-20°C_min		4.08	540°C	66.05	12.78
GR3-Kerogen-20°C_min		6.75	540°C	76.06	13.33

APPENDIX D

TEMPERATURE AND PRESSURE PROFILES

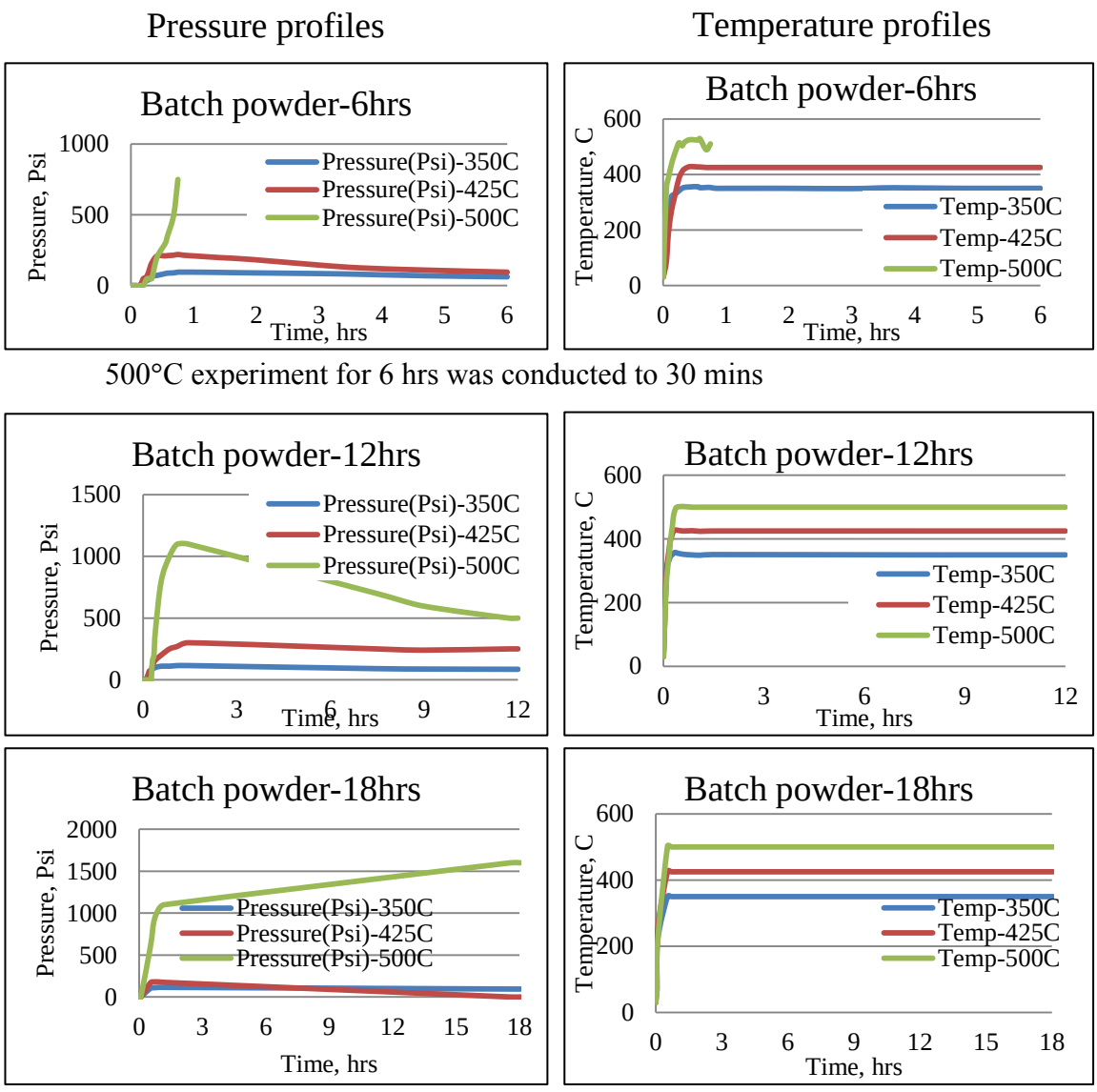

Figure D- 1: Pressure and temperature profiles during the batch pyrolysis of powdered (sample #1) oil shale (Table C-3).

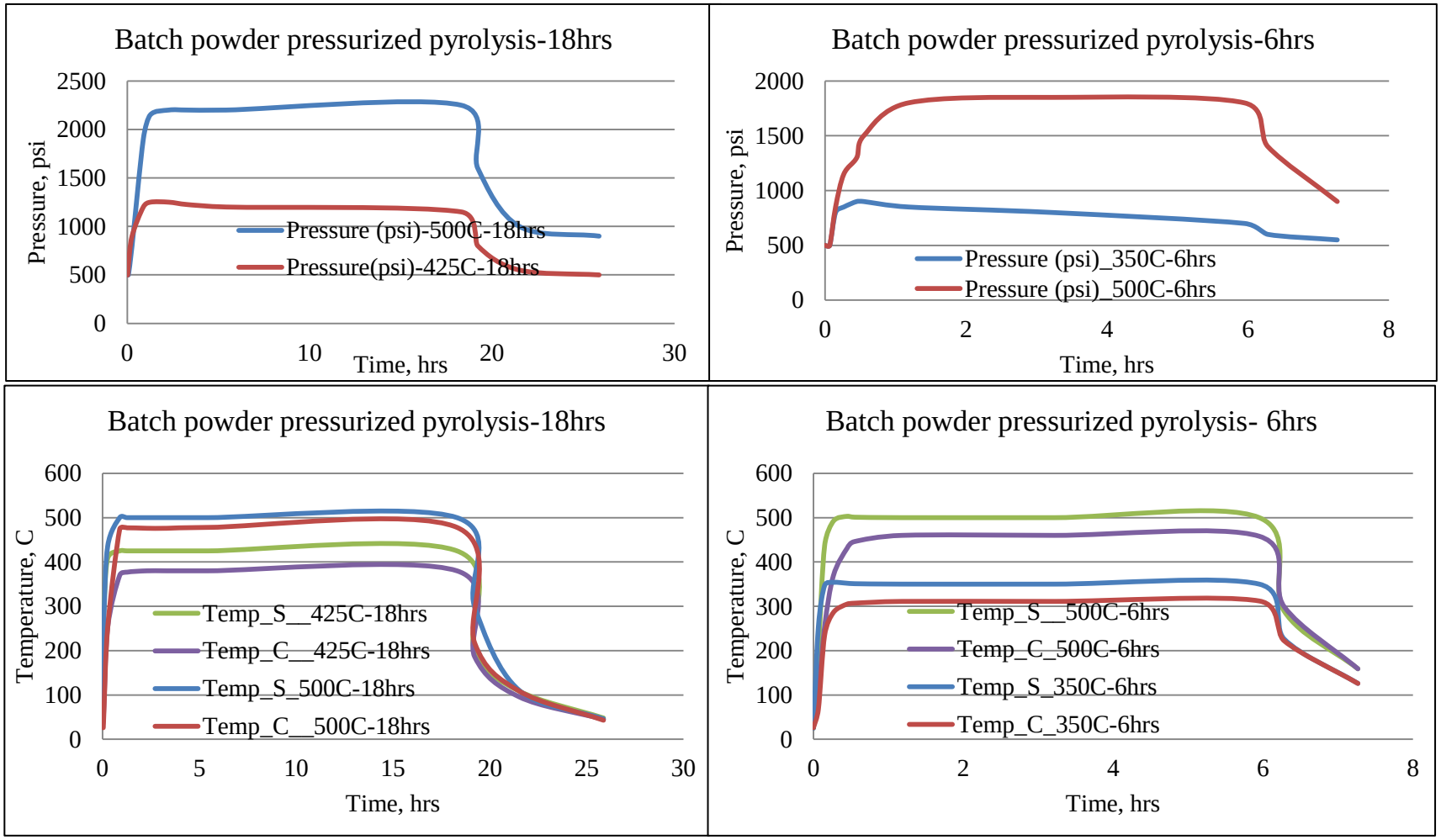

Figure D- 2: Pressure generated at different temperature during the batch pressurized pyrolysis of powdered (sample #1) samples and temperature profiles. S is the rector surface temperature and C is the temperature at the center of the sample (Table C-4).

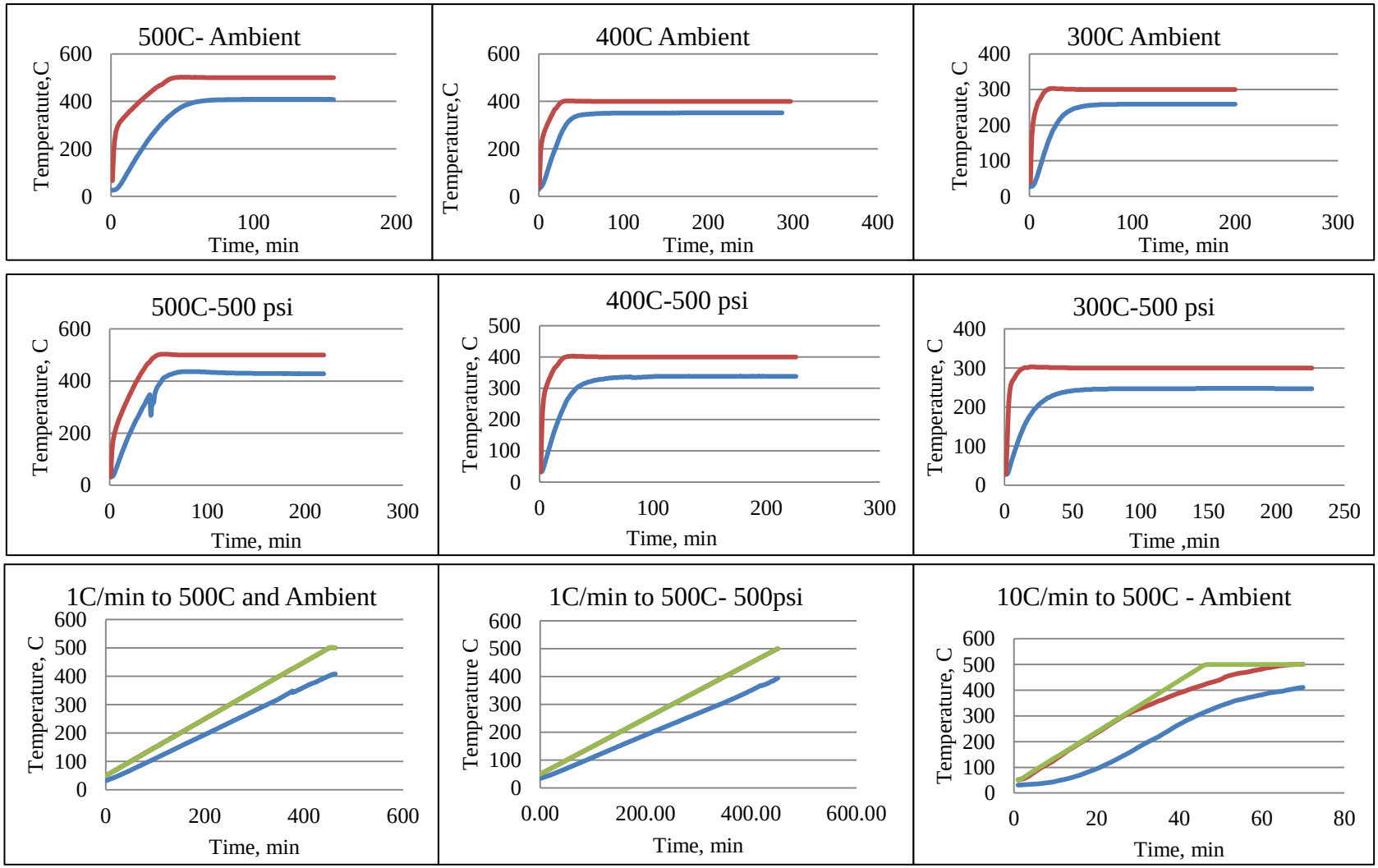

Figure D- 3: Temperature profiles for the pyrolysis of ¾" core (sample #2) samples (Table C-7).

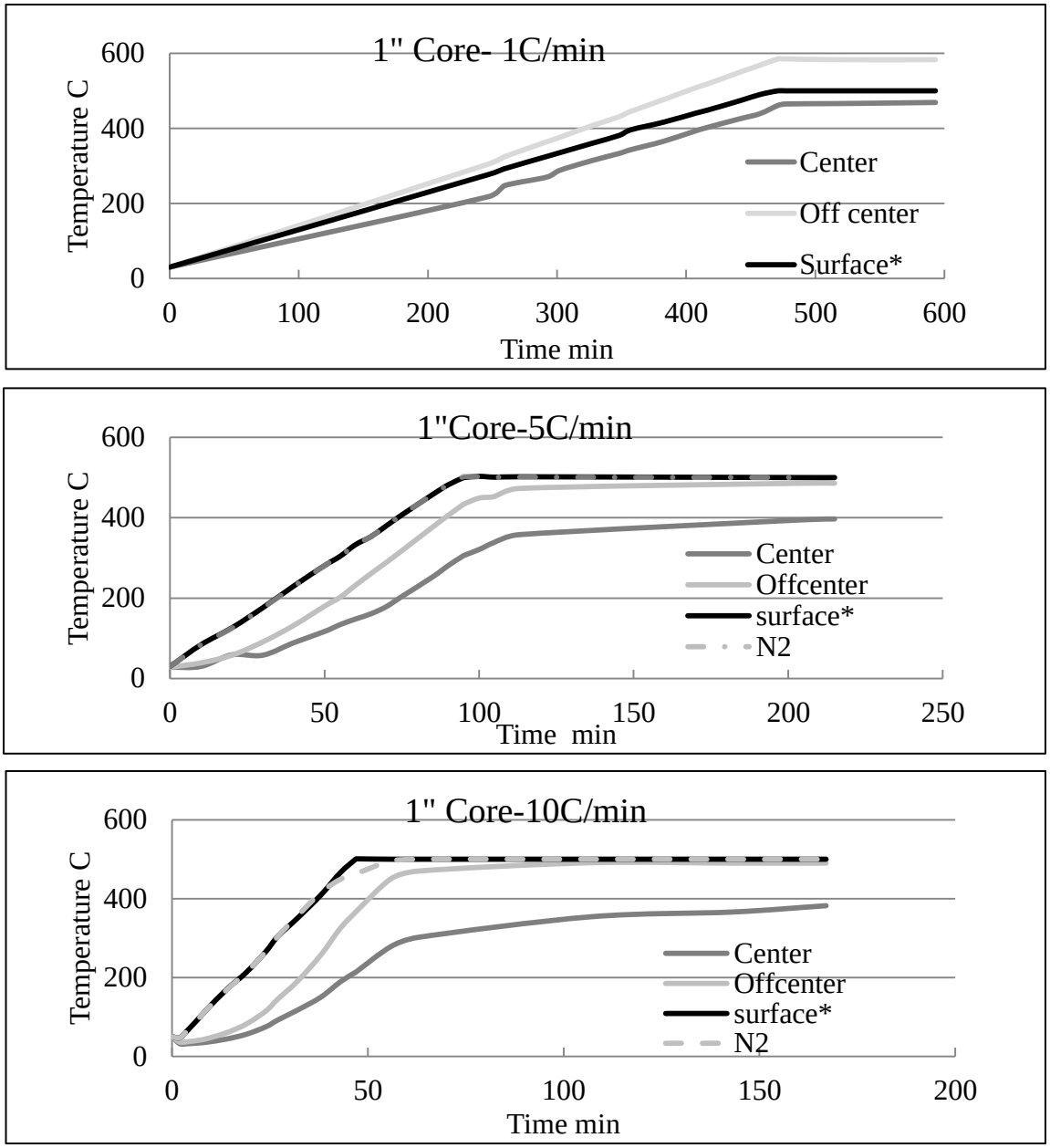

Figure D- 4: Temperature profiles for the pyrolysis of 1" core (sample #2) at three heating rates (Table 7-5).

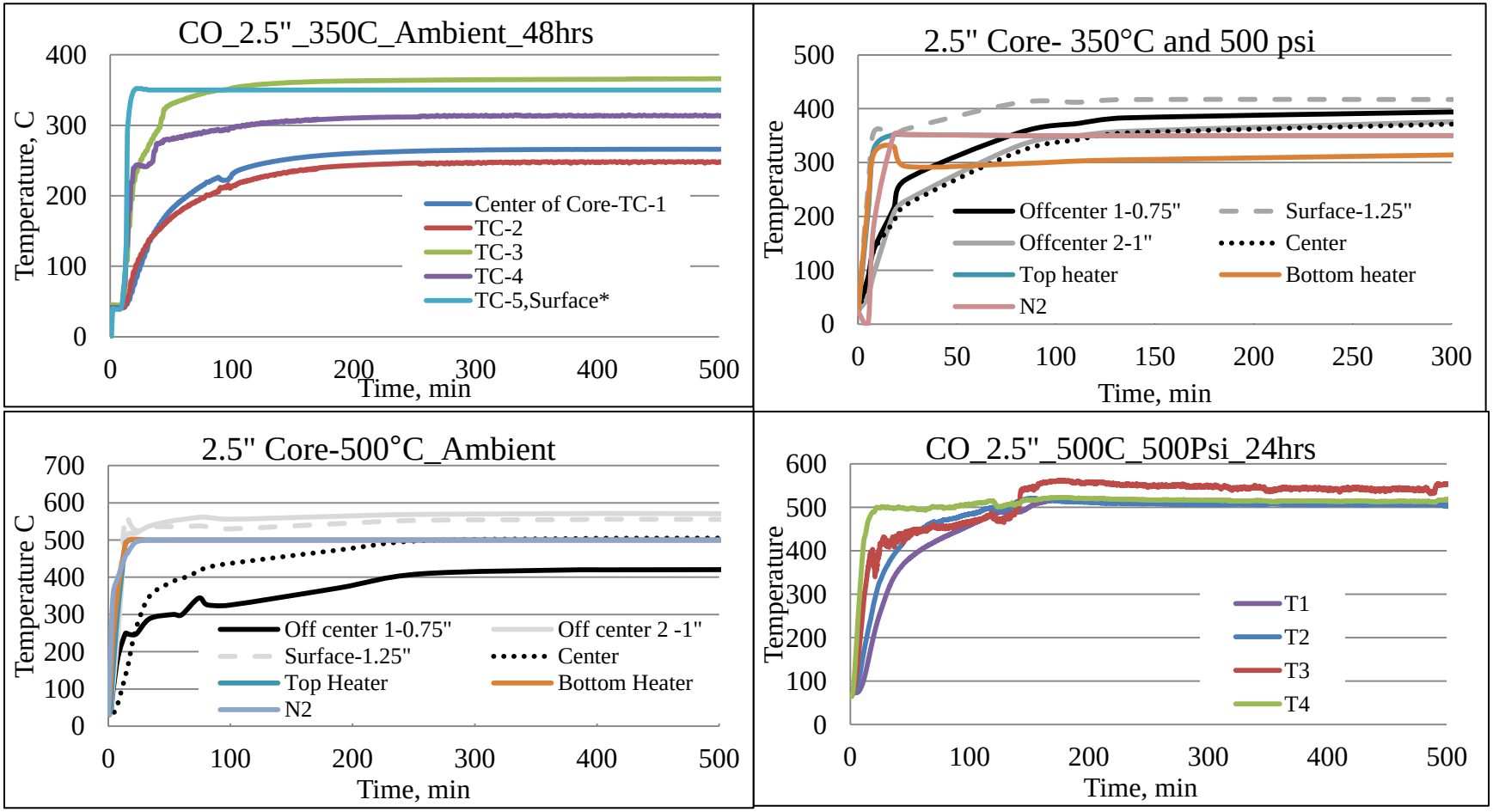

Figure D- 5: Temperature profiles during the pyrolysis of 2.5" core (sample #2) samples (Table 7-6).

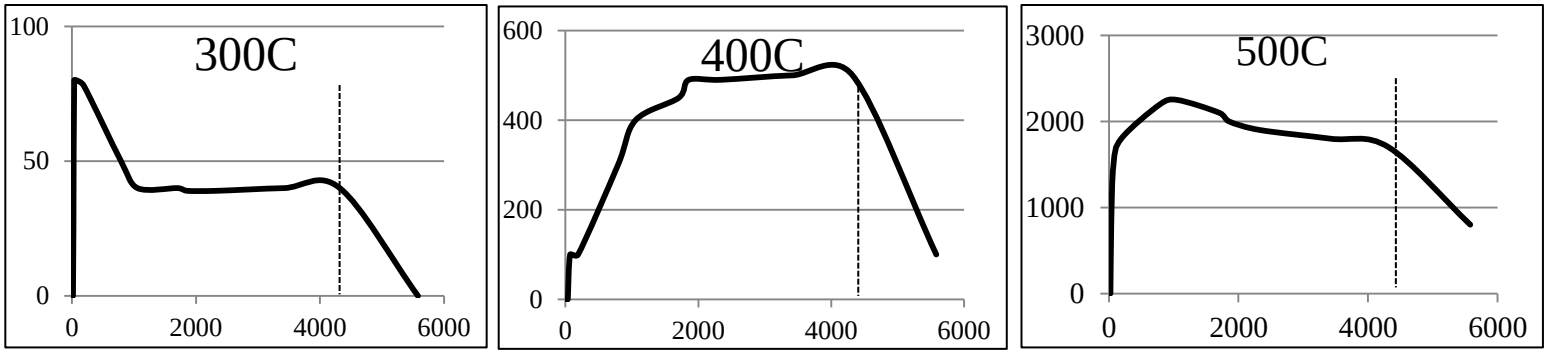

Figure D- 6: Pressure generated at different temperature during the batch pyrolysis of 3/4" core oil shale at different temperatures (Table C-8). The x axis is time in min and y axis is pressure in psi.

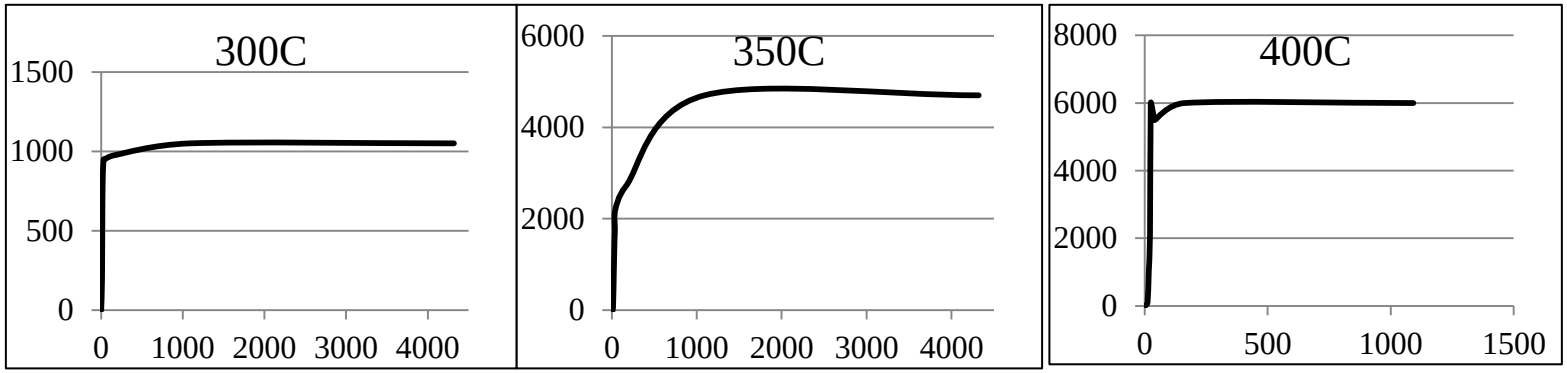

Figure D- 7: Increase in the pressure during batch hydrous pyrolysis experiments at different temperatures. The x axis is time in min and y axis is pressure in psi.

APPENDIX E

PHYSICAL PROPERTIES OF SHALE OILS

Table E- 1: Physical properties of the shale oils.

Size	SAMPLE ID	WAT °C	Density@ 25C-g/cc	Viscosity @30C-cp
PO	PO_SB_425C_6hrs	25.73		
	PO_SB_500C_30 mins	22.61		
¾" Core	CO_3/4"_Iso_500C_500psi	16.97	0.85	3.21
	CO_3/4"_Iso_400C_24hrs_TCC		0.91	22.1
	CO_3/4"_Noniso_10Cmin_Ambient	24.5	0.89	8.96
1" Core	CO_1"_1C/min_Ambient_Con_400C	21.78		
	CO_1"_1C/min_Ambient_Rec_400C	21.53		
	CO_1"_5C/min_Ambient_Con	21.90	0.91	
	CO_1"_10C/min_Ambient_Con	23.29	0.91	
	GR-2c_CO_1"_350C_24hrs	25.69		
	CO_1"_1C/min_500C_100psi_2hrs_400C	26.95		
	CO_1"_10C/min_500C_100psi_1hrs	27.49		
2.5" Core	CO_2.5"_500C_Ambient_1hr	26.30	0.90	
	CO_2.5"_500C_Ambient_Rec	30.72	0.92	
	CO_2.5"_500C_500psi_24hrs	19.27	0.89	4.19

APPENDIX F

GLOSSARY

Bitumen- Benzene soluble organic material in oil shale.

Batch Pyrolysis- Pyrolysis experiment in the closed system.

Carbonaceous Residue- Benzene insoluble portion of the kerogen product (char and coke) remaining in the spent shale.

Char- A solid product of the pyrolysis process in the spent shale, which can further be decomposed and produces gas and coke.

Coke- A solid product of the pyrolysis process which remains in the spent shale. The amount of the coke formed during the pyrolysis process is estimated by combusting the spent material after performing the second stage high temperature pyrolysis.

Combustion- Heating the oil shale in air environment.

Complete Conversion- Decomposition of all the organic matter in oil shale. The weight derivative peak returns to the base line.

Continuous Flow Pyrolysis- Pyrolysis of oil shale in an open system. The produced products are swept with hot nitrogen flow.

Conversion- Decomposition of the organic matter in oil shale to produce fluid products.

Gas- Uncondensed vapors formed from the organic matter during heating of oil shale.

Gas Loss- Difference of weight loss and oil yield during the process.

Hydrous Pyrolysis- Pyrolysis of oil shale in the presence of water.

Isothermal- Experiment at a constant temperature. A heating rate of 100°C/min was used to achieve the desired temperature.

Kerogen- Organic material in oil shale that is insoluble in ordinary solvents and that upon the application of heat decomposes and produces gas, oil and organic residue.

Nonisothermal- Heating the material with a constant temperature rate.

Nonhydorus Pyrolysis- Pyrolysis of the material in the absence of water.

Mahogany Zone- Organic rich oil shale section in the Green River Formation.

Mineral- Inorganic material in oil shale.

Mutiscale Pyrolysis- Pyrolysis of the samples of different sizes.

Oil- Condensable hydrocarbons formed during the pyrolysis of shale sample.

Oil Shale- A wide variety of compact, sedimentary rocks containing organic material

Oil Yield- The weight percent of oil produced per weight of initial oil shale.

Organic Matter- The portion of oil shale (kerogen and bitumen) which decomposes in the temperature range of 300-550°C and produces hydrocarbons.

Pyrolysis- Heating of oil shale in inert environment.

Secondary Reactions- Reactions occur in primary products such as coking and cracking.

Semibatch Pyrolysis- Pyrolysis with no sweep gas and fluid products escape the system by internal pressure.

Spent Shale- Pyrolyzed oil shale which may contain unreacted organic, coke and mineral materials.

Sample #1 – Oil shale samples (PO) which contain 10-12% organic matter.

Sample #2 – Oil shale samples (CO) which contain 17-18% organic matter.

Thermal Induction Period- Time required to achieve the isothermal condition.

Unreacted Organics- The amount of unpyrolyzed organic matter and unreleased oil in the spent shale.

Weight Loss- The difference of the weight between initial oil shale and spent shale.

REFERENCES

[1] George JH, Harris HG. Mathematical modeling of insitu oil shale retorting. Siam J Number Anal 1977;14.

[2] Bartis JT, LaTourrette T, Dixon L, Peterson DJ, Cecchine G. OIl shale development in the United States- Prospective and policy issues. In: Rand Corporation, Santa Monica, CA, 2005.

[3] Engler C. Die chemie und physik des erdols. Das Erdol 1913;1:1-37.

[4] ZNuttall HE, Guo T, Schrader S, Thakur DS. Pyrolysis kinetics of several key world oil shales. In: F.P. Miknis, J.F. McKay (Eds.) Geochemistry and chemistry of oil shales, American Chemical Society;1983, p. 269-300.

[5] Burham AK, Richardson JH, Coburn TT. Pyrolysis kinetics for western and eastern oil shale. In proceedings of the 17th intersociety energy conversion engineering conference, IEEE publishing: New York, 1982, pp. 912-7.

[6] Torrente MC, Galan MA. Kinetics of the thermal decomposition of oil shale from puertollano (Spain). Fuel 2001;80:327-34.

[7] Burnham AK. Oil evolution from a self purging reactor: Kinetic and composition at 2C/min and 2C/h. Energy Fuels 1991;5:205-14.

[8] Charlesworth JM. Oil shale pyrolysis. 1. Time and temperature dependence of product composition. Ind Eng Chem Process Des Dev 1985;24:1117-25.

[9] Burnham AK, Singleton MF. High-pressure pyrolysis of green river oil shale. in: F.P. Miknis, J.F. McKay (Eds.) Geochemistry and Chemistry of Oil Shales;1983, p. 335-51.

[10] Sohn HY, Yang HS. Effect of reduced pressure on oil shale retorting. 1. Kinetics of oil generation. Ind Eng Chem Process Des Dev 1985;24:265-70.

[11] Yang HS, Sohn HY. Mathematical analysis of the effect of retorting pressure on oil yield and rate of oil generation from oil shale. Ind Eng Chem Process Des Dev 1985;24:274-80.

[12] Stainforth JG. Practical kinetic modeling of petroleum generation and expulsion. Mar Petrol Geol 2009;26:552-72.

[13] Burnham AK, Happe JA. On the mechanism of kerogen pyrolysis. Fuel 1984;63:1353-6.

[14] Burnham AK. Relationship between hydrous and ordinary pyrolysis. In: NATO advanced study institute on composition, geochemistry and conversion of oil shales conference Akcay, Turkey, 1995 pp. 211–28.

[15] Pan C, Geng A, Zhong N, Liu J, Yu L. Kerogen pyrolysis in the presence and absence of water and minerals. 1. Gas components. Energy Fuels 2008;22:416-27.

[16] Lewan MD, Ruble TE. Comparison of petroleum generation kinetics by isothermal hydrous and non-isothermal open system pyrolysis. Org Geochem 2002;33:1457-75.

[17] Michels R, Landaisa P, Torkelsonb BE, Philpc RP. Effects of effluents and water pressure on oil generation during confined pyrolysis and high pressure hydrous pyrolysis. Geochim Cosmochim Acta 1995;59:1589-604.

[18] Hill GR, Johnson DJ, Miller L, Dougan JL. Direct production of low pour point high gravity shale oil. Ind Eng Chem Prod Res Dev 1967;6:52-9.

[19] Haung ETS. Retorting of single oil shale blocks with nitrogen and air. Soc Petrol Eng J 1977;17:331-6.

[20] Jaber JO, Probert SD. Nonisothermal thermogravimetry and decomposition kinetics of two Jordian oil shales under different processing conditions. Fuel Process Technol 2000;63:57-70.

[21] Kavianian HR, Yesavage VF, Dickson PF, Peters RW. Kinetic simulation model for steam pyrolysis of oil shale feedstock. Ind Eng Chem Res 1990;29:527-34.

[22] Fathoni AZ, Batts BD. A literature review of fuel stability studies with a particular emphasis on shale oil. Energy Fuels 1992;6:681–93.

[23] A technical, economical and legal assesment of North American heavy oil, oil sands, and oil shale resources; In responce to Energy Policy Act of 2005 Section 369(p); Prepared by Utah heavy oil program, 2007.

[24] Survey of energy resources. In: World Energy Council, 2007, pp. 93-115.

[25] Smith JW. Oil shale resources of the United States. CSM Mineral and Energy Resources Series 1980;23.

[26] Dyni JR. Geology and resources of some world oil shale deposits. Oil Shale 2003;20:193-252.

[27] Campbell JH, Kokinas GJ, Stout ND. Kinetics of oil generation from Colorado oil shale. Fuel 1978;57:372-6.

[28] VandenBerg MD. Basin wide evaluation of the uppermost green river formation's oil shale resource, Unita Basin, Utah and Colorado. In: Utah Geological Survey, 2008.

[29] Heistand RN. The Fishcer Assay, a standard method? in: Symposium on oil shale, tar sands, and related materials- production and utilization of sinfuels, San Francisco, 1976.

[30] Wellington SL, Berchenko IE, P. RE, Fowler TD, Ryan RC, Shalin GT, Stegemeier GL, Vinegar HJ. U.S. Patent 6,880,633, 2005.

[31] Symington WA, Olgaard DL, Phillps TC, Thomas MM, Yeakel JD. ExxonMobile's electrofrac^{TM} process for in situ oil shale conversion. In: 26th Oil Shale Symposium, Colorado Energy Research Institute, Colorado, 2006.

[32] Kasevich RS, Kolker M, Dwyer AS. U.S. Patent 4,140,179, 1979.

[33] Hubbard AB, Robinson WE. A thermal decomposition study of Colorado oil shale. in, U.S. Bureau of Mine:Report of investigation #4744, 1954.

[34] Pan Z, Feng HY, Smith JM. Rates of pyrolysis of colorado oil shale. AIChE J 1985;31:721-8.

[35] Allred VD. Kinetics of oil shale pyrolysis. Chem Eng Prog 1966;62:55-60.

[36] Braun RL, Rothman AJ. Oil shale pyrolysis: Kinetics and mechanism of oil production. Fuel 1975;54:129-31.

[37] Gregg ML, Campbell JH, Taylor JR. Laboratory and modelling investigation of a Colorado oil shale block heated to 900C. Fuel 1981;60:179-88.

[38] McKee RH, Lyder EE. Thermal decomposition of shales. Ind and Eng Chem 1921;13:613-8.

[39] Maier CG, Zimmerly SR. The chemical dynamics of the transformation of organic matter to bitumen in oil shale. Utah Eng Exper Sta Bull 1924;14:62-81.

[40] Franks AJ, Goodier BD. Preliminary study of the organic matter of Colorado oil shales. Quarterly of the Colorado School of Mines 1922;17:3-16.

[41] Bae JH. Some effects of pressure on oil shale retorting. Soc Petrol Eng J 1969;9:287-92.

[42] Parker JC, Zhang F. Efficient formulation of heat and mass transfer in oil shale retort models. In: 26th Oil Shale Symposium, Coloarodo School of Mines, 2006.

[43] Rajeshwar K, Nottenburg N, Dubow J. Review: Thermophysical properties of oil shales. J Mater Sci 1979;14:2025-52.

[44] Fausett DW, Mikinis FP. Simplified kinetics of oil shale pyrolysis. In: Colorado School of Mines Press, Golden, CO;1981.

[45] Campbell JH. The kinetics of decomposition of Colorado oil shale II. Carbonate minerals. Lawrence Livermore Laboratory Rep 1978;UCRL-52089-2.

[46] Jeong KM, Patzer IJF. Indigenous mineral matter effects in pyrolysis of Green River oil shale. In: F.P. Miknis, J.F. McKay (Eds.) Geochemistry and Chemistry of Oil Shales, Americal Chemical Society;1983, p. 529–42.

[47] Marshall CP, Kannangara GSK, Wilson MA, Guerbois JP, Hartung-Kagi B, Hart G. Potential of thermogravimetric analysis coupled with mass spectrometry for the evaluation of kerogen in source rocks. Chem Geol 2002;184:185-94.

[48] Galan MA, Smith JM. Pyrolysis of oil shale: Experimental study of transport effects. AIChE J 1983;29:604-10.

[49] Charlesworth JM. Oil shale pyrolysis. 2. Kinetics and mechanism of hydrocarbon evolution. Ind Eng Chem Process Des Dev 1985;24:1125-32.

[50] Burnham AK, Ward RL. A possible mechanism of alkene/alkane production. in: H.C. Stauffer (Ed.) Oil Shale, Tar Sands, and Related Materials, American Chemical Society, Washington DC;1981, p. 79-92.

[51] Burnham AK. Chemistry of shale oil cracking. in: H.C. Stauffer (Ed.) Oil Shale, Tar Sands, and Related Materials, American Chemical Society, Washington DC;1981, p. 79-92.

[52] Campbell JH, Koskians GJ, Coburn TT, D.Stout N. Oil shale retorting: The effects of particle size and heating rate on oil evolution and intraparticle oil degradation. InSitu 1978;2:1-47.

[53] Rajeshwar K. The kinetics of the thermal decomposition of green river oil shale kerogen by nonisothermal thermogravimetry. Thermochim Acta 1981;45:253-63.

[54] Hillier J, Fletcher J, Orgill J, Isackson C, Fletcher TH. An improved method for determination of kinetic parameters from constant heating rate TGA oil shale pyrolysis data. Am Chem Soc, Div Fuel Chem 2009;54:155-7.

[55] Li S, Yue C. Study of pyrolysis kinetics of oil shale. Fuel 2003;82:337-42.

[56] Li S, Yue C. Study of different kinetic models for oil shale pyrolysis. Fuel Process Technol 2003;85:51-61.

[57] Qing W, Baizhong S, Aijuan H, Jingru B, Shaohua L. Pyrolysis charactristic of Huadian oil shale. Oil Shale 2007;24:147-57.

[58] William PT, Ahmad N. Influence of process conditions on the pyrolysis of Pakistani oil shale. Fuel 1999;78:653-62.

[59] Thakur DS, Nuttal HE. Kinetics of pyrolysis of Moroccan oil shale by thermogravimetry. Ind Eng Chem Process Des Dev 1987;26:1351-6.

[60] Shin SM, Sohn HY. Nonisothermal determination of the intrinsic kinetics of oil generation from oil shale. Ind Eng Chem Process Des Dev 1980;19:420-6.

[61] Campbell JH, Koskinas GH, D SN. Kinetics of oil generation from Colorado oil shale Fuel 1978;57:372-6.

[62] Leavitt DR, Tyler AL, Kafesjiant AS. Kerogen decomposition kinetics of selected green river and eastern U.S. oil shales from thermal solution experiments. Energy Fuels 1987;1:520-5.

[63] Brown ME, Maciejewski M, Vyazovkin S, Nomen R, Sempere J, Burnham A, Opfermann J, Strey R, Anderson HL, Kemmeler A, Janssens J, Desseyn HO, Li CR, Tang TB, Roduit B, Malek J, Mitsuhasshi T. Computational aspects of kinetic analysis: Part A: The ICTAC kinetics project data, methods and results. Thermochim Acta 2000;355:125-43.

[64] Burnham AK. Computaional aspects of kinetic analysis. Part D: The ICTAC kinetic project multi thermal history model fitting methods and their relation to isoconversion methods in: Thermochim. Acta, 2000, pp. 165-70.

[65] Maciejewski M. Computational aspects of kinetic analysis: Part B- The ICTAC project- The decomposition kinetics of calcium carbonate revisited, or some tips on survival in the kinetic minefield. Thermochim Acta 2000;355:125-43.

[66] Roudit B. Computational aspects of kinetic analysis: Part E- Numerical techniques and kinetics of solid state processes. Thermochim Acta 2000;35:171-80.

[67] Vyazovkin S. Computational aspects of kinetic analysis: Part C- The ICTAC project- The light at the end of the tunnel? Thermochim Acta 2000;355:155-63.

[68] Burnham AK, Braun RL. Global kinetic analysis of complex materials. Energy Fuels 1999;13:1–22.

[69] Burnham AK, Dinh LN. A comparision of isoconversional and model fitting kinetic parameter estimation and application predictions. J Therm Anal Calorim 2007;89:479-90.

[70] Vyazovkin S. Reply to "What is meant by the term 'variable activation energy' when applied in the kinetics analyses of solid state decompositions (crystolysis reactions)?". Thermochim Acta 2003;397:269-71.

[71] Burnham AK. Chemistry and kinetics of oil shale retorting. In: Oil shale: A solution to the liquid fuel dilemma, ACS symposium series;2010, p. 115–34.

[72] Braun RL, Burnham AK. Analysis of chemical reaction kinetics using a distribution of activation energies and simpler models. Energy Fuels 1987;1:153-61.

[73] Burnham AK, Braun RL. General kinetic model of oil shale pyrolysis. InSitu 1985;9:1-23.

[74] Burnham AK, Braun RL, Coburn TT, Sandvik EI, Curry DJ, Schmidt BJ, Noble RA. An appropriate kinetic model for well-preserved algal kerogen. Energy Fuels 1996;10:49-59.

[75] Starink MJ. The determination of activation energy from linear heating rate experiments: A comparison of the accuracy of isoconversion methods. Thermochim Acta 2003;404:163-76.

[76] Sundararaman P, Merz PH, Mann RG. Determination of kerogen activation energy distribution. Energy Fuels 1992;6:793-803.

[77] Al-Ayed OS, Matouq M, Anbar Z, Khaleel AM, Abu-Nameh E. Oil shale pyrolysis kinetics and variable activation energy principle. Appl Energ 2010;87:1269-72.

[78] Friedman HL. Kinetics of thermal degradation of charforming plastics from thermogravimetry. In: Application to a phenolic plastic. J Polym SciPart C 1964;6:183–95.

[79] Vyazovkin S, Wight CA. Estimating realistic confidence intervals for the activation energy determined from thermoanalytical measurements. Anal Chem 2000;72:3171-5.

[80] Vyazovkin S, Wight CA. Isothermal and nonisothermal kinetics of thermally stimulated reactions of solids. Int Rev Phys Chem 1998;17:407-33.

[81] Vyzovkin SV, Lesnikovich AL. Practical application of isoconversional methods. Thermochim Acta 1992;203:177-85.

[82] Vyazovkin S, Wight CA. Kinetics in solids. Annu Rev Phys Chem 1997;48:125-49.

[83] Espitalie J, Ungerer P, Irwin I, Marquis F. Primary cracking of kerogens. Experimenting and modeling C_1, C_2–C_5, C_6–C_{15} and C_{15}+ classes of hydrocarbons formed. Org Geochem 1988;13.

[84] Huizinga BJ, Aizenshtat ZA, Peters KE. Programmed pyrolysis gas chromatography of artificially matured Green River kerogen. Energy Fuels 1988;2:74-81.

[85] Morandi JR, Jensen HB. Comparison of porphyrins from shale oil, oil shale, and petroleum by absorption and mass spectroscopy. J Chem Eng Data 1966;11:80-8.

[86] Wood KV, Narayan R, Stringham KR, Huang SL, Leehe H. Characterization of the oil extract of an Indiana shale. Fuel Process Technol 1990;26:73-81.

[87] Lee S. Oil shale technology. CRC Press Inc, Boca Raton, Florida, USA; 1991.

[88] Greenwood PF, George SC. Mass spectral characteristic of C_{19} and C_{20} tricylcic terpanes detected in Latrobe Tasmanite oil shale. Eur J Mass Spectrom 1999;5:221-30.

[89] Steck SJ, Muenow DW, Margrave JL. Mass spectrometric volatilization studies of oil shale. in: Division of Fuel Chemistry, American Chemical Society, Chicago, 1970.

[90] Chakravarty T, Windig W, Taghizadeh K, Meuzelaar HLC, Shadle LJ. Computer-assisted interpretation of pyrolysis mass spectra of two oil shales and their corresponding kerogens. Energy Fuels 1988;2:191-6.

[91] Campbell JH, Kokinas GJ, Gallegos G, Gregg M. Gas evolution during oil shale pyrolysis 1: Nonisothermal rate measurements. Fuel 1980;59:718-26.

[92] Campbell JH, Gallegos G, Gregg M. Gas evolution during oil shale pyrolysis 2: Kinetic and stoichiometric analysis. Fuel 1980;59:727-32.

[93] Huss EB, Burnham AK. Gas evolution during pyrolysis of various Colorado oil shales. Fuel 1982;61:1188-96.

[94] Burnham AK, Huss EB, Singleton MF. Pyrolysis kinetics for Green River oil shale from the saline zone. Fuel 1983;62:1199-204.

[95] Oh MS, Coburn TT, Crawford RW, Burnham AK. Study of gas evolution during oil shale pyrolysis by TQMS. Lawrence Livermore National Laboratory, UCRL 98233, 1988.

[96] Reynolds JG, Crawford RW, Burnham AK. Analysis of oil shale and petroleum source rock pyrolysis by triple quadrupole mass spectrometry: Comparisons of gas evolution at the heating rate of 10^0C/min. Energy Fuels 1991;5:507-23.

[97] Burnham AK, Braun RL, Gregg HR, Samoun AM. Comparison of methods for measuring kerogen pyrolysis rates and fitting kinetic parameters. Energy Fuels 1987;1:452-8.

[98] Burnham AK, Samoun AM, Reynolds JG. Characterization of petroleum source rocks by pyrolysis-mass spectroscopy gas evolution profiles. Lawrence Livermore National Laboratory, UCRL 111012, 1992.

[99] Burnham AK. Pyrolysis kinetics for the Bakken shale. Lawrence Livermore National Laboratory, UCRL 109622, 1992.

[100] Braun RL, Burnham AK, Reynolds JG. Oil and gas evolution kinetics for oil shale and petroleum source rocks determined from pyrolysis-TQMS data at two heating rates. Energy Fuels 1992;6:468-74.

[101] Oh MS, Taylor RW, Coburn TT, Crawford RW. Ammonia evolution during oil shale pyrolysis. Energy Fuels 1988;2:100-5.

[102] Oh MS, Fostera KG, Alcaraza A, Crawforda RW, Taylora RW, Coburna TT. Thermal decomposition of buddingtonite in oil shales. Fuel 1993;72:517-23.

[103] Wong CM, Crawford RW, Burnham AK. Determination of sulfur-containing gases from oil shale pyrolysis by triple quadrupole mass spectrometry. Anal Chem 1984;56:390-5.

[104] Wong CM, Crawforda RW. Application of a self-adaptive detector system on a triple quadrupole MS/MS to high explosives and sulfur-containing pyrolysis gases from oil shale. Int J Mass spectrom 1984;60:107-16.

[105] Meuzelaa HLC, Windig W, Futrell JH, Harper AM, Larter SR. Pyrolysis mass spectrometry and multivariable analysis of several key world oil shale kerogens and some recent alginites. In: T. Aczel (Ed.) Mass Spectrometric Characterization of Shale Oils: A Symposium;1986, p. 81-108.

[106] Khan MR. Influence of weathering and low-temperature preoxidation on oil shale and coal cevolatilization. Energy Fuels 1987;1:366-76.

[107] Stout ND, Koskinas GJ, Raley JH, Santor JD, Opila RL, Rothman AJ. Pyrolysis of oil shale, the effects of thermal history on oil yiled. In: 9th Oil Shale Symposium, Colorado School of Mines, 1976, pp. 153-72.

[108] Miknis FP, Maclel GE. In: 14th Oil Shale Symposium, 1981, pp. 270.

[109] Nazzal JM. Influnce of heating rate on the pyrolysis of Jordon oil shale. J Anal Appl Pyrolysis 2002;62:225-38.

[110] Nazzal JM. The influence of grain size on the products yiled and shale oil composition from the pyrolysis of Sultani oil shale. Energy Convers Manage 2008;49:3278-86.

[111] Litster J, Newell RB, Bhell PRF. Pyrolysis of Rundle oilshale in a continuous fluidized bed retort. Fuel 1988;67:1327-30.

[112] Yang HS, Sohn HY. Effect of reduced pressure on oil shale retorting. 2. Oil yield. Ind Eng Chem Process Des Dev 1985;24:271-3.

[113] Noble RD, Harris HG, Tucker WF. Isothermal oil shale pyrolysis. 2. Kinetic of product formation and composition at various pressure. Fuel 1981;60:573-6.

[114] Voge HH, Good GM. Thermal cracking and high paraffins. J Am Chem Soc 1949;71:593.

[115] Hillier JL, Fletcher TH. Pyrolysis kinetics of a Green River oil shale using a pressurized TGA. Energy Fuels 2011;25:232-9.

[116] Symington WA, Spiecker PM. Heat conduction modeling tools for screening insitu oil shale conversion processes. In: 28th Oil Shale Symposium, Colorado School of Mines, Colorado, 2008.

[117] Computer Modeling Group. STARS User Manual. 2007.

[118] Huang CK. Development of a general thermal oil reservoir simulator under a modularized framework. In: University of Utah, Salt Lake City, Utah, 2009.

[119] Granoff B, Nuttall HE. Pyrolysis kinetics for oil Shale particles Fuel 1977;56.

[120] Braun RL, Burnham AK. Mathematical model of oil generation, degradation, and expulsion. Energy Fuels 1990;4:132-46.

[121] Braun RL, Burnham AK. PMOD: A flexible model of oil and gas generation, cracking and expulsion. In: 15th International Metting on Organic Geochemistry, Manchester, England, 1991.

[122] Braun RL, Burnham AK. Chemical reaction model for oil and gas generation from type I and II kerogens. LLNL 1993.

[123] Stainforth JG. Practical kinetic modeling of petroleum generation and expulsion. Marine and Petroleum Geology 2009;26:552-72.

[124] Coburn TT, Oh MS, Crawford RW, Foster KG. Water generation during pyrolysis of oil shale. 1. Sources. Energy Fuels 1989;3:216-23.

[125] ASTM E1582-04 Standard Practice for Calibration of Temperature Scale for Thermogravimetry. ASTM International.

[126] Neer LA, Deo MD. Simulated distillation of oils with a wide carbon number distribution. J Chromatogr Sci 1995;33:133-8.

[127] ASTM D5307-97, Standard test method for determination of boiling range distribution of crude oils by gas chromatography. ASTM International 2002.

[128] Roehner RM, Hanson FV. Determination of wax precipitation temperature and amount of precipitated solid wax versus temperature for crude oils using FTIR spectroscopy. Energy and Fuels 2001;15:756—63.

[129] ASTM D1298-99, Standard test method method for density, relative density (specific gravity), or API gravity of crude petroleum and liquid petroleum products by hydrometer methods. ASTM International.

[130] ASTM D1217-93, Standard test method for density, relative density (Specific gravity) of liquids by Bingham pycnometer. ASTM International.

[131] ASTM D4052-96, Standard test method for density and relative density of crude oils by digital density analyzer. ASTM International.

[132] ASTM D5002-99, Standard test method for density and relative density of crude oils by digital density analyzer. .

[133] ASTM D2983-04, Standard test method for low-temperature viscosity of lubricants measured by brookfield viscometer. ASTM International.

[134] Hutton A, Bharati S, Robl T. Chemical and petrographical classification of kerogen/macerals. Energy Fules 1994;8:1478-88.

[135] Araújo HD, Silva NFD, Acchar W, Gomes UU. Thermal decomposition of illite. Mat Res 2004;7:359-61.

[136] Johnsona DR, Younga NB, Robb WA. Thermal characteristics of analcime and its effect on heat requirements for oil shale retorting. Fuel 1975;54:249-52.

[137] Behar F, Vandenbroucke M. Chemical modelling of kerogens. Org Geochem 1987;11:15-24.

[138] Vandenbroucke M, Largeau C. Kerogen origin, evaluation and structure. Org Geochem 2007;38:719-833.

[139] Blazek A. Thermal analysis. In: J.F. Tyson (Ed.) Thermal analysis, Van Nostrand Reinhold, London;1973.

[140] Vyazovkin S, A LL. Estimation of the pre-exponential factor in the isoconversional calculation of effective kinetic parameters. Thermochimica Acta 1988;128:297-300.

[141] Vyazovkin S, Linert W. Detecting isokinetic relationships in nonisothermal systems by the isoconversional method Thermochim Acta 1995;269/270:61-72.

[142] Vyazovkin S, Sbirrazzuoli N. Confidence intervals for the activation energy estimated by few experiments. Anal Chim Acta 1997;355:175-80.

[143] Doyle CD. Estimating isothermal life from thermogravimetric data. J Appl Polym Sci 1962;6:639-42.

[144] Senum GI, Yang RT. Rational approximations of the integral of the Arrhenius function. J Therm Anal Calorim 1977;11:445-7.

[145] Constable FH. The mechanism of catalytic decomposition. In: Proceedings of the Royal Society of London, The Royal Society, 1923, pp. 355-78.

[146] Boudreau BP, Ruddick BR. On a reactive continuum representation of organic matter diagenesis. Am J Sci 1991;291:507-38.

[147] Lakshmanan CC, White N. A new distributed activation energy model using weibull distribution for the representation of complex kinetics. Energy Fuels 1994;8:1158-67.

[148] Tiwari P, Deo M. Detailed kinetic analysis of oil shale pyrolysis TGA data. AIChE J 2011;57: n/a. doi: 10.1002/aic.12589.

[149] Galan MA, Smith JM. Pyrolysis of oil shale: Experimental study of transport effects. AIChE 2006 Spring National Meeting 1983;29.

[150] Brown ME, Maciejewski M, Vyazovkin S, Nomen R, Sempere J, Burnham A, Opfermann J, Strey R, Anderson HL, Kemmeler A, Janssens J, Desseyn HO, Li CR, Tang TB, Roduit B, Malek J, Mitsuhasshi T. Computational aspects of kinetic analysis: Part A-The ICTAC kinetics project-data, methods and results. Thermochim Acta 2000;355:125-43.

[151] Lewan MD. Water as a source of hydrogen and oxygen in petroleum formation by hydrous pyrolysis. Amer Chem Soc Div Fuel Chem 1992;37:1643-49.

[152] Vandergrift GF, Winans RE, Scott RG, Horwitz EP. Quantitative study of the carboxylic acids in Green River oil shale Bitumen. Fuel 1980;59:627-33.

[153] Bauman JH, Deo MD. Parameter space reduction and sensitivity analysis in complex thermal subsurface production processes. Energy Fuels 2011;25:251-9.

[154] Camp DW. Oil shale heat capacity relations and heats of pyrolysis and dehydration. LLNL. In: 20th Oil shale symposium, Golden, CO, 1987.

[155] Baughman GL. Synthetic fuels data handbook : U.S. oil shale, U.S. coal, oil sands. Denver : Cameron Engineers 1978

[156] Duvall EWF, Sohn HY, Pitt CH. Physical behaviour of oil shale at various temperatures and compressive loads: 2. Thermal expansion under various loads. Fuel 1985;64:184-8.

[157] Duvall EWF, Sohn HY, Pitt CH. Physical behaviour of oil shale at various temperatures and compressive loads: 3. Structure failure under loads. Fuel 1985;64:938-40.

[158] Duvall EWF, Sohn HY, Pitt CH, Bronson MC. Physical behavior of oil shale at various temperatures and compressive loads: 1. Free thermal expansion. Fuel 1983;62:1455-61.

[159] Chen WJ, Nuttall HE. Paper presented at the 86th AIChE National Meeting, Houston, Texas. 1979.

[160] Coats AW, Redfern JP. Kinetic parameters from thermodynamic data. Nature (London) 1964;201:68-9.

[161] Kissinger HE. Reaction kinetics in differential thermal analysis. Anal Chem 1957;29:1702-6.